
**Materials Research Report
Final Report**

August 2012

**UNF Project
Contract No. BDK82 977-02**

Sealing of Cracks on Florida Bridge Decks with Steel Girders

Principal Investigator: Adel ElSafty, P.E., Ph.D.

Co-Principal Investigator: N. Mike Jackson, P.E., Ph.D.

**School of Engineering
College of Computing, Engineering, and Construction
University of North Florida
Jacksonville, Florida 32224**



DISCLAIMER

The opinions, findings, and conclusions expressed in this publication are those of the authors and not necessarily those of the State of Florida Department of Transportation.

SI CONVERSION FACTORS

APPROXIMATE CONVERSIONS TO SI UNITS USED

SYMBOL	WHEN YOU KNOW	MULTIPLY BY	TO FIND	SYMBOL
LENGTH				
in	Inches	25.4	millimeters	mm
ft	Feet	0.305	meters	m
yd	Yards	0.914	meters	m

SYMBOL	WHEN YOU KNOW	MULTIPLY BY	TO FIND	SYMBOL
AREA				
in²	Square inches	645.2	square millimeters	mm ²
ft²	Square feet	0.093	square meters	m ²
yd²	square yard	0.836	square meters	m ²

SYMBOL	WHEN YOU KNOW	MULTIPLY BY	TO FIND	SYMBOL
VOLUME				
ft³	cubic feet	0.028	cubic meters	m ³
yd³	cubic yards	0.765	cubic meters	m ³

NOTE: volumes greater than 1000 L shall be shown in m³

SYMBOL	WHEN YOU KNOW	MULTIPLY BY	TO FIND	SYMBOL
MASS				
oz	ounces	28.35	grams	g
lb	pounds	0.454	kilograms	kg

SYMBOL	WHEN YOU KNOW	MULTIPLY BY	TO FIND	SYMBOL
FORCE and PRESSURE or STRESS				
lbf	Pound force	4.45	Newton	N
lbf/in²	Pound force per square inch	6.89	kilopascals	kPa

1. Report No. BDK82 977-02	2. Government Accession No.	3. Recipient's Catalog No.	
4. Title and Subtitle Sealing of Cracks on Florida Bridge Decks with Steel Girders		5. Report Date August 2012	
		6. Performing Organization Code	
7. Author(s) Adel ElSafty, P.E., Ph.D. & N. Mike Jackson, P.E., Ph.D.		8. Performing Organization Report No.	
9. Performing Organization Name and Address University of North Florida School of Engineering 1UNF Drive Jacksonville, FL 32224		10. Work Unit No. (TRAIS)	
		11. Contract or Grant No. BDK82 977-02	
12. Sponsoring Agency Name and Address State of Florida Department of Transportation 605 Suwannee St. MS 30 Tallahassee, FL 32399		13. Type of Report and Period Covered Final Report (1/14/2010) To (8/1/2012)	
		14. Sponsoring Agency Code	
15. Supplementary Notes			
16. Abstract One of the biggest problems affecting bridges is the transverse cracking and deterioration of concrete bridge decks. The causes of early age cracking are primarily attributed to plastic shrinkage, temperature effects, autogenous shrinkage, and drying shrinkage. The cracks can be influenced by material characteristics, casting sequence, formwork, climate conditions, geometry, vehicle loading, and time-dependent effects. The cracking of bridge decks not only creates unsightly aesthetic condition but also reduces deck durability. That can lead to corrosion problems of deck steel reinforcement and supporting steel girders (steel box girders and built-up steel girders). The lab testing, experimental field testing, and analytical study investigate the transverse cracking, especially early age cracking of bridge decks, and how to mitigate them. This research identifies suitable sealing materials for deck cracks showing their ability to span cracks of various widths and achieving performance criteria such as penetration depth, bond strength to crack walls, elongation, viscosity, penetration, and suitability of the type of sealant. Sealant performance was investigated by testing core samples to determine the depth of sealant penetration, bond, and tensile strength. Sealer samples were tested to verify their strength, modulus of elasticity, and elongation. A finite element model was developed to investigate the factors affecting tensile stresses and crack tendency. It also checks the live-load deflection limit, which is an important factor in bridge deck cracking. An Excel spreadsheet was also developed to predict the deck cracking accounting for shrinkage, thermal effect, creep, concrete mix design, deck restrain, loading, and environmental effects.			
17. Key Word Crack sealers, bridge deck, High Molecular Weight Methacrylate (HMWM).		18. Distribution Statement No restrictions.	
19. Security Classif. (of this report) Unclassified	20. Security Classif. (of this page) Unclassified	21. No. of Pages 201	22. Price

Form DOT F 1700.7 (8-72)

ACKNOWLEDGMENTS

The authors would like to thank the Florida Department of Transportation for their support and interest of this research. Also, appreciation is extended to BASF, Pilgrim, Unitex, and ChemMasters Corporations, for their participation and material donations regarding this research. In particular, special thanks go out to Ivan R. Lasa (the project manager), Mario Paredes, and the engineers of the FDOT Materials Research Center in Gainesville, Florida. The authors would also like to include special thanks to the laboratory staff and the technicians at the FDOT Materials Research Center.

EXECUTIVE SUMMARY

This report investigates the feasibility and performance of crack sealers that will meet the criteria set in the FDOT specifications 413 to repair transverse cracking on bridge decks. Many studies investigated deck cracking (Babaei et al., 1997, 1987; French et al., 1999; Krauss and Rogalla, 1996; La Fraugh et al., 1985; PCA, 1970). Transverse cracks have been a common problem in highway bridge decks in the past and continue to cause maintenance headaches today. Transverse cracks in bridge decks develop during the hardened concrete phase at early ages before service loads are applied. They are full-depth cracks and are typically spaced at 3 to 10 feet apart. They are the most frequently observed cracks in concrete bridge decks.

There are a number of problems associated with transverse cracking of bridge decks. Transverse cracks can reduce the service life of structures and increase maintenance costs. Structural problems include accelerated corrosion of reinforcing steel, deterioration of deck concrete, and possible damage to underlying components. Transverse deck cracking can also be detrimental to the overall bridge aesthetic. Transverse deck cracking also increases carbonation and chloride penetration leading to accelerated corrosion and deterioration.

Early age transverse deck cracking is a study of hardened concrete as compared to cracking of concrete while still in its plastic state. This research focuses on several mechanisms that contribute to cracking of hardened concrete: drying shrinkage, autogenous shrinkage, and thermal stresses.

Restrained drying shrinkage occurs due to the volume change induced by a loss of moisture in the cement paste. The concrete would not crack if this shrinkage could occur without the restraint from structural elements, the subgrade, or the moist interior of the concrete itself. This volume change coupled with restraint cause tensile stresses in the concrete that can lead to cracking. These tensile stresses are influenced by the amount and rate of shrinkage, the degree of restraint, the modulus of elasticity, and the amount of creep. The amount of drying shrinkage is a function of the amount and type of aggregate and the cement paste content of the concrete. Methods to reduce shrinkage cracking include using contraction joints, careful detailing of reinforcement, shrinkage-compensating admixtures, and reducing the sub slab restraint.

Autogenous shrinkage is a special type of drying shrinkage resulting from self-desiccation or internal drying, and typically occurs in concretes with water-cementitious (w/c) materials below 0.42. This type of shrinkage differs from typical drying shrinkage in that there is no loss of moisture from the bulk concrete. Autogenous shrinkage strain is typically about 40 to 100 microstrain, but has been measured as high as 2300 microstrain in concrete with a w/c ratio of 0.2. Autogenous shrinkage has been found to increase with increasing temperature, cement content, and cement fineness.

Temperature differences in a concrete structure result in volume changes causing tensile stresses. The dissipation of the heat of hydration of cement and changes in ambient temperature can create temperature differentials that cause tensile stresses in concrete structures. These tensile stresses are proportional to the temperature differential, the coefficient of thermal expansion, the

effective modulus of elasticity, and the degree of restraint. Methods of reducing thermal cracking include reducing maximum internal core temperature, delaying the onset of surface cooling, controlling the rate at which the concrete cools, and increasing the early age tensile strength of the concrete.

The ultimate goal for this research effort is to establish recommendations for new sealing materials that will withstand the cyclic movement of working deck cracks. Also, the project establishes some design provisions to assure improved live load deflection criteria for steel bridges, serviceability, good structural performance and economy in design and construction. This research develops a software program to specifically address the cracking in concrete decks supported by steel girders through the prediction of the generated temperature, thermal stress analysis, and finally tensile cracking predictions. The research team conducted extensive lab testing, experimental analysis, and field investigation to determine the feasibility and performance of repairing cracked bridge decks with crack sealers.

Based on conducted study, the following conclusions are drawn:

- For various crack widths, all of sealant materials used in field and laboratory investigation performed well with various crack widths. Slab with sealant material having 60% tensile elongation showed the best performance among slabs with other sealers. The research team recommends using sealant materials with large tensile elongation. The use of these materials was found to result in a better penetration and better overall performance.
- Performance of sealers complied with many of the requirements of the FDOT specifications 413. The research team recommends that the FDOT specifications should be modified to reflect elongation of a minimum of 10%
- The test results of all the sealers indicated discrepancies from the claimed values in the data sheets. It is worth noting that the tested material samples were prepared by the product suppliers and tested twice at the FDOT material labs.
- Sealing of slabs with induced cracks enhanced their performance to be comparable to that of the control slab (uncracked slab). Therefore, the use of sealant materials improved the performance of the slab.
- Analytical study predicted accurately the capacity and deflection of examined slabs.
- The primary cause of deck cracking is shrinkage alone or thermal alone.
- The FE analysis of bridges indicated that in most cases, no cracking occurred under truck loads. However, the combined effect of truck load and shrinkage or thermal effect causes transverse deck cracking.
- Deck cracks initiated due to shrinkage and/or temperature effects typically become working cracks, as external loads are ultimately applied to the deck. The cracks can widen due to these applied loads.

- Introducing continuity and increase of number of spans in bridges, may lead to larger likelihood of transverse cracking.
- There was a clear trend of increasing crack width with increasing deflection due to incrementally increasing truck loading.

TABLE OF CONTENTS

DISCLAIMER.....	ii
SI CONVERSION FACTORS	iii
ACKNOWLEDGMENTS	v
EXECUTIVE SUMMARY	vi
LIST OF FIGURES	xii
LIST OF TABLES	xix
1. INTRODUCTION.....	1
1.1. BACKGROUND	2
1.1.1. TYPES OF CRACKS.....	3
1.1.2. CRACK WIDTH.....	4
1.1.3. CRACK REPAIR.....	4
1.2. SEALERS	5
1.3. OBJECTIVES	5
1.4. RESEARCH APPROACH	6
2. LITERATURE REVIEW	7
2.1. REVIEW OF PREVIOUS RESEARCH.....	7
2.2. CAUSES OF AND FACTORS AFFECTING TRANSVERSE DECK CRACKING ..	15
2.2.1. SHRINKAGE AND CREEP EFFECTS.....	15
2.2.2. THERMAL CONTRACTION	18
2.2.3. ENVIRONMENTAL CONDITIONS.....	19
2.2.4. EFFECT OF COMPRESSIVE STRENGTH	19
2.2.5. LOAD EFFECT AND LIVE LOAD INDUCED TENSILE STRESS	20
2.2.6. MATERIAL AND MIX DESIGN FACTORS	21
2.2.7. CONSTRUCTION PRACTICE AND AMBIENT CONDITION FACTORS.....	23
2.2.8. STRUCTURAL DESIGN FACTORS.....	26
3. FIELD INVESTIGATION AND EXPERIMENTAL TESTING	31

3.1.	FLORIDA DISTRICTS' SURVEY	31
3.2.	INVESTIGATED BRIDGES.....	32
3.3.	SEALANT APPLICATION	39
3.4.	LAB TESTING AND RESULTS	39
3.4.1.	<i>CRACK SEALERS</i>	40
3.4.2.	<i>SEALER MATERIAL TESTING</i>	41
3.4.3.	<i>SLAB TESTS</i>	46
3.4.4.	<i>TESTING BEAM SAMPLES</i>	57
3.5.	FIELD MATERIAL TESTING AND RESULTS	58
4.	FINITE ELEMENT ANALYSIS OF SLAB	68
4.1.	FINITE ELEMENT MODEL OF SLABS	68
4.1.1.	<i>SPECIMEN DIMENSIONS</i>	68
4.1.2.	<i>MODELING</i>	69
4.1.3.	<i>ANALYTICAL STUDY</i>	70
4.1.4.	<i>LOADING</i>	71
4.1.5.	<i>RESULTS</i>	73
5.	FINITE ELEMENT ANALYSIS OF FULL BRIDGE	83
5.1.	SCOPE	83
5.2.	SELECTION OF BENCHMARK BRIDGE AND MODELING	83
5.3.	MODELLING.....	83
5.4.	ANALYTICAL STUDY.....	90
5.4.1.	<i>LOAD PATTERNS</i>	90
5.5.	RESULTS AND DISCUSSIONS	93
5.5.1.	<i>TRUCK LOAD APPLIED AS STATIC LOAD</i>	94
5.5.2.	<i>EFFECT OF TEMPERATURE</i>	94
5.5.3.	<i>EFFECT OF SECONDARY LOADS</i>	94
5.6.	DESIGN IMPLICATIONS - EFFECT OF LOADING ON DEFLECTION & CRACK WIDTH	127
5.7.	LOADING SCENARIO	128

6.	SPREADSHEET FOR EARLY AGE SHRINKAGE CRACK CALCULATIONS...	134
6.1.	INTRODUCTION	134
6.2.	NOTATIONS.....	134
6.3.	SPREADSHEET ORGANIZATION	136
6.4.	CONCRETE MIXTURE PROPORTIONING	137
6.4.1.	<i>WATER ADJUSTMENTS</i>	138
6.5.	TEMPERATURE PREDICTION	139
6.5.1.	<i>CONCRETE THERMAL PROPERTIES</i>	139
6.5.2.	<i>CONCRETE HEAT OF HYDRATION</i>	140
6.6.	BOUNDARY CONDITIONS.....	142
6.7.	THERMAL STRESS ANALYSIS.....	145
6.7.1.	<i>CONCRETE MECHANICAL PROPERTIES</i>	145
6.7.2.	<i>THERMAL EXPANSION</i>	148
6.7.3.	<i>SHRINKAGE</i>	148
6.7.4.	<i>CREEP</i>	148
6.8.	TENSILE CRACKING PREDICTION	149
6.8.1.	<i>DEGREES OF RESTRAINT</i>	149
6.8.2.	<i>TOTAL DEVELOPED STRESSES</i>	149
6.8.3.	<i>TIME OF FIRST DEVELOPED CRACK</i>	150
7.	CONCLUSIONS	152
8.	REFERENCES.....	154
9.	APPENDIX A: SEALERS MATERIAL APPLICATION	158
10.	APPENDIX B: INSPECTED BRIDGES	161
11.	APPENDIX C: SEALER TESTING.....	167
12.	APPENDIX D: SHRINKAGE STRAIN CALCULATIONS.....	171
12.1.	CALCULATIONS OF STRAIN DUE TO SHRINKAGE	171
13.	APPENDIX E: CREEP STRAINS CALCULATIONS.....	178
13.1.	CALCULATIONS OF CREEP COEFFICIENT	178

LIST OF FIGURES

Figure 1-1: Deck cracks in Ft. Lauderdale Bridge.....	2
Figure 1-2: Deck with pattern cracks.....	3
Figure 1-3: Deck with transverse linear cracks.....	4
Figure 2-1: Mechanism of transverse cracking.....	16
Figure 2-2: Mechanism of cracking.....	18
Figure 3-1: Blackwater River Bridge (Milton-Pensacola).....	32
Figure 3-2: Blackwater River Bridge crack pattern.....	33
Figure 3-3: Deck and soffit cracking.....	34
Figure 3-4: Core sampling showing crack development over the transverse reinforcement.....	34
Figure 3-5: Fort Lauderdale Bridge.....	35
Figure 3-6: Typical cross section.....	35
Figure 3-7: Deck and soffit cracking.....	36
Figure 3-8: Deck and soffit cracking map (general distribution of cracks).....	36
Figure 3-9: Internal investigation for corrosion shows detected corrosion spots.....	36
Figure 3-10: U.S. 1 Bridge.....	37
Figure 3-11: Deck cracking and supporting girders.....	37
Figure 3-12: JTB Bridge (Jacksonville).....	38
Figure 3-13: Deck crack pattern.....	38
Figure 3-14: Apply sealants to the cracked deck.....	40
Figure 3-15: Preparing the specimens for testing.....	42
Figure 3-16: Applying the sealant to concrete specimens before and testing.....	42
Figure 3-17: Sealent material testing.....	44
Figure 3-18: Construction of test slabs and placement of blades for crack width.....	46
Figure 3-19: Sealed slabs with LVDT's and dial gages and sealed cracks.....	46
Figure 3-20: Loading frame.....	46
Figure 3-21: Testing of control slab specimen and crack development.....	47
Figure 3-22: Slab Testing.....	48
Figure 3-23: Control slab load testing results.....	48

Figure 3-24: Slab 1-A load test.....	48
Figure 3-25: Slab 1-A LVDT results	49
Figure 3-26: Slab 1-A crack propagation and the double point load plate	49
Figure 3-27: Slab 1-A Test 2	50
Figure 3-28: Slab 1-A Test 2 LVDT results	50
Figure 3-29: Slab 1-B test 1	50
Figure 3-30: Slab 1-B test 2	50
Figure 3-31: Slab 1-B crack width results	51
Figure 3-32: Slab 2-A load test results	51
Figure 3-33: Slab 2-A crack width results	51
Figure 3-34: Slab 2-B load test results.....	52
Figure 3-35: Slab 2-B - crack width results	52
Figure 3-36: Slab 3-A load test results	52
Figure 3-37: Slab 3-A crack width results	53
Figure 3-38: Slab 3-B load test results.....	53
Figure 3-39: Slab 3-B crack width results	53
Figure 3-40: Slab 4-A load test results	54
Figure 3-41: Slab 4-A crack width results	54
Figure 3-42: Slab 4-B load test results.....	54
Figure 3-43: Slab 4-B crack width results	55
Figure 3-44: Concrete block schematic	57
Figure 3-45: Beam during split test procedure	57
Figure 3-46: Bridge testing locations.....	59
Figure 3-47: Mixing sealer materials	61
Figure 3-48: Cleaning the cracked deck	61
Figure 3-49: Applying sealers to the deck	61
Figure 3-50: Spreading the sealers.....	61
Figure 3-51: Sand spray	61
Figure 3-52: Sand spray by hand	61
Figure 4-1: Control slab dimensions.....	68
Figure 4-2: Slab with induced cracks.....	69

Figure 4-3: Control slab mesh detail.....	70
Figure 4-4: Slab with induced crack mesh detail.....	70
Figure 4-5: Control slab deflection comparison	74
Figure 4-6: Control slab cracking	74
Figure 4-7: ANSYS simulation cracking.....	74
Figure 4-8: Test setup	75
Figure 4-9: Induced crack deflection comparison	75
Figure 4-10: Numerical analysis deflection comparison	76
Figure 4-11: Cracks vs. deflection/length.....	77
Figure 4-12: Crack 1	77
Figure 4-13: Crack 2	77
Figure 4-14: Crack 3	78
Figure 4-15: Crack 4	78
Figure 4-16: Crack 5	78
Figure 4-17: Control 3-day temperature effect stress distribution.....	79
Figure 4-18: Control 7-day temperature effect stress distribution.....	79
Figure 4-19: Control 14-day temperature effect stress distribution.....	80
Figure 4-20: Control 28-day temperature effect stress distribution.....	80
Figure 4-21: Control 3-day shrinkage effect stress distribution	81
Figure 4-22: Control 7-day shrinkage effect stress distribution	81
Figure 4-23: Control 14-day shrinkage effect stress distribution	82
Figure 4-24: Control 28-day shrinkage effect stress distribution	82
Figure 5-1: Benchmark Bridge cross section.....	86
Figure 5-2: Four-node Shell element	87
Figure 5-3: Top and Bottom Flanges modelled using Shell Elements	87
Figure 5-4: Web modelled using Shell elements	88
Figure 5-5: Modelling of Steel I-girder	88
Figure 5-6: 8-node Solid element	89
Figure 5-7: Modelling of RC bridge decks	89
Figure 5-8: Typical 3-D bridge model	89
Figure 5-9: (a) Pin-roller condition and (b) Fixed-fixed condition.....	90

Figure 5-10: AASHTO HL-93 Truck load	93
Figure 5-11: Bridge Lane Definition for Truck loads.....	93
Figure 5-12: Stress contours due to (a) Truck load and (b) Tandem load	98
Figure 5-13: Development of deck stresses due to Truck load.....	99
Figure 5-14: Temperature effect	100
Figure 5-15: Effect of hydration (number of spans)	100
Figure 5-16: Effect of hydration (boundary conditions).....	101
Figure 5-17: Effect of hydration (deck thickness)	101
Figure 5-18: Deformed shape due to hydration	101
Figure 5-19: Effect of temperature (number of spans)	102
Figure 5-20: Effect of temperature and shrinkage (span length)	102
Figure 5-21: Effect of temperature (boundary conditions).....	103
Figure 5-22: Effect of temperature (deck thickness)	103
Figure 5-23: Effect of temperature (concrete compressive strength)	104
Figure 5-24: Stress contours due to 85°F increase of temperature	105
Figure 5-25: Stress contours due to 85°F decrease of temperature.....	105
Figure 5-26: Stress contours due to 85°F decrease of temperature and truck load.....	106
Figure 5-27: Shrinkage effect on bridge model single-span-N-4000-8.5-4.....	107
Figure 5-28: Shrinkage effect on bridge model two-span-N-4000-8.5-4	108
Figure 5-29: Shrinkage effect on bridge model three-span-N-4000-8.5-4	109
Figure 5-30: Shrinkage effect on bridge model two-span-half-4000-8.5-4 at 28 days.....	110
Figure 5-31: Shrinkage effect on bridge model three-span-N-4000-8.5-7 at 28 days	110
Figure 5-32: Shrinkage effect on bridge model two-span-N-4000-8.5-4-(F-F) at 28 days	111
Figure 5-33: Shrinkage effect on bridge model two-span-N-4000-7-4	112
Figure 5-34: Shrinkage effect on bridge model two-span-N-4000-10-4	113
Figure 5-35: Shrinkage effect on bridge model two-span-N-5000-8.5-4	114
Figure 5-36: Shrinkage effect on bridge model two-span-N-7000-8.5-4	114
Figure 5-37: Deformed shape due to shrinkage.....	114
Figure 5-38: Effect of shrinkage (number of spans).....	115
Figure 5-39: Effect of shrinkage (boundary conditions).....	115
Figure 5-40: Effect of shrinkage (deck thickness).....	116

Figure 5-41: Effect of shrinkage (concrete compressive strength).....	116
Figure 5-42: Longitudinal stress contours due to truck loads at 14 days for bridge model single-span-N-4000-8.5-4	117
Figure 5-43: Longitudinal stress contours due to truck loads at 14 days for bridge model two-span-N-4000-8.5-4	117
Figure 5-44: Longitudinal stress contours due to truck loads at 14 days for bridge model three-span-N-4000-8.5-4	117
Figure 5-45: Longitudinal stress contours due to truck loads at 28 days for bridge model two-span-half-4000-8.5-4.....	118
Figure 5-46: Longitudinal stress contours due to truck loads at 28 days for bridge model three-span-N-4000-8.5-7	118
Figure 5-47: Longitudinal stress contours due to truck loads at 14 days for bridge model two-span-N-4000-8.5-4-(F-F)	118
Figure 5-48: Longitudinal stress contours due to truck loads at 14 days for bridge model two-span-N-4000-10-4	118
Figure 5-49: Longitudinal stress contours due to truck loads at 28 days for bridge model two-span-N-5000-8.5-4.....	119
Figure 5-50: Longitudinal tensile stresses due to truck loads (number of spans).....	119
Figure 5-51: Bridge deflection (number of spans).....	120
Figure 5-52: Longitudinal tensile stresses due to truck loads at 14 days (number of spans)	120
Figure 5-53: Longitudinal tensile stresses due to truck loads at 28 days (number of spans)	121
Figure 5-54: Longitudinal tensile stresses due to truck loads (span length).....	121
Figure 5-55: Bridge deflection (span length).....	122
Figure 5-56: Longitudinal tensile stresses due to truck loads at 28 days (span length).....	122
Figure 5-57: Longitudinal tensile stresses due to truck loads (boundary conditions)	123
Figure 5-58: Bridge deflection (boundary conditions)	123
Figure 5-59: Longitudinal tensile stresses due to truck loads at 14 days (boundary conditions).....	124
Figure 5-60: Longitudinal tensile stresses due to truck loads at 28 days (boundary conditions).....	124
Figure 5-61: Longitudinal tensile stresses due to truck loads (deck thickness).....	125
Figure 5-62: Bridge deflection (deck thickness).....	125
Figure 5-63: Longitudinal tensile stresses due to truck loads at 14 days (deck thickness)	126

Figure 5-64: Longitudinal tensile stresses due to truck loads at 28 days (deck thickness)	126
Figure 5-65: Longitudinal tensile stresses due to truck loads (concrete compressive strength). 126	
Figure 5-66: Bridge deflection (concrete compressive strength).....	127
Figure 5-67: Longitudinal tensile stresses due to truck loads at 28 days (concrete compressive strength)	127
Figure 5-68: Bridge overview	128
Figure 5-69: Three-span bridge	128
Figure 5-70: Stress contours due to shrinkage	129
Figure 5-71: Bridge deformed shape due to shrinkage	129
Figure 5-72: Stress contours due to Truck load	130
Figure 5-73: Bridge deformed shape due to Truck load	130
Figure 5-74: Stress contours due to Shrinkage and Truck – Top of Slab	130
Figure 5-75: Stress contours due to shrinkage and Truck – bottom of slab	131
Figure 5-76: Stress contours due to 85°F increase of temperature	131
Figure 5-77: Bridge deformed shape due to 85°F increase of temperature	131
Figure 5-78: Stress contours due to 85°F decrease of temperature.....	132
Figure 5-79: Bridge deformed shape due to 85°F decrease of temperature	132
Figure 5-80: Stress contours due to 85°F decrease of temperature and Truck load	132
Figure 6-1: Visual example of deck and concrete user input tab.....	136
Figure 6-2: Visual example of structural and environmental user input tab.....	137
Figure 6-3: Concrete mixture portioning design tab of associated Excel spreadsheet	139
Figure 6-4: Example of “cement hydration” tab showing output graphs of hydration properties	142
Figure 6-5: Boundary conditions used for temperature analysis model in Excel	142
Figure 6-6: Depiction of temperature analysis tab, displaying output graphs of temperatures ..	144
Figure 6-7: Graphical depiction of example poisson’s ratio development from spreadsheet....	146
Figure 6-8: Example of stresses w/o relaxation calculated by spreadsheet	149
Figure 6-9: Screen cap of properties and strength tab displaying stresses and tensile strengths	150
Figure 6-10: Documented behavior of hardening concrete and crack identification.....	151
Figure 6-11: Spreadsheet calculated behavior of hardening concrete sample and crack identification	151

Figure 9-1: Sealer application.....	160
Figure10-1: Site inspection - Blackwater River Bridge (Pensacola).....	161
Figure 10-2: Sampling	162
Figure 10-3: Site inspection - Fort Lauderdale.....	163
Figure 10-4: Site inspection - U.S. 1 Bridge (Jacksonville).....	164
Figure 10-5: Concrete placement - U.S. 1 Bridge (Jacksonville).....	165
Figure 10-6: Crack locations - JTB Bridge (Jacksonville).....	166
Figure 11-1: Sealer tensile testing.....	168
Figure 11-2: Site core testing - site core testing	169
Figure 11-3: UNF – Lab testing and core testing	170
Figure 12-1: Bridge model single-span-N-4000-8.5-4, two-span-N-4000-8.5-4, three-span-N-4000-8.5-4.....	171
Figure 12-2: Bridge model two-span-half-4000-8.5-4.....	172
Figure 12-3: Bridge model two-span-N-4000-7-4.....	173
Figure 12-4: Bridge model two-span-N-4000-10-4.....	174
Figure 12-5: Bridge model two-span-N-5000-8.5-4.....	175
Figure 12-6: Bridge model two-span-N-7000-8.5-4.....	176
Figure 12-7: Another bridge model	177
Figure 13-1: PCA equations for creep	182

LIST OF TABLES

Table 3-1: FDOT Specifications 413 - Physical Properties of Methacrylate Resin	42
Table 3-2: Properties of Sealant Materials Investigated in the Study.....	43
Table 3-3: Characteristics of Selected Sealers	45
Table 3-4: Selected Sealer Tests	45
Table 3-5: Max Crack Width Obtained During the Load Test of All Slabs	56
Table 3-6: Tested Cores with Sealer Materials	58
Table 3-7: Selected Sealers Testing Results for Beams.....	58
Table 3-8: Results of Tests on the Cores from the Sealed Bridge Deck.....	60
Table 3-9: Sealant Test Results.....	62
Table 3-10: Tensile Testing of Deck Sealers	63
Table 3-11: Results for Control Slab Test	63
Table 3-12: Results for Slab Load Test and Crack Width Test (First Slab Set).....	64
Table 3-13: Results for Slab Load Test and Crack Width Test (Second Slab Set)	65
Table 3-14: Results for Slab Load Test and Crack Width Test (Third Slab Set)	66
Table 3-15: Results for Slab Load Test and Crack Width Test (Fourth Slab Set).....	67
Table 4-1: Concrete Material Properties	71
Table 5-1: Foremost Characteristics of Bridge Models	85
Table 5-2: Properties of Concrete	92
Table 5-3: Strain due to Shrinkage	92
Table 5-4: Loads and Loads Combinations Stresses, Moments, Deflections, and Crack Width	129
Table 5-5: Increase of Truck Load Effect with Shrinkage Load	133
Table 5-6: Increase of Truck Load Effect with Temperature Decrease Load	133
Table 6-1: Range of User Override Water Adjustment Factors	138
Table 6-2: Default Chemical Admixture Dosages Assumed If Selected But Not Specified.....	141
Table 6-3: Default CTE Values of Concrete Constituents Used If No Modifications are Selected by User	147

1. INTRODUCTION

Many studies investigated deck cracking (Babaei et al., 1997, 1987; French et al., 1999; Krauss and Rogalla, 1996; La Fraugh et al., 1989; PCA, 1970). Transverse cracks have always been a common problem in highway bridge decks. Transverse cracks in bridge decks develop during the hardened concrete phase at early ages before service loads are applied. They can be full-depth cracks and are typically spaced at 3 to 10 feet apart. They are the most frequently observed cracks in concrete bridge decks.

There are many problems associated with transverse cracking of bridge decks. Transverse cracks can reduce the service life of bridges and increase maintenance costs. Transverse deck cracking can lead to structural problems of deterioration of bridge decks, accelerated steel corrosion due to increased carbonation and chloride penetration, and possible damage to underlying components such as boxed steel girders. Transverse deck cracking can also be detrimental to the overall bridge aesthetic.

This review of early age transverse deck cracking addresses concrete cracks in hardened and plastic state. There are several mechanisms contributing to cracking of hardened concrete. Three of these mechanisms are drying shrinkage, autogenous shrinkage, and thermal stresses.

Restrained drying shrinkage occurs due to concrete volume change induced by loss of moisture in the cement paste. The concrete would not crack if this shrinkage could occur without the restraint from structural elements, or the moist interior of the concrete itself. The combined volume change and restraint may cause tensile stresses in the concrete. These stresses develop due to strains induced by early-age volume change and restraint as the concrete stiffness increases. These stresses may exceed the tensile strength of the concrete, thus resulting in deck cracking. These tensile stresses are influenced by the amount and rate of shrinkage, the degree of restraint, the concrete modulus of elasticity, and the amount of creep. The amount of drying shrinkage is a function of the amount and type of aggregate and the cement paste content of the concrete. Methods to reduce shrinkage cracking include using contraction joints, careful detailing of reinforcement, shrinkage-compensating admixtures, and reducing the sub slab restraint.

Autogenous shrinkage is a type of drying shrinkage resulting from self-desiccation or internal drying. It differs from typical drying shrinkage since there is no loss of moisture from the bulk concrete. It occurs in concretes with water-cementitious (w/c) materials below 0.42. Autogenous shrinkage strain is typically about 40 to 100 microstrain, but has been measured as high as 2300 microstrain in concrete with low w/c ratio of 0.2. Autogenous shrinkage could increase with increasing temperature, cement content, and cement fineness.

Temperature differences in a concrete structure result in volume changes causing tensile stresses. The dissipation of the heat of hydration of cement and changes in ambient temperature can create temperature differentials that cause tensile stresses in concrete structures. These tensile stresses are proportional to the temperature differential, the coefficient of thermal expansion, the effective modulus of elasticity, and the degree of restraint. There are several methods to reduce thermal cracking that include reducing maximum internal core temperature, delaying the onset of

surface cooling, controlling the rate at which the concrete cools, and increasing the early age tensile strength of the concrete.

1.1. BACKGROUND

Cracking and deterioration of concrete bridge decks is a major problem resulting in corrosion and consequently a reduction in service life by reducing the bridge load capacity and the riding surface quality. Cracks are classified as structural and nonstructural cracking. There are several types of deck deterioration: spalling, surface scaling, transverse cracking, and longitudinal cracking. Spalling is usually caused by reinforcement corrosion and freeze/thaw cycles of the concrete. Scaling is caused by improper finishing and curing of the concrete and the simultaneous effects of freeze/thaw cycles and deicing salts. The most common form of bridge deck deterioration is transverse cracking, which is attributed to plastic shrinkage of the concrete, drying shrinkage of the hardened concrete combined with deck restraint, settlement of the finished plastic concrete around the top mat of reinforcement, long-term flexure of continuous spans under service loads, and traffic induced repeated vibrations. Longitudinal cracks may result from poor mix design, temperature changes, live-load effects, or a reflection of shrinkage cracking. Multiple cracks appear on bridge decks (Figure 1-1) that are fatigued from heavy traffic due to pounding caused from the wheel impact on the expansion joints and surface irregularities.

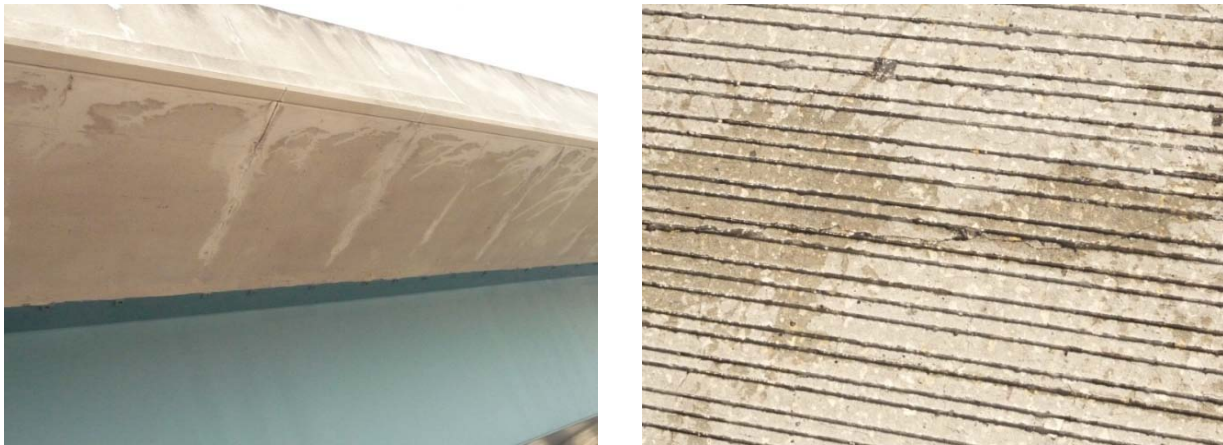


Figure 1-1: Deck cracks in Ft. Lauderdale Bridge

In some bridges with steel girders, especially with longer and shallower spans, live-load deflections may increase. Deflection magnitude allowed by the steel girders is greater than that of concrete girders. Bridges designed by the American Association of State Highway and Transportation Officials (AASHTO) Load and Resistance Factor Design (LRFD) specifications have an optional deflection limit or optional serviceability criteria. The AASHTO specifications limit live-load deflections to $L/800$ for ordinary bridges and $L/1000$ for bridges in urban areas that are subject to pedestrian use. This limit has not been a controlling factor in most past bridge designs. Previous research has shown that there is no clear justification for the current AASHTO live-load deflection limits, and that these limits were developed to control undesirable bridge vibration and to ensure user comfort. Due to the increased deflections with steel girders, the frequency of deck transverse cracks is greater than those on decks with concrete

girders. Therefore, the problem of deck cracking, especially with steel-girder bridges, might prompt more rational live-load serviceability criteria to be adopted. The bridge design specifications of the Ontario Highway Bridge Design Code (OHBDC) and Australian Code do not explicitly employ live-load deflection limits. Instead, vibration control is achieved through a relationship between the first flexural natural frequency of the bridge and live-load deflection. However, no specific equations are provided regarding the calculation of the first flexural natural frequency in the OHBDC. Australian Code uses a curve to control superstructure vibration of road bridges with footways.

It is also noted that early age bridge deck cracking may primarily result from shrinkage and thermal effects. Some literature also indicates that deck cracking may result from construction practices, specifically the sequence of concrete placement. Typically, concrete decks are placed in symmetrical locations across spans to avoid excessive moment imbalance during placement. If cracks are developed during construction, they typically become working cracks, as external loads are ultimately applied to the deck. This proposed research effort aims to help identify the primary sources of concrete deck cracking in Florida when steel girders are used, and further provides guidance with respect to the sealing of such cracks when they occur.

1.1.1. TYPES OF CRACKS

Pattern Cracks

Pattern cracks typically have a random orientation and are interconnected in the most severe situations. Examples of cracking that often appear as pattern cracking include checking, craze cracks, map cracking, pattern cracking, plastic cracking, shrinkage cracking and temperature cracking. Figure 1-2 shows a deck with pattern cracks.

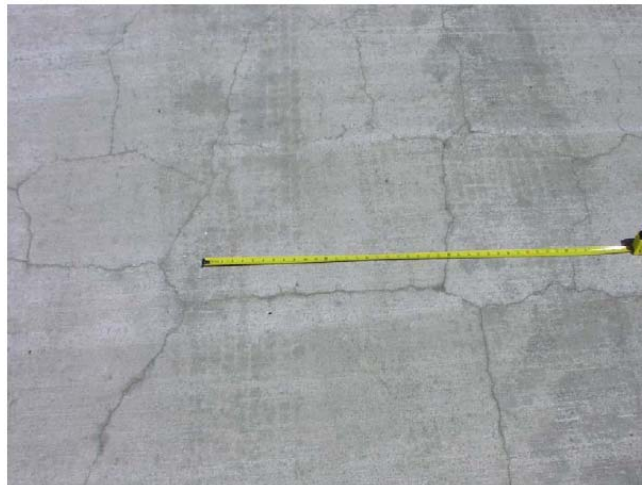


Figure 1-2: Deck with pattern cracks

Linear Cracks

Linear cracks typically have an orientation that is either perpendicular (transverse cracks) or parallel (longitudinal cracks) to the longitudinal axis of the bridge. Occasionally, the orientation of the cracks is diagonal. Examples of linear cracking include diagonal, longitudinal and transverse cracks. Figure 1-3 shows a deck with linear cracks.



Figure 1-3: Deck with transverse linear cracks

Linear cracks, particularly transverse cracks, can be caused by thermal contraction, drying shrinkage, and construction loads, continuous span deck construction sequence and live load-induced tensile stress. The width of the cracks may be a function of thermal contraction, drying shrinkage, crack spacing, concrete age, and loads applied to the deck.

1.1.2. CRACK WIDTH

The disposition of concrete cracks shall be in accordance with FDOT method section 400-21.

Measuring Crack Width

Crack width should be measured using a scaled magnifying device or transparent crack comparator placed on the surface of the concrete. The width should be measured and recorded prior to three hours past sunrise.

Determining the Total Width of Linear cracks in 100-ft of Bridge Deck

The total width of cracks in 100 ft. shall be measured by placing a 100-ft tape or string line approximately perpendicular to the direction of the cracks in the center of the cracked surface. The crack widths shall be measured next to the intersection of the cracks and the tape or string line. The crack width in 100 ft. shall be computed in accordance with FDOT method section 400-21 or as the sum of all the crack widths intersected by the tape or string line over a distance of 100 ft. The crack width in 100 ft. shall be computed for each bridge span. When the length or width of the cracked span is less than 100 ft., the crack width in 100 ft. shall be computed by multiplying the total crack width in the distance measured by 100 ft. and dividing the quantity by the measured distance.

1.1.3. CRACK REPAIR

Cracks That Cannot Be Filled

Deck cracks that are less than 0.0079 in. (0.2 mm) in width typically do not need to be filled if subjected to moderate or slight aggressive (MA or SA) environmental conditions (FDOT specifications- section 400-21.5.2 - Table2).

Cracks that are less than 0.0059 in. (0.15mm) in width at a drying age of six months (< 0.004 in. or < 0.1 mm in width at a drying age of one month) have no significant problematic effect on either the deck. Therefore, there is no need to be filled.

Cracks That Should Be Filled

Cracks that are greater than 0.0059 in. (0.15mm) in width at a drying age of six months (> 0.004 inch or >0.1mm in width at a drying age of one month) should be filled to prevent water and chlorides from penetrating the cracks.

1.2. SEALERS

The characteristics of crack sealing materials were identified to determine their suitability in relation to the crack deck movements. That identification required an extensive testing of different sealing materials to explore their physical and chemical behavior. High Molecular Weight Methacrylate (HMWM) is used for deck crack sealing. The methacrylate system must be a three-component system consisting of: a) methacrylate monomer, b) cumene hydroperoxide (CHP) initiator, and c) cobalt promoter. The sealing materials for deck cracks usually have a specific elongation factor, for example, 10%. Once applied and cured, the crack filling material will fail upon placing the loads on the deck and deflections occur, if greater than the specified 10% elongation occurs. If failure of the sealant occurs, this allows water and moisture to penetrate through the cracks. The following were accomplished in the study:

- Find concrete crack sealers that can be used in bridge decks to help protect and extend the life of the reinforced concrete bridge decks.
- Determine their structural property, and their ability to prevent chloride ion ingress.
- Determine their elongation, bond strength, tensile strength, and viscosity for penetration.

1.3. OBJECTIVES

The ultimate goals for this research effort are:

- To investigate the causes of transverse concrete deck cracking;
- To determine the feasibility and performance of repairing cracked bridge decks with crack sealers;
- To establish recommendations for new sealing materials that will withstand the cyclic movement of working deck cracks;
- To establish some design provisions to assure improved live load deflection criteria for Steel Bridges, serviceability and good structural performance in design and construction;

- To develop an Excel spreadsheet to specifically address the cracking in concrete decks supported by steel or concrete girders;
- To conduct extensive lab testing, field investigation, and analytical investigation to properly achieve the goals of the research.

1.4. RESEARCH APPROACH

The tasks conducted to achieve these objectives are:

- Literature review and evaluation of previous research recommendations.
- Literature review of current design and construction practices.
- Development of 3-D finite element models and parametric study.
- Development of simplified Excel spreadsheet to predict early age deck cracking.
- Field investigation of bridges, sealing, cores, and analysis of results.
- Laboratory testing of sealers used to repair slabs and beams. Cores are also taken and tested.

2. LITERATURE REVIEW

2.1. REVIEW OF PREVIOUS RESEARCH

An earlier study was conducted by the Portland Cement Association, the Bureau of Public Roads, and 10 state highway departments, and was released in 1970. The purpose of the study was to determine concrete bridge deck durability problems, causes of the types of deterioration, methods to improve durability, and methods to inhibit existing deterioration. In this study, transverse cracking was observed to be the most common type of cracking. Older decks and longer spans showed more transverse cracking, and continuous span bridges and steel girders appeared to exacerbate transverse cracking. As indicated by Frosch et al. (2002), the three important factors affecting deck cracking included:

1. Restraint from the girders on the early and long-term shrinkage of the deck;
2. Influence of top slab reinforcement as a source of internal restraint;
3. Internal restraint of the concrete due to differential drying shrinkage.

As indicated by Frosch et al. (2003), the researchers concluded that vibration characteristics were not a factor in the deterioration of bridge decks. Restraint to thermal variations was also believed to contribute to cracking. Recommendations by the Portland Cement Association included:

1. Limit slump to 2 in. \pm 0.5 in.
2. Maintain the water/cement ratio less than 0.48.
3. Use large sized aggregates.
4. Reduce bleeding by having a smooth grading curve and test mixes for bleeding.
5. Select aggregates with low shrinkage.
6. Avoid placement temperatures over 80° F and consider nighttime deck placement.
7. Provide 1.5 in. minimum concrete cover for top mat reinforcement.
8. Consider further research on the amount of temperature and shrinkage reinforcement.

Frosch et al. reported that, in a study conducted for the Pennsylvania Department of Transportation, Cady et al. surveyed four-year old bridge decks in Pennsylvania to investigate the extent and causes of concrete bridge deck deterioration. The researchers found transverse cracks in 60% of all spans and 71% of all bridges. They concluded that:

1. Decks constructed with stay-in-place forms exhibited much less cracking than those built with removable forms.
2. The transverse crack intensity (total length of cracks per 100 ft²) increased as the span length increased.
3. Superstructure type had a significant effect on the amount of cracking observed. Steel bridges had more cracking than prestressed concrete bridges
4. Cracking is more prevalent on continuous spans than simple spans.
5. Construction practices were the single most influential variable in the extent of cracking observed in bridge decks
6. The use of retarder in the concrete mix is not an important factor.

Assessment of bridges in Pennsylvania was conducted by Purvis et al. through surveys to determine the causes of transverse cracking. These surveys included crack mapping, crack width measurements, rebar location and depth surveys, concrete coring, and construction records. The researchers found that the transverse cracks intersected coarse aggregate particles. This indicated that transverse cracking occurred in hardened concrete rather than plastic concrete. Drying and thermal shrinkage could have caused the transverse cracking. Recommendations and/or conclusions from this study included that temperature difference between deck and girder should be limited to 22° F for at least 24 hours.

A study was also conducted by Schmitt and Darwin on the effects of different variables on bridge deck cracking. The variables included material properties, site conditions, construction procedures, design specifications, and traffic and age. The material properties considered included admixtures, slump, percent volume of water and cement, water content, cement content, water-cement ratio, air content, and compressive strength. As indicated by Frosch et al. (2002), the conclusions of Schmitt and Darwin regarding material properties were:

1. Deck cracking increased with increasing slump, water content, cement content, and water-cement ratio.
2. Cracking increased as the water and cement volumes grew above 27.5%.
3. Cracking increased as compressive strength increased corresponding to increasing cement content.
4. Cracking decreased as air content increased, particularly above 6%.
5. Use of silica fume may significantly increase cracking if precautions are not taken to prevent plastic cracking.
6. No correlation between deck cracking and the type of admixture was determined.

As indicated by Frosch et al. (2003), the site condition factors considered in the study of Schmitt and Darwin (1995) were average air temperature, low air temperature, high air temperature, daily temperature range, relative humidity, average wind velocity, and evaporation. Conclusions regarding site conditions included:

1. There were no obvious correlations concerning cracking and average or low air temperature, relative humidity, average wind velocity, or evaporation rate.
2. Cracking increased significantly as the maximum daily air temperature increased.
3. Cracking increased when the daily temperature range increased.

Regarding the construction procedure factors considered in the study, there were no observed relationships between length of placement or type of curing materials and cracking. No correlation between cracking and placing sequence could be determined due to lack of information.

As indicated by Frosch et al. (2002), the design factors considered in the study of Schmitt and Darwin (1995) included structure type, deck type, deck thickness, top cover, transverse reinforcing bar size, transverse reinforcing bar spacing, girder end conditions, span length, bridge length, span type, and skew. Conclusions from the study were:

1. Girder end condition appeared to affect deck cracking with fixed girders having more cracks than pinned girders.
2. Cracking increased as transverse reinforcement spacing increased.
3. Cracking increased as bar size increased.
4. There were no noticeable correlations concerning cracking and top cover, span length, span type, or skew.

Regarding traffic and age, the researchers found that cracking increased with traffic volume and that bridges constructed prior to 1988 exhibited less cracking than bridges constructed after 1988, as indicated by Frosch et al. (2003). The increase in cracking in newer bridges was attributed to changes in construction, material properties, and design specifications.

Krauss and Rogalla (1996) conducted a comprehensive study to evaluate early age transverse cracking. To evaluate the early age transverse cracking, the researchers surveyed 52 transportation agencies in the United States and Canada. Over 100,000 bridges were found to have developed early transverse cracks. The researchers also performed analytical studies using both theoretical and finite element analysis to evaluate the influence of several different parameters on transverse cracking. The researchers determined that span type, concrete strength, and girder type were the most important design factors influencing transverse cracking. Material properties such as cement content, cement composition, early-age elastic modulus, creep, aggregate type, heat of hydration, and drying shrinkage also influenced deck cracking. Conclusions and/or recommendations included:

1. Recommended clear cover is between 1.5 and 3 inch.
2. Recommended minimum thickness of the deck is between 8 and 9 inch.
3. Use the largest possible size aggregate and use low shrinkage aggregate.
4. Type II cement reduces cracking in bridge decks.
5. Increasing cement content increases the amount of deck cracking due to higher drying shrinkage, higher temperature rise during hydration, and higher early modulus of elasticity.
6. Increase in deck cracking since the 1970s may coincide with AASHTO's 1973 increase of minimum strength from 3000 psi to 4500 psi; consequently, use of concrete with low early strength is recommended.
7. There is not relationship between slump and cracking tendency.
8. Use of retarders may reduce the rate of early temperature rise and early gain of modulus of elasticity.
9. Silica fume may significantly increase cracking if precautions are not taken to prevent plastic cracking.
10. Concrete placement temperature should be no greater than 80°F and should be 10-20°F cooler than ambient temperature.
11. Special consideration should be taken when evaporation rates are more than 0.2 lb/ft²/hr for normal concrete and 0.1 lb/ft²/hr for low w/c ratio concrete.
12. The following procedure is recommended for curing:
 - a. Use of fog nozzle water spray in hot weather to cool concrete and to cool the steel and forms immediately ahead of placement—ponding of water on the forms or plastic concrete should not be allowed.
 - b. Use of wind breaks and enclosures when the evaporation rates exceed 0.2 lb/ft²/hr for normal concrete and 0.1 lb/ft²/hr for low w/c ratio concretes susceptible to plastic cracking.
 - c. Application of water mist or monomolecular film immediately after strike-off or early finishing.
 - d. Application of white-pigmented curing compound as soon as bleed water diminishes.

- e. Application of pre-wetted burlap as soon as concrete resist indentation—the burlap must be kept wet by continuous sprinkling or by covering the burlap with plastic sheeting and periodic sprinkling.
 - f. Continuation of wet curing for a minimum of 7 days, preferably, 14 days—curing should be extended in cold weather until the concrete has gained adequate strength.
13. Early finishing reduces cracking.
 14. SIP forms sometimes increase deck cracking.
 15. Decks on steel girders tend to crack more when compared to decks on concrete girders and cracking is more prevalent on continuous spans than on simple spans.
 16. Girder restraint and studs cause significant cracking.
 17. Increasing deck thickness reduces deck cracking. Increasing the amount of longitudinal reinforcement is recommended (#4 bars at 6 in. spacing).
 18. Reducing deck stiffness reduces deck cracking.

Eppers et al. (1998) conducted a field investigation of 72 bridge decks in Minnesota. The researchers determined that design factors most related to transverse cracking were longitudinal restraint, deck thickness, and top transverse bar size. The researchers also determined that the material factors affecting transverse deck cracking were cement content, aggregate type and quantity, and air content. As indicated by Frosch et al. (2003), recommendations from the study of Eppers et al. (1998) included:

1. Decks constructed on simply supported prestressed girder bridges were in good condition relative to those on continuous steel girder bridges.
2. Diaphragms caused stress concentrations and staggered diaphragms with close spacing resulted in more closely spaced, more narrow cracks.
3. Restraint should be reduced using bridge expansion joints, simply supported spans, increasing girder spacing, and providing fewer shear connectors.
4. Use #5 bars for top transverse reinforcement in concrete bridge decks on steel girders.
5. Reduce the paste volume of the mix designs used.
6. Use lower water-cement ratios
7. Select minimum air content between 5.5% and 6.0%.
8. Maximize coarse and fine aggregate content.

9. Improve curing in the field.

Le, French, and Hajjar (1998) performed a parametric study to also study the deck cracking. The researchers considered bridges with steel and prestressed concrete girders. The researchers investigated several variables for steel girder bridges that included: end conditions, girder stiffness, locations of cross frames, girder splices, supplemental reinforcing bars, shrinkage properties, concrete modulus of elasticity, and temperature differential due to heat of hydration. Frosch et al. listed the following conclusions from the study of Le, French, and Hajjar (1998):

1. Steel girder bridges exhibited cracking in both the positive and negative moment regions of the bridge deck.
2. The main cause of cracking was due to differential shrinkage between the deck and the girders.
3. Ultimate shrinkage did not significantly affect the tensile stresses in the deck because the creep of the concrete mitigated the stress.
4. End conditions significantly affected the amount of transverse cracking. Cracking was most extensive in the fixed-fixed case and not observed in the simply supported case.
5. Girder stiffness, cross frames, and splices dictated crack locations.
6. Longitudinal restraint should be reduced by using expansion joints on continuous girders, increasing girder spacing, and minimizing shear connector restraint by using fewer rows of smaller-diameter studs.

In a research study sponsored by the Indiana Department of Transportation, Frosch et al. (2003) conducted a field study and constructed laboratory specimens to investigate the behavior of transverse cracks. Using these specimens, the researchers could evaluate the effects of differing bridge deck designs on the control of overall shrinkage and the contribution of Stay-in-Place (SIP) steel forms to the formation of transverse cracking. The researchers concluded from the field investigation and laboratory study that:

1. Bridges cast monolithically with a concrete superstructure had the fewest cracks.
2. The restraint of the concrete deck on steel superstructure bridges, through the use of composite action and/or stay-in-place steel forms, induced more transverse cracking than those not incorporating composite action and/or stay-in-place steel forms.
3. Transverse cracks were observed on more bridges with a steel girder superstructure than bridges with a concrete superstructure than bridges with a concrete superstructure. Precast, prestressed concrete superstructure bridges likely behave similar to the monolithic concrete bridges and shrink with the deck instead of restraining the shrinkage when the concrete girders and deck are close in age.

4. Transverse cracking was not influenced by live loads or vibrations caused by live loads.
5. SIP deck forms increased the amount of restraint in specimens.
6. The stiffness of SIP deck forms contribute to reducing overall shrinkage. The sealing effect of SIP forms tended to reduce the total amount of shrinkage, but also increased curling in the specimens.
7. SIP forms produce curling that can exacerbate cracking on the top surface.
8. Decks constructed with removable forms may experience larger total shrinkage than those constructed with SIP forms.
9. As steel reinforcement spacing increased, crack widths increased.
10. Additional reinforcement should be provided above current practice to control crack widths in concrete decks.
11. As epoxy coating thickness of rebar increased, average and maximum crack widths increased.
12. Less shrinkage should be achieved through mix designs.
13. Concrete strength should be minimized.

In a research study sponsored by the Colorado Department of Transportation (CDOT), Xi et al. (2003) reviewed CDOT practices and compared them with the practices of other DOT's for the construction of bridges. A database analysis was conducted on field inspection results in 72 bridges built by CDOT between 1993 and 2002. The database analysis was confirmed with field inspections conducted on nine newly constructed bridge decks that show excessive cracking. Recommendations made by the researchers included:

1. Use Type I or Type II Portland cement for bridge deck construction.
2. Limit cement content to about 470 lb/yd³ or lower if possible.
3. Use a water/cement ratio of around 0.40.
4. Limit silica fume to 5% by weight of cement to reduce permeability.
5. Use large sized and well-graded aggregate.
6. Use smaller bars for transverse reinforcement.
7. Concrete girders should be preferred for equivalent coefficients of thermal expansion.
8. Consider a minimum deck thickness of 8.5”.

9. Do not cast decks when ambient temperature is below 45° F or over 80° F.
10. Avoid concrete placement when the evaporation rate is above 0.20 lb/ft²/hr for normal concrete and 0.10 lb/ft²/hr for low water/cement ratios.

In a research study sponsored by the New Jersey Department of Transportation, Xi et al. (2003) surveyed 24 bridges in New Jersey built after 1994. Based on the surveys and design and construction documents a database was developed. Statistical analysis of the database was conducted to identify major factors causing transverse deck cracking. Some factors were also investigated using finite element analysis. As indicated by Saadeghvaziri and Hadidi (2002), recommendations made by the researchers included:

1. Specify an upper limit on concrete strength and use low early strength concrete when possible.
2. Minimize the ratio of girder/deck stiffness through changes in deck thickness, girder spacing, and girder moment of inertia.
3. Increase the deflection limits to employ a more flexible superstructure.
4. Uniform reinforcement meshes on top and bottom are recommended to control cracking. Increasing the volume of reinforcement above code requirement does not have an effect on cracking.
5. Reduce cement content to 650-660 lb/yd³ and consider using fly ash.
6. Use Type II cement for bridge deck construction.
7. Limit the water/cement ratio to 0.4-0.45.
8. Maximize the aggregate content and use the largest possible aggregate size.
9. Employ the following pouring sequence:
 - a. Pour complete deck at one time whenever feasible within the limitation of the maximum placement length based on drying shrinkage consideration.
 - b. If multiple placements must be made and the bridge is composed of simple spans, then place each span in one placement.
 - c. If bridge is simple span but cannot be placed in a single placement, divide the deck longitudinally and make two placements.
 - d. If the bridge is simple span and single placement cannot be made over the full span length, then place the center of span segment first and make this placement as large as possible.

- e. If multiple placements must be made and the bridge is continuous span, then place concrete in the center of positive moment region first and observe a 72 hour delay between placements.
 - f. When deck construction joints are created, require priming existing interfaced surfaces with a primer/bonding agent prior to placement of new concrete.
10. Wet cure for at least 7 days; consider 14 day wet cure when possible.

2.2. CAUSES OF AND FACTORS AFFECTING TRANSVERSE DECK CRACKING

When a restraint mass of concrete tends to change volume, concrete cracks occur, as shown in Figure 2-1. Volume change in concrete is affected by the proportions and properties of concrete constituents. Also, environmental conditions such as ambient temperature changes and humidity could affect the concrete cracking. Restraint could be due to composite action of deck and girder, and depends on bridge design characteristics. As indicated by Saadeghvaziri and Hadidi (2002), some researchers indicated that construction techniques could also contribute to volume change and/or to degree of restraint of concrete mass.

Curtis and White (2007) identified some of the most influential factors on bridge deck cracking. The factors included strength of concrete, thickness of concrete cover above reinforcing steel, and temperature at which the concrete was poured. It was also noted that the main causes of tensile stresses in concrete bridge decks are thermal effects from heat of hydration during curing and daily temperature cycling, live load stresses, such as those from the flow of traffic along the bridge, and shrinkage of concrete. In a finite element study, Hadidi and Saadeghvaziri (2005) performed linear and non-linear analyses to show the effect of design factors on transverse cracking in bridges. Through an investigation of crack patterns and stress histories, it was concluded that design factors, such as structural stiffness, can have a significant impact on transverse cracking. The researchers identified a variety of recommendations to reduce transverse bridge deck cracking during the design phase. For example, steel reinforcement should be placed in uniform meshes on the top and bottom of the deck. Shrinkage should be accounted for during the design process. Another recommendation suggested that an accurate crack prediction model should include a shrinkage model that takes into account a variety of concrete and structural design properties: strength of concrete, thickness of concrete cover above reinforcing steel, structural stiffness, and live load stresses.

2.2.1. SHRINKAGE AND CREEP EFFECTS

Many studies indicated that shrinkage and creep stresses are considered to be among the leading causes of transverse bridge deck cracking. Restrained shrinkage of concrete bridge decks is considered to be the main cause of transverse deck cracking (Frosch 2003). Bridge deck cracking occurs when restrained volumetric changes associated with moisture and temperature changes take place. Volumetric changes mainly result from autogenous shrinkage, drying shrinkage, plastic shrinkage, thermal shrinkage, and creep. This concrete volume change depends primarily on the properties of concrete and mix design, design details, construction practices, and

environmental conditions. Researchers concluded that concrete properties are the most important factors affecting transverse deck cracking since they control the shrinkage and thermal strains that cause stresses.

Drying shrinkage is a change in concrete volume due the change in water content. That occurs during the time after exposure to atmosphere. Autogenous shrinkage is the change in concrete volume without change in its water content and usually occurs in very low w/c ratios. Plastic shrinkage is caused by excessive evaporation of surface water. Thermal shrinkage is caused by cooling of concrete after initial hydration. However, creep strains counteract the effect of shrinkage. Many studies indicated that drying shrinkage and thermal shrinkage are considered to be the major cause of concrete deck cracking (Babaei et al., 1997, 1987; French et al., 1999; Krauss and Rogalla, 1996; La Fraugh et al., 1989; PCA, 1970). As indicated by Saadeghvaziri and Hadidi, some studies reported correlation between deck cracking, drying shrinkage (Babaei and Hawkins, 1987, La Fraugh, 1985, PCA, 1970) and higher placement temperatures (PCA, 1970).

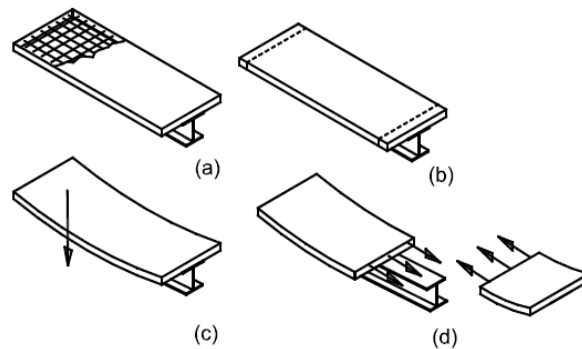


Figure 2-1: Mechanism of transverse cracking. (a) Concrete is poured. (b) Concrete shrinks, (c) Due to restraint from girder, concrete shrinkage produces downward deflection. (d) Tensile stress is developed in deck, which causes transverse cracks - Courtesy of New Jersey D.O.T. (2002)

Babaei and Purvis (1994) showed higher cracking tendency for mixes with higher thermal and drying shrinkage values. Also, according to Krauss and Rogalla (1996) drying shrinkage and temperature changes through the section are responsible for deck cracking. Frosch et al. (2002) showed through field instrumentation and test of constructed deck in laboratory that drying shrinkage is the most important cause of transverse cracking.

Types of Shrinkage

Generally there are three different kinds of shrinkage for concrete: plastic shrinkage, autogenous shrinkage and drying shrinkage. Plastic shrinkage and autogenous shrinkage happen at an early age of the concrete, while drying shrinkage takes place over a long period of time.

Plastic Shrinkage

Plastic shrinkage is caused by a rapid loss of water on the concrete surface before the concrete hardens. This loss of water can be caused by many reasons, such as evaporation or suction by a dry sub-base. In fresh concrete, the concrete materials have not formed into a solid matrix and are still

surrounded by water. When too much water rapidly evaporates, the water that remains in the concrete will not be sufficient, and voids occur within concrete, leading to the occurrence of plastic shrinkage cracking.

Environmental conditions, such as wind and temperature, have great influence on plastic shrinkage cracking of concrete. To reduce plastic shrinkage, the rate of water evaporation should be reduced. Therefore, when there are high wind speeds, concrete casting should be avoided, or wind breaks and fogging should be used to prevent water loss. Because water evaporation only happens at the surface, plastic shrinkage cracking only occurs at the surface, and it is usually small.

Autogenous Shrinkage

Autogenous shrinkage happens when the concrete begins to hydrate. It is caused by the self-desiccation of concrete during the hydration process due to lack of water in concrete that has a low water-cement ratio. Autogenous shrinkage is also usually small. However, for concrete using high-range-water-reducing admixture (HRWRA) and fine materials, such as silica fume, it may become an important factor leading to shrinkage cracking. To prevent autogenous shrinkage, low water-cement ratios are not preferred because there is not enough water for the cement to hydrate. When it is necessary to use a low water-cement ratio, other methods should be used to compensate for the lack of water in the concrete mix design.

Drying Shrinkage

Indicated by the pattern of early-age transverse cracking, drying shrinkage is associated with bridge decking shrinkage cracking (Krauss and Rogalla 1996). It is caused by loss of water in the hardened concrete. Drying shrinkage can be explained by three main mechanisms: capillary stress, disjoining pressure and surface tension, each of which plays an important role within a certain range of relative humidity. Normally bridge decks will experience relative humidity from 45% to 90%, which is when the capillary stress mechanism plays the important role.

Many factors can directly affect the drying shrinkage of concrete, such as paste volume, water-cement ratio, aggregates type, environment conditions, and curing methods. Of all these factors, paste volume is the most important one. Drying shrinkage will be greatly reduced if the paste volume is reduced (Xi et al. 2003, Tritsh et al. 2005, Darwin et al. 2007, Delatte et al. 2007).

Effect of Shrinkage on Deck Crack

Restraint of deck by girder against deck volume change provides the cracking condition. The composite action between the deck and the girders provides restraining to the deck. It has been observed that reducing the ratio of cross sectional area of girder to deck reduces risk of cracking. When concrete shrinks, the external restraint from the girder, as well as the internal restraints from the reinforcement and aggregates, produces tensile stresses in the longitudinal direction of the deck. When these stresses reach the tensile strength of concrete which is low at early ages, transverse cracks are developed in the deck starting sometimes from the bottom and extending to the top surface. In continuous beams or in beams with fixed-end restraint, the combined tensile stress from loads and shrinkage stresses could exceed the tensile strength of the bridge deck, thus initiating the deck cracking.

D'Ambrosia et al. (2004) studied early age creep and shrinkage of a concrete bridge under restrained conditions and experiencing a constant applied load for the first week after it was cast.

A uniaxial test procedure was employed to measure the shrinkage stress and strain, while the tensile creep and resultant stress relaxation were determined using superposition analysis. Modifications were made to an existing prediction model to account for the early age of the concrete at the time the measurements were taken in this study. The validity of the early age model was assessed by comparison against current creep and shrinkage models. The early age model was shown by these comparisons to be accurate. Goel et al. (2006) found the GL2000 model to exhibit the greatest accuracy in predicting creep and shrinkage strains in prestressed concrete. This model and several others, including the ACI-209R-82 model, B3 model, and CEB-FIP model code 90, were compared to experimental results. All models are derived from ACI-209 R-82 but modified by each agency/researcher to suit their needs, CEB/FIP is the European Concrete Committee/International Federation of Prestressing, B-3 Model is by Bazant((1995).

Creep

While early-age cracking in bridge deck is mainly due to concrete shrinkage, creep helps to relax shrinkage. The study by Altoubat et al. (2001) found that the tensile creep relaxes the shrinkage stress by 50% and doubles the failure strain capacity. It is generally believed that creep will help reduce shrinkage of concrete, as shown in Figure 2-2.

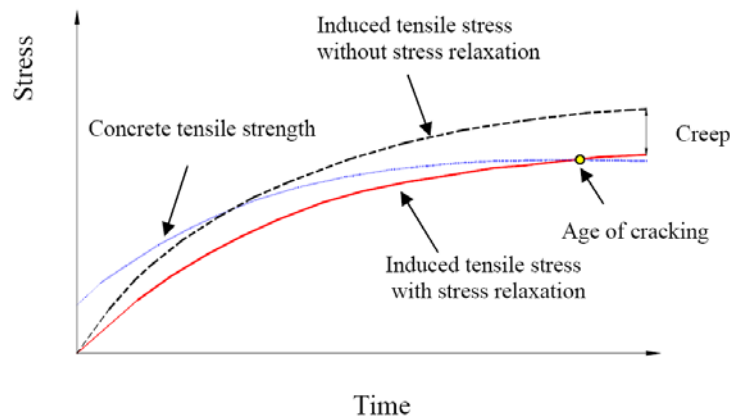


Figure 2-2: Mechanism of cracking (from Neville 1996)

2.2.2. THERMAL CONTRACTION

Thermal effects from heat of hydration during curing and daily temperature cycling affects deck stresses and cracking tendency. Also, temperature at which the concrete was poured has an effect. The delivered concrete temperature is typically higher than the air temperature and the temperature of the bridge girders and form work. The temperature of concrete is affected by the heat of hydration from the curing process and from changes in environmental conditions due to daily and seasonal cycling of temperatures. The higher concrete temperature has the potential to cause cracks after the concrete cools to an equilibrium temperature with the air, bridge girders and form work. The cracks may have a width and spacing that is a function of the temperature difference and the coefficient of thermal expansion of the concrete. For example, if the delivered concrete temperature is approximately 10 degree F higher than the air, girder and form work temperatures during the concrete placement, the theoretical thermal contraction is 0.084 inch per

100 ft of deck length, assuming a thermal coefficient of 7×10^{-6} in/in/degree F. If the temperature difference is 40 degrees F the theoretical thermal contraction is 0.336 in. per 100 ft of deck length. To calculate the theoretical crack width, first determine the difference in temperature between the concrete and the average of the temperatures of the air and the top flanges of the girders and the formwork. Multiply the temperature difference by 8.4×10^{-3} to get the theoretical crack width as inches per 100 ft. of deck length. Literature indicates that computer models that can simulate the temperature variations taking place during the curing process of concrete have been developed. One model is accurate within 2°C. It was created based on fundamental heat and mass transfer principles and also has the capability to track the water mole fraction and unreacted cement fraction for the first 72 hours of curing. Considered in this model are various environmental factors, such as wind speeds and the changes in solar radiation during different hours of the day and different seasons in the year. Also an empirical model for concrete curing that considers thermal and moisture behaviors during the first several days after concrete placement has been developed. The investigation performed looks at the curing process from the standpoint of energy balances and heat transfer between the atmosphere and the concrete surface. No previous or additional work had been done to understand these energy balances.

2.2.3. ENVIRONMENTAL CONDITIONS

Previous research indicated that the exposure to environmental conditions, e.g. ambient humidity and temperature, has a major effect on transverse cracks. For structures exposed to harsh environments, such as bridge decks exposed to deicing salts, ACI 350 recommends limiting crack width in the range of 0.0079 inch to 0.010 inch (0.20 mm to 0.25 mm). If the HP concrete mix and current construction practices are maintained, then longitudinal temperature and shrinkage steel needs to be increased sufficiently to limit bridge deck crack size to 0.010 inch. Minimum temperature and shrinkage steel (#5 at 18 inch) required by AASHTO 17th Edition Bridge Design Manual has been sufficient to limit crack sizes for conventional concrete but is not sufficient to limit crack widths for high strength concrete. It has been shown that for high strength concrete, with current construction practices, if the maximum crack size at the negative moment regions is to be limited to 0.010 inch, then for a typical bridge deck #5 epoxy coated bars at 4.14 inch maximum spacing are required for the top layer of temperature and for shrinkage reinforcement at the negative moment regions (Minnetyan and Assamany 2004).

2.2.4. EFFECT OF COMPRESSIVE STRENGTH

Transverse cracks in high performance concrete decks are characteristically more distinct and wider than those in conventional concrete bridge decks. High performance (HP) concrete of greater than 6,000 psi has higher strength and significantly lower creep properties. It has been shown that the higher compressive strength f_c' of concrete cannot be the main reason affecting the crack size. This is reasonable since compressive strength increases stiffness as well as bond strength and tensile strength by the same proportions. The effect of higher stiffness will increase crack width. However, higher bond/tensile strengths will decrease crack width. Therefore, the net effects of higher f_c' cannot account for the wider cracks on high performance concrete decks. Yet, several researchers indicated the great increase of cracks for higher strength concrete of 6,500 psi versus typical 4000 psi concrete.

Compressive strength and elastic modulus increase with increasing amounts of silica fume included in the concrete mix. Presence of silica fume increases shrinkage by approximately 20 to 25 percent, especially if HP concrete is allowed to experience early age drying shrinkage. Creep is reduced by more than 60 percent due to the presence of 10 percent silica fume (Wiegrink et al. 1996). Shrinkage of concrete produces tensile stresses that generate cracks. Conventional concrete is able to creep, therefore the tensile stresses caused by shrinkage are relaxed and crack size is limited. HP concrete with greatly reduced creep is unable to dissipate tensile stresses, therefore, it cracks. The combination of increase in shrinkage due to early age mishandling and reduced creep properties of HP concretes containing silica fume and super plasticizers is detrimental and produces large cracks. From the shrinkage and creep data, one can deduce that HP concretes containing silica fumes are likely to develop crack widths that are at least twice those developed in conventional concrete decks without significant amounts of silica fume (Minnetyan and Assamany 2004). Yazdani et al. (2007) investigated a means by which HP concrete can be cured more rapidly without an increase in shrinkage cracks. Silica fume, a common additive in HP concrete mixes, causes accelerated curing of the concrete. This causes an elevation in heat of hydration and increased water demand. Steam curing has been tested in an effort to offset the increased shrinkage caused by accelerated curing. A bridge steam cured for 12 hours was found to have no cracking at one year.

A case study was performed on a bridge in Tennessee, half of which was built with high strength concrete and the other half built with normal strength concrete. Its construction included instruments for monitoring the strains and temperature variations in its beams, deck, and diaphragms. The study found that the high strength concrete experienced differential shrinkage to the standard concrete in the bridge deck. Rapidly developed creep and shrinkage strains were observed, as well as rapidly developed time-dependent cambers. Recommendations were made for using a fogging system during placement of high strength concrete in order to reduce moisture loss due to evaporation, leading to a decrease in shrinkage.

2.2.5. LOAD EFFECT AND LIVE LOAD INDUCED TENSILE STRESS

Dead load and live load stresses have a significant impact on transverse cracking of bridge decks. Previous work has been done to understand the effects of repeated loading on transverse deck cracking. A fracture mechanics approach was used to develop a design equation capable of predicting maximum crack width and crack spacing in precast reinforced concrete slabs. It was found that steel stress ratio, reinforcement ratio, and repeated loading do affect the maximum crack width in concrete. A finite element model capable of predicting, with good accuracy, the load level at which cracking will initiate in a composite steel girder bridge, the ultimate load capacity that will be experienced, and the overall crack pattern has been developed. Oh and Kim adjusted a previous crack width prediction model to account for the stress-slip behavior between concrete and its reinforcing steel. This model focuses on repeated loading of reinforced concrete beams. The software developed in this research quantifies all temperature, shrinkage, and load effects that produce cracking.

In continuous span bridges designed using AASHTO design requirements, concrete deck can be in tension under live loading. The location and frequency of the majority of the transverse deck

cracks suggest that most of the cracks were initiated by the addition of live load induced tensile stress to the already existing stress in the concrete caused by thermal contraction, drying shrinkage, and deck construction sequence.

Saadeghvaziri and Hadidi indicated that some researchers (Krauss and Rogalla, 1996, Stewart and Gunderson, 1969, Cady et al., 1971) reported no relationship between daily traffic of bridge and tendency for deck cracking. However, others (Mc Keel, 1985) observed that bridges that carry fewer trucks at lower speeds exhibit less cracking than those that carry large number of truck at higher speeds.

2.2.6. MATERIAL AND MIX DESIGN FACTORS

Aggregate

As indicated by Saadeghvaziri and Hadidi, type, size, volume and properties of aggregate have great effects on concrete properties. Previous studies recommended using the largest possible size of aggregate (Babaei and Purvis, 1994; Kosel et al., 1985; Krauss and Rogalla, 1996; PCA, 1970). The studies also recommended maximizing aggregate volume (French et al., 1999; Kochanski, 1990; Kosel et al., 1985) and using low shrinkage aggregate (Krauss and Rogalla, 1996; PCA, 1970) to reduce cracking.

Water Content

Many researchers found increased cracking with increased water content and recommended reducing water content (Schmitt and Darwin, 1999, Babaei and Hawkins, 1985; Babaei and Purvis, 1994; Issa, 1999). As indicated by Saadeghvaziri and Hadidi, Schmitt and Darwin (1999) suggested that the volume of water and cement should not exceed 27% of total volume of concrete. Also, Babaei and Purvis (1994) recommended the maximum water content to be 192 kg/m³ (323 lb/yd³).

Cement Type, Cement Content, and Water/Cement Ratio

Many researchers concluded that the use of type II cement reduces cracking and recommended its use in bridge deck construction (Krauss and Rogalla, 1996; Babaei and Purvis, 1994; Kosel et al., 1985; La Fraugh, 1989). The good performance of type II cement is usually attributed to reduced early thermal gradient and shrinkage. Babaei and Purvis (1994) presented the effect of cement type and source on curing temperature. As indicated by Saadeghvaziri and Hadidi, many studies have observed increased deck cracking when using higher amount of cement in the concrete mix (French et al., 1999; Krauss and Rogalla, 1996; La Fraugh, 1989; Iowa DOT, 1986; Kochanski et al., 1990; Kosel et al., 1985; La Fraugh, 1989; Schmitt and Darwin, 1999). Higher cement content is usually related to higher drying shrinkage, higher temperature rise during hydration, and higher early modulus of elasticity of concrete. Saadeghvaziri and Hadidi indicated that different amounts of cement have been recommended by researchers as the maximum acceptable cement content in concrete mixes: 360 kg/m³ (611 lb/m³), 370 kg/ m³ (620 lb/yd³), 446 kg/ m³ (725 lb/yd³), and 385-390 kg/ m³ (650-660 lb/yd³).

Also, as indicated by Saadeghvaziri and Hadidi, many researchers (Schmitt and Darwin, 1999, French et al., 1999; Iowa DOT, 1986; Kochanski et al., 1990; PCA, 1970) noticed reduced cracking with reduction in water cement ratio. Saadeghvaziri and Hadidi indicated that reducing

water cement ratio of concrete is believed to reduce shrinkage of concrete. The following maximum water cement ratios have been recommended: 0.48, 0.41, 0.40, and 0.40-0.45 (standard w/c ratio is 0.445). La Fraugh, 1989 also recommended reducing water cement ratio using water reducers and pozzolans.

Slump

Saadeghvaziri and Hadidi indicated that there are many contradictions in the results of the previous studies performed so far on the effect of slump on deck cracking. An experimental study by Dakhil et al. (1975) indicated that increased cracking was reported with increasing slump. Saadeghvaziri and Hadidi also indicated that some studies have recommended reducing the slump (PCA, 1970, Babaei and Hawkins, 1987, Isaa, 1999, Kosel, 1985, Schmitt and Darwin, 1999). The researchers of these studies proposed values for maximum slump as follows:

- 50 + 12 mm (2 + ½ in.) (PCA, 1970)
- 60+12 mm (2 ½ + ½ in.) (Iowa DOT, 1986)
- 76 mm (3in.) (Florida DOT)

However, as presented in the study by Saadeghvaziri and Hadidi, Krauss and Rogalla (1996) found that there is no relation between slump and cracking tendency. Cheng and Johnson (1985), on the other hand, even noticed a decrease in transverse cracking with an increase in slump.

Concrete Strength

The increase of concrete strength is usually accompanied by increase in cement content. That results in an increase in paste volume and higher hydration temperatures, which could cause more cracking in concrete decks. As indicated by Saadeghvaziri and Hadidi, Krauss and Rogalla (1996) related the increase in deck cracking since 1970s to AASHTO's 1973 increase of minimum strength from 3,000 psi to 4,500 psi and lowering w/c from 0.53 to 0.445. The strength gain of concrete is usually accompanied by a gain in modulus of elasticity. There is no general agreement among studies that higher concrete strength reduces cracking. Although Schmitt and Darwin (1999) noticed increased cracking with increased compressive strength, Ramey et al. (1997) recommended increasing compressive strength. Yet, Krauss and Rogalla (1996) recommended the use of concrete that has low early strength.

Admixtures

Saadeghvaziri and Hadidi indicated that the effect of different types of admixtures on cracking is not yet completely understood. Many researchers including Cady et al. (1971) reported that the use of retarder is not an important factor; yet, some studies (Krauss and Rogalla, 1996; La Fraugh, 1989) encourage the use of retarders. They believe that deck cracking would decrease with reduced rate of early rise of temperature and early gain of modulus of elasticity. There are other studies (Krauss and Rogalla, 1996; Schmitt and Darwin, 1999) that have shown that use of silica fume may significantly increase cracking. That occurs if precautions are not taken to prevent plastic cracking.

Cheng and Johnson (1985) observed cracking reduction with the increase of air content. Saadeghvaziri and Hadidi indicated that Schmitt and Darwin (1999) even noticed significant decreases in cracking with air content more than 6%. Schmitt and Darwin also recommend at least 6% air content. French et al. (1999) recommended an air content of 5.5-6%. However, no relationship between air content and cracking was found by Stewart and Gunderson (1969).

2.2.7. CONSTRUCTION PRACTICE AND AMBIENT CONDITION FACTORS

Weather Condition and Concrete Temperature

As indicated by Saadeghvaziri and Hadidi, weather condition during placement of concrete and relative concrete temperature can greatly affect deck cracking. Researchers (Cheng and Johnson, 1985, Mayers, 1982, Schmitt and Darwin, 1999) have shown that hot and cold weather may increase cracking. Thermal stresses developed in concrete deck at early age, depend greatly on concrete temperature and weather conditions. The restraint to the thermal variations contributes to cracking (PCA, 1970). Temperature change between girder and deck may cause thermal stresses in the section. Researchers proposed some allowable ambient temperatures and concrete temperature during placement as follows:

- Maximum concrete placement temperature of 27°C (80°F) (PCA, 1970);
- Minimum ambient temperature of 7.2°C (45°F) (Cheng and Johnson, 1985);
- Minimum and maximum ambient temperature of 4 and 32°C (40 and 90°F) and reducing temperature difference between deck and girder;
- Maximum concrete placement temperatures 27°C (80°F) (Krauss and Rogalla, 1996);
- Concrete temperature of at least 5-10°C (10-20°F) cooler than ambient temperature (Krauss and Rogalla, 1996);
- Girder temperature of 12-24°C (55-75°F) should be maintained in cold weather (Babaei and Purvis, 1994);
- Some other studies specified the allowable differential temperature of deck and girder, for example: temperature difference of at least 12°C (22°F) for at least 24 hours is recommended by Babaei and Purvis (1994).

Low levels of humidity and high wind speed may also contribute to increased cracking. Plastic shrinkage cracks are often attributed to higher evaporation rates than concrete bleeding, where evaporation rates increase with high temperatures, low humidity, and high wind speed. Evaporation rates of concrete under different conditions can be found using an evaporation chart such as that developed by Portland Cement Association. Krauss and Rogalla (1996) recommended that special consideration should be taken when evaporation rates are more than 1.0 kg/m²/hr (0.2 lb/ft²/hr) for normal concrete and 0.5 kg/m²/hr (0.1 lb/ft²/hr) for low w/c ratio concrete. PCA (1970) recommends testing mixes for bleeding. Kochanski et al. (1990)

recommend estimating evaporation rate and reducing it to a maximum of 1.25 kg/m²/hr (0.25 lb/ft²/hr).

Curing

Proper curing is a key factor in reducing cracking and enhancing the properties of hardened concrete, such as durability and strength. The literature listed initial fogging, applying wet burlaps, and applying curing compounds among the recommendations proposed to reduce deck cracking. As indicated by Saadeghvaziri and Hadidi, the following curing procedure was recommended by Krauss and Rogalla (1996):

- Use of fog nozzle water spray in hot weather to cool concrete and to cool the steel and forms immediately ahead of placement – ponding of water on the forms or plastic concrete should not be allowed.
- Use of wind breaks and enclosures when the evaporation rates exceed 1kg/m²/hr (0.2 lb/ft²/hr) for normal concrete or 0.5 kg/m²/hr (0.1 lb/ft²/hr) for low water cement ratio concretes susceptible to plastic cracking.
- Application of water mist or monomolecular film immediately after strike-off or early finishing.
- Application of white-pigmented curing compound as soon as bleed water diminishes.
- Application of prewetted burlap as soon as concrete resist indentation – the burlap must be kept continuously wet by continuous sprinkling or by covering the burlap with plastic sheeting and periodic sprinkling.
- Continuation of wet curing for a minimum of 7 days, preferably 14 days.

As indicated by Saadeghvaziri and Hadidi, extended curing time is suggested by La Fraugh (1989). Kosel and Michols (1985) and Frosh et al. (2002) recommended minimum curing of 7 days for type I and 14 days for type II cement. Kochanski et al. (1990) recommended covering the decks with permeable membranes to reduce temperature.

Pour length, Pour Sequence, and Time of Casting

As indicated by Saadeghvaziri and Hadidi, earlier studies (Cheng and Johnson, 1985, Perfetti et al., 1985) reported that pour length and sequence do not influence cracking. However, later studies suggested that pour length, sequence, and rate may affect deck cracking. Issa (1999) attributes cracking to sequence of pour and recommends placing concrete first in positive moment regions. Ramey et al. (1997) recommend the following detailed pouring procedure:

- When possible, place complete deck at one time.
- Place simple span bridges one span per placement or if span is long, divide the deck longitudinally and place each stripe at one time. If this cannot be done, then place the center of span first and then place other portions.

- If multiple placements should be made on continuous beams, place middle spans first and observe 72-hour delay between placements. Use bonding agent to enhance bond at joint.

As reported by Saadeghvaziri and Hadidi, PCA (1970) recommended nighttime casting and Krauss and Rogalla (1996) recommended early or mid-evening placing.

Revolutions in Concrete Truck and Vibration of Fresh Concrete

It was noticed that excess revolution in truck does not affect cracking. Saadeghvaziri and Hadidi indicated that sufficient vibration of concrete is essential to good concrete. Issa (1999) considers insufficient vibration of fresh concrete as a contributing factor in concrete cracking. It was noticed that under-vibrated areas tend to develop more cracks.

Finishing

Krauss and Rogalla (1996) reported that early finishing reduces cracking. Researchers reported that hand finishing increases cracking; however, mechanical grooving is recommended by Krauss and Rogalla (1996). It is also reported that applying water to concrete surface during finishing operation has adverse effects on cracking.

Form Type

Saadeghvaziri and Hadidi indicated that there are inconsistent reports on the effect of form type on deck cracking. Issa (1999) attributes cracking to weight of the forms and their deflection. Cady et al. (1971) reported that Stay-In-Place (SIP) forms perform better than removable forms. However, Cheng and Johnson (1985) reported that use of SIP or conventional forms have little effect on transverse deck cracking. Also, Krauss and Rogalla (1996) and Frosh et al. (2002) have found that SIP forms sometimes increase cracking due to the additional restraint from SIP forms.

Construction Loads

Saadeghvaziri and Hadidi indicated that the effect of traffic and construction loads on deck cracking is not completely known. Researchers found that no adverse effect can be attributed to traffic in adjacent lanes during construction. Also researches showed that good quality concrete is not adversely affected by vibrations of low frequency and amplitude during the period of setting and early strength development. However, Issa (1999) attributes cracking to weight and vibration of machinery. It has been suggested that shoring girders may reduce deck cracking due to construction loads.

Continuous Span Deck Construction Sequence Effect

Construction practice, such as curing procedures, pouring sequence, and form type can also affect deck cracking. Cady et al. (1971) studied 249 bridges in Pennsylvania and has shown that the construction practice plays a major role in cracking of concrete bridge decks. Several researchers have emphasized effect of curing and weather. Although construction methods may increase or decrease the risk of cracking, cracking has been observed on decks built with different construction techniques. Consequently, transverse deck cracking cannot be solely attributed to a certain type of construction technique.

For continuous span steel plate girder bridges, deck construction sequence can contribute to transverse cracking. Positive moment areas should be placed before negative moment areas to

minimize tensile stress in the concrete in negative moment areas. For continuous placements the concrete is retarded to help prevent tensile stresses in the concrete placed at the beginning of each placement. While the concrete placed at the beginning may not have set when the last concrete is placed, it is rare that the concrete placed at the beginning is still workable when the last concrete is placed. Consequently, continuous placements can contribute to transverse cracking.

2.2.8. STRUCTURAL DESIGN FACTORS

There are some studies which have considered the structural design factors.

Girder Type, Boundary Condition, and Spacing

As indicated by Saadeghvaziri and Hadidi, several studies (Krauss and Rogalla, 1996; PCA, 1970; Cheng and Johnson, 1985; Mayers, 1982; Frosh et al., 2002) have found that decks on steel girders tend to crack more when compared to deck on concrete girders. The researchers believed that since concrete girders conduct heat slower than steel girders, thermal stresses in concrete girder bridges are lower than steel girder bridges. That results in less cracking tendency. Krauss and Rogalla (1996) found that have deep steel beams have performed worse than cast in place concrete girders and young prestressed girders. Girder end conditions also affect deck cracking. For example, cracking is more prevalent on continuous spans when compared to simple spans (Krauss and Rogalla, 1996; Mayers, 1982; Cady et al., 1971; Cheng and Johnson, 1985). Portland Cement Association study (PCA, 1970) indicated that regardless of type of span, the same pattern of uniformly spaced cracks is observed on decks supported on steel girder.

Stud Configuration and Properties

Krauss and Rogalla (1996) have found that girder restraint and studs may cause significant cracking. They recommended using fewer studs with smaller rows and lengths

Concrete Cover

Dakhil et al. (1975) performed an experimental study and reported that concrete cover over reinforcement is the most important factor affecting crack formation. They concluded that increased cover depth reduces risk of cracking. However, they also indicated that excessive increase in cover depth increases probability of settlement cracks over reinforcement. As indicated by Saadeghvaziri and Hadidi, optimum values are proposed for the cover depth over top reinforcing bars:

- Minimum of 38 mm. (1.5 in.) (PCA, 1970)
- 88 mm (3.5 in.) (Babaei and Hawkins, 1987)
- 50 mm (2 in.), where deicing chemicals are used use 64 mm (2 ½ in.) and maintain 76 mm (3 in.) limit (Ramey et al., 1997)
- 38 - 76 mm (1.5 - 3 in.)

Saadeghvaziri and Hadidi indicated that the study conducted by Dakhil et al. found that decks with cover of 76 mm (3 in) and more seem to be more susceptible to cracking.

Reinforcement Type, Spacing, Size and Distribution

Reinforcing details (size, type, spacing, and distribution) affect cracking tendency of concrete decks. It was reported that cracking increases with an increase in bar size (Dakhil et al., 1975, Babaei and Hawkins, 1987, Schmitt and Darwin, 1999, Kochanski et al., 1990, Ramey et al., 1997). To control deck stresses and reduce cracking tendency, an increase in the amount of longitudinal reinforcement without increasing bar size is recommendation (Krauss and Rogalla, 1996, PCA, 1970, Kochanski et al., 1990, Frosh et al., 2002). Researchers also indicated that deck tends to crack over transverse reinforcing bars due to the settling of fresh concrete over the reinforcing bars. Researchers also recommended limiting transverse bar size and/or maximize transverse bar spacing. As indicated by Saadeghvaziri and Hadidi, it was noticed that tightly tied reinforcements initially develop more small cracks than loosely tied reinforcements. Yet, cracking was ultimately the same. Saadeghvaziri and Hadidi also reported that Issa (1999) attributed some cracking to insufficient reinforcing detail at joints between new and old decks. Saadeghvaziri and Hadidi also listed the following recommendations suggested by Ramey et al. (1997) for reducing deck cracking:

- Limiting the size of deck reinforcement to No. 5
- Reversing lying transverse and longitudinal rebars in the top mat and staggering top and bottom rebars so as not to create significant plane of weakness and using higher percentage of longitudinal steel
- Using $\rho=0.002$ for top mat longitudinal steel and using the same for bottom mat and trying to use No. 4 bars
- Reducing splices
- Extending deck transverse steel to full width

Deck Thickness and Section Stiffness

It was found that an increase in deck thickness reduces deck cracking (French et al., 1999; Krauss and Rogalla, 1996; Kochanski et al., 1990; Ramey et al., 1997; Mayers, 1982). Saadeghvaziri and Hadidi reported that the effect of section stiffness on deck cracking is somehow contradicting, based on the results of the research studies. Babaei and Hawkins (1987) suggested minimizing the flexibility of structure. However, Ducret et al. (1996) showed that cracking tendency increases with an increase in the ratio of girder to deck area (reducing flexibility). This finding is in agreement with the findings of Krauss and Rogalla (1996) who also reported that increasing deck section stiffness increases cracking. Some literature indicated that since restraint volume change of deck is the principal cause of deck cracking, reducing section stiffness seems to decrease deck cracking.

Vibration and Impact Characteristics

There have been several studies dealing with bridge superstructure deflection and vibration. Burke stated that bridge superstructure flexibility had adverse influence on the integrity and

durability of the reinforced concrete deck slabs. Increasing the stiffness of the bridge superstructure could be a remedy to reduce deck cracking.

Cao and Shing (1999) stated that the maximum bending moment in a deck depends on the stiffness ratio of girders and the ratio of the girder spacing to bridge span length.

S. Zhou et al. (2004) indicated that published research works are based on parametric studies, using computer simulations. However, there are significant limitations in such studies. As an example, yielding of the reinforcement of the concrete deck and the non-linear behavior of bridge structure has been routinely ignored in finite element models (FEM models). In addition, the limitation of computing equipment and supporting software packages has also been restricting factors. Parametric studies were conducted and identified the following issues:

1. At low load levels, the effects of the composite action and the presence of the diaphragms are very small. The stiffness of the concrete slab is proportional to the slenderness ratio.
2. At intermediate load levels, and while the slab has entered the inelastic range, the effects of the composite action are more profound both in the stiffness of the slab and crack distribution.
3. The presence of diaphragms has minimal effects on the composite bridge deck at lower load levels. However, at intermediate loads the diaphragms stiffen the noncomposite deck to the levels of the composite deck. In both the composite and non-composite cases and when diaphragms are present, local failures of the slab are detected in the vicinity of the connection of the diaphragms to the girders. In the non-composite case, the load distribution is significantly different between the case of a structure with diaphragms and without diaphragms. However, the distribution of cracks between composite structures with and without diaphragms shows little difference.
4. The slenderness ratio has significant effect on the stiffness of the non-composite superstructure and the load distribution. Higher slenderness ratio yields greater net deflection of the slab. Cases of same slenderness ratio involving thinner slabs show more extensive damage of the slab. These effects are more profound at higher loads. Composite decks are more sensitive to changes of slenderness ratio, especially at lower load levels.

The New York State Department of Transportation initiated a study to ascertain if a correlation exists between bridge deck cracking and bridge vibration due to vehicular traffic. Their study involved 233 slab-on-steel girder style bridges built between 1990 and 1997. Each of the bridges was inspected to assess the type and severity of deck cracking and the severity of bridge vibrations. Statistical analysis was then used to determine if a relationship exists between four different parameters and deck cracking. Their results concluded that: 1) the vibration severity influences the cracking severity significantly; 2) Average Annual Daily Traffic (AADT) does influence the cracking severity and very low volume bridges exhibit less cracking; 3) span length does influence the cracking severity, with longer spans exhibiting more cracking; and 4) there is no statistically significant difference between the cracking severity and type of bearing.

The researchers in Champaign, Illinois found that some bridges were very flexible with a deflection limit at the center span of $L/625$ and $L/560$. This caused excessive deflection and vibration to the superstructure which deteriorated the decks of all the studied bridges to the point of the deck needing full replacement.

Due to dynamic loading caused by moving traffic: "Structures with significant traffic induced deflection reversals, or high traffic-induced vibration amplitudes and frequencies, are more likely than other structures to crack or to have their existing cracks lengthen and deepen. More flexible structures result in vibrations with larger amplitudes at essentially the same frequency"

In a study of the necessity of the top mat of reinforcing bars in bridge decks it was stated that "Girder flexibility can be an important parameter that affects the level of bending stresses in a bridge deck". When looking at the relative importance of the influence of the superstructure components on concrete deck durability, it was stated that "Cracking patterns and propagation are affected by the load distribution on the slab and the stiffness characteristics of the superstructure". They state further that "The relative rigidity between the concrete bridge deck and the remaining structural components of the bridge superstructure is considered as one of the important factors that affect the durability and lifespan of the concrete deck". "Increasing the stiffness of the bridge superstructure could be a remedy to reduce cracking". Steel girder bridges are more flexible than reinforced or prestressed concrete girder bridges. Therefore, a concrete deck supported on steel girders will be subjected to stress fluctuations of a larger magnitude due to traffic loads.

Results of phase I of this investigation indicated that the new LRFD provisions result in generally more conservative designs. The results of phase II investigation showed that there is no significant change in the dynamic properties of I-girder bridges designed by either AASHTO (1989) code provisions. Box girder bridges designed with the new code do exhibit more flexibility than previous AASHTO (1989) based designs.

The deflection computations in the new LRFD code are based on the assumption that all girders deflect equally. Hence, the deflections computed under the service load must be factored by a constant = ratio of the number of traffic lanes to number of girders. This results in much smaller deflections than the previous AASHTO (1989) version of the design code.

There are no significant changes in the dynamic characteristics (frequencies) of bridge configurations designed with AASHTO (1989) for I-girder bridges. In fact, I-girder bridges using the new LRFD result in stiffer bridges due to typically reduced girder spacing for spans up to about 35 m.

There is an increase in the flexibility of box-girder bridges for LRFD designs. Corresponding change in frequencies of the order of 20% were observed for spans in excess of 60 m. Dynamic amplification due to moving trucks shows minimal changes for I-girder bridges and significant changes for box-girder bridges.

Some researchers indicated that the concrete industry has for some time been trying to blame the observed cracking in bridge deck to flexibility of steel bridges. Some of the recent work by David Darwin at Kansas also contradicts this conclusion. His research team has a pooled funding on development of crack free bridge deck. He contributes the cracking to curing and construction practices. New York State DOT also concluded that over the last 40 years there has been major change on construction practices, namely moving away from sequential casting where positive sections should be poured first, followed by negative regions, and changes to cement chemistry and mix designs. Nowadays we use concrete mixes that have more than 650 pounds of cement, whereas in the past 550 pounds of cement per cubic yard was a norm. On top of everything else the deflection check is an indirect approach to control the vibration. According to several researches, it was found that no relationship between frequency of vibration of superstructure, speed and impact parameters and transverse cracking. However, Babaei and Hawkins (1987) suggested reducing the amplitude and frequency of structure vibration under live load.

3. FIELD INVESTIGATION AND EXPERIMENTAL TESTING

This study aimed at gaining a better understanding of early concrete cracking of bridge decks, identifying the key factors which cause early concrete cracking in bridge deck, investigating whether live-load deflection limits or vibration control are important factors in bridge deck cracking, modeling the behavior of cracks based on deflection, and identifying the most suitable materials for crack sealing with their ability to span cracks of various widths. The benefits and limitations of each material are also presented.

3.1. FLORIDA DISTRICTS' SURVEY

Data has been collected from different districts to know about their bridges problems and status. Following are some of the districts responses:

- District 4: We currently have 12 steel box girders in Broward County that is in the work program for deck sealing as the decks have many cracks over the steel box girders and can be seen going thru the deck at the overhangs. We have some rusting of the galvanized stay-in-place forms. We also have one area that may be leaking into the box. The project is for year 2014.
- District 3: I am not aware of any widespread issue of water infiltrating steel box girder bridges, but by copy of this email I am asking the District Structures Maintenance Engineers to respond directly to you with any occurrences. About a year ago the Construction Office conducted a survey on cracking of concrete decks of steel bridges, to determine if there was a need to update the construction specifications regarding the curing of concrete decks on steel bridges.
- District 2: Construction Structures Engineer, FDOT, Jacksonville indicated: My investigation concluded that the current curing procedures are very effective and that the problem is design related since the coefficient of expansion for steel beams is significantly larger than it is for the concrete deck, the deck is put into tension during times of maximum expansion of the beams and this causes the deck cracking. This is a nationwide issue and has been for a very long time but is generally considered benign in Florida since we do not use deicing salts and the cracking is typically minor. The State Structures Design Office looked into a solution to this problem and concluded, based on the lack of deck deterioration problems reported by Maintenance, that the cost of adding enough crack control rebar to eliminate or dramatically reduce the cracking would not be worth the cost. In other words, there is a good cost benefit to allowing minor deck cracks to form since performance or durability of the decks is not reduced significantly during their service life.

In this study, the researchers investigated a database on bridge information that include, crack location, concrete mix ingredients and properties, construction method, superstructure type, possible causes for cracking, and other relevant data for selected bridges in Florida (Blackwater River Bridge, Fort Lauderdale Bridge, US1 Bridge, and JTB Bridge)

3.2. INVESTIGATED BRIDGES

1. Blackwater River Bridge (Milton - Pensacola)

The research team investigated Blackwater River Bridge in Pensacola to investigate the extent of cracking for steel bridge decks. Figures 3-1 through 3-4 show some cracking extending to the sides and bottom of the bridge deck and the cores taken for analysis.



Figure 3-1: Blackwater River Bridge (Milton-Pensacola)

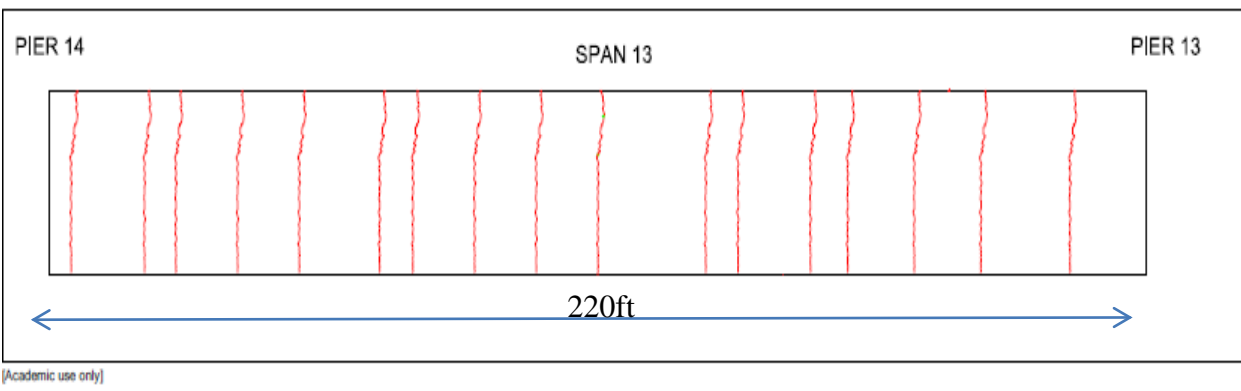
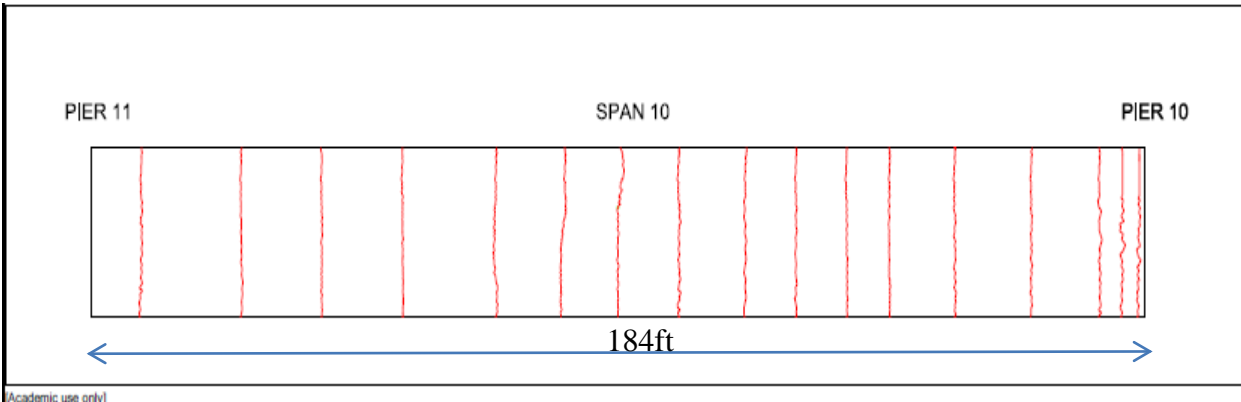
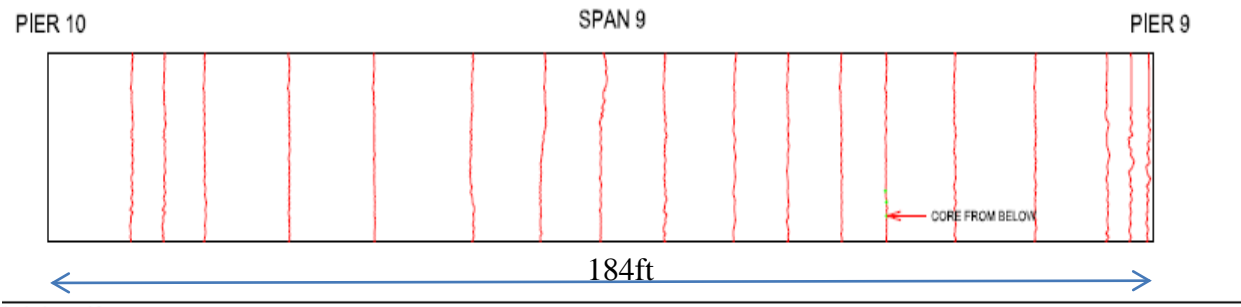


Figure 3-2: Blackwater River Bridge crack pattern

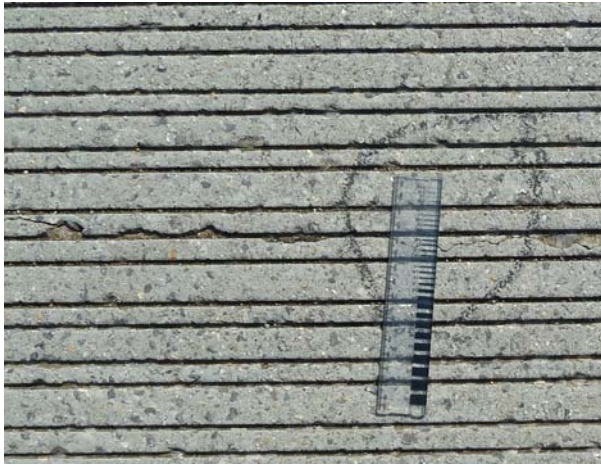


Figure 3-3: Deck and soffit cracking



Figure 3-4: Core sampling showing crack development over the transverse reinforcement

2. Fort Lauderdale Bridge (Fort Lauderdale)

The research team investigated some bridges in Fort Lauderdale to see the extent of cracking for steel bridge decks. Figures 3-5 through 3-9 show some cracking extending to the sides and bottom of the bridge deck, cross-section, deck cracking, and corrosion in the steel girders.



Figure 3-5: Fort Lauderdale Bridge

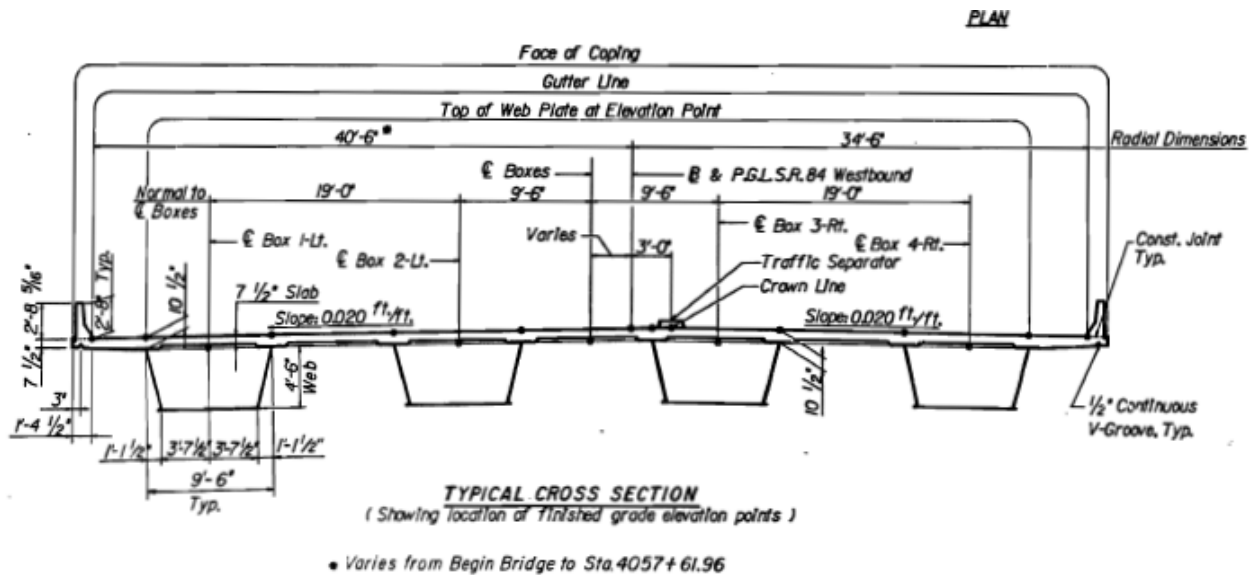


Figure 3-6: Typical cross section

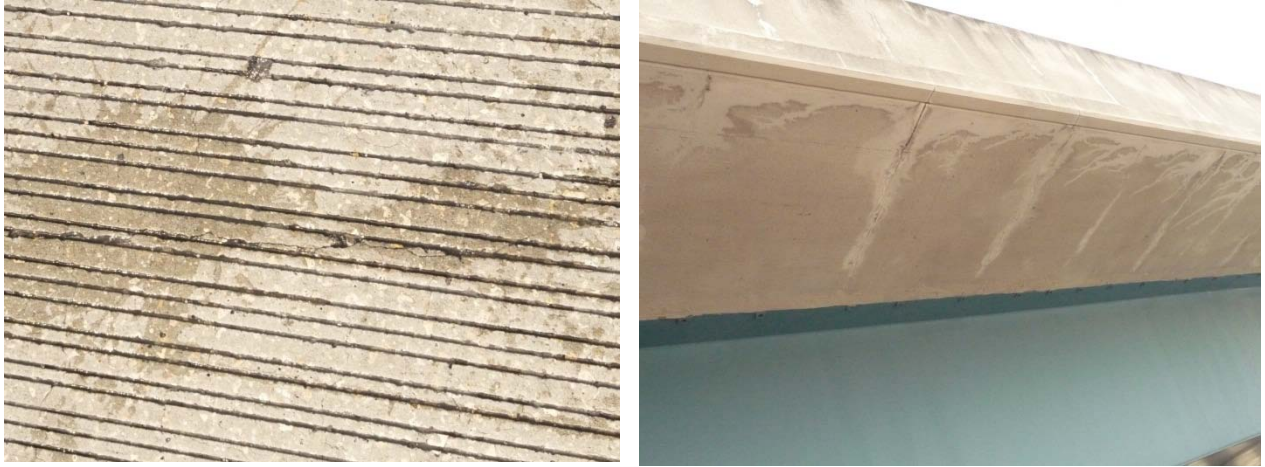


Figure 3-7: Deck and soffit cracking

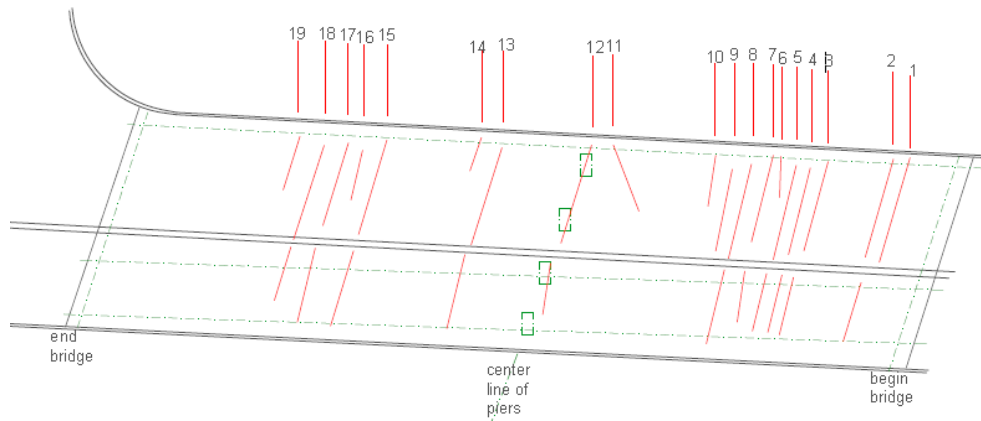


Figure 3-8: Deck and soffit cracking map (general distribution of cracks)



Figure 3-9: Internal investigation for corrosion shows detected corrosion spots

3. U.S. 1 Bridge (Jacksonville)

The research team also investigated the U.S. 1 Bridge in Jacksonville as a new construction. Figure 3-10 and Figure 3-11 show the bridge structural system and cracking in the bridge deck.



Figure 3-10: U.S. 1 Bridge



Figure 3-11: Deck cracking and supporting girders

4. JTB Bridge (Jacksonville)

The following figures, Figures 3-12 and 3-13, show the deck cracking of the bridge deck.



Figure 3-12: JTB Bridge (Jacksonville)

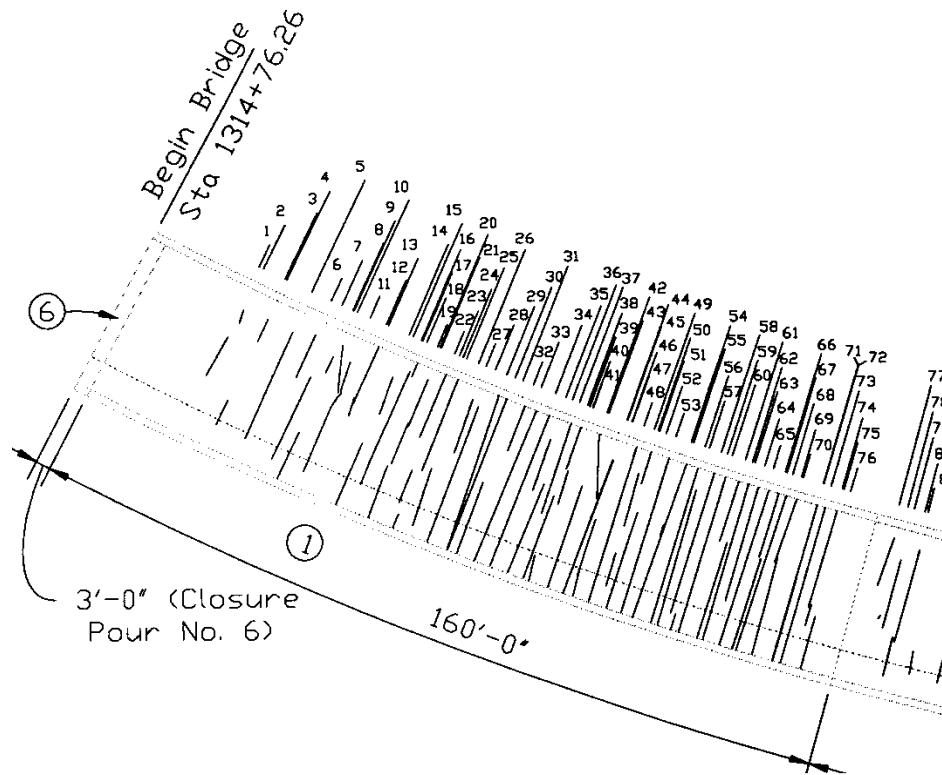


Figure 3-13: Deck crack pattern

3.3. SEALANT APPLICATION

The most commonly marketed sealers include epoxies, reactive methyl methacrylates (MMA), methacrylates, high-molecular weight methacrylates (HMWM), and polyurethanes. All these products have distinct characteristics that make them favorable for some uses and unfavorable for others. Properties include volatility, viscosity, initial shrinkage, tensile strength, and tensile elongation. Some surveys of 40 states have been conducted. They showed that 60% of these states did not have a crack sealing program and 24% use epoxies and methacrylates. Another survey stated that epoxy was the predominant sealer. Only four of sixteen states that had a crack sealing program claimed to use HMWM sealers. In another study, ten specimens were tested that had sealed cracks; two with HMWM, two with methacrylates, one with urethane polurea hybrid, four with epoxies, and one with epoxy resin. All ten sealers showed good penetration (2.5 in) at three different crack widths. Another study was also conducted with similar results of good penetration at varying crack widths. A sealant performance research study conducted by MNDOT focused on percent of penetration obtained an average of 90.3 percent of penetration over varying crack widths.

Our research concentrates on epoxies and methacrylates, both HMWM and MMA, as they possess the properties closest to the requirements in the FDOT specifications 413, five manufacturers were contacted and a field test was scheduled for August 24, 2010 at the Blackwater River Bridge at Milton, Florida. The field test was completed and it included four manufacturers (BASF, ChemMasters, Pilgrim, and Unitex), and five products which were applied by the manufacturers in accordance with FDOT requirements. The sealants were tested for ease of application, gel time, pot life, penetration, and water ingress prevention capabilities. The FDOT took core samples of the sealants applied as well as control core samples to compare the results of the application.

3.4. LAB TESTING AND RESULTS

In previous literature, researchers found that a HMWM sealer had a penetration of 0 and 3 inches into cracked pavements. Another research study indicated that epoxy did not penetrate satisfactory and the researchers replaced it with a HMWM which penetrated to the reinforcement. A study conducted in 1990 at the Seven Mile Bridge grouped cracks into three categories. Group one, crack width of 0.005 in., group two crack width between 0.005 and 0.010 in., and group three all crack widths wider than 0.010 inch. After 11.5 months of application, an average depth of penetration of 0.76, 0.93, and 0.95 inch occurred. The depth of penetration was measured 16 years after application with the resulting depth of penetration; 0.24, 0.35, and 0.42-inch. The depth of penetration was not expected to change with time. The reasons for penetration reduction were that resin dulled over time and became harder to see, and that fewer cores were taken 16 years after application compared to 11 months. Another study involving sealing eight bridges of varying ages with HMWM and epoxy showed scattered data retrieved from cores. The average percent penetration indicated that HMWM performed better than the epoxy. The Seven Mile bridge study indicated that penetration was impeded due to considerable amounts of contaminants found in the cracks.

3.4.1. CRACK SEALERS

In this study, laboratory tests were performed on crack sealants with the following performance criteria; penetration depth, bond strength plus elongation, and crack bonding test. Field tests of sealant were performed on bridges and on slab samples. Tests also included core sampling to determine crack bonding test and depth of sealant penetration using dissection/stereo microscopes and fluorescent and long-wave UV lighting to determine resin depth. The research team also investigated whether new cracks formed near newly sealed cracks. All testing was performed at the FDOT testing facility. Figure 3-14 shows applying sealants to the cracked deck.



Figure 3-14: Apply sealants to the cracked deck

Material Criteria and Performance Measures

Crack sealers are measured in four primary ways: depth of penetration, bond strength, chloride content/resistance to corrosion, and seepage rate. There is lack of standardized tests to investigate the performance of crack sealers making it more challenging to compare results. The research team only concentrated on three of the performance measures for crack sealers; depth of penetration, bond strength, and elongation.

Depth of penetration: Sealers are used to fill a formed crack. The deeper a sealer can penetrate the better seal it will create. Yet, due to the variability of crack widths it may be more useful to measure the percentage of penetration versus the actual penetration depth. The method conducted in this study of testing penetration depth involved taking cores from the concrete deck and examining a cross section of the crack with a microscope. If the resin has faded or is not readily visible, a florescent dye was applied to the crack and viewed under an ultraviolet light. Another method involved cracking the core sample and placing drops of water until the water stops beading then obtaining the average depth from all the cores.

Bond strength: The ability of a resin to repair the structural problem in a cracked deck is measured by its bond strength. There is no standard method to test for bond strength. In this study, the tensile splitting test ASTM C496 was used. This test involves placing a core sample on its side in a compression machine. The repair crack is placed perpendicular with the compressive load, which causes a tensile load to develop in the crack. The compressive load required for the repaired crack to fail is then compared to compressive load used to fail the uncracked core sample. A ratio is obtained by dividing the cracked sample capacity by the uncracked sample capacity. This is the percentage of the strength retained by the sealer. Another method is the three-point bending flexural test ASTM C293. This test is normally performed with beams and a ratio is developed to obtain the percent of strength retained by the sealer. Once the test is chosen and conducted, the failure surface is observed and documented. From these data three different types of failure planes can be produced, these are concrete, bond, and sealer failure.

Chloride content/resistance to corrosion: Chloride ions can infiltrate the concrete and corrode the reinforcement if there exists any cracking on the bridge deck. Crack sealers act as a barrier to slow down this ingress of chloride ions into the concrete. This problem occurs mainly in the northern states where there is tendency of having freeze/thaw cycles and the use of road salt for deicing.

Seepage: The indication of how well the repaired pavement will prevent chloride ion ingress is called seepage. Seepage is measured by the volume of water that passes through the cracked concrete. It is suggested that the least amount of water that passes through the crack the better the rebar of the deck is protected. Several tests are used to check for seepage. One test involves forming a barrier around the top of the concrete core sample, after the sides are waterproofed; water is poured into the barrier on top of the core sample. The water height is kept constant and the rate in which water passes through the core is recorded. The number of leaks before the cracks were sealed is compared to the number of leaks after the cracks were sealed. This test is mainly used in the field to give an indication of the success of the repair.

The research team only concentrated on three of the performance measures for crack sealers; depth of penetration, bond strength, and elongation.

3.4.2. SEALER MATERIAL TESTING

Tests were performed on the sealing materials according to ASTM specifications. Figure 3-15 shows samples of dog bone prepared sealing materials. Figure 3-16 shows the testing of the sealant material using bonded concrete specimen. Other tests were conducted on deck panels sealed with the sealing materials that had the best performance.



Figure 3-15: Preparing the specimens for testing



Figure 3-16: Applying the sealant to concrete specimens before and testing

Table 3-1 presents the FDOT specifications 413 - the physical properties of Methacrylate resins. From the list of sealers shown in Table 3-2, the research team chose the five sealers that more closely matched the FDOT specifications 413, as shown in Table 3-3.

Table 3-1: FDOT Specifications 413 - Physical Properties of Methacrylate Resin (FDOT Products Manual)

Viscosity (Brookfield RVT)	14-20 cps at 50 rpm
Density (ASTM D1481)	8.5 – 9.0 lb/gl at 77° F
Flash Point (ASTM D93)	>200° F (Pensky Martens CC)
Odor	Low
Bulk Cure Speed	3 Hours @ 73° F (max)
Surface Cure	8 Hours @ 73° F (max)
Gel Time (ASTM 2471)	60 minutes (max)
Tack Free Time	5 Hours (max.) (at 72° F and 50% Relative Humidity)
Compressive Strength (ASSHTO T106)	6,500 psi (min)
Tensile Strength (ASTM C307)	1,300 psi (min.)
Shear Bond Adhesion (ASTM C882)	600 psi (min.)
Wax Content	0

The characteristics of the chosen five manufacturers' materials are shown in Table 3-3. They were further tested in the lab to verify that the properties reported in the manufacturer's data sheet were accurate. Test process and results are shown in Figure 3-17 and Table 3-4.

Table 3-2: Properties of Sealant Materials Investigated in the Study

Sealant	Company	Description
Sealate T-70	Pilgrim Permocoat, Inc.	Methacrylate. Bond Strength 615 psi, Tensile Elongation 3-5%. Viscosity <20 cps, Flash Point >210F. Pot Life 70F: 25-40 min, Tack Free 70F: 4-7 hrs
Sealate T-70 MX-30	Pilgrim Permocoat, Inc.	Methacrylate. Bond Strength 615 psi. Tensile Elongation 30%. Viscosity <25 cps, Flash Point >200F. Pot Life 70F: 40-60 min, Tack Free 70F: 5-8 hrs
Sikadur 55 SLV	Sika Costal Construction	Is a 2-Component, 100% solids, Moisture-tolerant, epoxy crack healer/Penetrating sealer. Bond Strength 14 days – 2,500psi. Tensile Strength 7, 100 psi, Elongation 10%. Viscosity 105 cps, Flash Point N/A. Pot Life 20 min, Tack Free 73F: 6hrs, 90F: 2.5 hrs
Duraguard 401	ChemMasters, Inc	Methacrylate. It is a 3 component, low viscosity, solvent free, high molecular weight methacrylate penetrating sealer and crack healer. Tensile Strength 2,800 psi, Elongation 40-50%. Viscosity 5-20 cps, Flash Point >200F. Pot Life 45 min, Tack Free up to 6 hrs
Epoxeal GS – Structural	BASF Construction	Epoxy Sealer. It is two components, ultra-low viscosity, gravity feed or pressure injected. Bond Strength 14 days – 3,450 psi. Tensile Strength 7,100 psi, Elongation 2.9%. Viscosity 95 cps, Flash Point >200F. Pot Life 45 min, Tack Free 70F: 12 hrs, 80F: 6 hrs
Degadur 332	BASF Construction	Methyl Methacrylate (MMA). Is a solvent free, 2 component, 100% reactive resin. Tensile Strength 1,200 psi, Elongation 220-300%. Viscosity 95 cps, Flash Point 48F. Pot Life 25 min, Tack Free 1hr
Degadeck Crack Sealer Plus	BASF Construction	Methacrylate. It is a low viscosity, low surface tension, solvent free, penetrating sealer and crack healer. Tensile Strength 8,100 psi, Elongation 5.5%. Viscosity 5-15 cps, Flash Point 48F. Pot Life 15-20 min, Tack Free 1hr
Traffic Guard EP-35	BASF Construction	Epoxy. It is a rapid-curing, skid-resistant epoxy concrete overlay system. Tensile Strength 2,500 psi, Bond Strength 2,500 psi. Elongation 30%, Viscosity 1000-2500 cps. Flash Point 200F, Pot Life 15-25 min, Tack Free 2hrs
Degadeck Deck overlay System	BASF Construction	Methacrylate. It is a 3 component, reactive resin used as a wearing course. Tensile Strength 1,290-1,380 psi (Body coat), 2,150 psi (Top coat). Elongation 13% (Body coat), 35% (Top coat). Viscosity N/A, Flash Point 48F, Pot Life N/A. Tack Free 1hr
Zero-C Horizontal Extended Mortar	BASF Construction	Cementitious Material. It is a two component screedable, shrinkage-compensated pre-extended cementitious repair material. Tensile Strength 500 psi Bond Strength >2,000 psi (28 days).

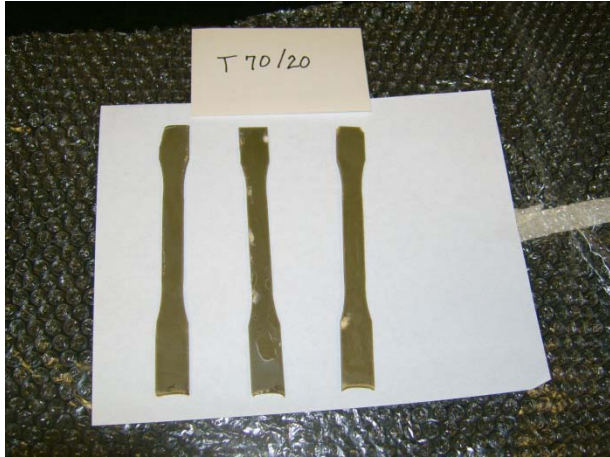


Figure 3-17: Sealent material testing

Table 3-3: Characteristics of Selected Sealers

Test Site #	Tested Products	Components	Viscosity	Elongation	Curing time	Skid Ave.	Tensile strength Ave. (lbf)
TS -1	CM DuraGuard HM Sealer	2 part Epoxy	30 cps	5.5%	2-3 Hr	62	1591
TS -2	CM DuraGuard 401	3 part Methacrylate	5-20 cps	40-50%	4-6 Hr	37	2363
TS -3	BASF DegaDeck Sealer Plus	2 comp Methacrylate	5-15 cps	5.5%	1 Hr	22	1276
TS -5	Pilgrim T-70/20	3 part Methacrylate	14-15 cps	20%	4-6 Hr	37	1731
TS -6	Unitex ProPoxy 40 LV	Epoxy	80 cps	60%	2 Hr	<u>6A/6B</u> 50/74	<u>6A/6B</u> 2236/2240
TS-4	Controls	No sealer applied				48	2290

Note: In the field, the average penetration of the material in the cracks ranged from 0.5 to 1 inch. However, because of the different crack widths, the information should not be used for direct comparison of the materials. All materials appear to have acceptable penetration. Then, it was decided to perform a secondary lab test on the crack sealer products, as shown in Table 3-4.

Table 3-4: Selected Sealer Tests

Manufacturer's Data					Lab Test Data (7/29/10)		Lab Test Data (12/8/10)	
Actual Product Name	Product labeling	Tensile strength (MPa)	Viscosity (cps)	Elongation (%)	Tensile strength (MPa)	Elongation (%)	Tensile strength (MPa)	Elongation (%)
DegaDeck Crack Sealer Plus	1-A	56.4	5-15	5.5	22.6	2.1	25.3	2.6
DuraGuard 401	2-B	19.3	5-20	40-50	0.9	99.6	7.3	17.2
DuraGuard HM Sealer	3-C	41.0-48.0	30	3-7	23.4	10.5	27.2	N/A
ProPoxy 40LV	4-D	6.9	80	60	3.36	213	5.5	102
Sealate T70/20	5-E	8.2	10-25	30	No test	No test	5.7	1.3

3.4.3. SLAB TESTS

Further lab testing was conducted, as shown in Figures 3-18 to 3-21, on slab model construction having blade placement to create “ideal” cracks of 0.01 to 0.02 in. of width and a spacing of 4 inches from center. Sealing of the slab cracks was performed to check the characteristics of sealants and their applicability that simulate actual bridge deck cracks. Results are shown in Table 3-5.



Figure 3-18: Construction of test slabs and placement of blades for crack width



Figure 3-19: Sealed slabs with LVDT's and dial gages and sealed cracks

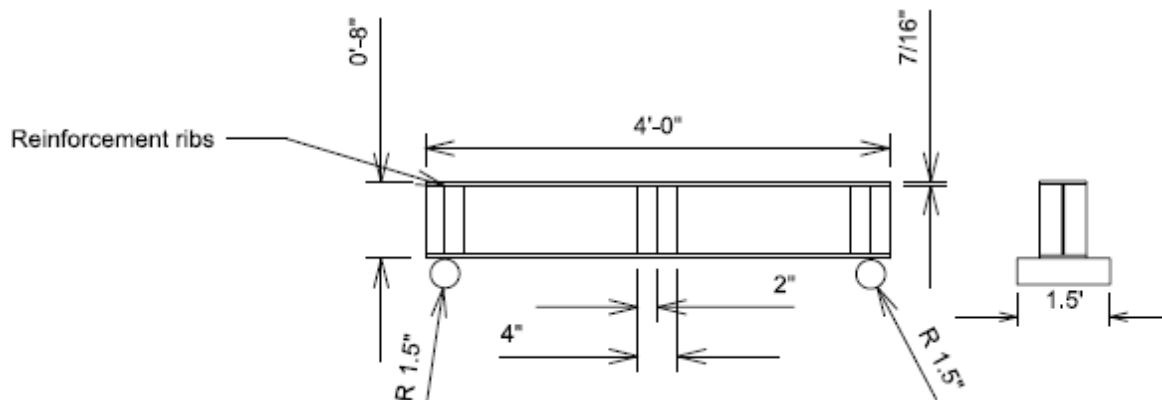


Figure 3-20: Loading frame



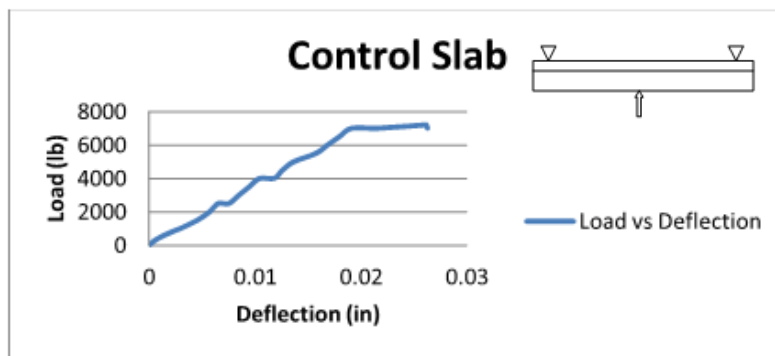
Figure 3-21: Testing of control slab specimen and crack development

After slabs were cast (Figure 3-18), blades were used to induce three cracks, at top of the slabs. The center crack spans along the entire slab width with crack width of 0.02 in. (0.51 mm) and is in the graph as CH-0 while one of the offset cracks spans along the entire slab width with crack width of 0.01 in. (0.25 mm) and is in the graph as CH-1. As shown in Figure 3-21, the other offset crack spans from the edge of the slab to mid-width with crack width of 0.01 in. (0.25 mm). For all of the three induced cracks, crack depth is 1.5 in. (38 mm) reaching the slab reinforcements. The center crack is at the mid-span of the slab while the other two are spaced at 4 in. (101.6 mm) from the center crack. The control slab did not have any induced cracks, however, the remaining five specimens had three cracks with 9 in. and 18 in. (229 mm and 457.2 mm) of crack length as explained earlier and presented in Figure 3-18. The specimens were tested under static loads at age of 28 days. All of specimens were fully instrumented as shown in Figures 3-19 and 3-20. LVDT's were installed to monitor crack openings and deflection while dial gages were used to monitor crack openings as well. Figure 3-20 presents the load frame used to test the specimens. When the load is applied, load, time, deflection, and crack opening are monitored for all of the specimens. It is important to note that crack opening was monitored for cracks that run through the entire slab width only. Shorter cracks were monitored for propagation of crack only. The control slab was tested to a force of 7,200 lb and three cracks equally spaced at approximately 4 in. (101.6 mm) were developed, as shown in Figure 3-21.

Based on previous research and observation on the tested bridge, control slab was tested as shown in Figure 3-21 to a force of 7,200 lb and obtained three cracks spaced at approximately 4 inches beginning at the center line of the slab as shown in Figure 3-21 with the load results shown in Figure 3-22. The results of the load testing of the control slab are shown in Figure 3-23.



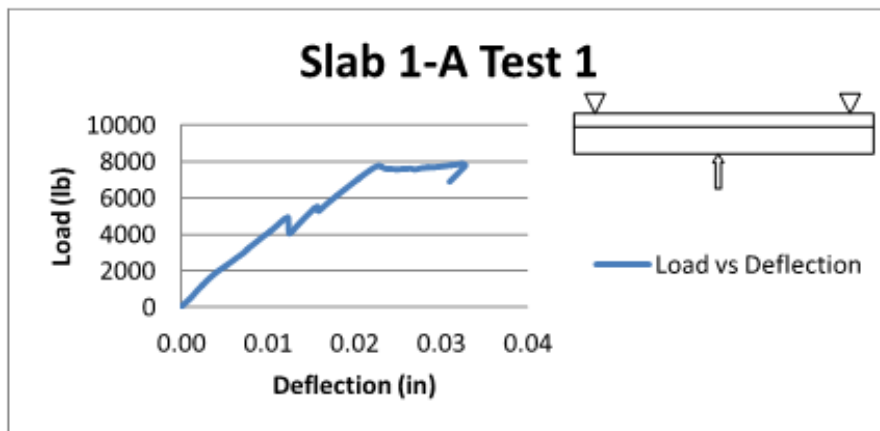
Figure 3-22: Slab Testing



Deflection at 7000 lb = 0.01914 in

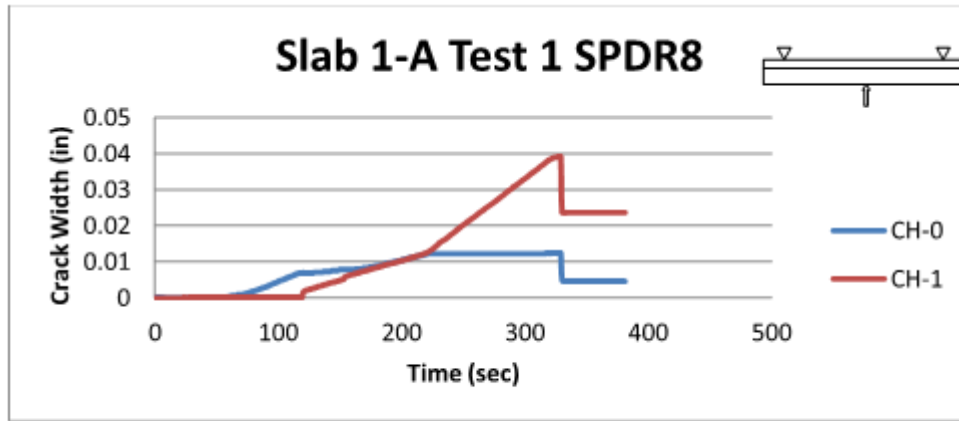
Figure 3-23: Control slab load testing results

The rest of the slabs were sealed with the appropriate sealer, as shown in Figure 3-19 and allowed to cure, then subjected to the single point load to observe the behavior of the sealer under load. The results of the load testing of the slabs are shown in Figures 3-24 and Figure 3-25.



Deflection at 7000 lb = 0.0203 in

Figure 3-24: Slab 1-A load test



Max crack width CH-0 (center crack) 0.012549 in. CH-1 (LH crack) 0.039124 in

Figure 3-25: Slab 1-A LVDT results

Slab 1-A was tested with a single line load. Center crack occurred at 6500 lbs but other cracks did not appear. Therefore, a second test with two point loads was performed, whereas the outside crack propagated but no visible sealant debonding as shown in Figure 3-26. The test results are shown in Figures 3-27 and 3-28. The test results for the other slabs are shown in Figures 3-27 to 3-43.

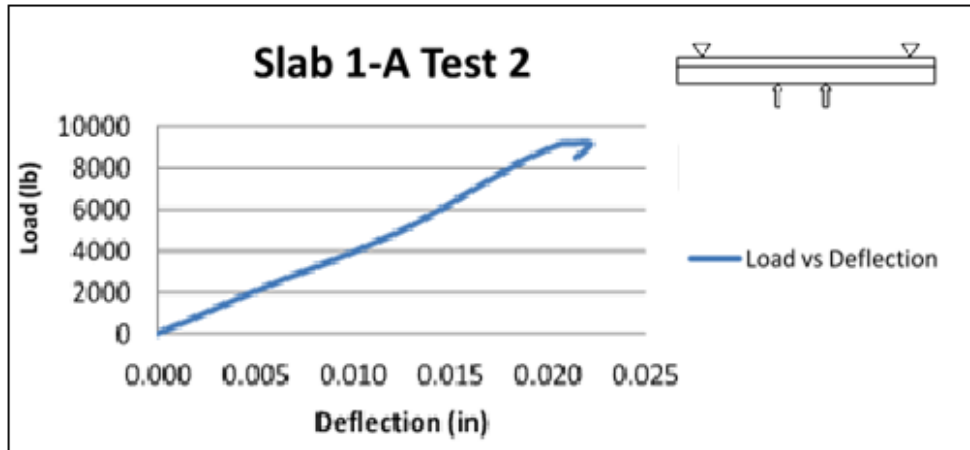


(a)



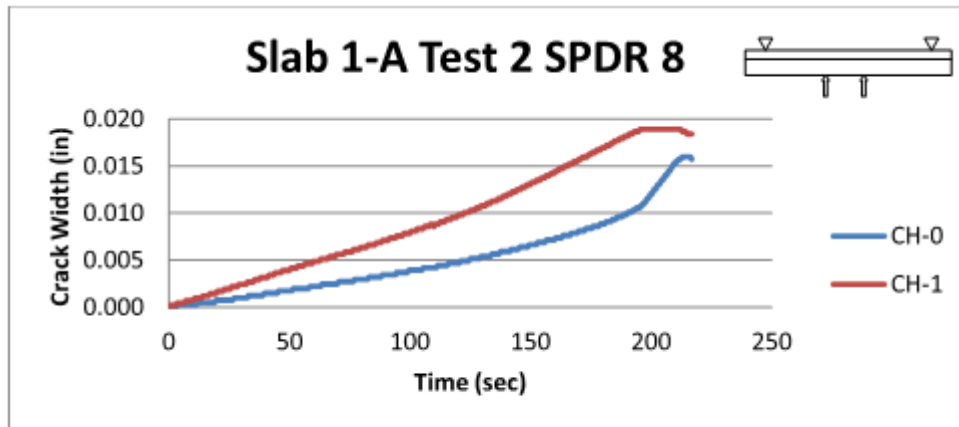
(b)

Figure 3-26: Slab 1-A crack propagation and the double point load plate



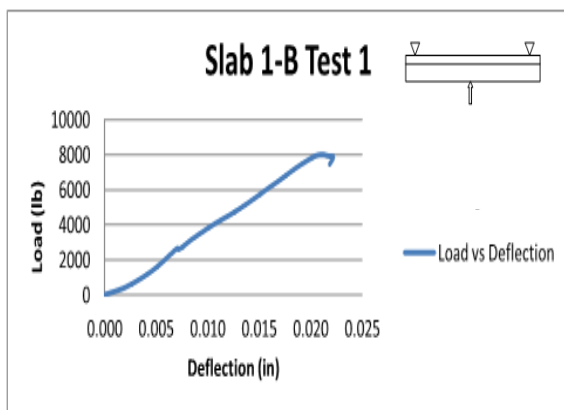
Deflection at 7000 lb = 0.0163 in

Figure 3-27: Slab 1-A Test 2



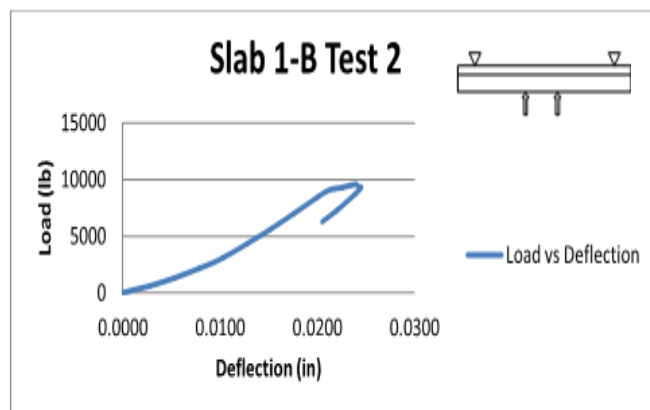
Max crack width CH-0 = 0.015994 in, CH-1 = 0.018947 in

Figure 3-28: Slab 1-A Test 2 LVDT results



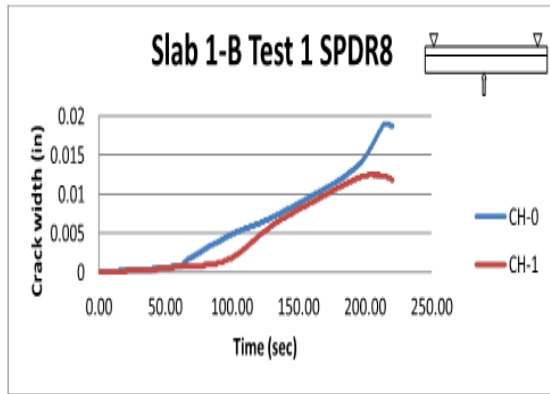
Deflection at 7000 lb = 0.0180 in

Figure 3-29: Slab 1-B test 1

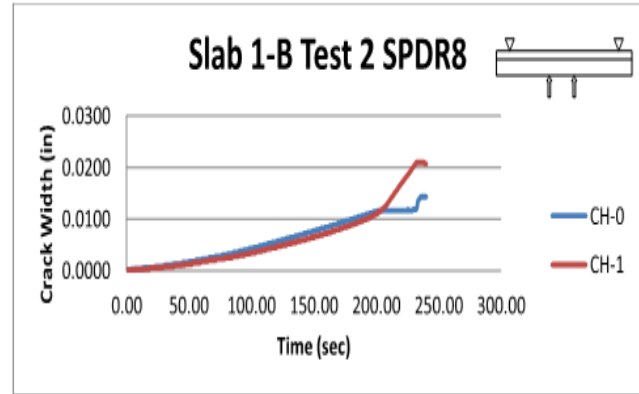


Deflection at 7000 lb = 0.0176 in

Figure 3-30: Slab 1-B test 2

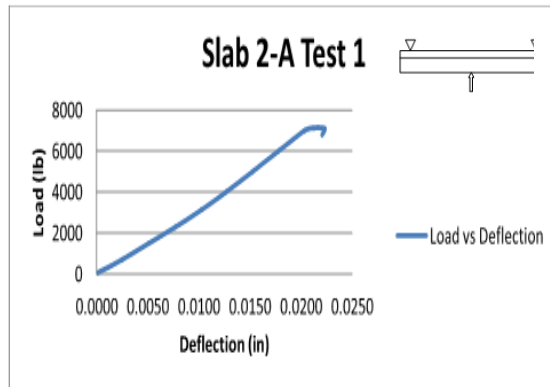


Max crack width CH-0 = 0.018947 in, CH-1 = 0.012549 in

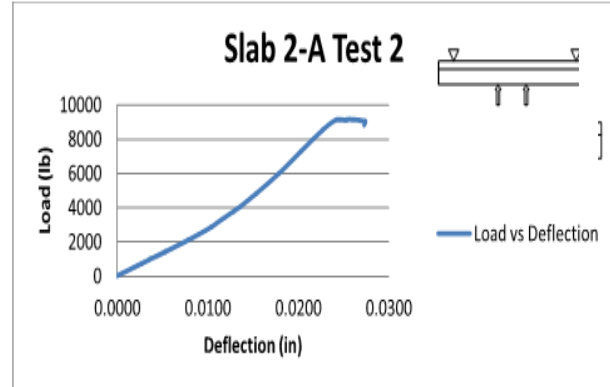


Max crack width CH-0 = 0.014272 in, CH-1 = 0.020915 in

Figure 3-31: Slab 1-B crack width results

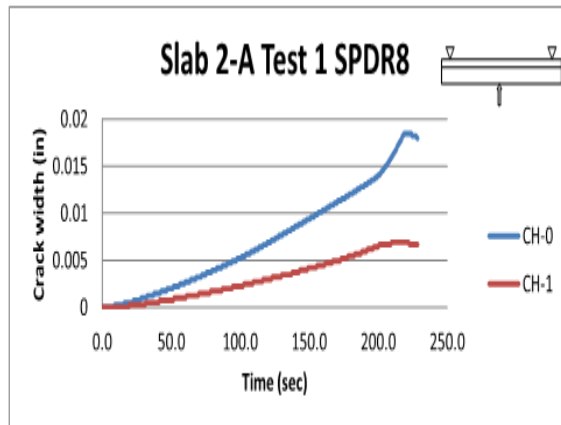


Deflection at 7000 lb = 0.0203 in

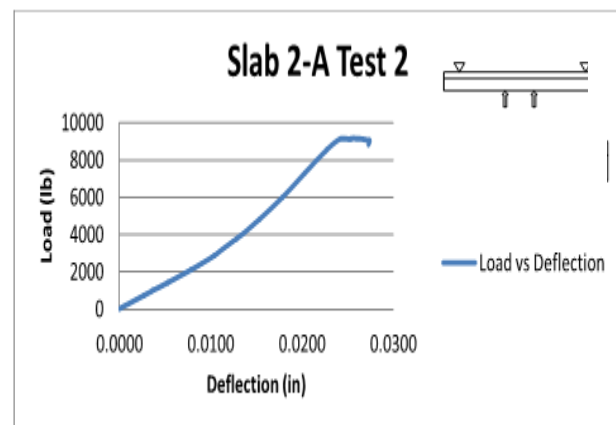


Deflection at 7000 lb = 0.0197 in

Figure 3-32: Slab 2-A load test results

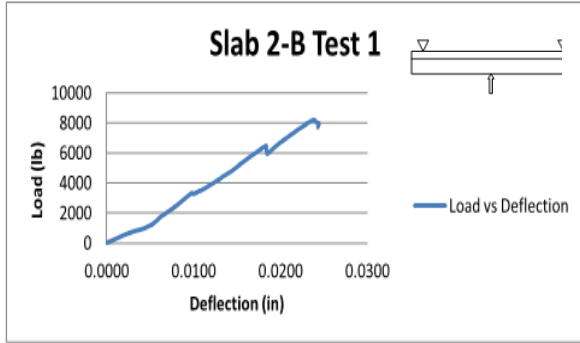


Crack width CH-0 = 0.018455 in, CH-1 = 0.00689 in

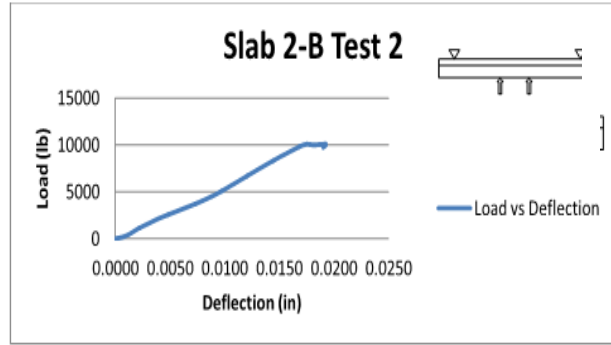


Deflection at 7000 lb = 0.0197 in

Figure 3-33: Slab 2-A crack width results

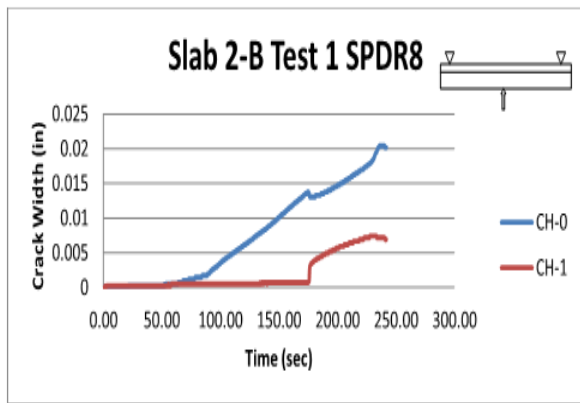


Deflection at 7000 lb = 0.0207 in

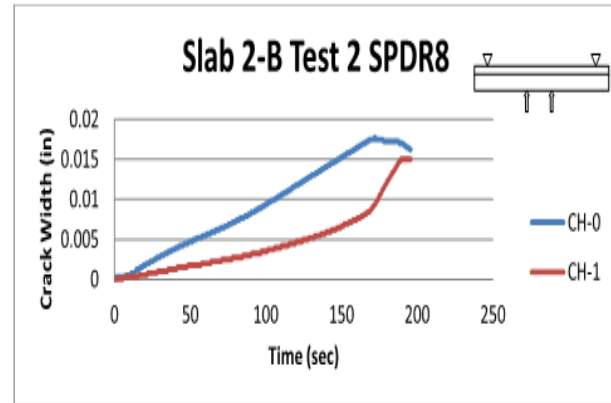


Deflection at 7000 lb = 0.0125 in

Figure 3-34: Slab 2-B load test results

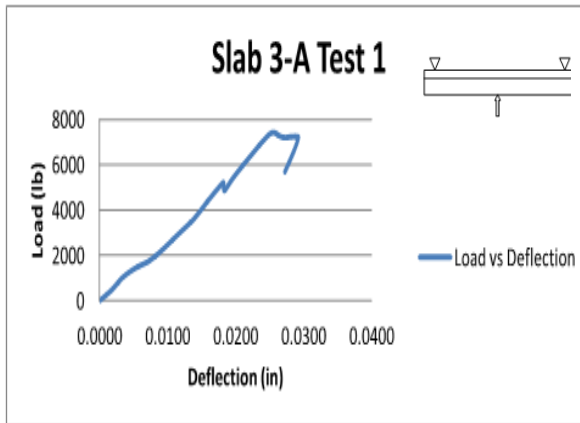


Crack width CH-0 = 0.02042 in, CH-1 = 0.00738 in

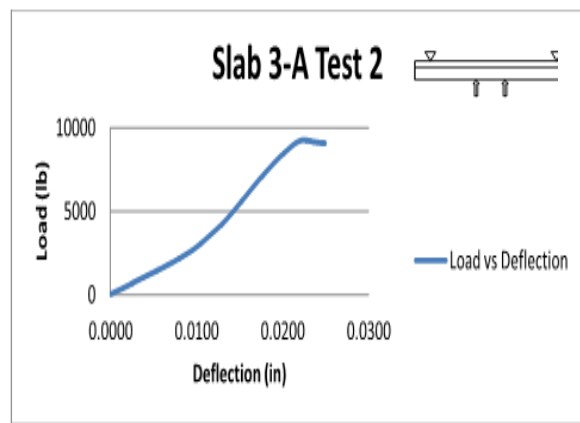


Crack width for CH-0 = 0.01772 in, CH-1 = 0.01501 in

Figure 3-35: Slab 2-B - crack width results

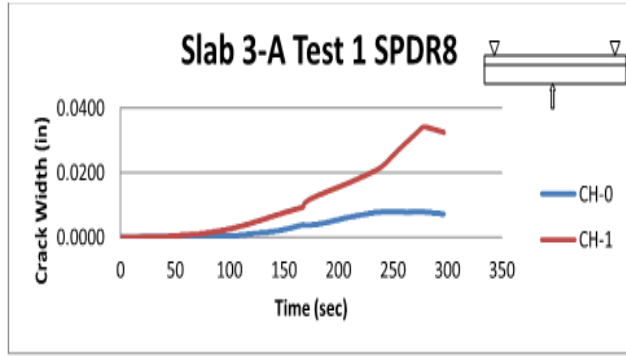


Deflection at 7000 lb = 0.0239 in



Deflection at 7000 lb = 0.0175 in

Figure 3-36: Slab 3-A load test results

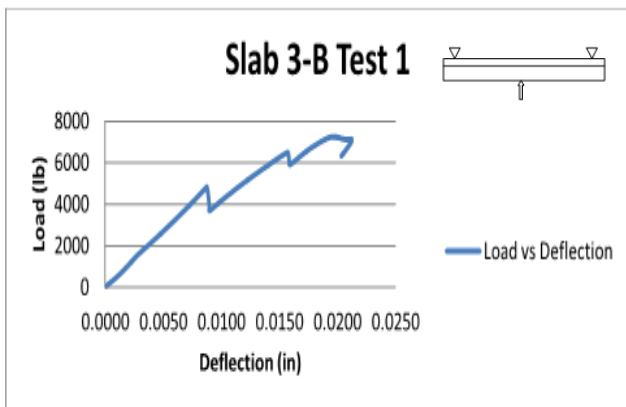


Crack width for CH-0 = 0.00787 in, CH-1 = 0.03420 in

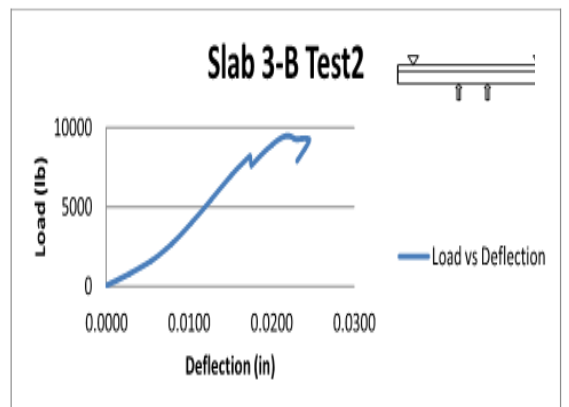


Crack Width for CH-0 = 0.02313 in, CH-1 = 0.02067 in

Figure 3-37: Slab 3-A crack width results

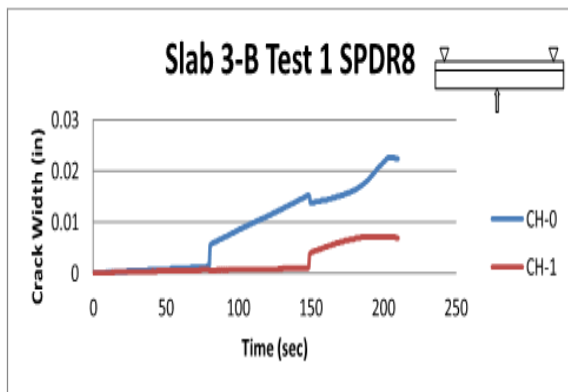


Deflection at 7000 lb = 0.0185 in

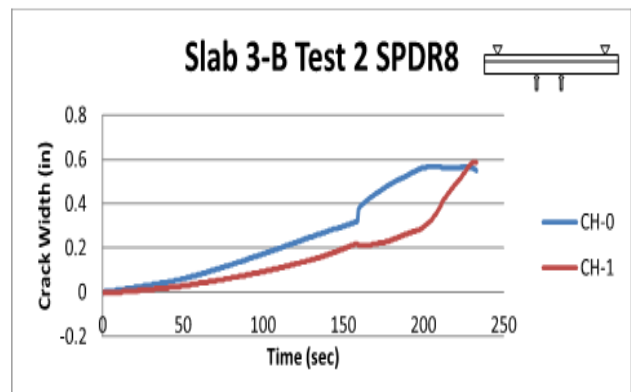


Deflection at 7000 lb = 0.0152 in

Figure 3-38: Slab 3-B load test results

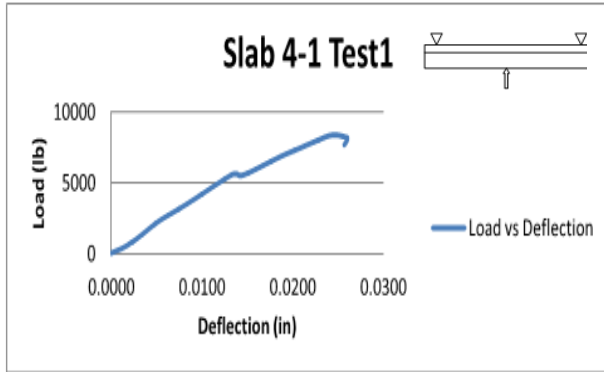


Crack width CH-0 = 0.02264 in, CH-1 = 0.00714 in

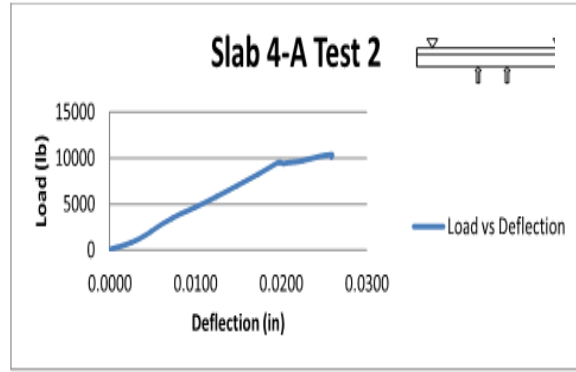


Crack width CH-0 = 0.02239 in, CH-1 = 0.02313 in

Figure 3-39: Slab 3-B crack width results

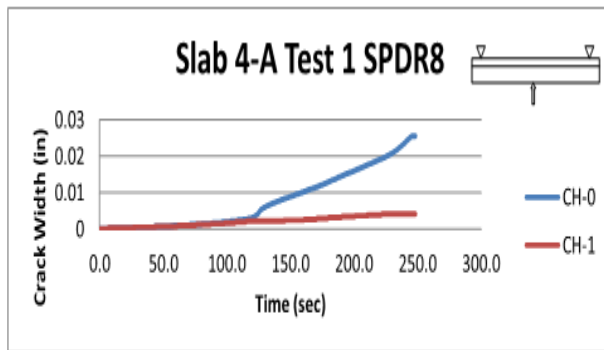


Deflection at 7000 lb = 0.0192 in

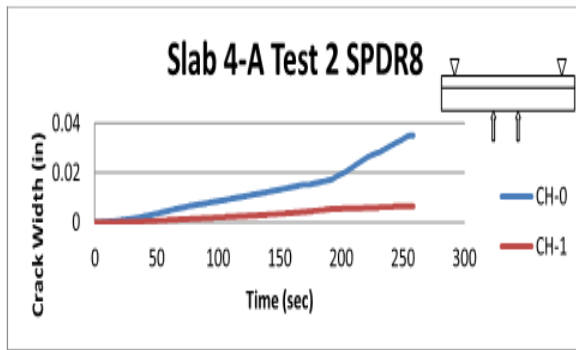


Deflection at 7000 lb = 0.0150 in

Figure 3-40: Slab 4-A load test results

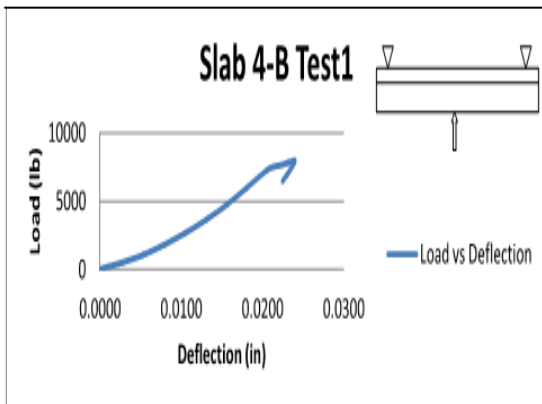


Crack width of CH-0 = 0.02559 in, CH-1 = 0.00418 in

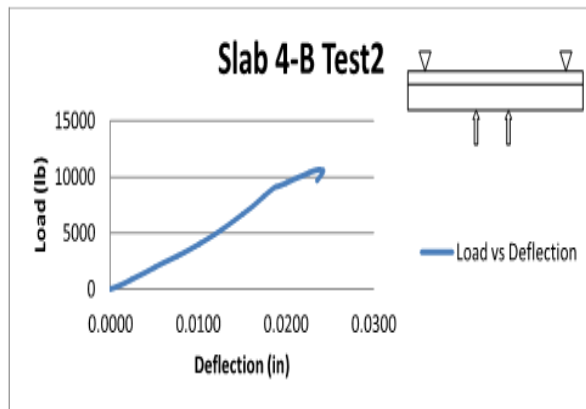


Crack Width at CH-0 = 0.03519 in, CH-1 = 0.00664 in

Figure 3-41: Slab 4-A crack width results

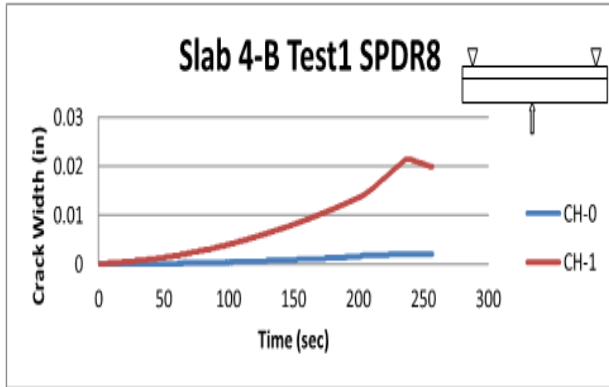


Deflection at 7000 lb = 0.0200 in

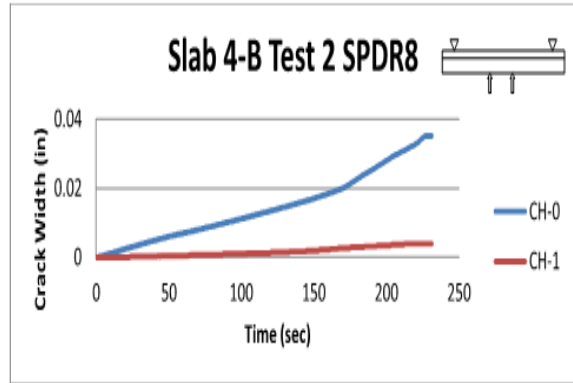


Deflection at 7000 lb = 0.0156 in

Figure 3-42: Slab 4-B load test results



Crack width at CH-0 = 0.00197 in, CH-1 = 0.02141 in



Crack width at CH-0 = 0.03519 in, CH-1 = 0.00394 in

Figure 3-43: Slab 4-B crack width results

Table 3-5: Max Crack Width Obtained During the Load Test of All Slabs

Test	Slab ID.	CH-0 Max Width (mm)	CH-0 Max Width (in.)	CH-1 Max Width (mm)	CH-1 Max Width (in.)
1	1-A	0.03188	0.01255	0.09938	0.03912
2	1-A	0.40625	0.01599	0.48125	0.01895
1	1-B	0.48125	0.01895	0.31875	0.01255
2	1-B	0.36250	0.01427	0.53125	0.02092
1	2-A	0.46875	0.01846	0.17500	0.00689
2	2-A	0.65625	0.02584	0.41875	0.01649
1	2-B	0.51875	0.02042	0.18750	0.00738
2	2-B	0.45000	0.01772	0.38125	0.01501
1	3-A	0.02000	0.00787	0.86875	0.03420
2	3-A	0.58750	0.02313	0.52500	0.02067
1	3-B	0.57500	0.02264	0.18125	0.00714
2	3-B	0.56875	0.02239	0.58750	0.02313
1	4-A	0.06500	0.02559	0.10625	0.00418
2	4-A	0.89375	0.03519	0.16875	0.00664
1	4-B	0.05000	0.00197	0.54375	0.02141

3.4.4. TESTING BEAM SAMPLES

Small beams were tested to validate the slab testing. Cracks were sealed with the best performing products. Cores were taken at the crack location and tested. A concrete block design that allowed for controlled cracking was developed. A schematic of the block is shown in Figure 3-44. All blocks were made from concrete mixed and cured in a moist room for at least 28 days. The blocks were cut in half to create 6"x6"x8" specimens. Each specimen was cracked by applying compressive force through round bars positioned in the grooves. Cracks were formed by placing small aluminum foil spacers along the edge of one half and clamping the two halves together. Crack width was determined by averaging the measured crack width at 1-in. intervals on both ends of the specimens and averaging the values. The width was then adjusted by tightening or loosening the clamping pressure. The ends and bottom were sealed with silicone caulk. A splitting test was then applied as shown in Figure 4-45. The samples were glued back together with sealers after cracking and retested. Cores were taken and investigated for tensile strength and penetration. Table 3-6 shows the results of the core testing. Table 3-7 presents the results of the beam testing.

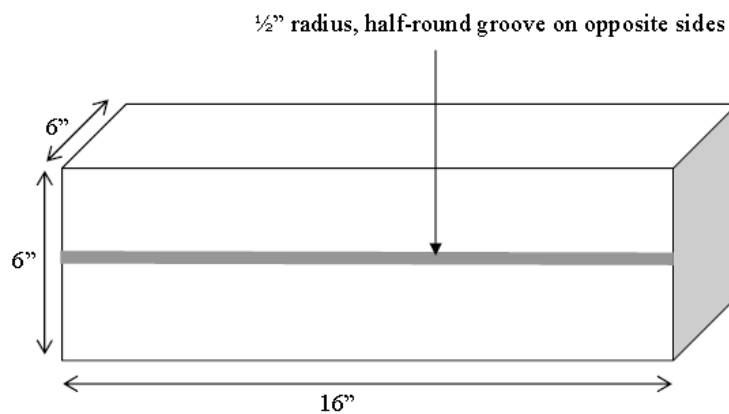


Figure 3-44: Concrete block schematic



Figure 3-45: Beam during split test procedure

Table 3-6: Tested Cores with Sealer Materials

GROUP	CORE #	Diam. (in.)	Length (in.)	Load (lbf)	Tensile Strength (psi)	Penetration (in.)
Control	1	1.98	2.57	4654	582.25	N/A
Control	2	1.99	2.56	4432	553.84	N/A
Control	3	1.98	2.56	4527	568.57	N/A
Control	4	1.99	2.55	4389	548.47	N/A
1 BASF	1-A	1.99	2.56	3609	450.99	3.9
1 BASF	1-B	1.98	2.55	3393	427.82	3.4
2 ChemM	2-A	1.97	2.54	4003	509.29	4.1
2 ChemM	2-B	1.98	2.57	3988	498.93	4.4
3 Pilgrim	3-A	1.99	2.55	3612	453.14	4.2
3 Pilgrim	3-B	1.98	2.55	3410	429.96	4.1
4 Unitex	4-A	1.98	2.53	4008	509.35	3.1
4 Unitex	4-B	1.98	2.54	4001	506.46	2.8

Table 3-7: Selected Sealers Testing Results for Beams

Company	Average Load (lbf)	Average Tensile strength (psi)	Penetration (in.)
Control	4,501	563.28	
BASF	3,501	439.41	3.65
ChemMaster	3,996	504.11	4.25
Pilgrim	3,511	441.55	4.15
Unitex	4,004	507.91	2.95

Beams of 6x6x16 inches were cracked longitudinally down the center and cut to 6x6x8 inches prisms. The two split parts of each prism (6x6x8 inches) were then clamped together to form an average crack width of 0.0145 inches wide and were sealed with the corresponding sealers. The sealed prisms were allowed to dry for 48 hours. Then one slice of approximately 1 inch was cut to test for sealers penetration. Also, 2-inch cores were taken from the remainder of the prisms for tensile/bond strength of sealers.

3.5. FIELD MATERIAL TESTING AND RESULTS

After researchers tested the sealants in the lab, researchers applied the sealants to selected areas of the Blackwater River Bridge in Pensacola to evaluate their applicability under service conditions. Figure 3-46 depicts the pilot bridge plan and test areas on the Blackwater River Bridge.

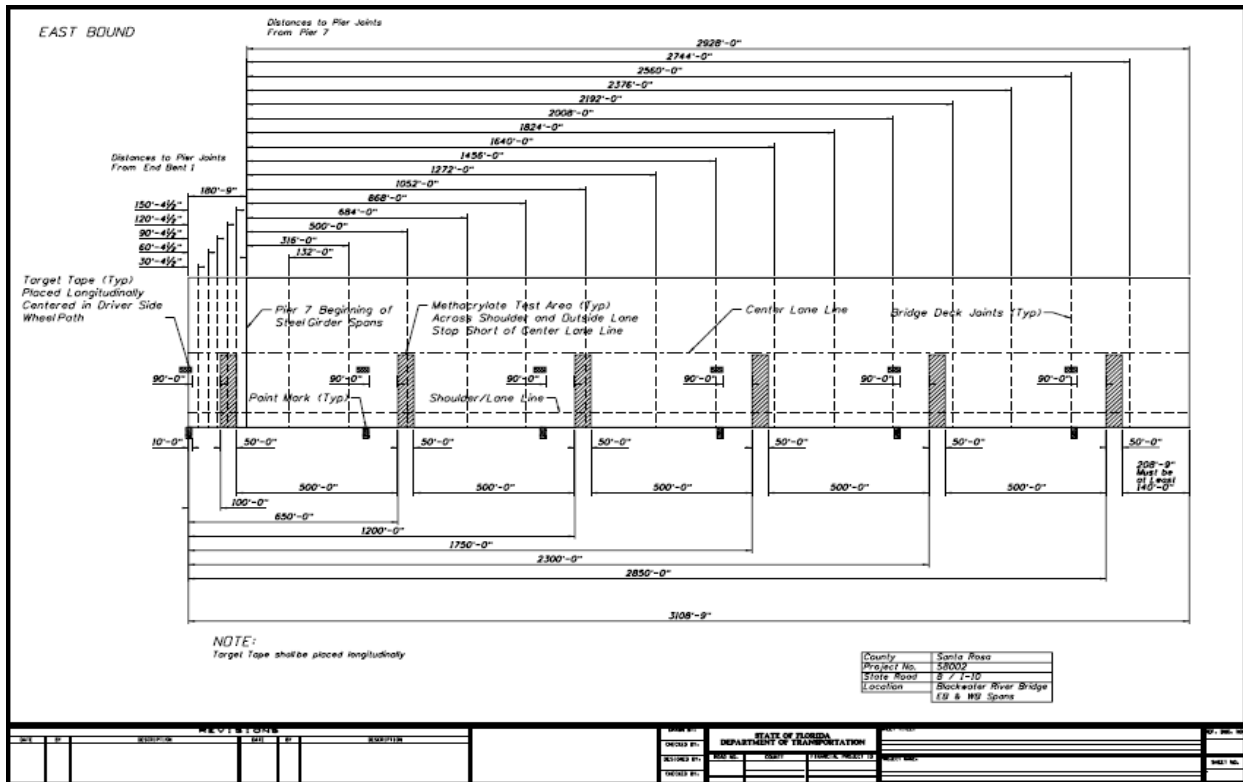


Figure 3-46: Bridge testing locations

Figures 3-47 through 3-52 show a brief of the applying the sealers materials. Table 3-8 shows the field test results for several sealants applied to parts of the same bridge. The surface was prepared, the cracks were cleaned properly, the sealant materials were applied according to the specified procedure in the manufacturer’s data sheet, and sand was sprinkled to provide skid resistance. Cores were taken after curing of the sealant and tests were performed. Table 3-9 also shows the test results.

Table 3-8: Results of Tests on the Cores from the Sealed Bridge Deck

Sample ID	Material Type	Location	Peak Load* (lbf)	Ave (lbf)	Penetration (in.)	Ave (in.)
Core 1-1	Concrete 1.75" core	Test section 1	1391	1591	0.70	0.475
Core 1-2			1131		--	
Core 1-3			2250		0.25	
Core 1-4			2540		N/A	
Core 2-1		Test section 2	1809	2363	0.70	0.767
Core 2-2			2230		0.70	
Core 2-3			3050		0.90	
Core 3-2		Test section 3	1954	1277	0.90	0.850
Core 3-3 ¹			599		0.80	
Core 5-1		Test section 5	2090	1731	N/A	0.483
Core 5-2			2320		0.50	
Core 5-3			3000		N/A	
Core 5-5			1035		0.45	
Core 5-6			1838		0.50	
Core 6A-1		Test section 6 – first part	1973	2237	1.00	1.000
Core 6A-2			2770		N/A	
Core 6A-3			2340		N/A	
Core 6A-4 ²			2500		--	
Core 6B-1 ³		Test section 6 – second part	1641	2241	0.60	0.600
Core 6B-2 ⁴			2840		0.60	
Core 6B-3	1799		N/A			
Core 6B-4	1921		N/A			
Core 6B-5	1860		N/A			

- * Modified split tensile test to compare bond
- Core 3-3¹ Individual cracks were treated prior to application
- Core 6A-4² Excessive amount of sand were used
- Core 6B-1³ Not representative of long-term performance
- Core 6B-2⁴ Excessive sand also effect strength

Figures 3-47 to 3-52 show the seal application to the cracked bridge deck.



Figure 3-47: Mixing sealer materials



Figure 3-48: Cleaning the cracked deck



Figure 3-49: Applying sealers to the deck



Figure 3-50: Spreading the sealers



Figure 3-51: Sand spray



Figure 3-52: Sand spray by hand

Table 3-9: Sealant Test Results

Test Site #	Product	Components	Viscosity (cps)	Elongation (%)	Curing time (hr)	Skid Ave.	Tensile strength Ave. (lbf.)
TS -1	1	2 part Epoxy	30	5.5	2-3	62	1,591
TS -2	2	3 part Methacrylate	5-20	40-50	4-6	37	2,363
TS -3	3	2 comp Methacrylate	5-15	5.5	1	22	1,276
NA*	4	2 comp Methacrylate	1100-1500	220-300		---	---
TS -5	5	3 part Methacrylate	14-15	20	4-6	37	1,731
NA*	6	3 part Methacrylate	14-15	30	6	---	---
TS -6	7	Epoxy	80	60	2	50/7 4	2,236/ 2,240
TS-4	Control	No sealer applied				48	2,290

*Not applied

The average penetration of the material in the cracks ranged from 0.5 to 1 inch. However, because of the different crack widths, the information should not be used for direct comparison of the materials. All materials appear to have acceptable penetration. From the Field test and the lab results it was decided to perform a secondary lab test on the crack sealer products with the following results as shown in Table 3-10.

Table 3-10: Tensile Testing of Deck Sealers

Manufacturer's Data				Lab Test Data (7/29/10)		Lab Test Data (12/8/10)	
Product	Tensile Strength (MPa)	Viscosity (cps)	Elongation (%)	Tensile Strength (MPa)	Elongation (%)	Tensile Strength (MPa)	Elongation (%)
1-A	56.4	5-15	5.5	22.6	2.1	25.3	2.6
2-B	19.3	5-20	40-50	0.9	99.6	7.3	17.2
3-C	41.0-48.0	30	3-7	23.4	10.5	27.2	N/A
4-D	6.9	80	60	3.36	213	5.5	102
5-E	8.2	10-25	30	No test	No test	5.7	1.3

Tables 3-11 through 3-15 present the results of the load and crack widths for the tested slabs.

Table 3-11: Results for Control Slab Test

SAMPLE	LOAD (kips)	CRACK Cond.
CONTROL	0	N/A
CONTROL	1	N/A
CONTROL	2	N/A
CONTROL	3	N/A
CONTROL	4	Micro
CONTROL	5	Micro
CONTROL	6	Center
CONTROL	7	right/left

$f_c=7,966$ psi (avg)

Table 3-12: Results for Slab Load Test and Crack Width Test (First Slab Set)

SAMPLE	LOAD (kips)	HALF CRACK(0.01") Test 1		HALF CRACK(0.01") Test 2		CRACK Cond.	PEAK LOAD (lbf)	
		Width	Bond	Width	Bond		Test 1	Test 2
1-A	0	0	1	0	1	1		
1-A	1	0	1	0	1	1		
1-A	2	0.02	1	0.02005	1	1		
1-A	3	0.03	1	0.03003	1	1		
1-A	4	0.04	1	0.04006	2	2		
1-A	5	0.05	1	0.06003	3	3		
1-A	6	0.07	1	0.09002	3	3		
1-A	7	0.08	1	0.1	3	3	7875	
1-A	8	0.1	1	0.106	3	3		
1-A	9					3		9219
1-B	0	0	1	0	1	1		
1-B	1	0	1	0	1	1		
1-B	2	0.008	1	0.01	1	1		
1-B	3	0.009	1	0.02004	2	1		
1-B	4	0.01	2	0.03001	2	1		
1-B	5	0.01	2	0.03008	2	2		
1-B	6	0.01002	2	0.04005	2	3		
1-B	7	0.01002	3	0.05001	3	4		
1-B	8	0.01003	3	0.05008	3	4	8002	
1-B	9					4		9604

Notes:

Full cracks extend along the entire width of the slab or 18 inches long, and the widths of the cracks are 0.01 in. (3mm) and 0.02 in. (6mm).

Half cracks are 9 inches long and 0.01 in. (3mm) wide

1-A,B BASF

2-A,B C.M.

3-A,B Pilgrim

4-A,B Unitex

Table 3-13: Results for Slab Load Test and Crack Width Test (Second Slab Set)

SAMPLE	LOAD (kips)	HALF CRACK(0.01") Test 1		HALF CRACK(0.01") Test 2		CRACK Cond.	PEAK LOAD (lbf)	
		Width	Bond	Width	Bond		Test 1	Test 2
2-A	0	0	1	0	1	1		
2-A	1	0.01	2	0.01	1	1		
2-A	2	0.01006	4	0.01009	1	1		
2-A	3	0.02003	4	0.02006	1	1		
2-A	4	0.04001	4	0.03003	2	2		
2-A	5	0.06002	4	0.05	2,3	3		
2-A	6	0.06008	3,4	0.08006	3	3		
2-A	7	0.09002	3	0.09005	4	4	7153	
2-A	8	0.101004	3,4	0.101007	4	4		
2-A	9			0.103005	4	4		9180
2-B	0	0	1	0	1	1		
2-B	1	0.01003	1	0.001	1	1		
2-B	2	0.01007	1	0.002	1	1		
2-B	3	0.02004	1	0.01	1	1		
2-B	4	0.03006	1	0.03	1	1		
2-B	5	0.04002	1	0.05002	1	1		
2-B	6	0.05002	2	0.08001	2	2		
2-B	7	0.07004	2	0.103004	2	2		
2-B	8	0.103004	2	0.104001	2	2	8196	
2-B	9	0.106002	2	0.105007	2	2		10093

Notes:

Full cracks extend along the entire width of the slab or 18 inches long, and the widths of the cracks are 0.01 in. (3mm) and 0.02 in. (6mm).

Half cracks are 9 inches long and 0.01 in. (3mm) wide

- 1-A,B BASF
- 2-A,B C.M.
- 3-A,B Pilgrim
- 4-A,B Unitex

Table 3-14: Results for Slab Load Test and Crack Width Test (Third Slab Set)

SAMPLE	LOAD (kips)	HALF CRACK(0.01") Test 1		HALF CRACK(0.01") Test 2		CRACK Cond.	PEAK LOAD (lbf)	
		Width	Bond	Width	Bond		Test 1	Test 2
3-A	0	0	1	0	1	1		
3-A	1	0.008	1	0.002	1	1		
3-A	2	0.01002	1	0.004	1	1		
3-A	3	0.02005	1	0.005	1	1		
3-A	4	0.03002	1	0.01004	1	1		
3-A	5	0.04003	1	0.02009	1	1		
3-A	6	0.05005	2	0.04003	2	2		
3-A	7	0.07003	2	0.05007	2	2	7416	
3-A	8	0.102004	2	0.07003	2	2		
3-A	9			0.1006		2		9279
3-B	0	0	1	0	1	1		
3-B	1	0.002	1	0.002	1	1		
3-B	2	0.003	1	0.004	1	1		
3-B	3	0.004	1	0.005	1	1		
3-B	4	0.004	1	0.007	1	1		
3-B	5	0.006	2	0.009	1	1		
3-B	6	0.01007	2	0.01009	1	1		
3-B	7	0.02008	3	0.02008	2	2	7265	
3-B	8	0.04004	3	0.03004	3	3		
3-B	9			0.04008	3	3		9484

Notes:

Full cracks extend along the entire width of the slab or 18 inches long, and the widths of the cracks are 0.01 in. (3mm) and 0.02 in. (6mm).

Half cracks are 9 inches long and 0.01 in. (3mm) wide

- 1-A,B BASF
- 2-A,B C.M.
- 3-A,B Pilgrim
- 4-A,B Unitex

Table 3-15: Results for Slab Load Test and Crack Width Test (Fourth Slab Set)

SAMPLE	LOAD (kips)	HALF CRACK(0.01") Test 1		HALF CRACK(0.01") Test 2		CRACK Cond.	PEAK LOAD (lbf)	
		Width	Bond	Width	Bond		Test 1	Test 2
4-A	0	0	1	0	1	1		
4-A	1	0.002	1	0.003	1	1		
4-A	2	0.002	1	0.005	1	1		
4-A	3	0.003	1	0.01003	1	1		
4-A	4	0.003	2	0.01009	1	1		
4-A	5	0.007	2	0.02001	2	2		
4-A	6	0.01008	2	0.03002	2	2		
4-A	7	0.02	2	0.04003	2	2,3		
4-A	8	0.03	3	0.07003	3	4	8388	
4-A	9	0.04	3	0.08007	4	4		10357
4-B	0	0	1	0				
4-B	1	0.005	1	0.009				
4-B	2	0.006	1	0.01004				
4-B	3	0.01002	1	0.02004				
4-B	4	0.02003	1	0.03003				
4-B	5	0.04006	2	0.04005				
4-B	6	0.05001	2	0.05003				
4-B	7	0.06008	4	0.06008				
4-B	8	0.07004	4	0.101003			8009	
4-B	9			0.102006				10645

Notes:

Full cracks extend along the entire width of the slab or 18 inches long, and the widths of the cracks are 0.01 in. (3mm) and 0.02 in. (6mm).

Half cracks are 9 inches long and 0.01 in. (3mm) wide

- 1-A,B BASF
- 2-A,B C.M.
- 3-A,B Pilgrim
- 4-A,B Unitex

4. FINITE ELEMENT ANALYSIS OF SLAB

4.1. FINITE ELEMENT MODEL OF SLABS

A model was developed to capture the behavior of experimental concrete slabs without cracks, with cracks and with sealed cracks. Various factors influence the performance of concrete on bridges, for example: loading conditions, allowed deflection limits and support systems among others. To address this issue, all factors that have a significant influence on bridge deck cracking must be carefully considered. This research investigates the many reasons of the increase of transverse cracks including deflection, temperature effects, the effect of secondary loads and concrete material properties. The developed model will be used to better understand the effect of different parameters.

4.1.1. SPECIMEN DIMENSIONS

Experimental testing was conducted in the laboratory to investigate the deflection of specimens without cracks, with cracks and with sealed cracks. Figures 4-1 and 4-2 show the geometry of the control slab, and the slab with cracks. The slab with the induced cracks (Figure 4-2) was sealed with the experimental material and tested.

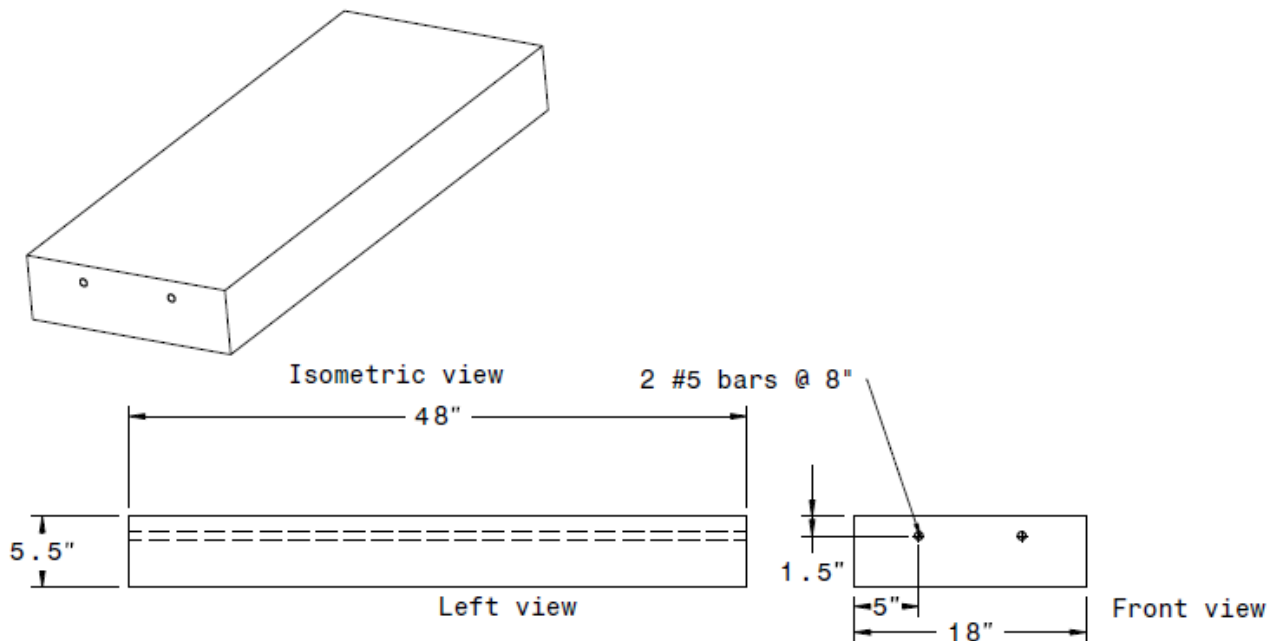


Figure 4-1: Control slab dimensions

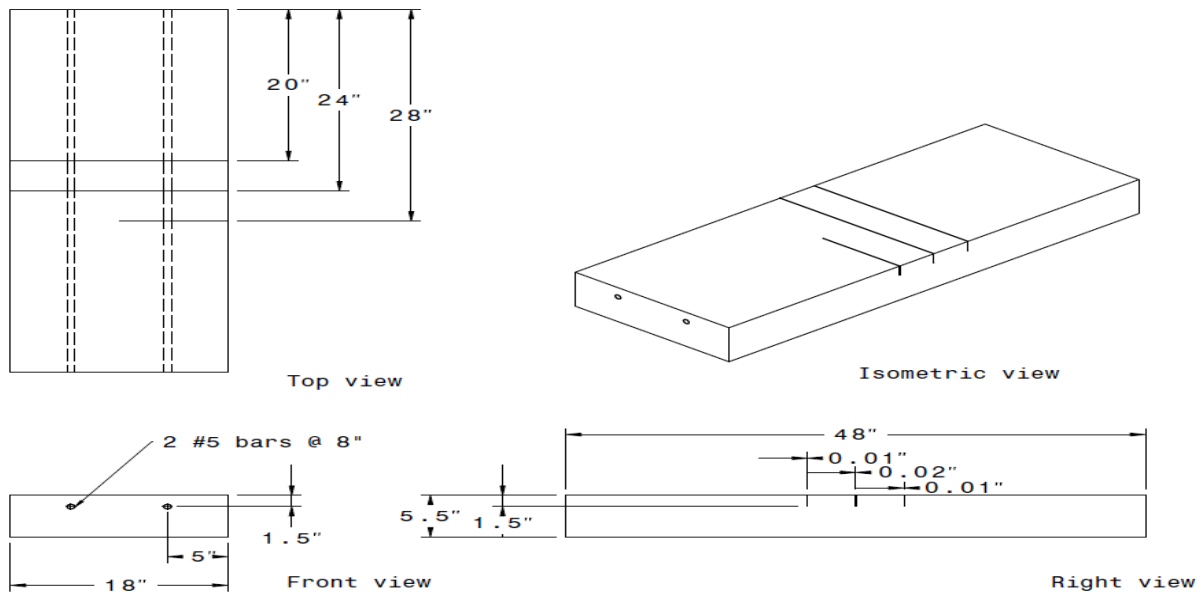


Figure 4-2: Slab with induced cracks

Both slabs were tested to a load of approximately 7,800 lbs. The slabs were carefully observed to capture the load when cracking started.

4.1.2. MODELING

The numerical analysis was conducted using ANSYS Parametric Design Language. Beam and solid elements were used to model the rebar, concrete, and sealant material. The reinforcing bars were modeled using BEAM189 elements that include special features of plasticity, creep, large deflection and strain. BEAM189 is a quadratic 3-D 3-Node Beam that has 6 degrees of freedom. The concrete was modeled using SOLID65 elements that are specifically designed to model concrete. SOLID65 is a 3-D 8-Node Reinforcing Concrete Solid that includes special features of cracking, crushing, plastic deformation and creep. The sealant material was modeled using SOLID185 elements. SOLID185 is a 3-D 8-Node Structural Solid that includes special features of elasticity, plasticity and nonlinear stabilization. In addition, BEAM189, SOLID65 and SOLID185 elements are capable of running nonlinear analyses. The developed models were thus capable of running a nonlinear analysis to take into consideration the concrete material nonlinearity.

The SOLID65 element can capture concrete cracking. As the concrete cracks, the results display first crack denoted by a red circle outline, the second crack denoted with a green outline and the third crack denoted with a blue outline. ANSYS however, does not indicate the depth or width of the crack. While ANSYS does not directly report the load that causes the first crack, this load may be evaluated using the load substep numbers and load step time elapsed. The ANSYS results; nonetheless provides us with important information to approximate cracking load, location and depth of the crack. The developed model had a hybrid mesh that maintained full connectivity of the nodes to ensure that the rebar and the concrete are in complete contact.

The control slab was modeled using 1" BEAM189 and 1" SOLID65 elements. The model contained 6,613 nodes, 96 BEAM189 elements and 5,280 SOLID65 elements. Figure 4-3 shows the mesh detail of the control slab.

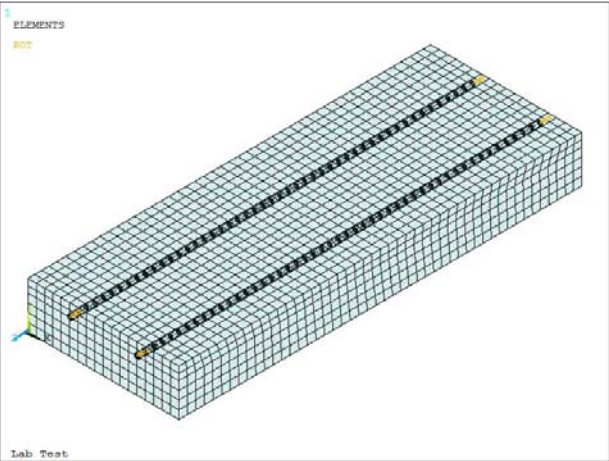


Figure 4-3: Control slab mesh detail

The slab with the induced crack was also modeled using 1" BEAM189 elements and 1" SOLID65 elements. This model was approached a little differently due to the need of a refined mesh around the induced crack region. The geometry was constructed from key points which forced nodes at the location of the key points. This method improved meshing because the geometry can now be volume swept as opposed to being meshed freely. The model contained 20,338 nodes, 198 BEAM189 elements and 17,280 SOLID65 elements. Figure 4-4 shows the mesh detail of the slab with induced crack.

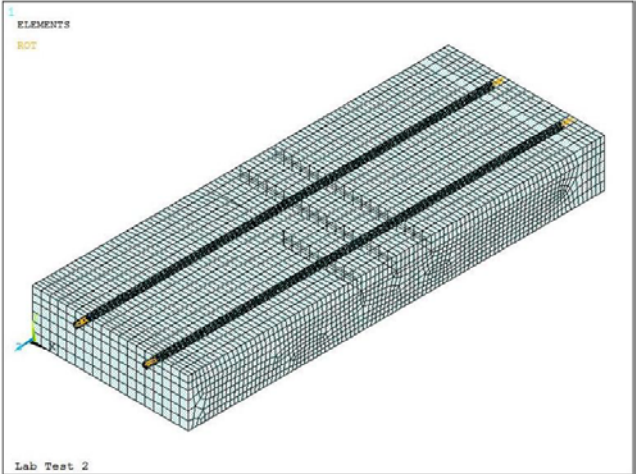


Figure 4-4: Slab with induced crack mesh detail

4.1.3. ANALYTICAL STUDY

The immediate deflection of the concrete slab was calculated in accordance with ACI (318) 9.5.2.3 utilizing the effective moment of inertia I_e as calculated using the following equation, but

not greater than the gross moment of inertia of the concrete section I_g (American Concrete Institute, 2008):

$$I_e = \left(\frac{M_{cr}}{M_a}\right)^3 I_g + \left[1 - \left(\frac{M_{cr}}{M_a}\right)^3\right] I_{cr} \quad (\text{Equation 4-1})$$

where

$$M_{cr} = \frac{f_r I_g}{y_t} \quad (\text{Equation 4-2})$$

and

$$f_r = 7.5\lambda\sqrt{f'_c} \quad (\text{Equation 4-3})$$

The modulus of elasticity for concrete, E_c , as identified in ACI 8.5.1 was computed as follows:

$$E_c = 57,000\sqrt{f'_c} \quad (\text{Equation 4-4})$$

The slabs without and with cracks have a concrete compressive strength, f'_c , of 4,775 psi. This strength was used in the deflection analysis and deflection parametric study. The additional parameters were analyzed using an ultimate compressive strength of 4,000 psi, at different ages of the concrete. The following concrete properties were used for the 3, 7, 14, and 28 day strength, as shown in Table 4-1.

Table 4-1: Concrete Material Properties

Time (days)	f'_c	E_c	f_r
3	2,160	$2,649 \times 10^3$	348.6
7	3,080	$3,163 \times 10^3$	416.2
14	3,652	$3,445 \times 10^3$	453.2
28	4,000	$3,605 \times 10^3$	474.3

4.1.4. LOADING

Numerous loading parameters were modeled for this research. The deflection of the slabs, a deflection parametric study and secondary loads were covered. The secondary loads include the temperature effect due to hydration, temperature, shrinkage, and creep. The effect of hydration was modeled by applying a 68°F uniform temperature load to the slab. The temperature effect was modeled by applying an 85°F increase in temperature to the slab. Shrinkage was modeled by applying a strain due to shrinkage to the slab. The strain was uniform throughout the depth of the slab. The proposed shrinkage formula established by Tadros, Al-Omaishi, Seguirant and Gallt (2003) was used to define the strain due to shrinkage:

$$\varepsilon_{sh} = 480 * 10^{-6} \gamma_{sh} \quad (\text{Equation 4-5})$$

where

$$\gamma_{sh} = k_{td}k_s k_{hs}k_f \quad (\text{Equation 4-6})$$

and

$$k_{td} = \frac{t}{61 - 4f'_{ci} + t} \quad (\text{Equation 4 - 7})$$

$$k_s = \frac{1064 - 94\frac{V}{S}}{735} \quad (\text{Equation 4 - 8})$$

$$k_{hs} = 2.00 - 0.0143H \quad (\text{Equation 4 - 9})$$

$$k_f = \frac{5}{1 + f'_{ci}} \quad (\text{Equation 4 - 10})$$

where; k_{td} is the time development factor, f'_{ci} is the specified compressive strength of concrete at time of loading for nonprestressed members and is taken as $0.8f'_c$, t is maturity of concrete in days, k_s is the factor for the effect of the volume-to-surface area ratio of the component, V is the volume of concrete, S is the surface area of concrete, k_{hs} is the humidity factor for shrinkage, H is the relative humidity in percent and is taken as 70% for the Florida region and k_f is the factor for the effect of concrete strength.

Creep was modeled by applying a strain and was only taking the effect of the dead load in to account. The creep strain was evaluated using the product of the creep coefficient and strain due to dead load. The proposed creep formula established by Tadros, Al-Omaishi, Seguirant and Gallt (2003) was used to define the creep coefficient:

$$\psi(t, t_i) = 1.9\gamma_{cr} \quad (\text{Equation 4 - 11})$$

where

$$\gamma_{cr} = k_{td}k_{la}k_s k_{hc}k_f \quad (\text{Equation 4 - 12})$$

and

$$k_{td} = \frac{t}{61 - 4f'_{ci} + t} \quad (\text{Equation 4 - 13})$$

$$k_{la} = t_i^{-0.118} \quad (\text{Equation 4 - 14})$$

$$k_s = \frac{1064 - 94\frac{V}{S}}{735} \quad (\text{Equation 4 - 15})$$

$$k_{hc} = 1.56 - 0.008H \quad (\text{Equation 4 - 16})$$

$$k_f = \frac{5}{1 + f'_{ci}} \quad (\text{Equation 4 - 17})$$

where; k_{td} is the time development factor, f'_{ci} is the specified compressive strength of concrete at time of loading for nonprestressed members and is taken as $0.8f'_c$, t is maturity of concrete in days, k_{la} is the loading factor, t_i is the age of concrete at time of load application, k_s is the factor for the effect of the volume-to-surface area ratio of the component, V is the volume of concrete, S is the surface area of concrete, k_{hc} is the humidity factor for creep, H is the relative humidity in percent and is taken as 70% for the Florida region and k_f is the factor for the effect of concrete strength.

4.1.5. RESULTS

As stated, the parameters used in this research include deflection, a deflection parametric study and secondary loads. The secondary loads include hydration, temperature, shrinkage and creep. Results on each area are discussed in the following:

Deflection

Prior to comparing the experimental against numerical results, Figure 4-5 shows a graph of the analytical and numerical deflection of the slabs. This graph shows that the analytical and numerical deflections closely follow the same path in the elastic region until the material yields. After the material has yielded, the deflection for both the analytical and numerical analysis continues with a comparable slope. In addition to the deflection, the experimental and numerical cracking loads of the concrete slab were compared to each other. The crack initiation load for the experimental slab occurred at 4,800lbs and the average load the crack propagated at occurred at 5,500lbs. The average load that propagation occurred at for the simulated slab occurred at 5,400lbs. Figures 4-6 and 4-7 show the cracks for the experimental concrete slab and the simulated model, respectively. The experimental results, however, follows a different path in the elastic region and then continues with a similar slope after the material has yielded.

The slab was modeled given the same constraints as the experimental test. The slab was constrained in the vertical direction and free to move at one support in the horizontal direction. Due to the nature of the test setup the slab was flipped such that the tension side is faced up so that the cracking can be viewed during testing. Figure 4-8 shows an image of the test setup.

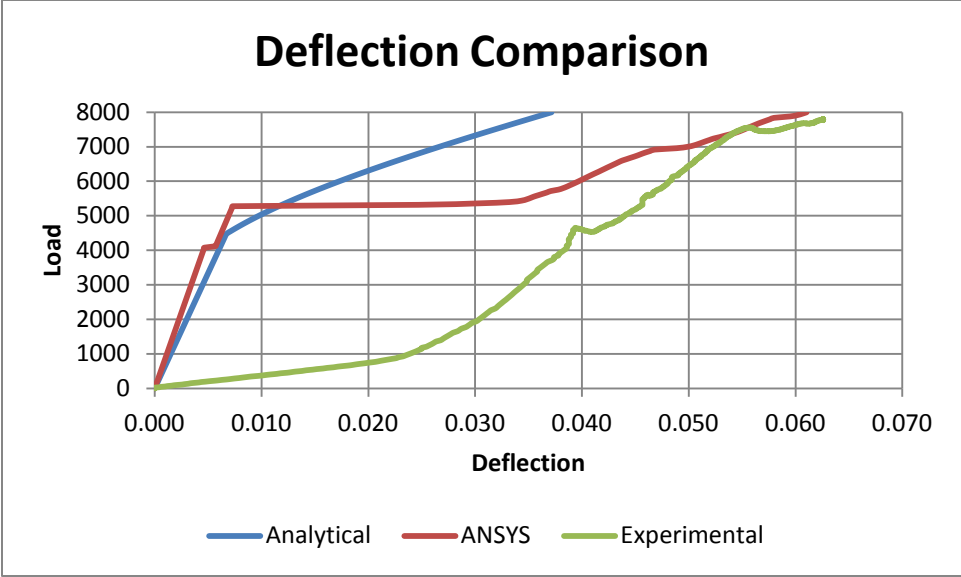


Figure 4-5: Control slab deflection comparison



Figure 4-6: Control slab cracking

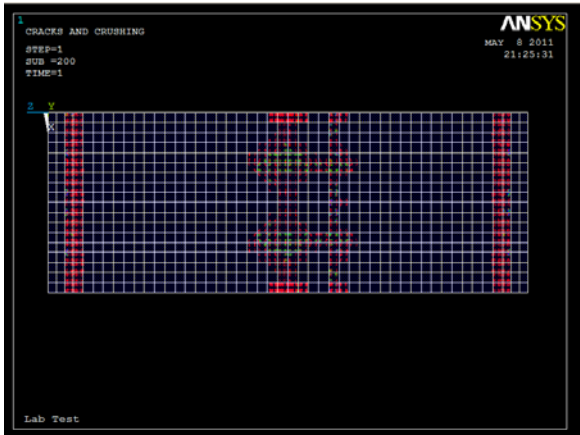


Figure 4-7: ANSYS simulation cracking



Figure 4-8: Test setup

From Figures 4-6 and 4-7, it can be seen that the cracks of both the simulated model and experimental model are in the approximate locations. Figure 4-9, shows the deflection comparison between the slab with induced crack and the numerical model with induced crack. The deflections in Figure 4-9 indicate that both specimens have reduced stiffness compared to the analysis of the control slab. This behavior is expected since the slab has an induced crack; hence, the inertia has decreased. The slopes for both deflections are also comparable.

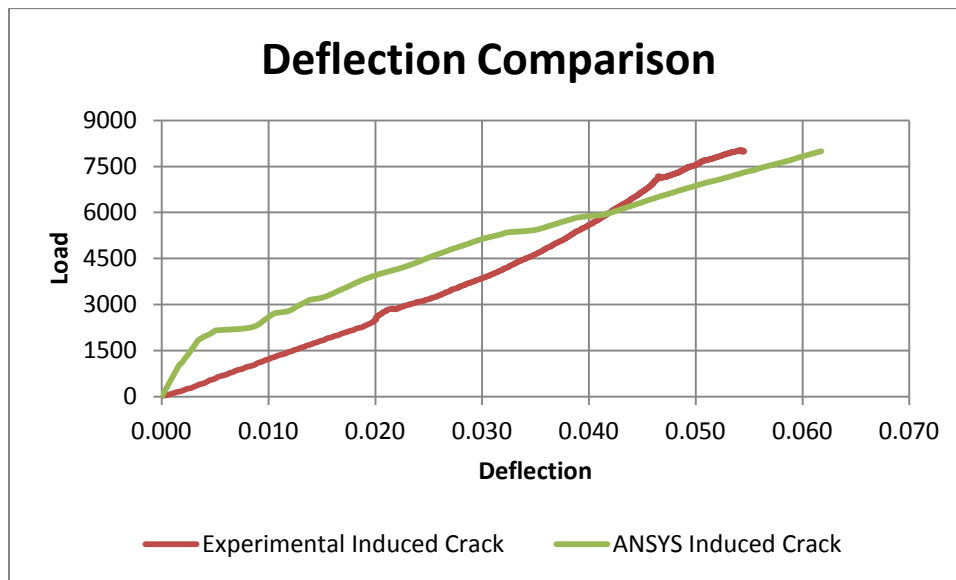


Figure 4-9: Induced crack deflection comparison

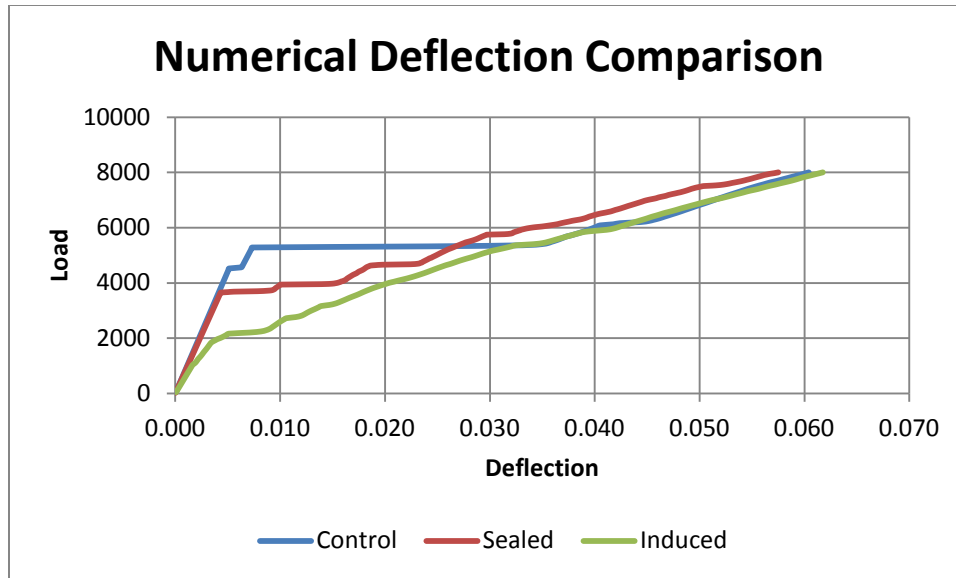


Figure 4-10: Numerical analysis deflection comparison

Figure 4-10 shows a graph of the numerical analysis of the control slab, slab with induced crack and sealed slab. As seen, the slab with induced crack has a smaller slope compared to the control slab. This is due to the reduced inertia of the cross section. The slab with induced crack follows this path until the control slab cracks and both slabs continue with comparable slope. The slab with sealed crack implies that stiffness would be added to the slab with induced crack. The sealed slab has a slope greater than the slab with induced crack and less than the control slab. This means that the sealant material will provide some structural rigidity after the slab has cracked.

Deflection Parametric Study

A parametric study was conducted on the control slab to identify the number of cracks that will occur with respect to the deflection per unit length. This approach can then be used to predict when the slab will crack given then deflection. The ratio of deflection to length will be expressed as a percentage. Figure 4-11 shows a graph of the number of cracks versus the deflection per unit length. Figures 4-12 through 4-16 show the cracked slab after each new crack has occurred.

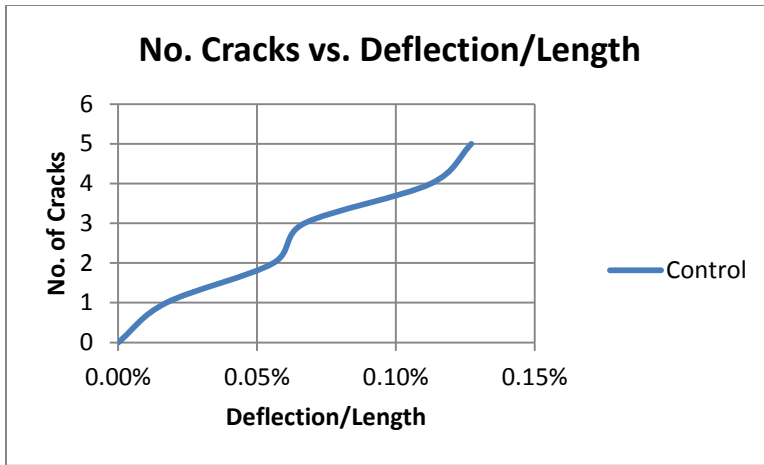


Figure 4-11: Cracks vs. deflection/length

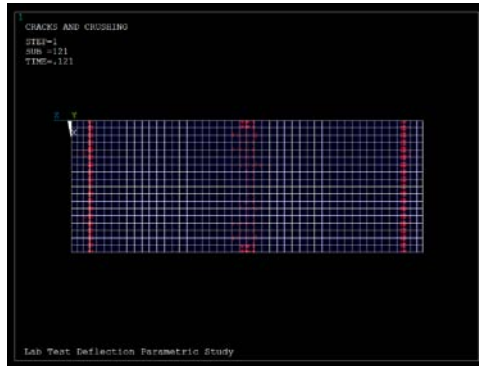


Figure 4-12: Crack 1

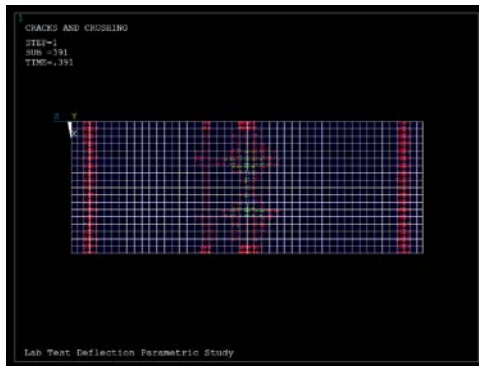


Figure 4-13: Crack 2

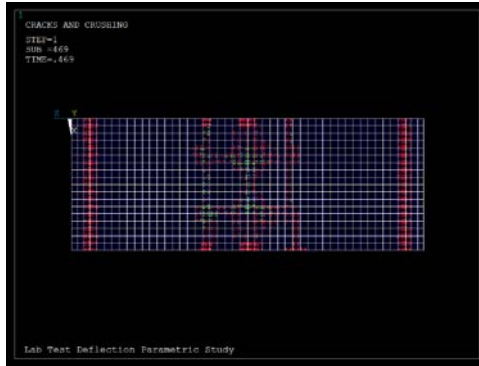


Figure 4-14: Crack 3

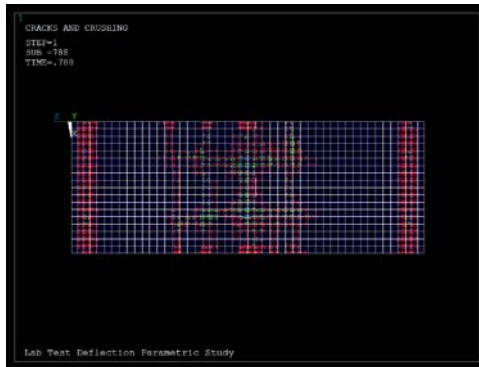


Figure 4-15: Crack 4

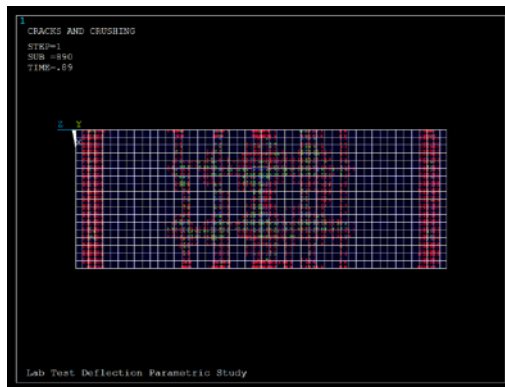


Figure 4-16: Crack 5

Secondary Loads – Hydration

The temperature effect of hydration was modeled by applying a 68°F uniform temperature load to the slab. The tensile stresses were developed on the tension side of the slab. The stresses did not exceed the cracking stress and no cracking occurred due to hydration.

Secondary Loads – Temperature

The temperature effect was modeled by applying an 85°F increase in temperature to the slab. Figures 4-17 through 4-20 show the tensile stresses develop in the slab at 3, 7, 14, and 28 days, respectively. The constraints of this model are different to that of the deflection as described

earlier. The tension side of the slab is to the bottom; hence the reinforcement is to the bottom. The slab is constrained at the bottom at two locations for an effective length of 42 inches in the vertical direction and is free to move at one support in the horizontal direction. This setup better resembles the constraints of a simple supported bridge and will provide practical results to view. The temperature effect at 3, 7, 14, and 28 days yields tensile stresses on the top of the slab; however, these tensile stresses are not capable of producing cracking on the deck.

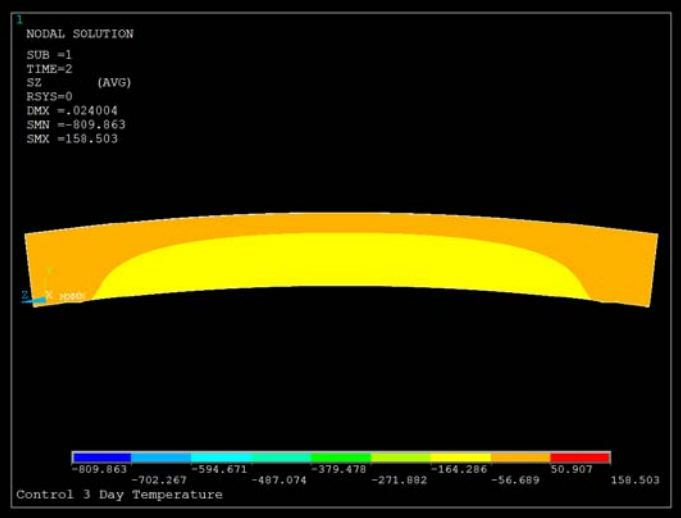


Figure 4-17: Control 3-day temperature effect stress distribution

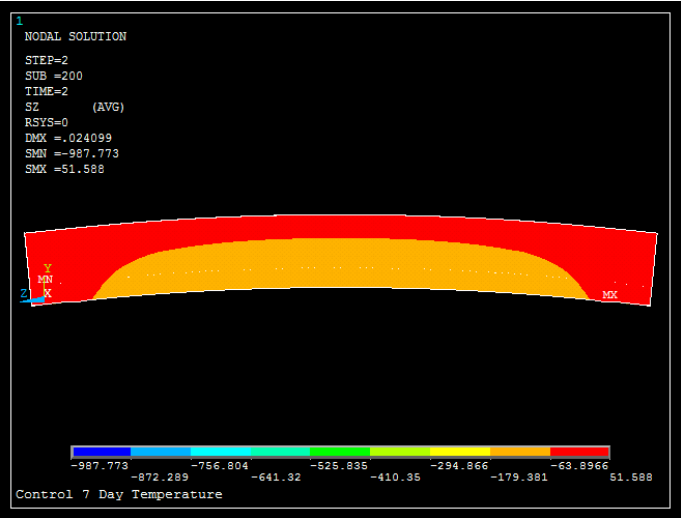


Figure 4-18: Control 7-day temperature effect stress distribution

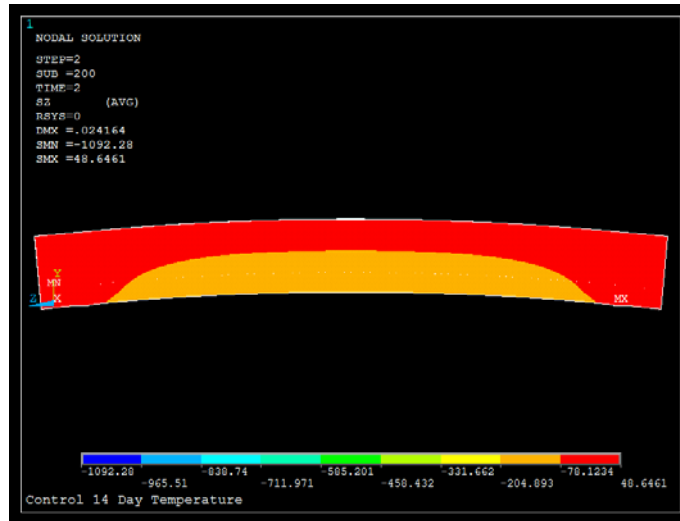


Figure 4-19: Control 14-day temperature effect stress distribution

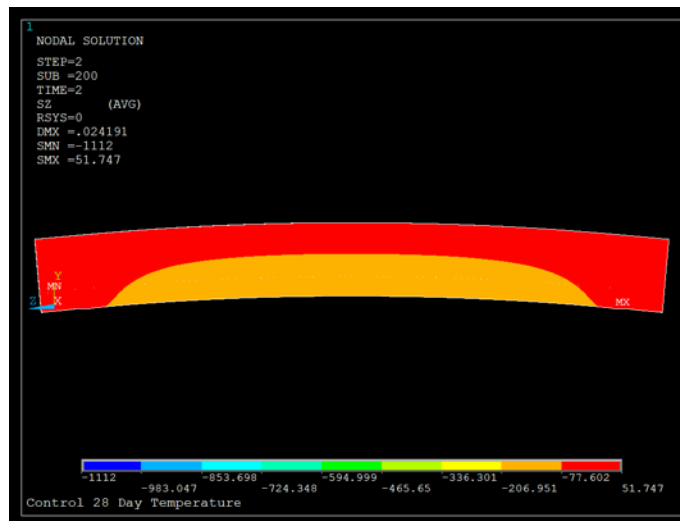


Figure 4-20: Control 28-day temperature effect stress distribution

Shrinkage

As stated, the effect of shrinkage was modeled by applying a strain to the slab. The stress incurred on the model due to shrinkage was found to be much smaller than the cracking stress. Tensile stresses were initially developed on the top of the deck at 3 and 7 days. At 14 and 28 days, it can be observed that tensile stresses begin to develop on the top of the deck. It can be concluded that, as the concrete ages the tensile stresses developed on the top of the slab increases with time. It can also be noted that the tensile stress in the deck will be greater for a higher concrete compressive strength. Figures 4-21 through 4-24 show the stress distribution of the deflected model due to shrinkage at 3, 7, 14 and 28 days for the control slab. As a result, shrinkage does not produce transverse cracks on the model during the curing period.

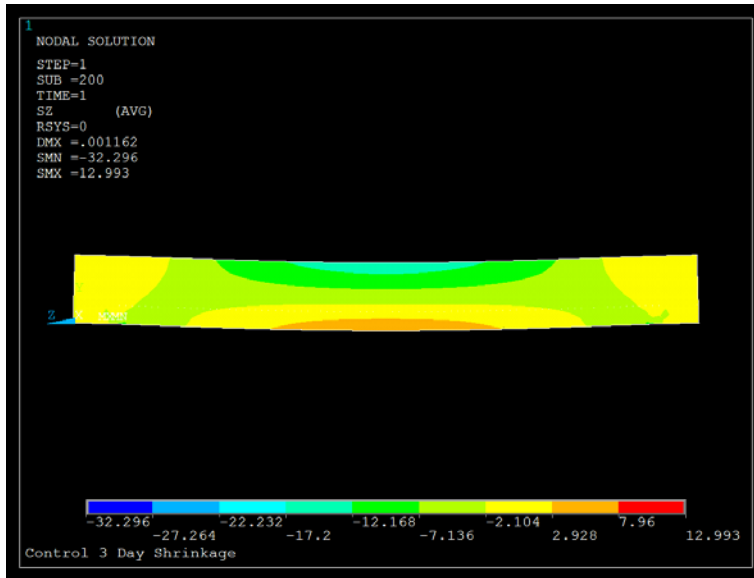


Figure 4-21: Control 3-day shrinkage effect stress distribution

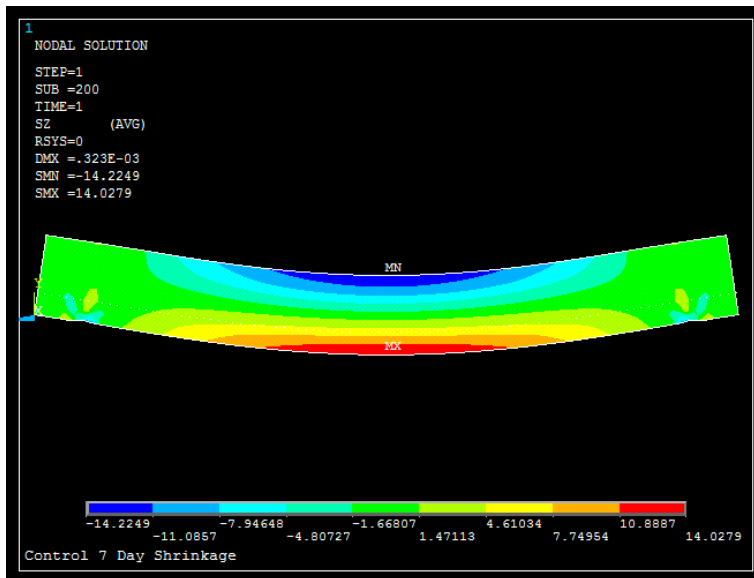


Figure 4-22: Control 7-day shrinkage effect stress distribution

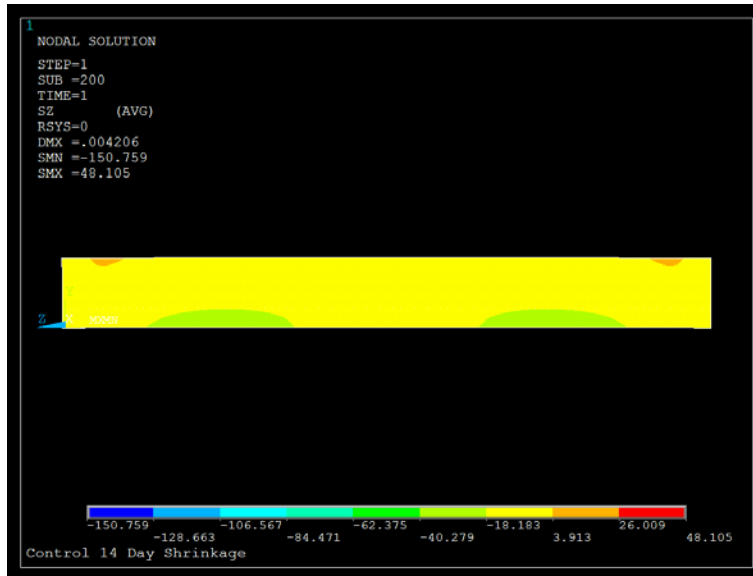


Figure 4-23: Control 14-day shrinkage effect stress distribution

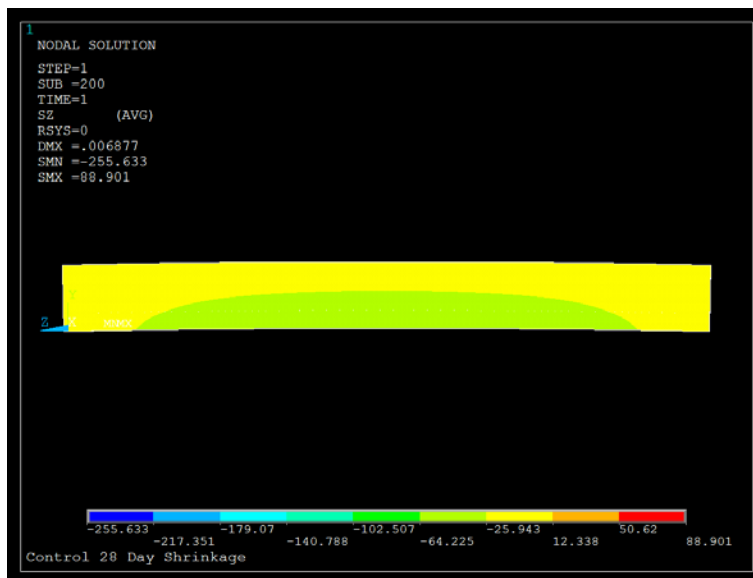


Figure 4-24: Control 28-day shrinkage effect stress distribution

Creep

Creep was also modeled by applying a strain to the slab. The tensile stress results are much smaller than the shrinkage results. The deflected shape is opposite to the shrinkage results and bows downward. This behavior is expected during the curing period and follows the premise that creep strains tend to counteract the effect of shrinkage (Saadeghvaziri and Hadidi, 2002).

5. FINITE ELEMENT ANALYSIS OF FULL BRIDGE

5.1. SCOPE

The objective of this study is to perform finite element modeling, analyses, and discussion of Florida department of transportation (FDOT) Steel Girder Bridges in order to limit the development of transverse bridge deck cracking. Many parameters may affect the performance of steel girder bridge such as; load patterns, load magnitudes, deflection limits, bridge span length, bridge continuity, structural system, and others. It was crucial to identify all of parameters that have a major effect on the development of transverse deck cracking. The effect of parameters which were expected to significantly affect the performance and deck cracking of this type of bridges, were examined. The presented study examines the effect of several parameters on the development of transverse cracking in bridge decks including the effect of creep, shrinkage, thermal expansion, strength of concrete, deck thickness, bridge spans, bridge continuity, traffic load and load patterns, and boundary conditions.

5.2. SELECTION OF BENCHMARK BRIDGE AND MODELING

The analytical part of the project consisted of five tasks. After looking at a number of FDOT bridge drawings, a benchmark bridge (Figure 5-1) was selected. The bridge has reinforced concrete (RC) bridge deck, which is 8.5 inch thick, and supported by four steel plate girders. The spacing between girders is 11'-3". The span of the bridge is 184 ft. The selected bridge was altered to cover different parameters of interest (number of spans, span length, deck aspect ratio, etc.).

5.3. MODELLING

Modeling of the benchmark bridge took place first. A 3-D finite element model of the bridge was completed. The model includes a 3-D finite element model of RC deck and steel I-girders. The steel plate girders of A992 steel were modeled using shell elements (Figure 5-2). The shell elements are four-node quadrilateral elements. The shell elements were used to model top and bottom flanges and the web as well (Figure 5-3, Figure 5-4, and Figure 5-5). Each flange was modeled using a large number of shell elements; elements were in the longitudinal direction and in the transverse direction. Each web was modeled using shell elements ensuring compatibility with flanges. Since the objective of the study is to investigate the tendency of bridge decks to develop transverse cracks, the RC bridge deck was modeled more accurately using 8-node solid element (Figure 5-6). Fifteen elements were used in the longitudinal direction and 6 elements were used between girder flanges. It is important to note that the same distribution and number of elements used to model girder flanges were used to model the parts of deck above flanges to ensure joint connectivity and compatibility. All of what mentioned above was used to model a single span bridge, however, this was used to give an indication of type of elements used to model bridges with different geometry. It is important to examine the significance of parameters on the development of transverse deck cracking therefore it was necessary to include a large number of parameters in the study. The following parameters were expected to affect the behavior; therefore, the current study considered the effect of:

- Number of Spans
- Span Length
- Boundary Conditions
- Deck Thickness
- Bridge Continuity
- Concrete Compressive Strength
- Load Patterns
- Thermal Loads
- Shrinkage
- Creep

To include all of the above parameters, the properties of Benchmark Bridge were altered to produce models which are general enough to cover all of the listed parameters. Table 5-1 shows the main characteristics of bridge models developed to address the first six parameters of the above list; however, the remaining four parameters were examined in application of loads on bridge models. Load applied on bridge models were diverse enough to address all of the four remaining parameters which will be discussed later. The bridge models are denoted as Single-Span-N-4000-8.5-4, Two-Span-N-4000-8.5-4, Three-Span-N-4000-8.5-4, Two-Span-Half-4000-8.5-4, Three-Span-N-4000-8.5-7, Two-Span-N-4000-8.5-4-(F-F), Two-Span-N-4000-7-4, Two-Span-N-4000-8.5-4, Two-Span-N-5000-8.5-4, and Two-Span-N-7000-8.5-4. It is important to note that the generated models are 3-D finite element models as presented in Figure 5-8. Figure 5-9 presents side view of bridge models to show the end condition cases (pin-roller and fixed-fixed) included in the parametric study. In general, the produced bridge models addressed all of the listed parameters.

Table 5-1: Foremost Characteristics of Bridge Models

Model Nom enclature	Number of Spans	Span Length (ft)	Num ber of Girders	Deck Thickness (in.)	Concrete Com pressive Strength, fc' (psi)	End Conditions at Abutment Locations
Single-Span-N-4000-8.5-4	1	184'	4	8.5	4000	Pin-Roller
Two-Span-N-4000-8.5-4	2	184'	4	8.5	4000	Pin-Roller
Three-Span-N-4000-8.5-4	3	184'	4	8.5	4000	Pin-Roller
Two-Span-Half-4000-8.5-4	2	92'	4	8.5	4000	Pin-Roller
Three-Span-N-4000-8.5-7	3	184'	7	8.5	4000	Pin-Roller
Two-Span-N-4000-8.5-4-(F-F)	2	184'	4	8.5	4000	Fixed-Fixed
Two-Span-N-4000-7-4	2	184'	4	7	4000	Pin-Roller
Two-Span-N-4000-10-4	2	184'	4	10	4000	Pin-Roller
Two-Span-N-5000-8.5-4	2	184'	4	8.5	5000	Pin-Roller
Two-Span-N-7000-8.5-4	2	184'	4	8.5	7000	Pin-Roller

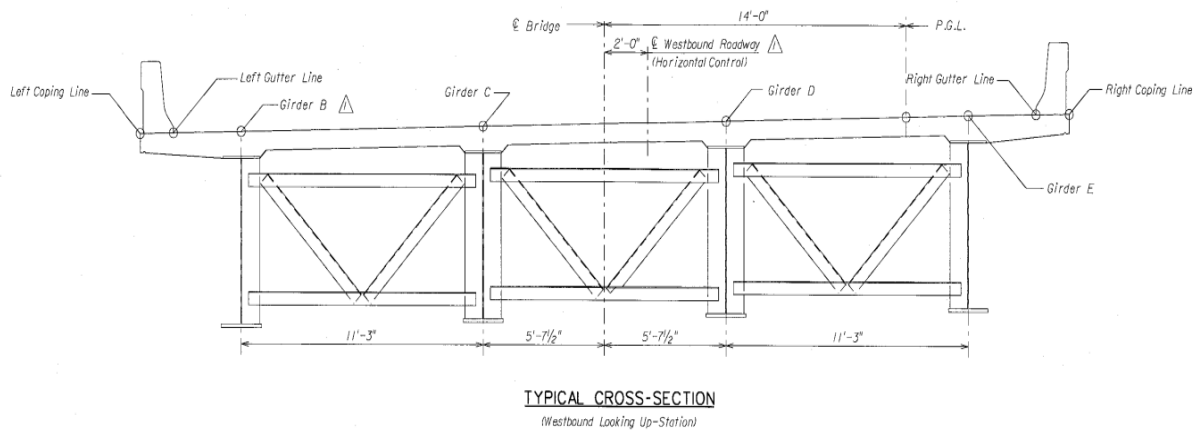


Figure 5-1: Benchmark Bridge cross section

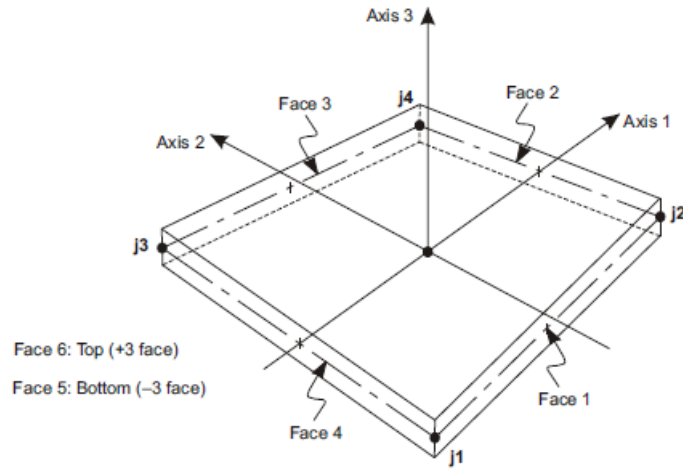


Figure 5-2: Four-node Shell element

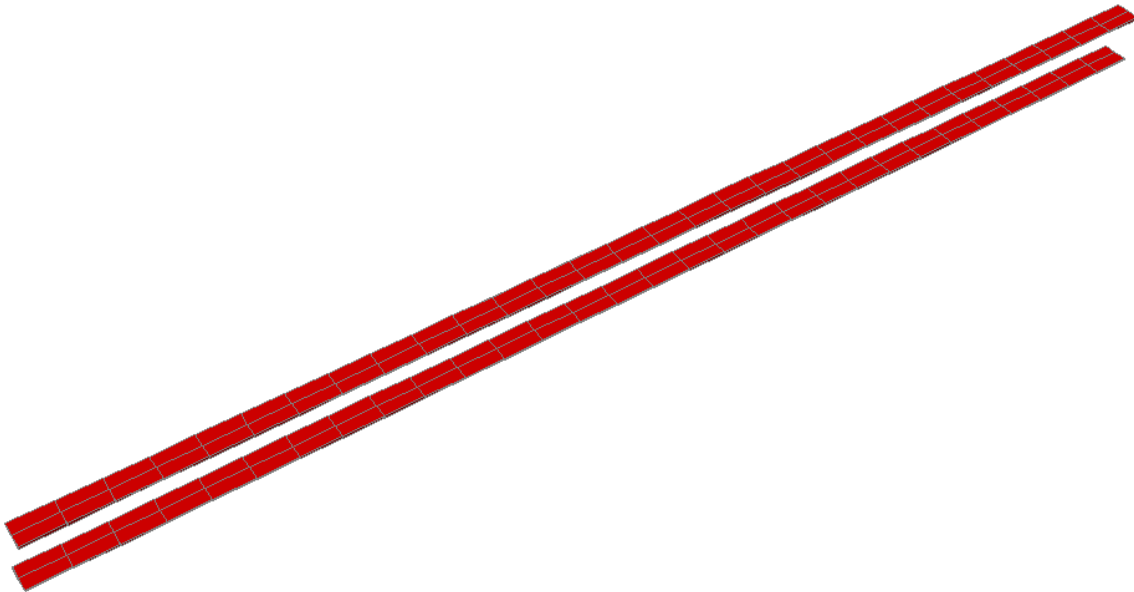


Figure 5-3: Top and Bottom Flanges modelled using Shell Elements

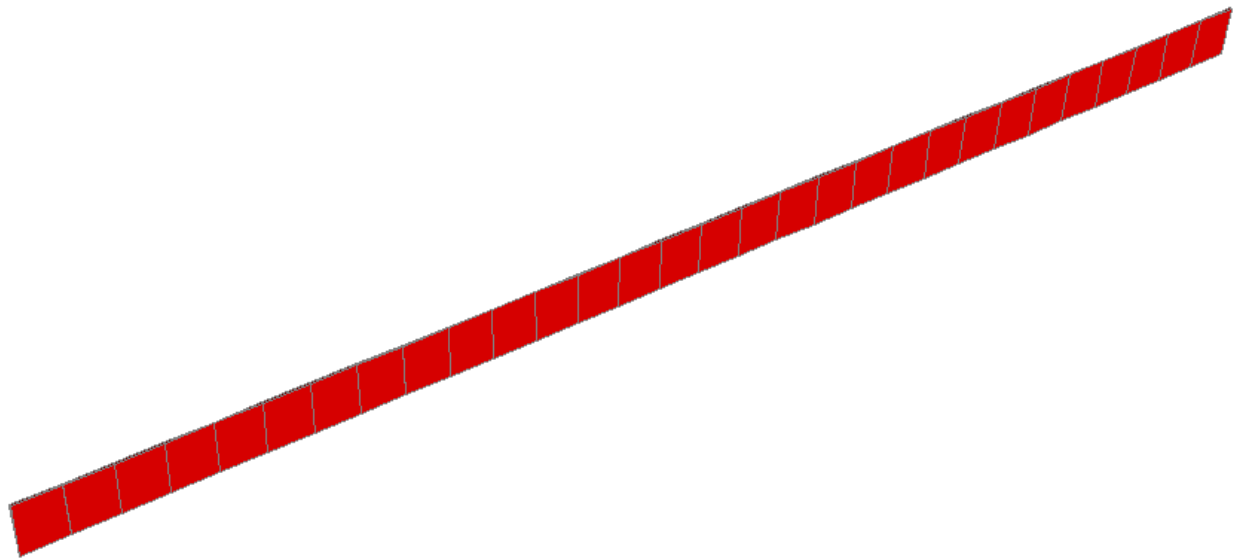


Figure 5-4: Web modelled using Shell elements

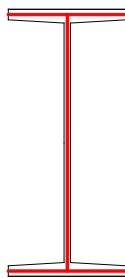
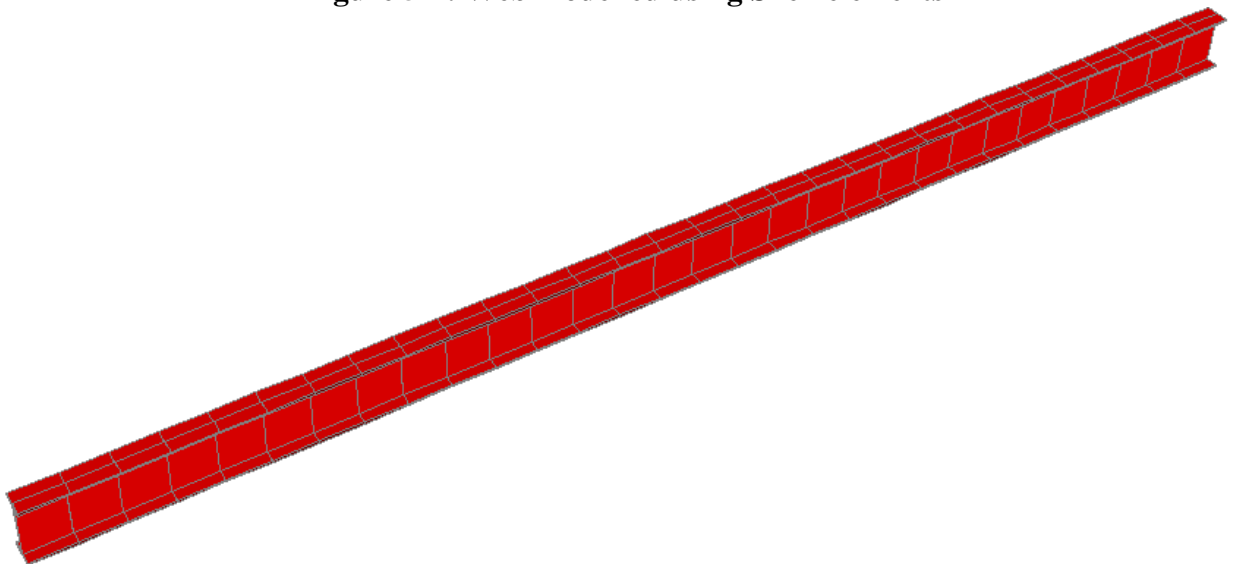


Figure 5-5: Modelling of Steel I-girder

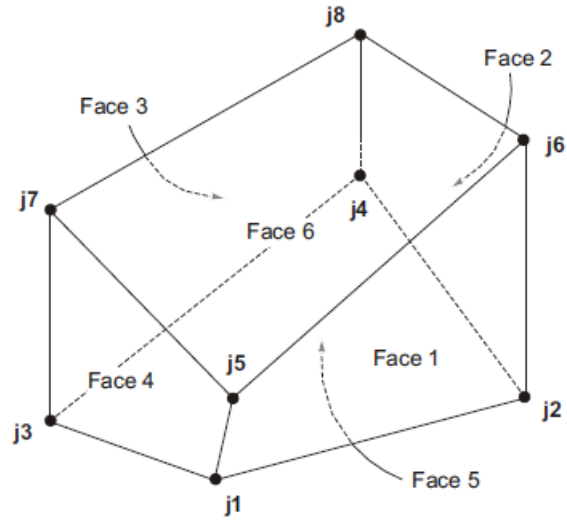


Figure 5-6: 8-node Solid element

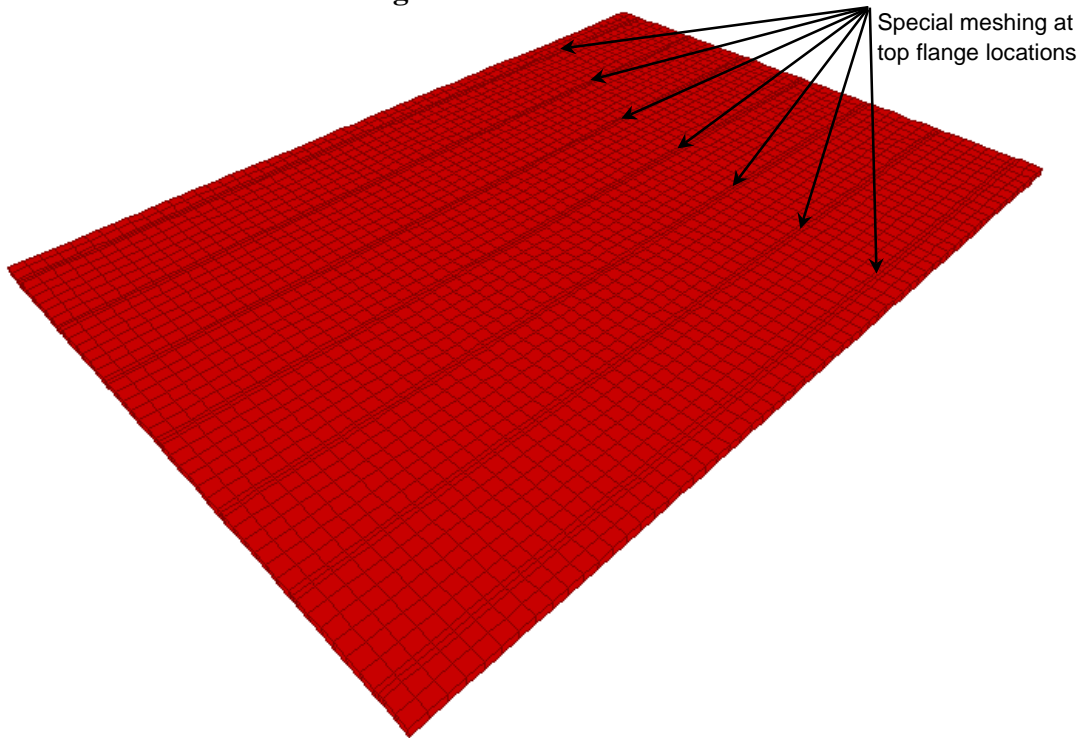


Figure 5-7: Modelling of RC bridge decks

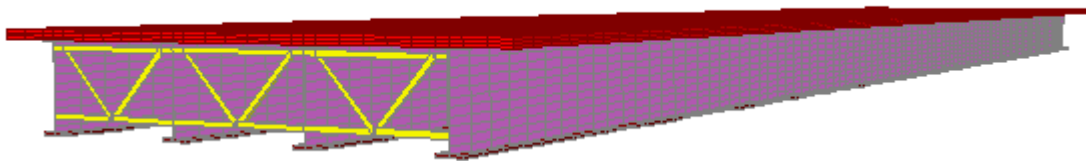


Figure 5-8: Typical 3-D bridge model

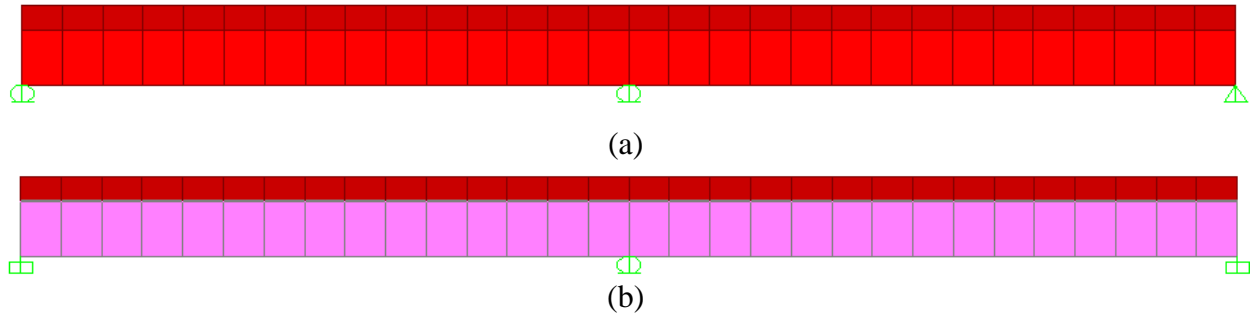


Figure 5-9: (a) Pin-roller condition and (b) Fixed-fixed condition

5.4. ANALYTICAL STUDY

Forty five 3-D finite element models were developed to address all of the parameters under study. The parameters were examined in light of the development of transverse deck cracking. Different load patterns were included in the analyses. The analysis was completed following the assumptions:

- The modulus of elasticity of concrete remains constant
- The modulus of elasticity of steel remains constant
- Stresses in concrete will not exceed the elastic limit
- Plane sections remain plane

As mentioned earlier, compressive strengths of concrete, f_c' , of 4000 psi, 5000 psi, and 7000 psi were studied. The ultimate concrete compressive strength of 4000 psi matches the strength used in the study conducted by Wan et al. (2010). Therefore, the same values of concrete compressive strength at different ages of concrete (3, 7, 14, and 28 days) were used (Table 5-2). The modulus of elasticity of concrete, E_c , was determined using the ACI 318-08 (2008) relationship for normal weight concrete. For this study, the transverse deck cracking was considered to occur once the longitudinal stress produced in bridge decks exceeds the modulus of rupture, f_r (Table 5-2).

$$E_c = 57000\sqrt{f_c'} \quad \text{(Equation 5-1)}$$

$$f_r = 7.5\sqrt{f_c'} \quad \text{(Equation 5-2)}$$

5.4.1. LOAD PATTERNS

Several load patterns were included in the study. Load patterns included dead load, increase in temperature due to hydration, temperature, shrinkage, creep, and truck loads. Only bridge deck was subjected to increase in temperature due to hydrations which was assumed to be 20 (68°F). The temperature load was taken as both increase and decrease in temperature of bridge deck and girders by 85°F. The effect of shrinkage was considered through applying the strain due to shrinkage on bridge decks. The strain was assumed to be constant throughout the total depth

of the bridge deck. The following equation developed by Saadeghvaziri and Hadidi (2002) was used to determine the strain due to shrinkage (ξ_{sh}) at different ages of concrete. The strain due to shrinkage was calculated as summarized in Table 5-3. Appendix D presents the calculation of strain due to shrinkage for all of bridge models under study.

$$\varepsilon_{sh} = -(1.2)k_{vs}k_{hs}k_fk_{td}(0.78 \times 10^{-3}) \quad (\text{Equation 5-3})$$

Where;

$$k_{vs} = 1.45 - 0.13(V/S) \geq 1.0$$

$$k_{hs} = 2.00 - 0.014H$$

$$k_f = \frac{5}{1 + f'_{ci}}$$

$$k_{td} = \frac{t}{61 - 4f'_{ci} + t}$$

Where; k_{vs} is a factor to consider the effect of volume-to-surface area ratio of concrete, V is the volume of concrete, S is the surface area of concrete, k_{vs} is a humidity factor, H is % of relative humidity, k_f is a factor to take into account the effect of concrete strength, f'_{ci} is the specified compressive strength of concrete at the time of initial loading (ksi). Tadros and Hadidi (2003) suggests the use of $0.80f'_c$. When this factor is calculated, k_{td} is a time development factor, and t is the maturity of the concrete (in days).

The effect of creep was considered with dead load only. To account for effect of creep, creep coefficient was calculated and was multiplied by the strain due to dead load to obtain the strain due to creep. The creep strain was applied to the bridge deck. The creep coefficient was calculated using PCA (1969) equations, as shown in Equation 5-4.

$$\psi_{(\infty,1)} = 3.5k_c k_f (1.58 - H/120)t_i^{-0.118} \left[(t - t_i)^{0.6} / (10 + (t - t_i)^{0.6}) \right] \quad (\text{Equation 5-4})$$

Where;

$$k_c = \left[\frac{\left(\frac{t}{26e^{0.36(V/S)_b} + t} \right)}{\left(\frac{t}{45 + t} \right)} \right] \left[\frac{1.80 + 1.77e^{-0.54(V/S)_b}}{2.587} \right]$$

$$k_f = \frac{1}{\left[0.67 + \frac{f'_c}{9} \right]}$$

Where; k_c is the volume-to-surface area factor, k_f is the concrete compressive strength factor, H is the % of relative humidity, t is the age of concrete at time of interest, t_i is the age of concrete when load is initially applied, e is natural log base (approximately 2.71828), f'_c is the specified compressive strength of concrete (ksi), V is volume of concrete, and S is the surface area of concrete. Appendix E presents the calculation of creep strains for all of bridge models under study.

The AASHTO LRFD HL-93 loading (Figure 5-10), which is either HS20 truck and lane load of 0.64 kip/ft. or tandem load and lane load of 0.64 kip/ft., was used to load the bridge models. The truck loading was applied at 14 days of age of concrete and was called construction load. Also, the truck loading was applied at 28 days of age of concrete while the bridge can be fully loaded at that stage. Figure 5-11 shows the bridge lane for truck loading.

Initially, truck loading was applied as a static load to produce maximum positive moment and maximum negative moment. For maximum positive moment, the truck load was positioned close to mid-span. However, for maximum negative moment, two adjacent spans were loaded with truck load at the same time to produce maximum negative moment at the intermediate support. It is important to note that the live load truck loading case followed the dead load case.

In order to accurately investigate the performance of bridge models, more accurate approach was introduced. Lanes for truck loads were defined for all of 3-D bridge models. The truck loads were defined as moving load to take into account all of cases of loading that can produce cracks. Also, impact factor of 33% was applied to accompany the truck loads as per AASHTO-LRFD (2007). Several load combination cases were included in the analyses; moving load was accompanied with dead load for one case, accompanied with hydration, accompanied with temperature, accompanied with shrinkage at 14 days of concrete age and at 28 days of concrete age, and accompanied with dead load and creep.

Table 5-2: Properties of Concrete

Time (days)	Concrete Compressive Strength (psi)	Concrete Modulus of Elasticity (psi)	f_r (psi)
3 ($f_c'=4000$ psi)	2160	2649×10^3	348.6
7 ($f_c'=4000$ psi)	3080	3163×10^3	416.2
14($f_c'=4000$ psi)	3652	3445×10^3	453.1
28($f_c'=4000$ psi)	4000	3605×10^3	474.3
28($f_c'=5000$ psi)	5000	4030.5×10^3	530.3
28($f_c'=7000$ psi)	7000	4769×10^3	627.5

Table 5-3: Strain due to Shrinkage

Bridge Model	Time (days)	ξ_{sh}
4000 psi & 7 in. thick deck	3	-0.000092
	7	-0.0002
	14	-0.00035
	28	-0.00057
4000 psi & 8.5 in. thick deck	3	-0.000090
	7	-0.0002
	14	-0.00035
	28	-0.00057
4000 psi & 10 in. thick deck	3	-0.000089
	7	-0.00019
	14	-0.00034
	28	-0.00056
5000 psi & 7 in. thick deck	3	-0.000082
	7	-0.00018

	14	-0.00031
	28	-0.0005
5000 psi & 7 in. thick deck	3	-0.000072
	7	-0.00015
	14	-0.00026
	28	-0.00042

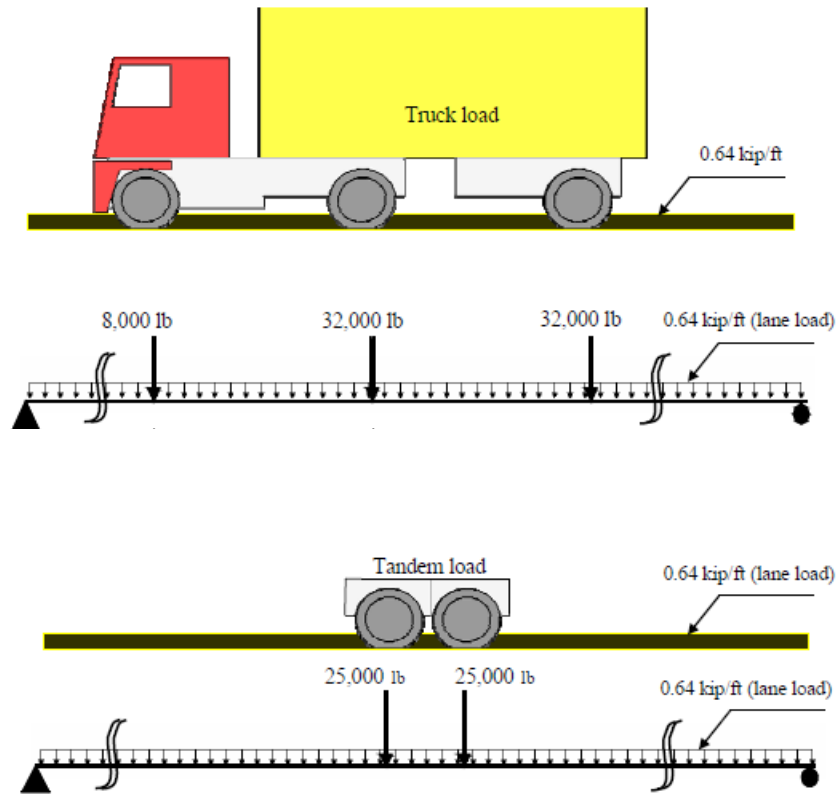


Figure 5-10: AASHTO HL-93 Truck load

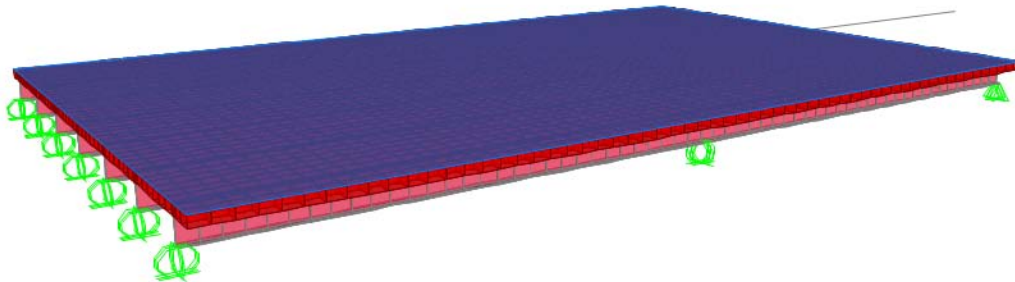


Figure 5-11: Bridge Lane Definition for Truck loads

5.5. RESULTS AND DISCUSSIONS

As mentioned earlier, truck loading followed dead load and was applied as a static load to produce maximum positive moment and maximum negative moment. Load cases include dead

load, hydration, temperature, shrinkage, and creep. When the moving load was introduced, moving load was accompanied with hydration, temperature, shrinkage, and creep. The described load patterns were applied to different 45 bridge models. The development of transverse deck cracking was monitored in light of deflection produced.

5.5.1. TRUCK LOAD APPLIED AS STATIC LOAD

The truck load followed the dead load case (Figure 5-12). Two cases of live load were considered; one case to produce maximum positive moment and other case to produce maximum negative moment. For one-span bridge (single-span-N-4000-7-7), no cracking occurred and maximum stresses take place under loads. For two-span bridge (two-span-N-4000-7-7) and maximum positive moment loading, no cracking occurred and maximum stresses take place under loads. On the other hand, for maximum negative moment loading, no cracking occurred and maximum stresses take place under loads and at intermediate support. For the three-span bridge (the three-span-N-4000-7-7) and maximum negative moment loading, no cracking occurred and maximum stresses take place under loads and at intermediate support. For the three-span bridge with spacing between girders larger than the width of the truck (three-span-N-4000-7-4), transverse deck cracking occurred for maximum positive moment load case. Also, maximum stresses take place at bottom of the deck. For maximum negative moment load case, transverse cracking occurred as well. Maximum stresses took place at the bottom and at top over intermediate support. For two-Span Bridge with same width and longer spans (two-span-D-4000-7-7), no cracking occurred. However, maximum stress took place at top over intermediate support for maximum negative load case.

From Figure 5-13, It was determined that aspect ratio did not seem to have a considerable effect on transverse cracking. Number of spans did not show tendency to affect transverse cracking; however, in continuous bridge tendency was demonstrated to produce larger tensile stresses at intermediate support locations. Truck loading did not cause transverse cracking in most of bridge models studied. Shrinkage solely or in combination with truck loading may cause transverse cracking in bridge decks.

5.5.2. EFFECT OF TEMPERATURE

To show the effect of temperature, the two-span bridge was modeled by only modeling one of the intermediate girders and its associated tributary portion of the deck (Figure 5-12). This allowed for better accuracy through refining the mesh. The bridge deck was subject to decrease of temperature of 5°F. The developed stress distribution through the depth of the bridge superstructure is presented in Figure 5-14. It is important to note that the stress distribution varies through the span of the bridge. The distribution shown is at the intermediate support. It was concluded that the temperature effect alone or combined with truck loading can result in transverse deck cracking.

5.5.3. EFFECT OF SECONDARY LOADS

The secondary loads included hydration, temperature, shrinkage, and creep. As mentioned, hydration effect was considered by applying 68°F of temperature load to all of decks of bridge models. Temperature effect was considered by applying both increase and decrease of temperature of 85°F. Shrinkage effect was considered by applying the proper value of strain due to shrinkage for the deck of each bridge model. Creep was accounted for also by applying a strain to bridge deck.

HYDRATION

By applying the hydration effect to the decks of bridge models, it was determined that the maximum tensile stress to produce transverse cracking takes place at the top of the bridge decks and at the girders locations. From Figure 5-15 to Figure 5-17, tensile stress due hydration does not seem to have potential to produce transverse cracking for the pin-roller boundary conditions. Therefore, it can be stated that, for bridges with seat-type abutment, hydration will not lead to development of transverse deck cracking. However, when the boundary conditions became fixed, the fixity restrained the deformation of the bridge due to hydration which led to larger stresses. Therefore, the fixed boundary condition shall be avoided. Also, it was observed that the tensile stresses developed in bridge decks increased with the age of the concrete. Figure 5-18 shows a sample of a deformed shape due to hydration.

TEMPERATURE

By applying the temperature effect to all of the bridge models, it was determined that the maximum tensile stress to produce transverse cracking took place at the bottom of the bridge decks and at the location of girders. From Figure 5-19 to Figure 5-23, tensile stresses developed due to temperature were small and did not resemble a potential cause for transverse deck cracking. It should be noted that this behavior is noticed when the bridge experiences an increase in temperature, however, if a decrease of temperature takes place transverse cracks may develop. However, when the fixity was introduced, tensile stresses increased significantly and transverse cracking took place. It was observed that stresses increased slightly with the number of spans. Therefore, continuity in bridges can lead to larger likelihood of transverse cracking development. It seems that increase in span length does not affect the stresses due to temperature. On the other hand, introducing fixity restrained significantly the deformation of bridge due to temperature and transverse cracking occurred. It seems that the stiffer (thicker) the concrete deck, the lower the tensile stresses are. However, the effect of deck thickness is marginally pronounced. It was also found that the higher the concrete compressive strength, the higher the tensile stresses developed which could lead to transverse deck cracking. It is recommended to use average concrete compressive strength and to avoid the use of concrete with very high compressive strength to avoid development of such transverse cracks. Stress contour developed due to the effect of temperature are shown in Figures 5-24 through 5-26.

SHRINKAGE

As mentioned earlier, shrinkage was applied as a strain to the decks of bridge models. Figure 5-27 to Figure 5-36 show the stress contours developed due to the effect of shrinkage. Figure 5-37 shows a sample of bridge deformed shape due to the effect of shrinkage. Tensile stresses developed due to shrinkage were found to be larger than those developed due to hydration and temperature. Shrinkage can be considered as a parameter that has the highest influence on the

bridge to produce transverse cracking. It is determined that transverse cracking starts to produce at 7 days. The transverse cracks initiated near the steel girders and deck overhang. Figures 5-36 through 5-41 present a comparison between tensile stresses developed in bridge models and effect of parameters studied in light of the likelihood of transverse deck cracking. It was observed that continuity increased the stress slightly; however, all of bridges developed transverse cracks due to shrinkage at 7, 14, and 28 days. There were not any cracks developed at 3 days. Introducing fixed boundary conditions increased the stresses, considerably at especially at 7, 14, and 28 days. In addition, the increase of the deck thickness reduces the developed stress which may lead to fewer cracks throughout. When the concrete compressive strength increases, the developed stress becomes smaller. This trend is opposite to what was presented before. Increase of span length did not seem to have a significant effect on the likelihood of transverse deck cracking to increase. In light of presented observations, it is recommended to avoid fixed boundary conditions and to use a thicker bridge decks as well as a moderate concrete compressive strength.

CREEP

The effect of creep was found to be similar to the effect of shrinkage and it showed similar trend as well. However, stresses due to creep effect were smaller than those produced due to shrinkage.

EFFECT OF TRUCK LOADS

The truck load was applied as a moving load with an impact factor of 33%. The moving load acts within the limits of the defined bridge lane. When the bridge is loaded at 14 days, the load is called “construction load”, however, when the bridge is loaded at 28 days, the case is called “loaded bridge”. Also, the truck load was applied associated with dead load, hydration, temperature, shrinkage, or creep. The combination of load cases was considered at 14 days and 28 days. It is important to note that, when hydration and temperature were combined with truck loads, the overall stress decreased. Therefore, this case was not addressed in the following discussion.

Figure 5-42 to Figure 5-49 present the stress contours developed due to truck load. In general, there were no cracks produced due to truck load. Figure 5-50 to Figure 5-80 show results including deflections and a comparison between longitudinal tensile stresses developed in all bridge models considering all studied parameters affecting transverse cracking. For truck only, it can be observed that continuity increased the amount of stress developed; however, cracking takes place for all of bridge models. When the truck load was combined with other loads, cracks take place for all of the cases. Stress was maximum when truck was combined with shrinkage while at the same time deflection was maximum.

For truck only, it can be observed that stress increases with the increase of span length. Increase of span length led to a larger deflection.

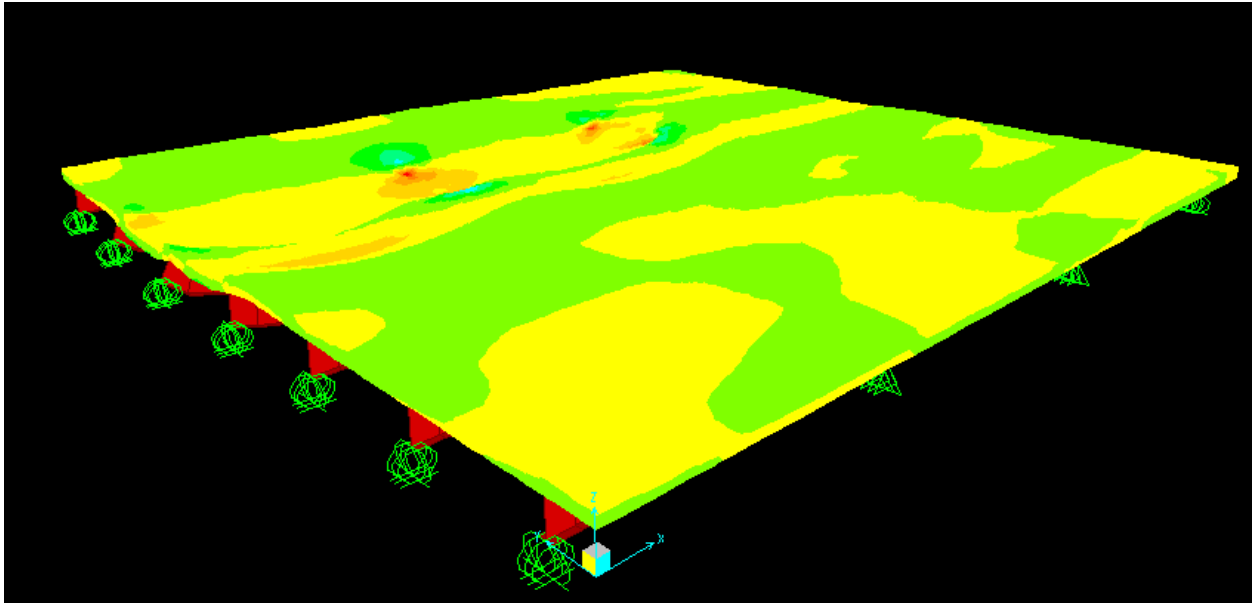
For truck only, it was observed that fixed boundary condition has a marginal effect on the stress developed. As fixity was introduced, the stress reduced slightly. When the truck load was combined with other loads such as thermal and shrinkage, cracks took place for all of these

cases. Bridge decks with fixed boundary conditions experienced larger stress. Stress was maximum when truck was combined with shrinkage and deflection was maximum as well.

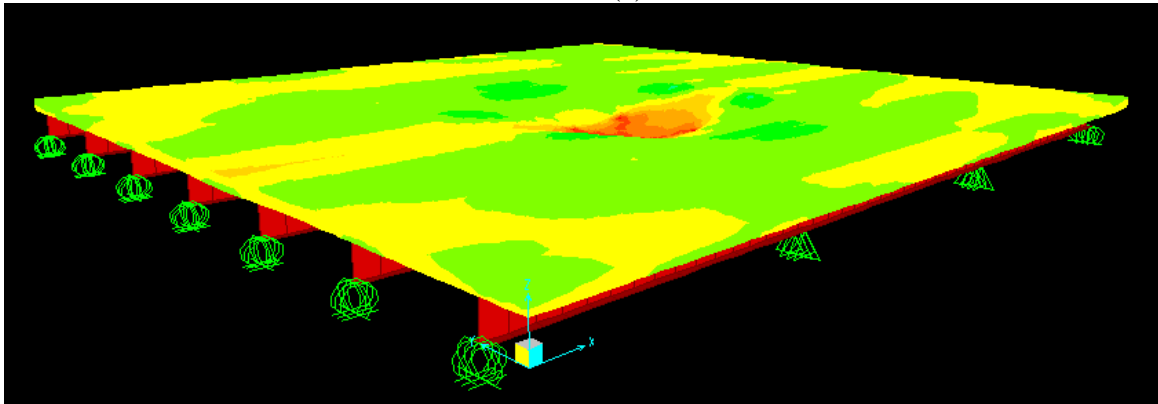
For truck only, it can be observed that increase of deck thickness led to a lower stress to be developed. When the truck load was combined with other loads, cracks take place for all of the cases. The same trend was observed since the stress reduced for larger thickness while deflection follows the same trend. Stress was maximum when truck was combined with shrinkage.

For truck only, it was observed that increase of concrete compressive strength led to a higher stress to be developed. When the truck load was combined with other effects such as shrinkage and thermal, cracks took place for all of these cases. Stress increased with the increase of concrete compressive strength except when truck is combined with shrinkage. Stress and deflection were maximum when truck was combined with shrinkage.

The FE analysis present the deflection developed due to all cases of load. Also, tensile stress was reported as well as the rupture stress at which crack took place. The deflection at which crack does not took place was calculated and the deflection limit was computed backward as a fraction of span length. The AASHTO Standard Specification limits live-load deflections to $L/800$ for ordinary bridges and $L/1000$ for bridges in urban areas that are subject to pedestrian use. In light of presented results, the current deflection limits provided by AASHTO does not serve the current need to limit such transverse deck cracking. Therefore, there was a need for a new deflection limits to help limit transverse deck cracking.



(a)

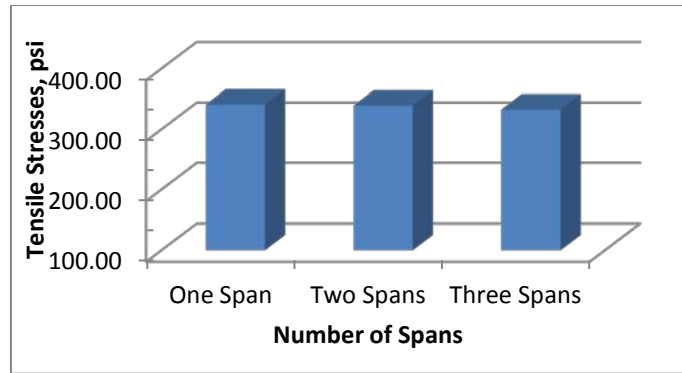


(b)

Figure 5-12: Stress contours due to (a) Truck load and (b) Tandem load

W/L= 2.8

Criteria	F _t (psi)
One Span	341.04
Two Spans	339.28
Three Spans	332.70



2-span bridge

Aspect ratio	F _t (psi)
2.8	339.28
1.4	329.23

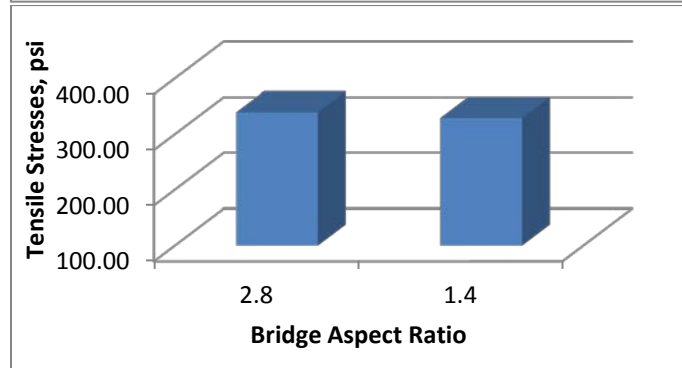


Figure 5-13: Development of deck stresses due to Truck load

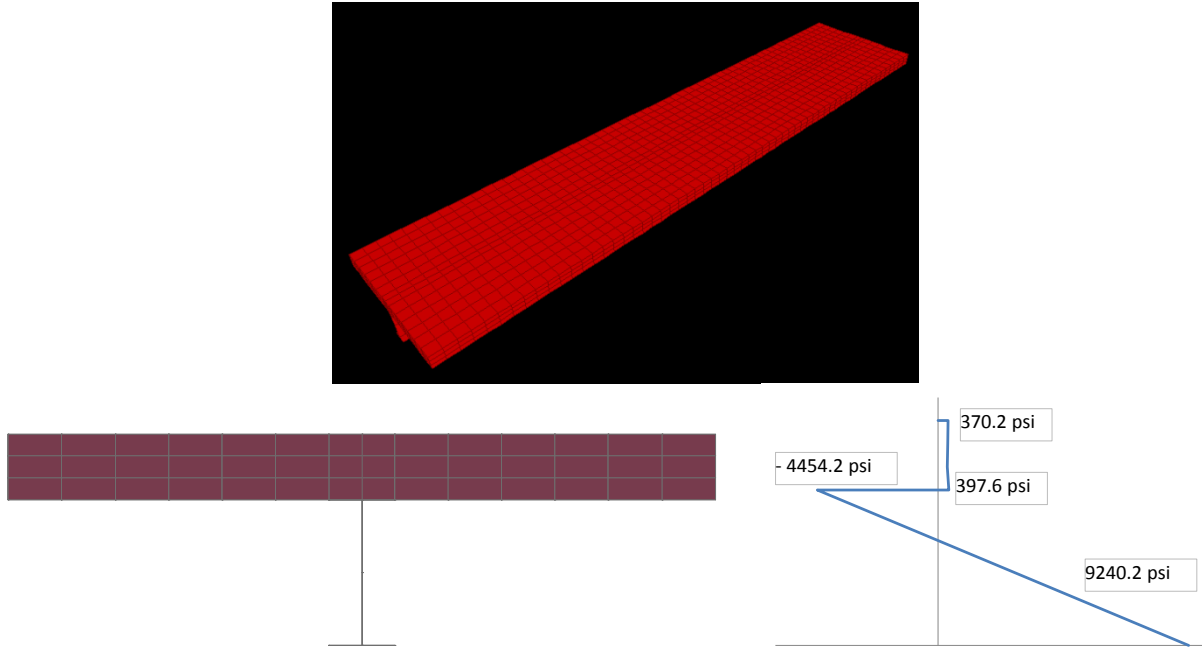


Figure 5-14: Temperature effect

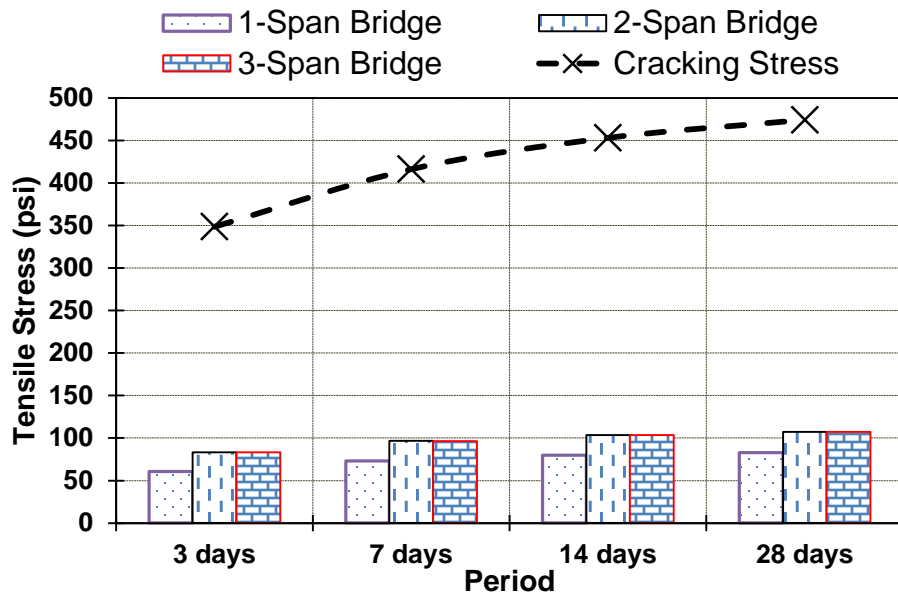


Figure 5-15: Effect of hydration (number of spans)

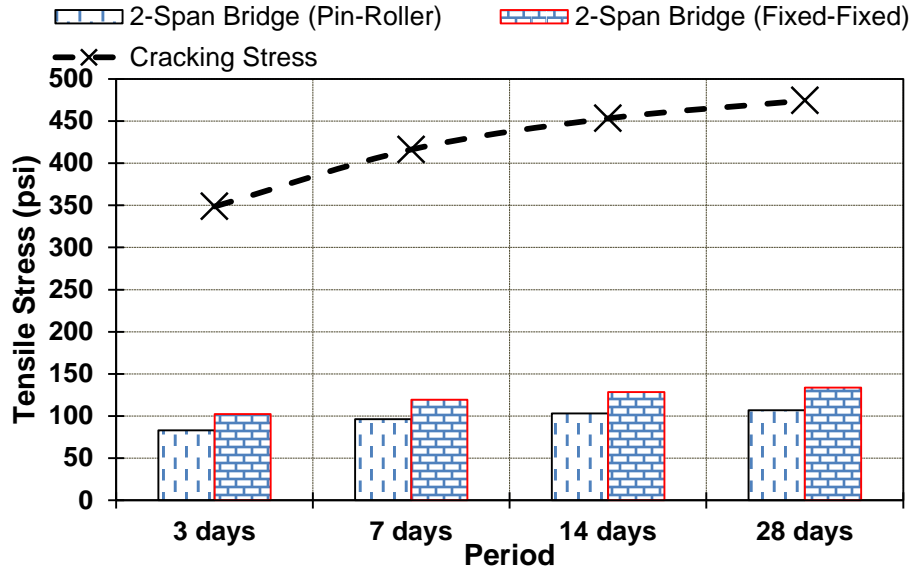


Figure 5-16: Effect of hydration (boundary conditions)

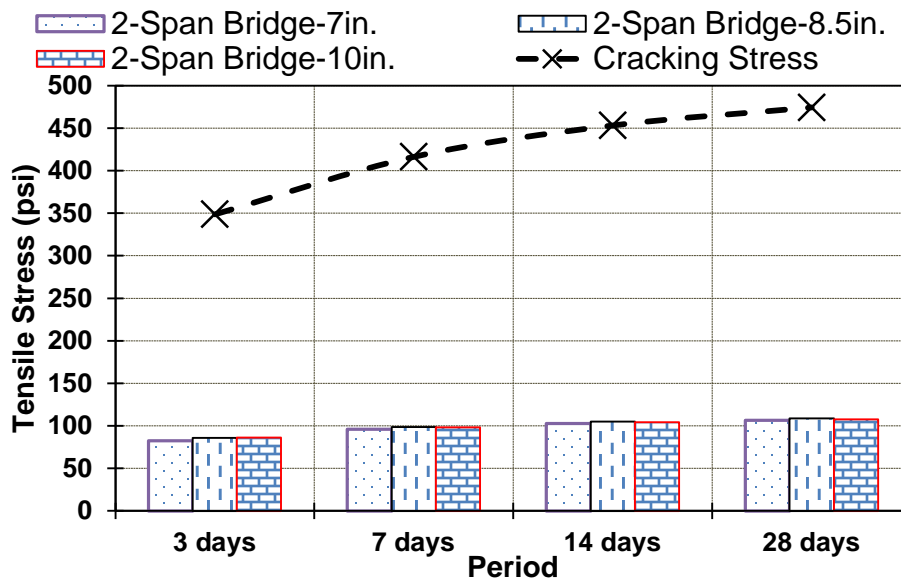


Figure 5-17: Effect of hydration (deck thickness)

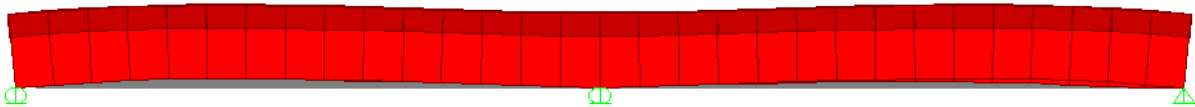


Figure 5-18: Deformed shape due to hydration

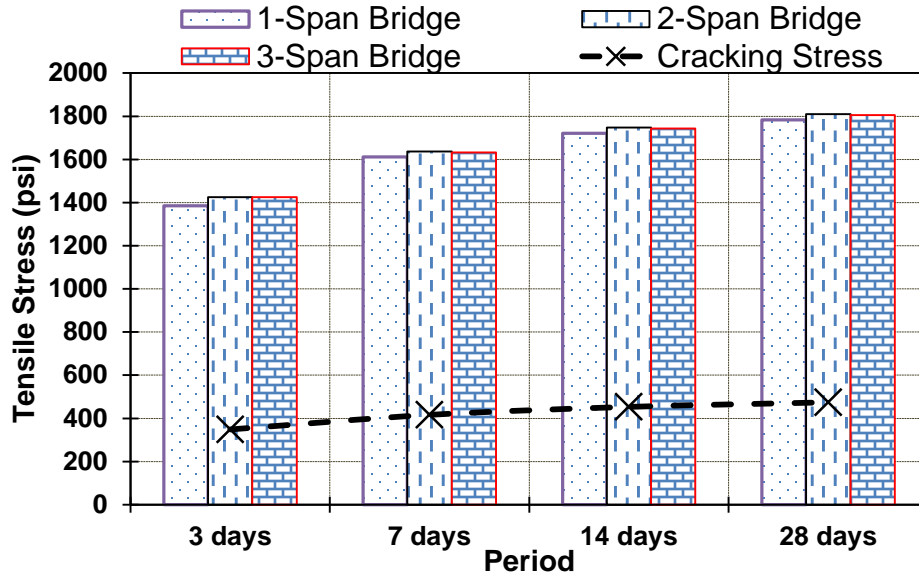


Figure 5-19: Effect of temperature (number of spans)

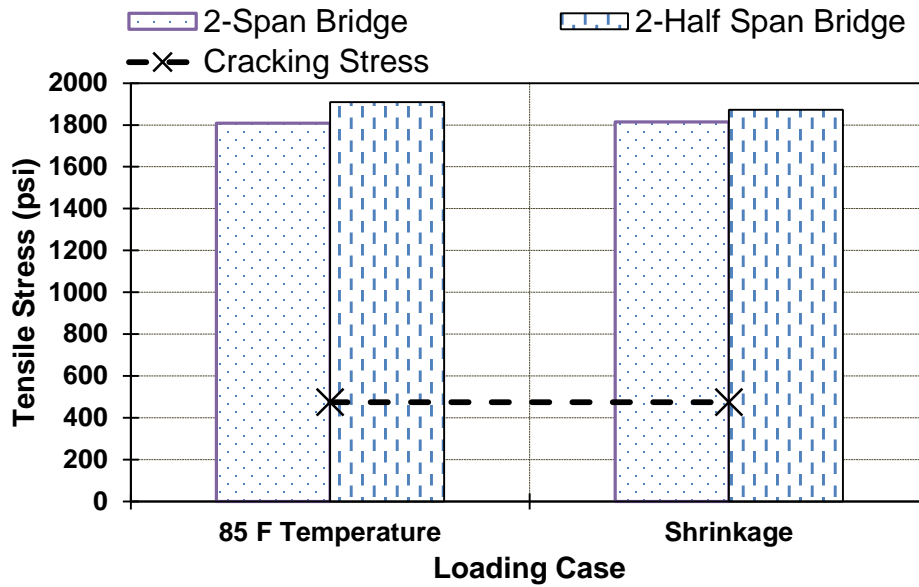


Figure 5-20: Effect of temperature and shrinkage (span length)

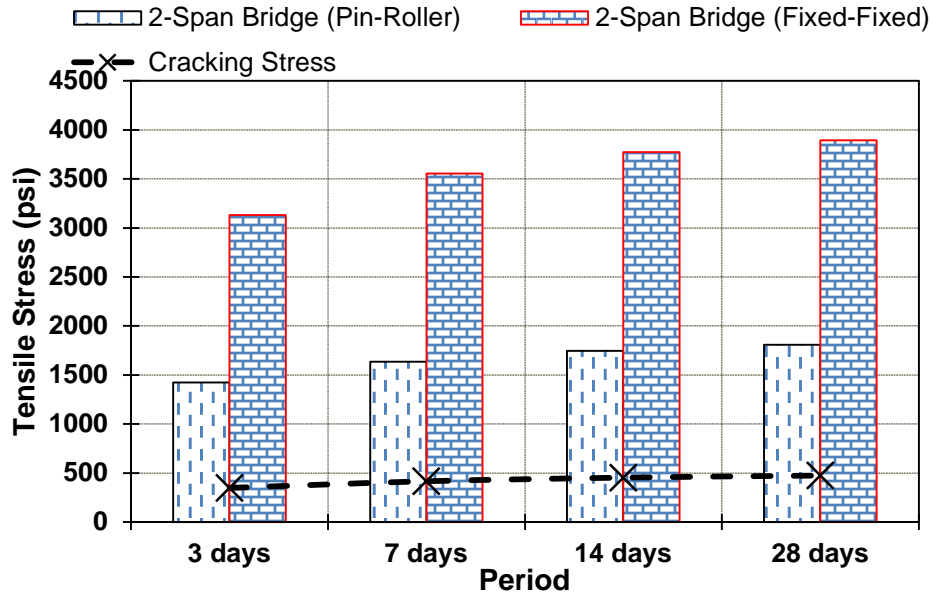


Figure 5-21: Effect of temperature (boundary conditions)

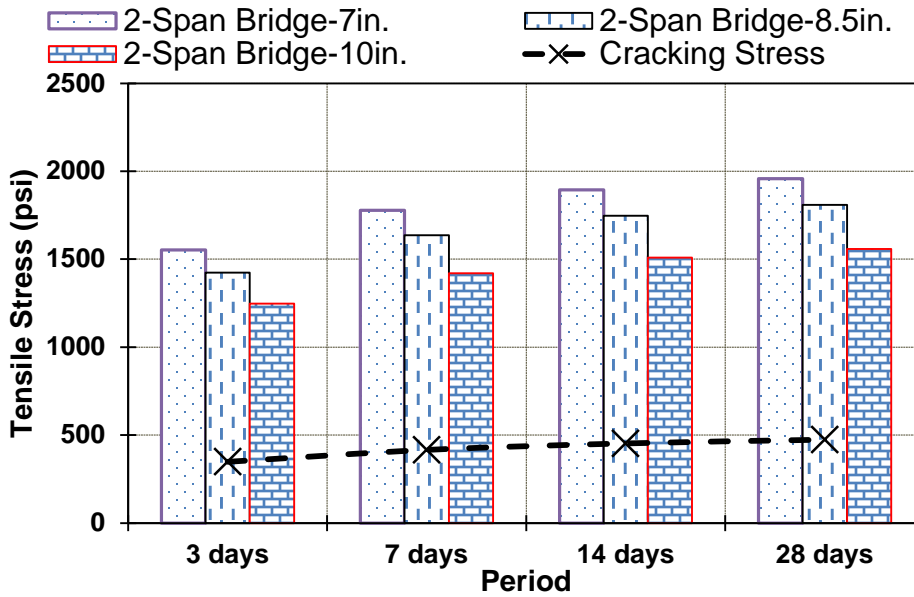


Figure 5-22: Effect of temperature (deck thickness)

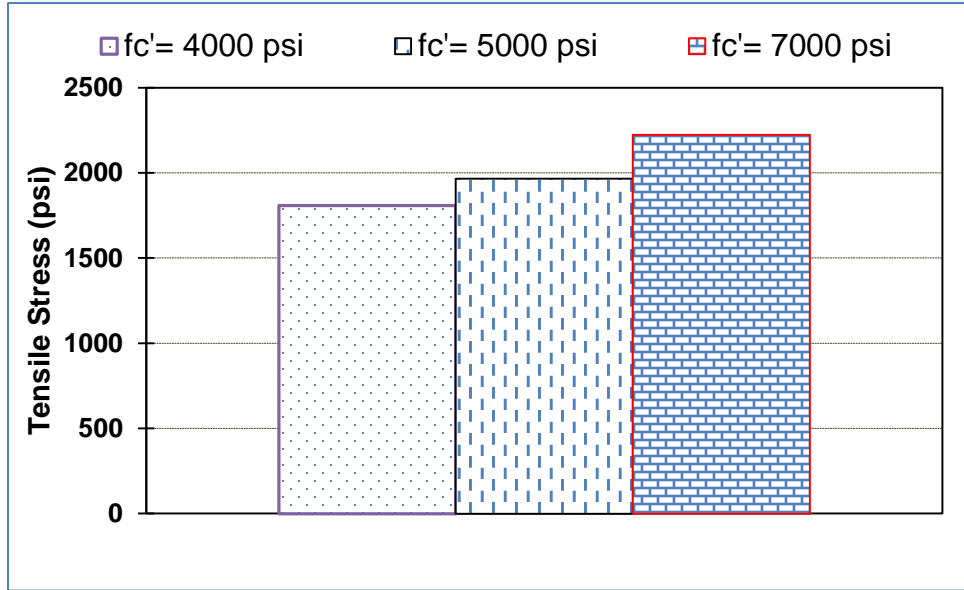


Figure 5-23: Effect of temperature (concrete compressive strength)

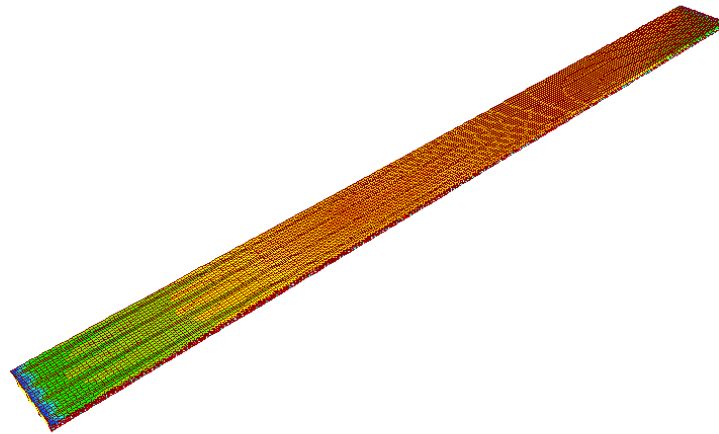


Figure 5-24: Stress contours due to 85°F increase of temperature

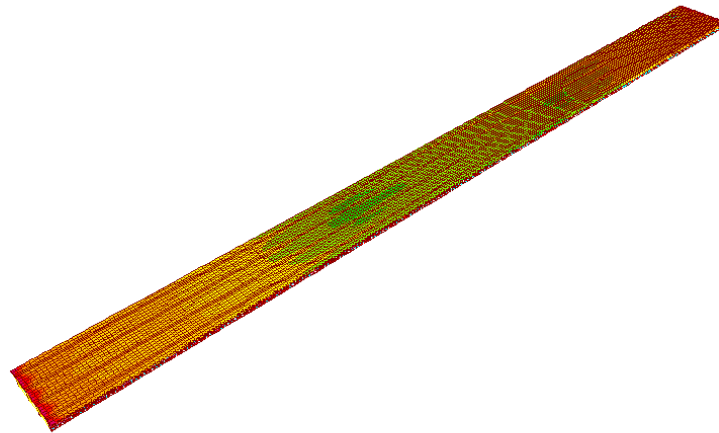


Figure 5-25: Stress contours due to 85°F decrease of temperature

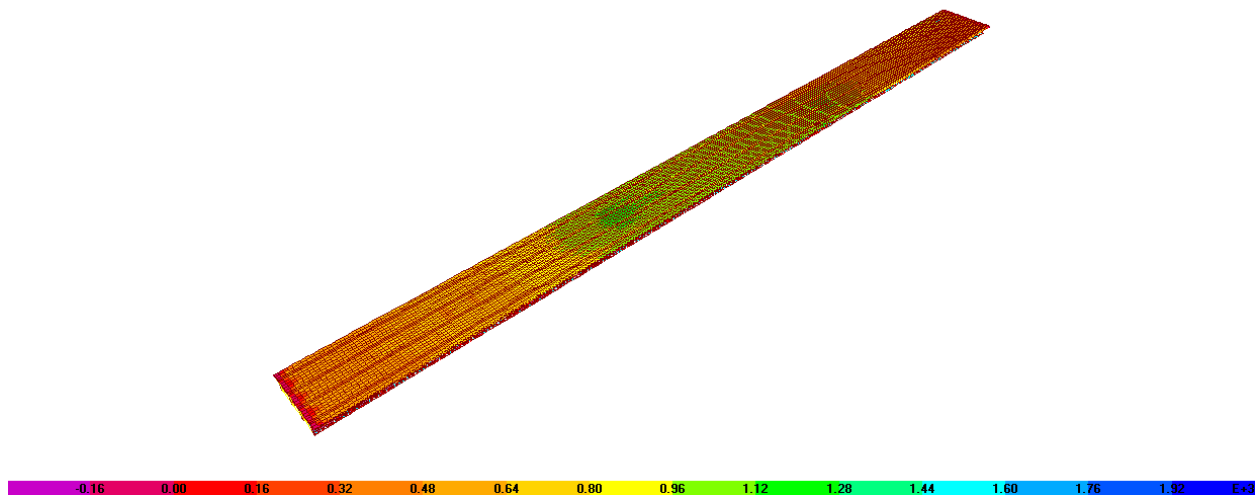
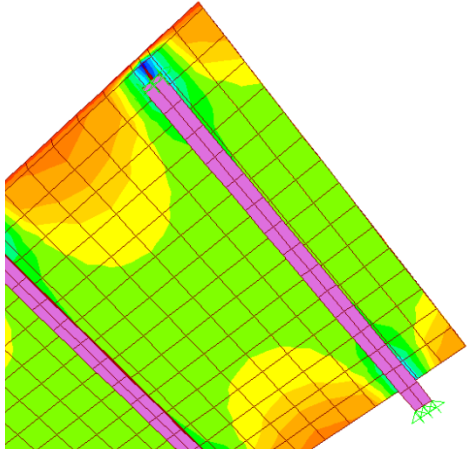
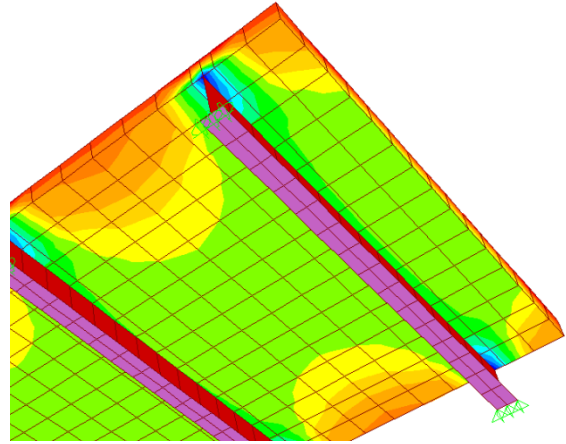


Figure 5-26: Stress contours due to 85°F decrease of temperature and truck load

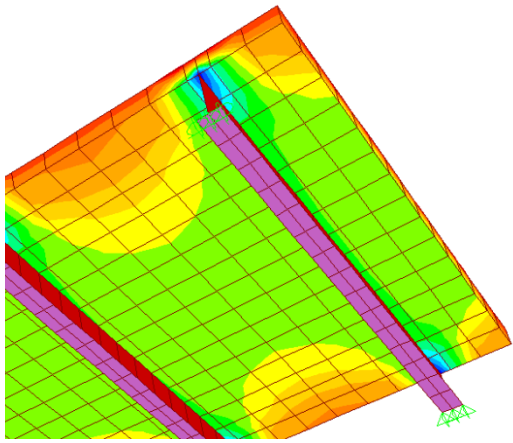
In order to study the effect of the increase of the live load applied on the bridge model on the elongation of developed transverse cracks, the live load due to truck load was incrementally increased. The live load cases included application of 50%, 75%, 100%, and 125% of HS-20 truck load. The increase of the live load tended to further open the crack up and hence the crack width increased. It was important to specifically conduct this study on combined case of truck load with either shrinkage or decrease of temperature since shrinkage and decrease of temperature cases were proven to drive the development of transverse deck cracking.



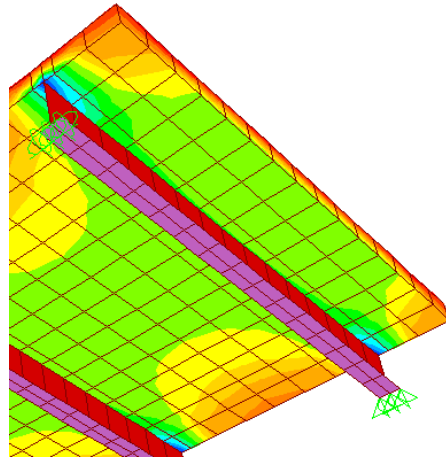
(a) 3-day Shrinkage



(b) 7-day Shrinkage

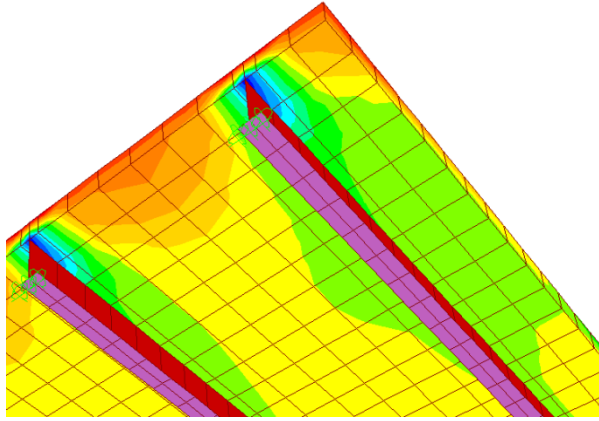


(c) 14-day Shrinkage

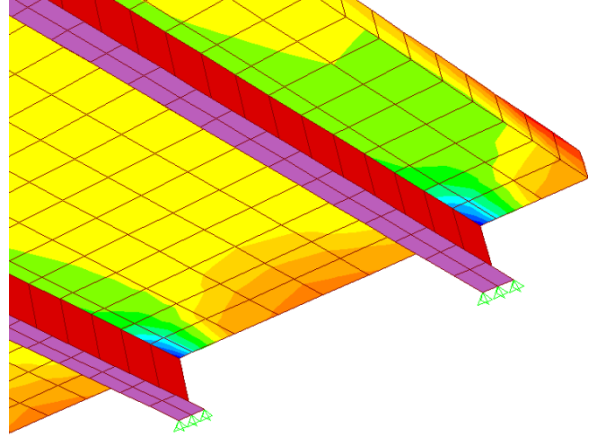


(d) 28-day Shrinkage

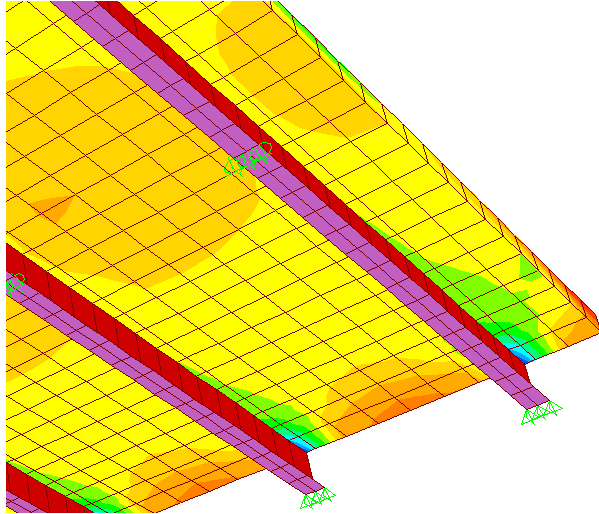
Figure 5-27: Shrinkage effect on bridge model single-span-N-4000-8.5-4



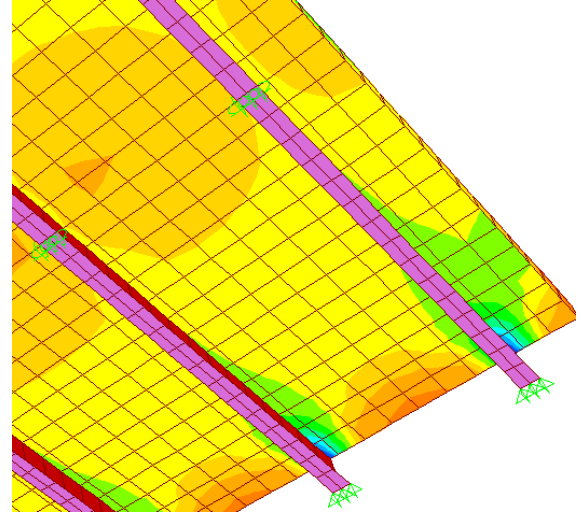
(a) 3-day shrinkage



(b) 7-day shrinkage

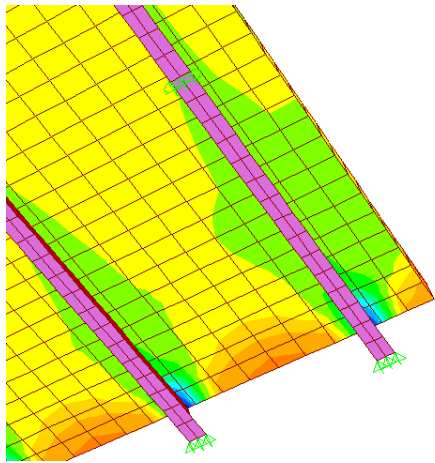


(c) 14-day Shrinkage

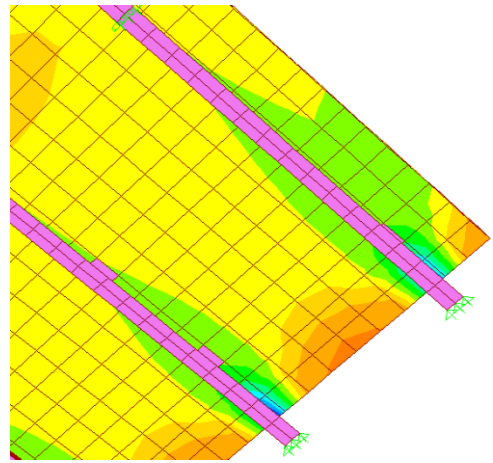


(d) 28-day Shrinkage

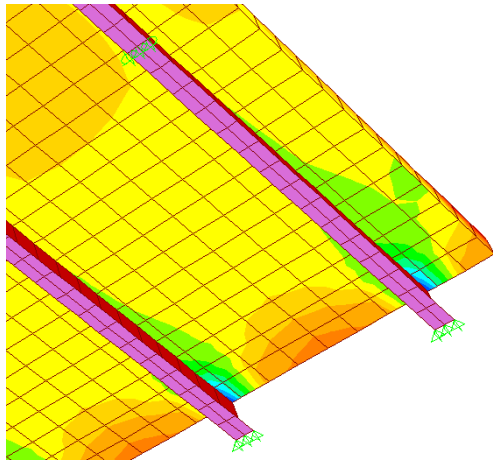
Figure 5-28: Shrinkage effect on bridge model two-span-N-4000-8.5-4



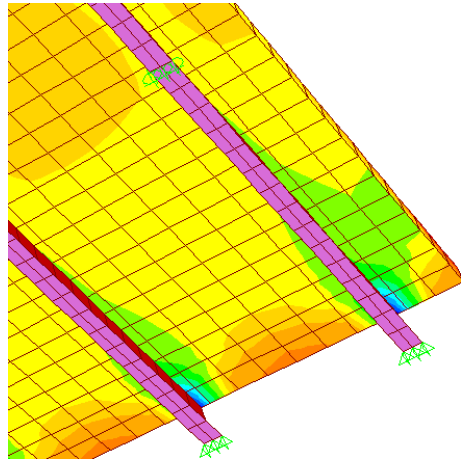
(a) 3-day Shrinkage



(b) 7-day Shrinkage



(c) 14-day Shrinkage



(b) 28-day Shrinkage

Figure 5-29: Shrinkage effect on bridge model three-span-N-4000-8.5-4

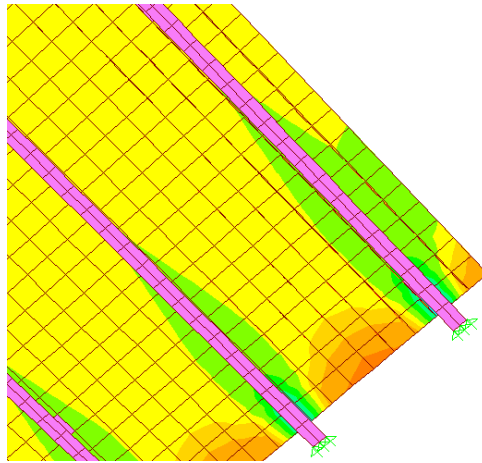


Figure 5-30: Shrinkage effect on bridge model two-span-half-4000-8.5-4 at 28 days

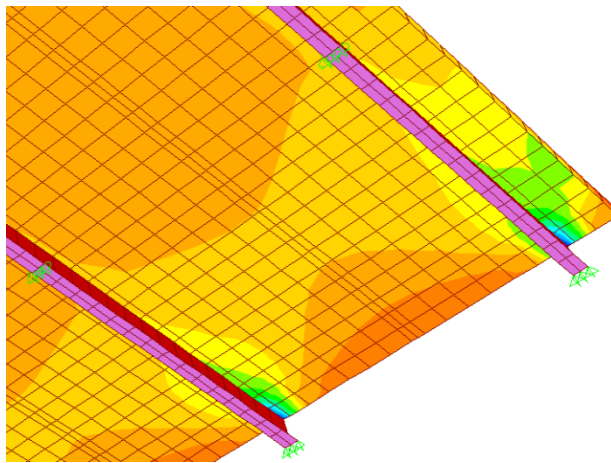
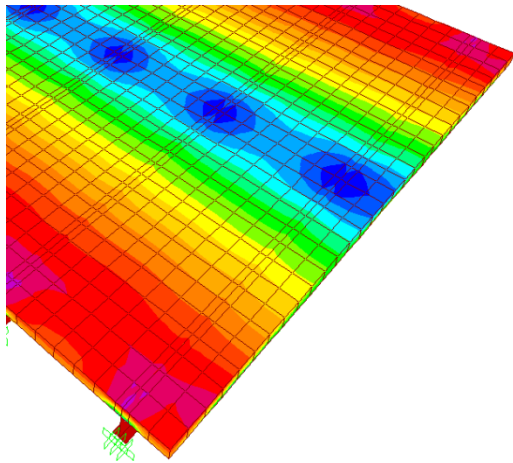
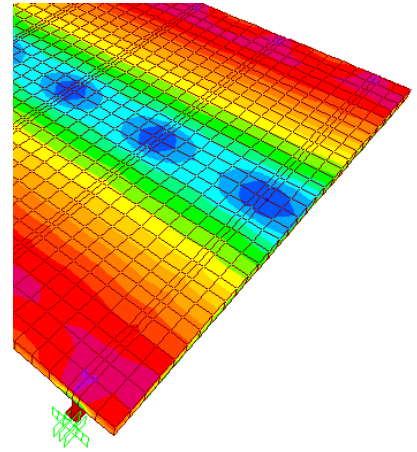


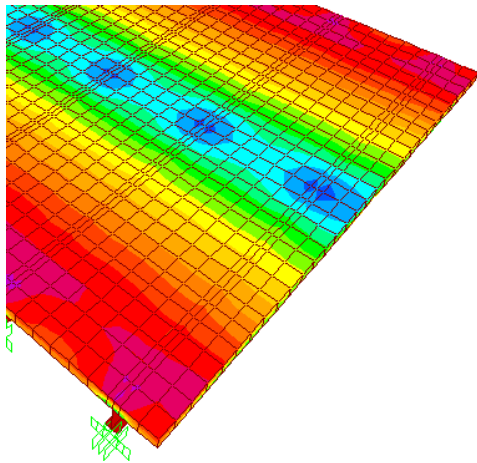
Figure 5-31: Shrinkage effect on bridge model three-span-N-4000-8.5-7 at 28 days



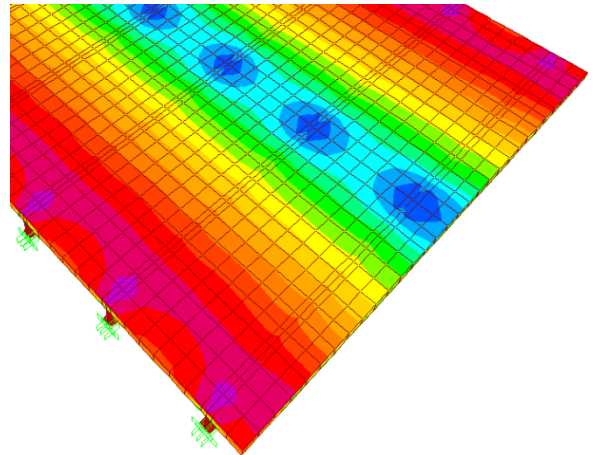
(a) 3-day Shrinkage



(b) 7-day Shrinkage

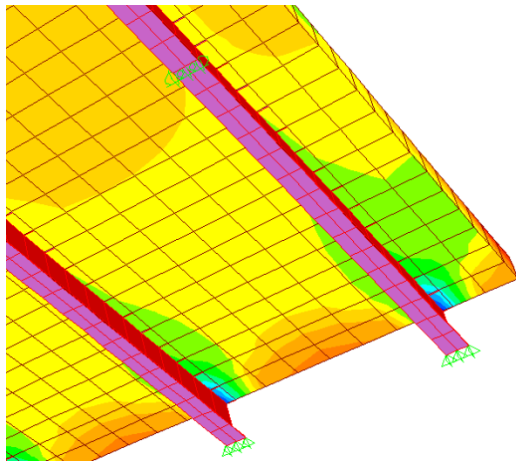


(c) 14-day Shrinkage

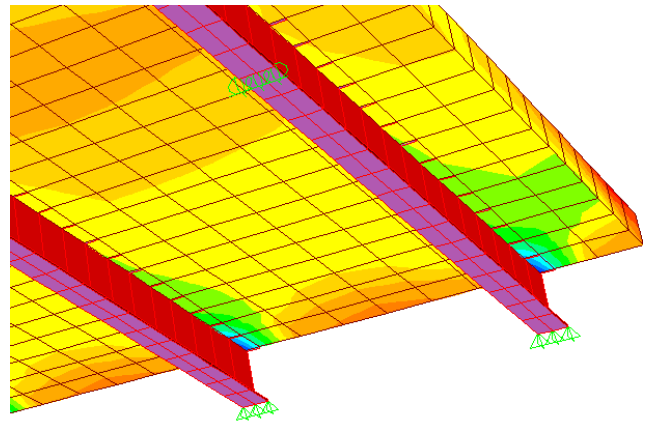


(d) 28-day Shrinkage

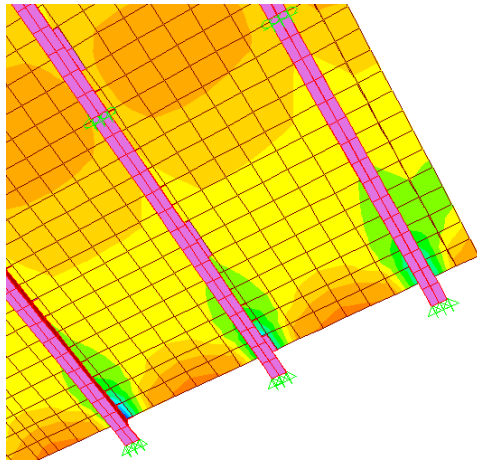
Figure 5-32: Shrinkage effect on bridge model two-span-N-4000-8.5-4-(F-F) at 28 days



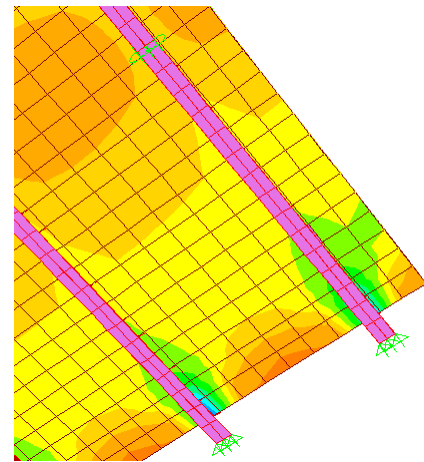
(a) 3-day Shrinkage



(b) 7-day Shrinkage

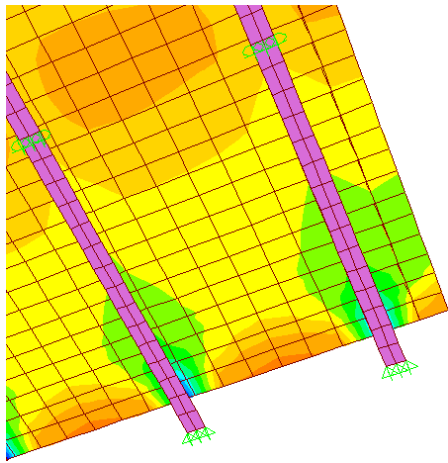


(c) 14-day Shrinkage

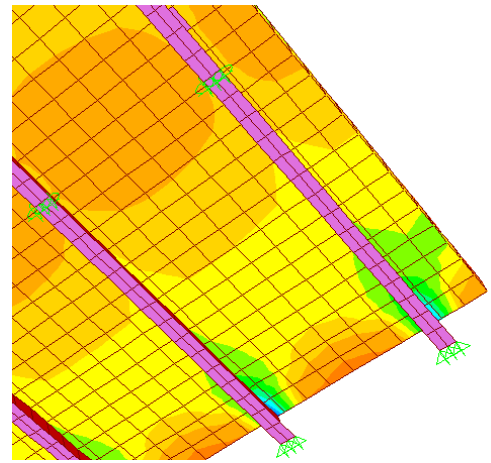


(d) 28-day Shrinkage

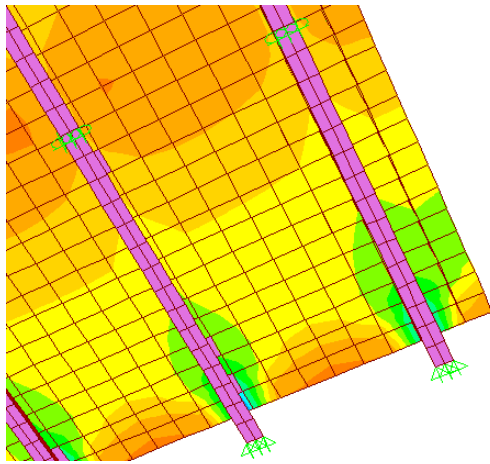
Figure 5-33: Shrinkage effect on bridge model two-span-N-4000-7-4



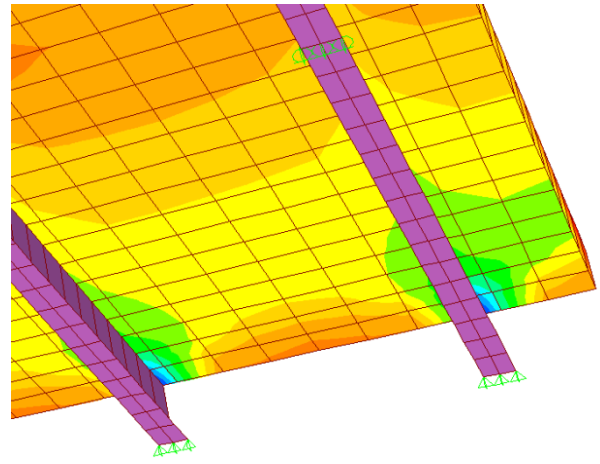
(a) 3-day Shrinkage



(b) 7-day Shrinkage



(c) 14-day Shrinkage



(d) 28-day Shrinkage

Figure 5-34: Shrinkage effect on bridge model two-span-N-4000-10-4

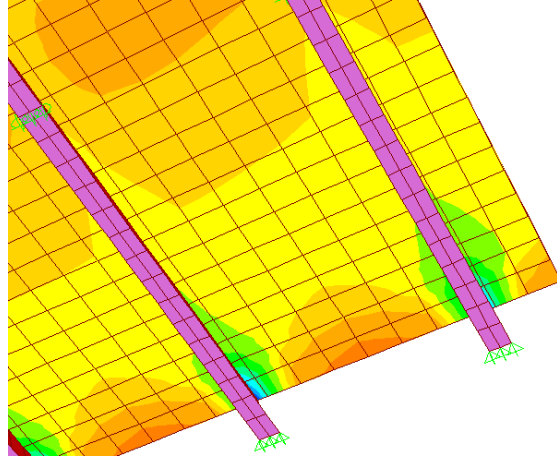


Figure 5-35: Shrinkage effect on bridge model two-span-N-5000-8.5-4

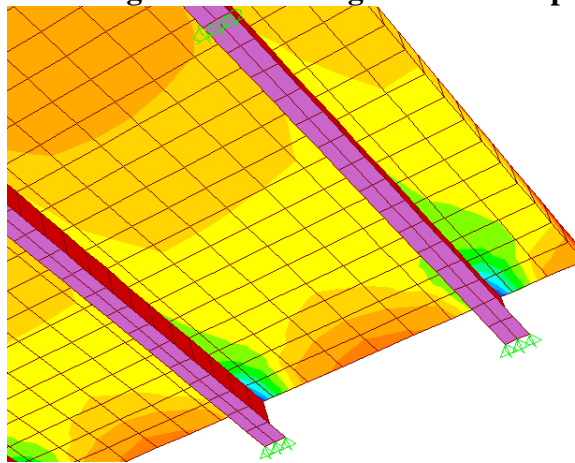


Figure 5-36: Shrinkage effect on bridge model two-span-N-7000-8.5-4

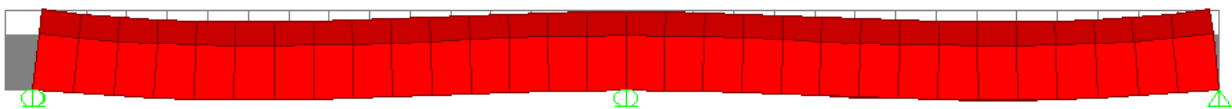


Figure 5-37: Deformed shape due to shrinkage

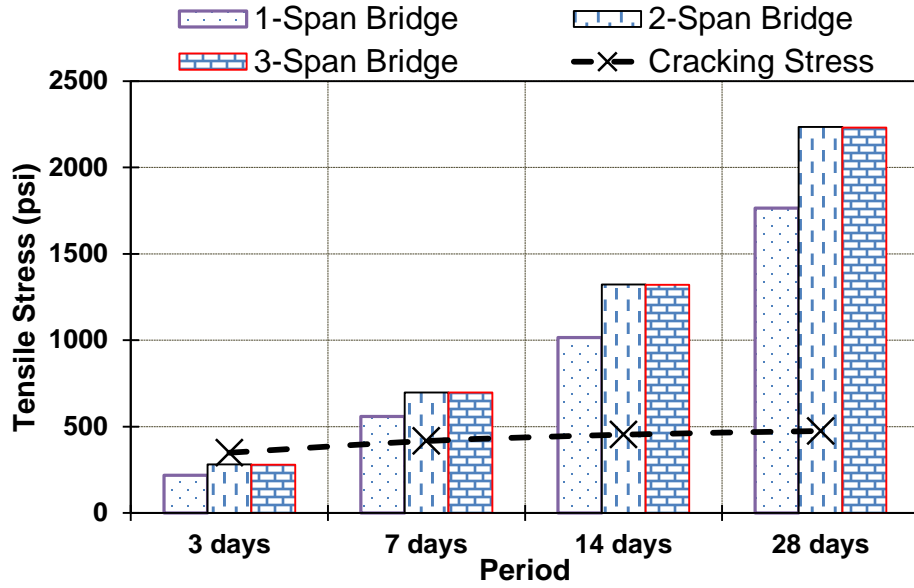


Figure 5-38: Effect of shrinkage (number of spans)

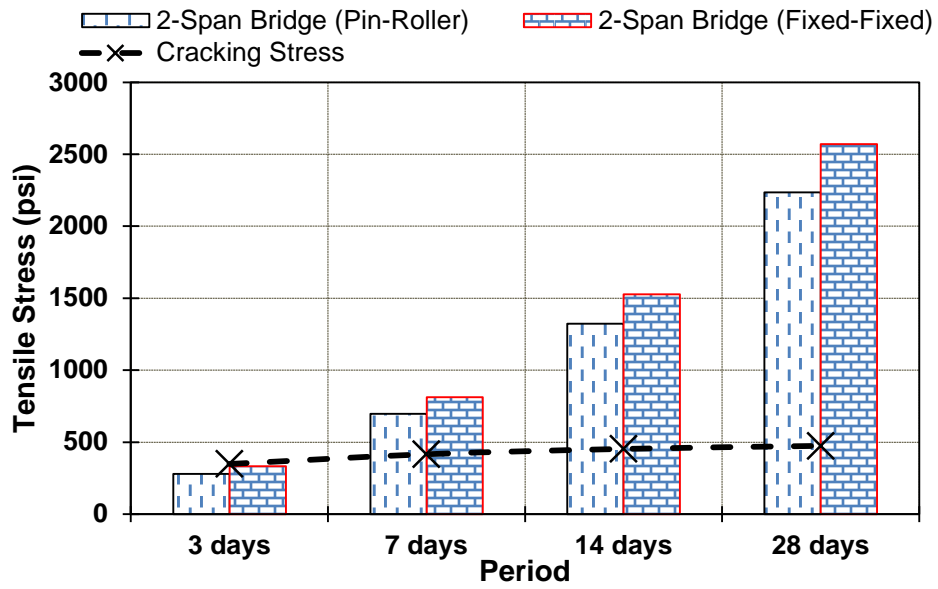


Figure 5-39: Effect of shrinkage (boundary conditions)

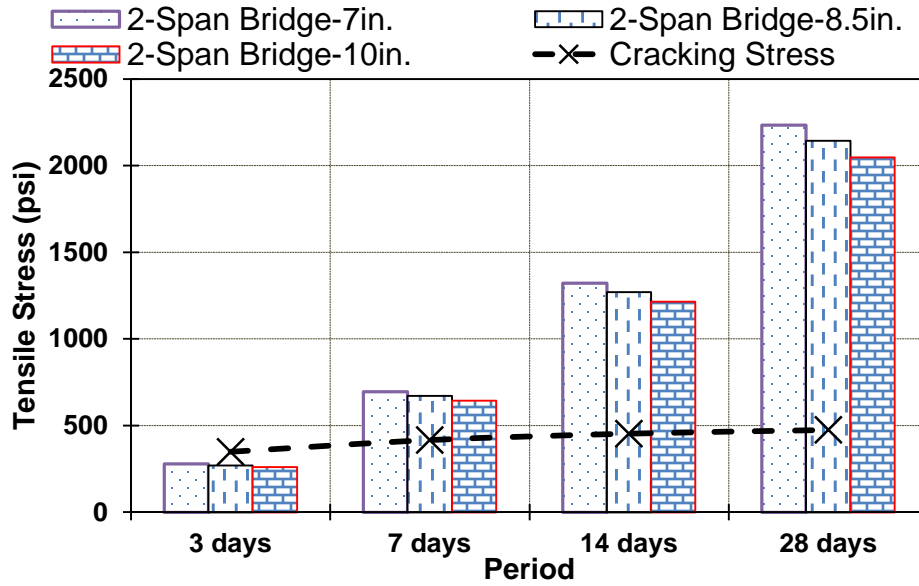


Figure 5-40: Effect of shrinkage (deck thickness)

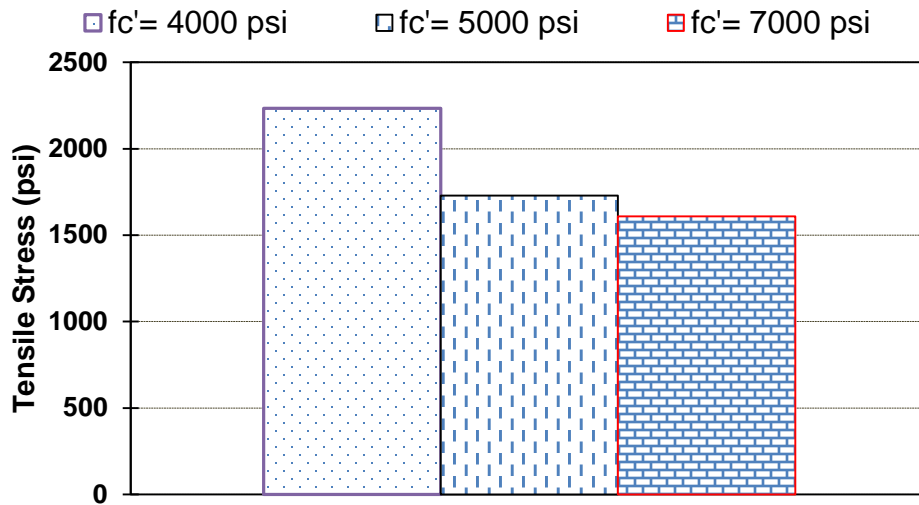


Figure 5-41: Effect of shrinkage (concrete compressive strength)

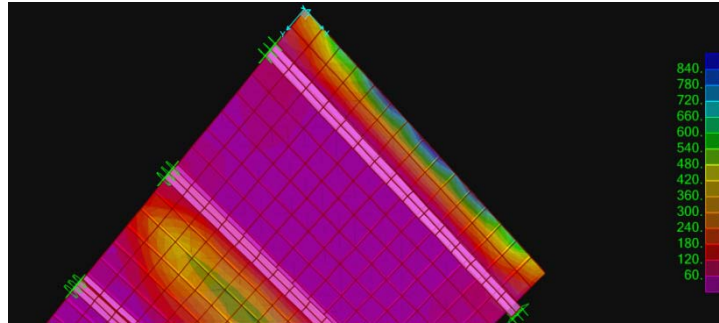


Figure 5-42: Longitudinal stress contours due to truck loads at 14 days for bridge model single-span-N-4000-8.5-4

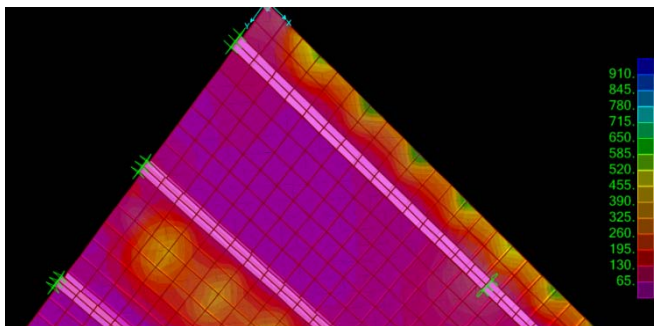


Figure 5-43: Longitudinal stress contours due to truck loads at 14 days for bridge model two-span-N-4000-8.5-4

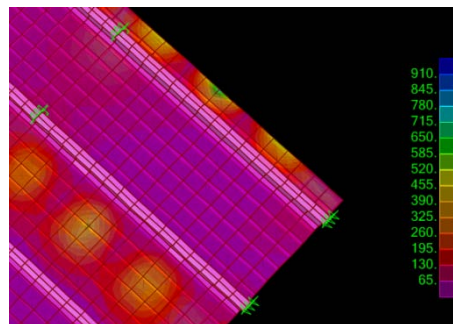


Figure 5-44: Longitudinal stress contours due to truck loads at 14 days for bridge model three-span-N-4000-8.5-4

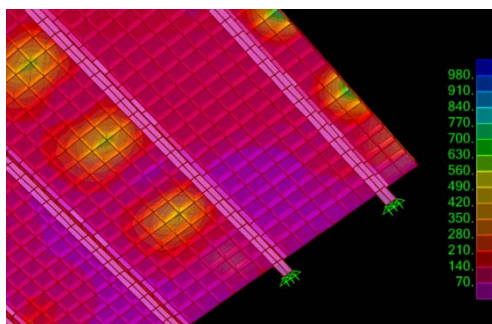


Figure 5-45: Longitudinal stress contours due to truck loads at 28 days for bridge model two-span-half-4000-8.5-4

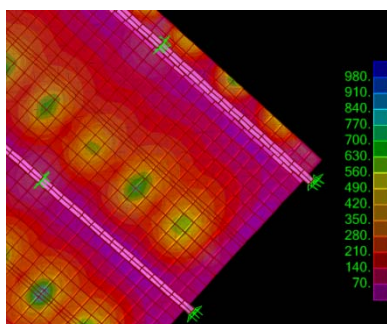


Figure 5-46: Longitudinal stress contours due to truck loads at 28 days for bridge model three-span-N-4000-8.5-7

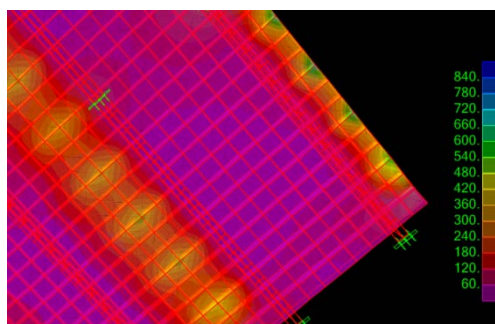


Figure 5-47: Longitudinal stress contours due to truck loads at 14 days for bridge model two-span-N-4000-8.5-4-(F-F)

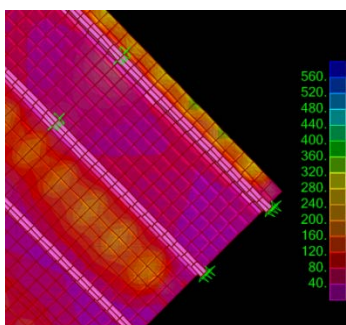


Figure 5-48: Longitudinal stress contours due to truck loads at 14 days for bridge model two-span-N-4000-10-4

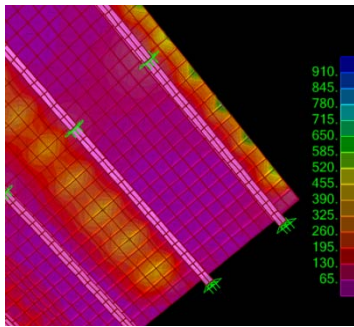


Figure 5-49: Longitudinal stress contours due to truck loads at 28 days for bridge model two-span-N-5000-8.5-4

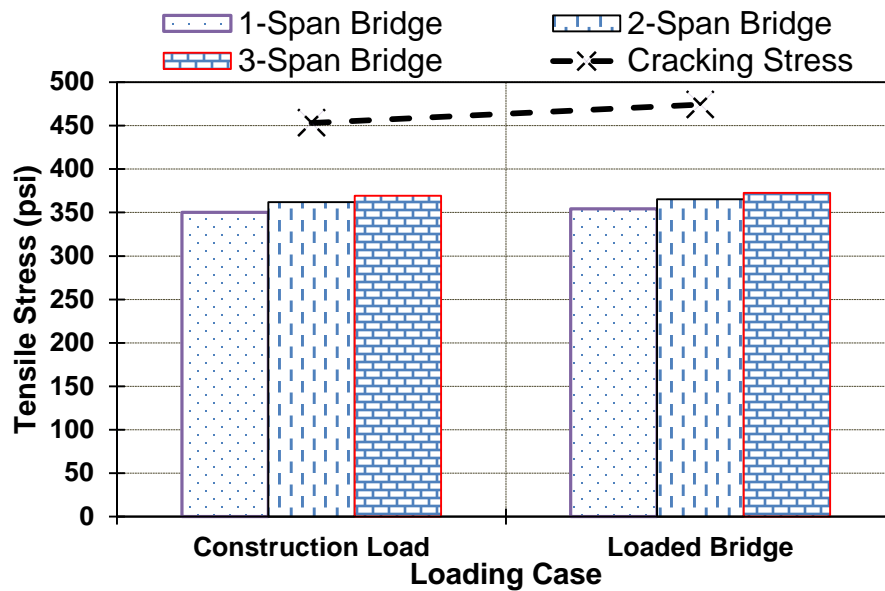


Figure 5-50: Longitudinal tensile stresses due to truck loads (number of spans)

In many cases, temperature change could result in higher tensile stresses causing deck cracking. In other cases of temperature changes, the developed tensile stresses did not reach the tensile capacity of concrete at specific points of consideration along the bridge span length.

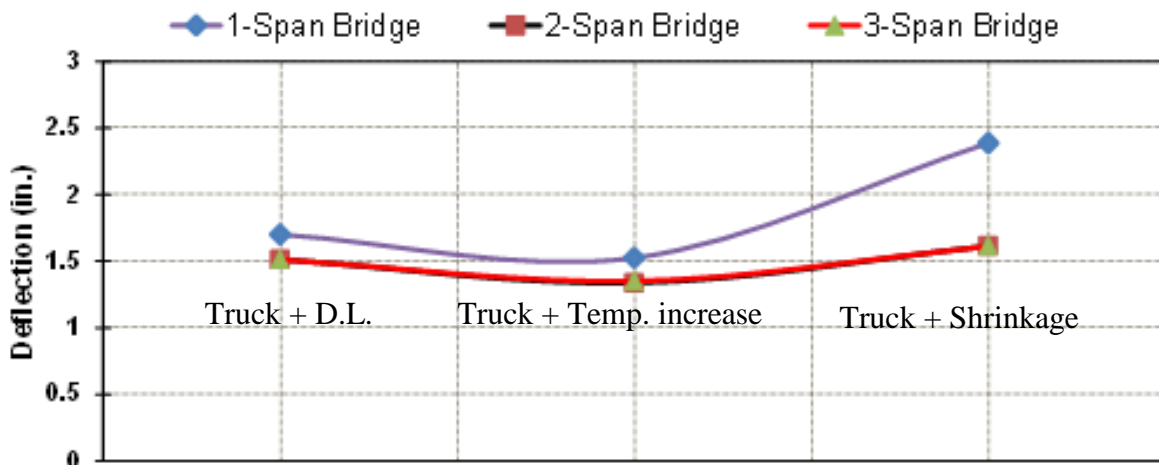


Figure 5-51: Bridge deflection (number of spans)

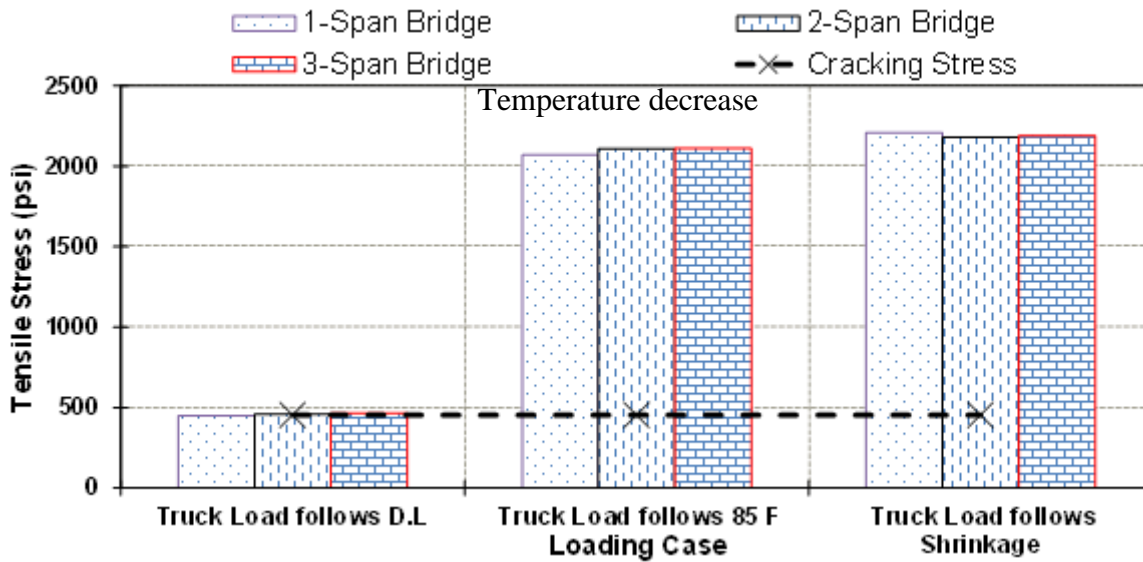


Figure 5-52: Longitudinal tensile stresses due to truck loads at 14 days (number of spans)

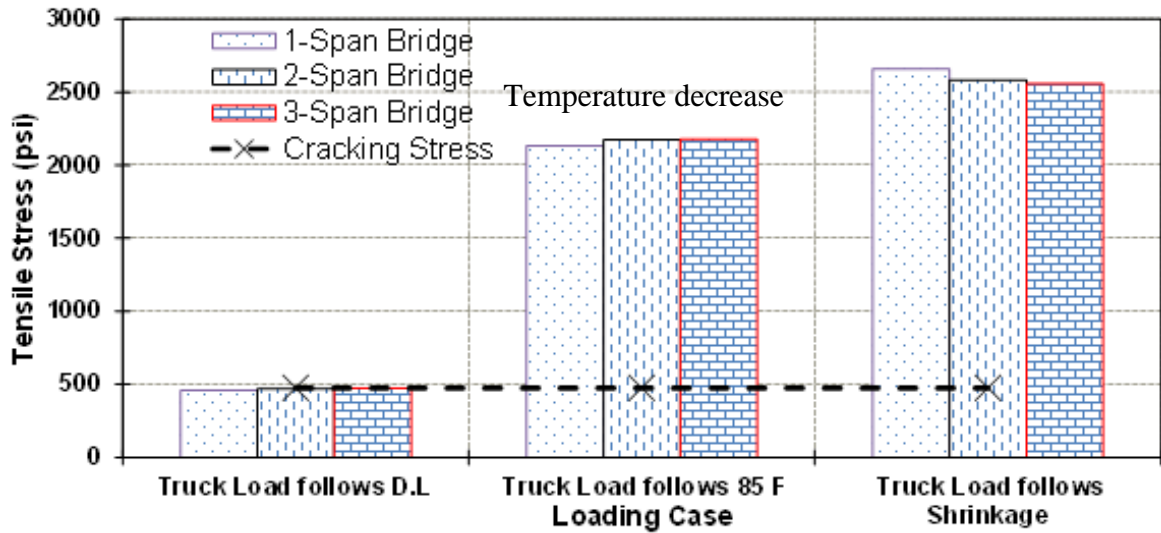


Figure 5-53: Longitudinal tensile stresses due to truck loads at 28 days (number of spans)

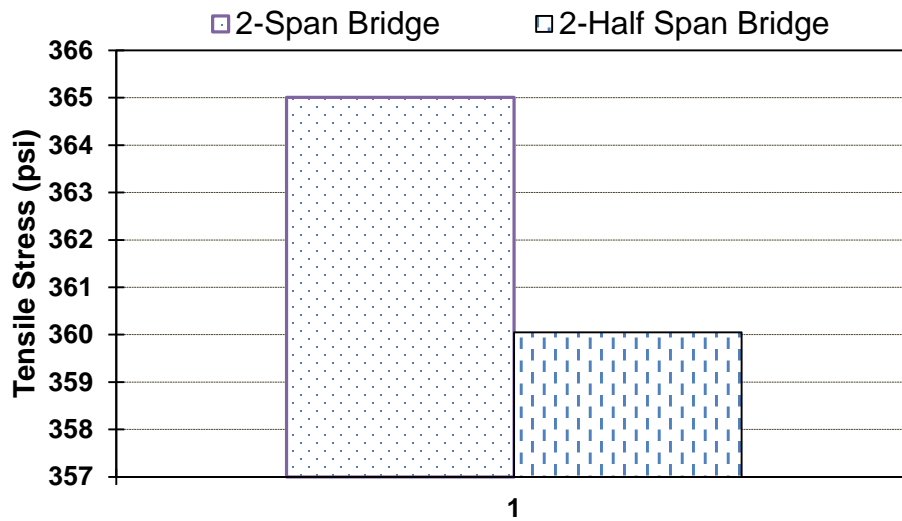


Figure 5-54: Longitudinal tensile stresses due to truck loads (span length)

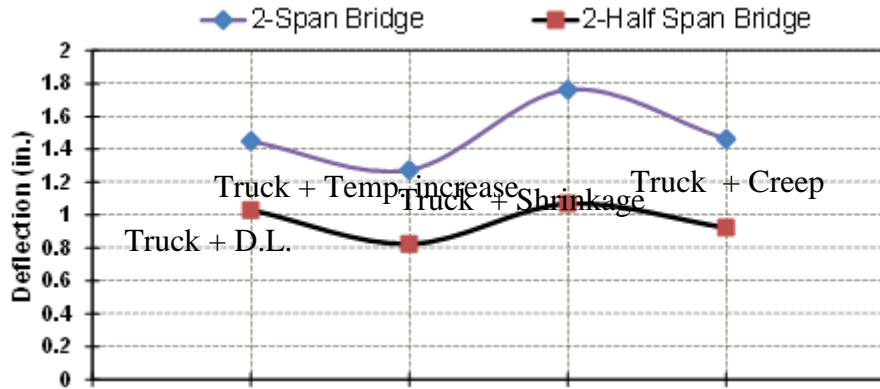


Figure 5-55: Bridge deflection (span length)

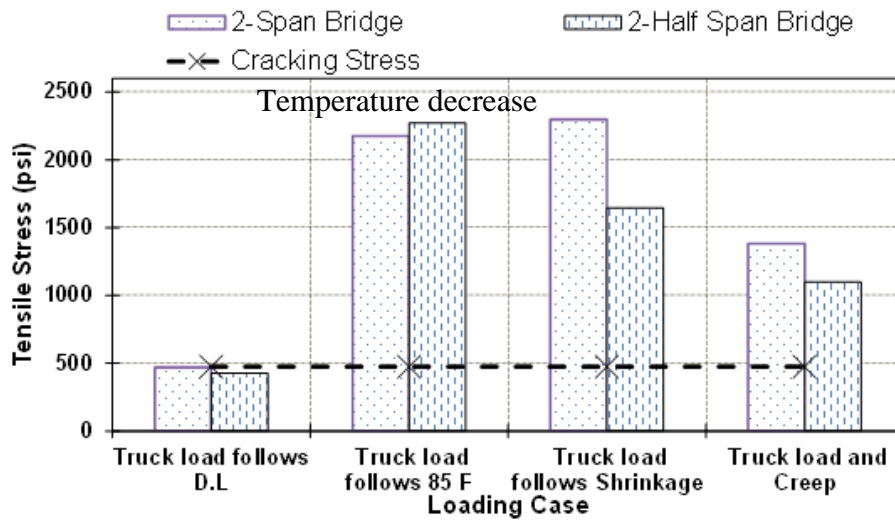


Figure 5-56: Longitudinal tensile stresses due to truck loads at 28 days (span length)

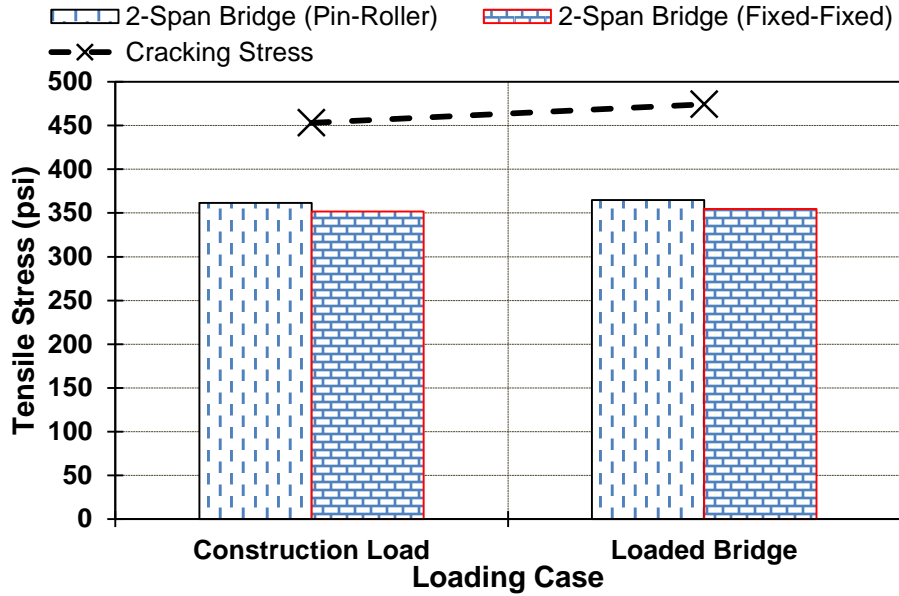


Figure 5-57: Longitudinal tensile stresses due to truck loads (boundary conditions)

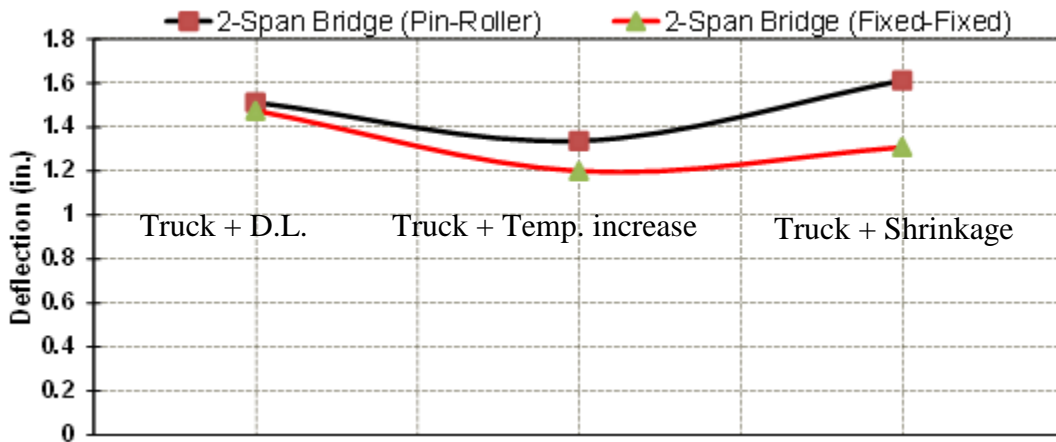


Figure 5-58: Bridge deflection (boundary conditions)

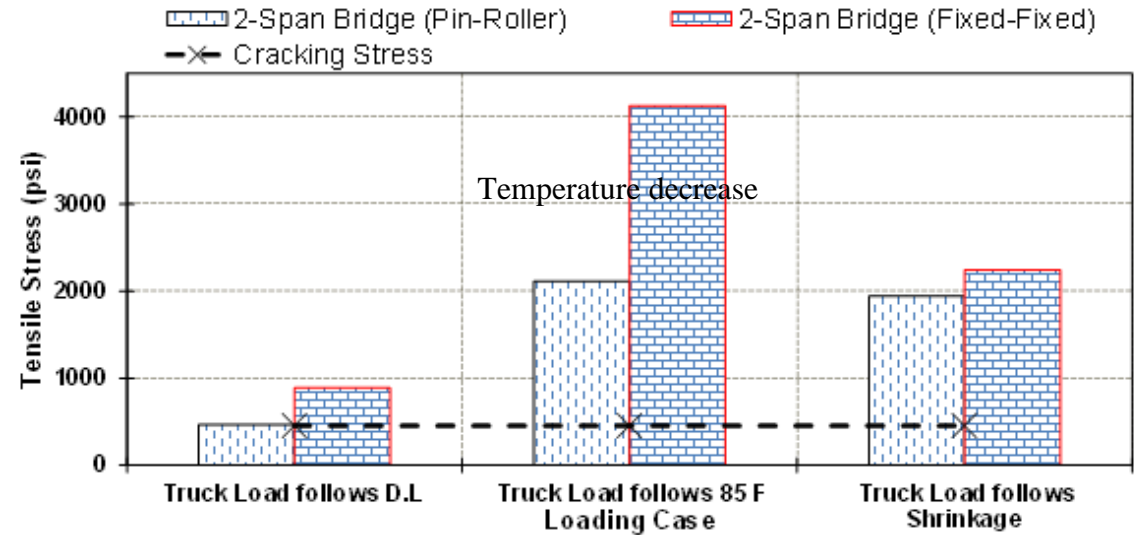


Figure 5-59: Longitudinal tensile stresses due to truck loads at 14 days (boundary conditions)

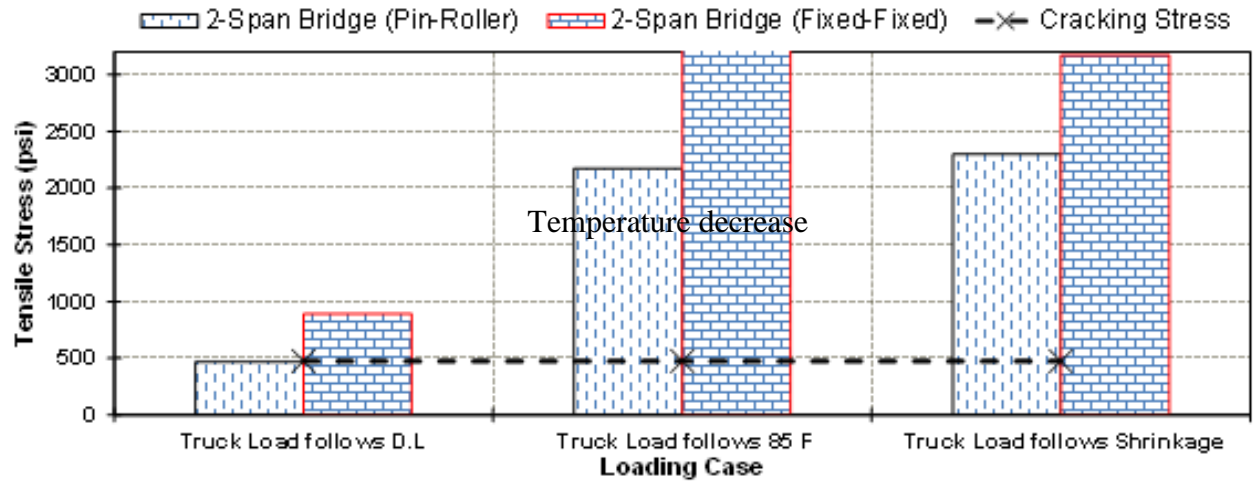


Figure 5-60: Longitudinal tensile stresses due to truck loads at 28 days (boundary conditions)

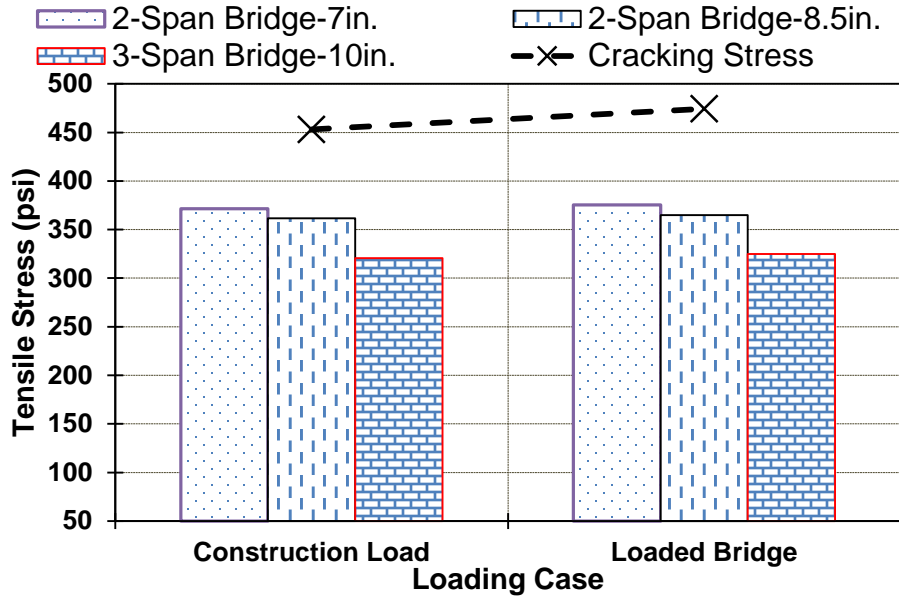


Figure 5-61: Longitudinal tensile stresses due to truck loads (deck thickness)

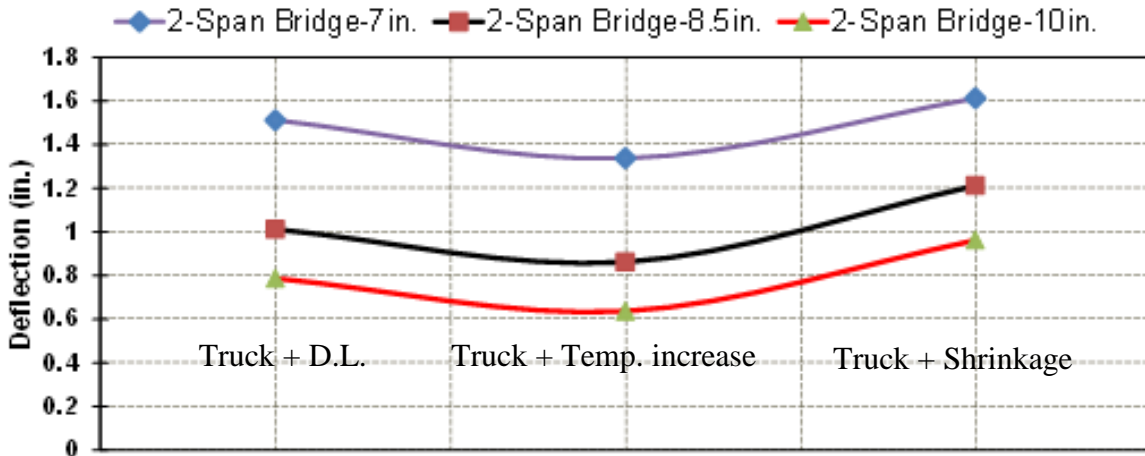


Figure 5-62: Bridge deflection (deck thickness)

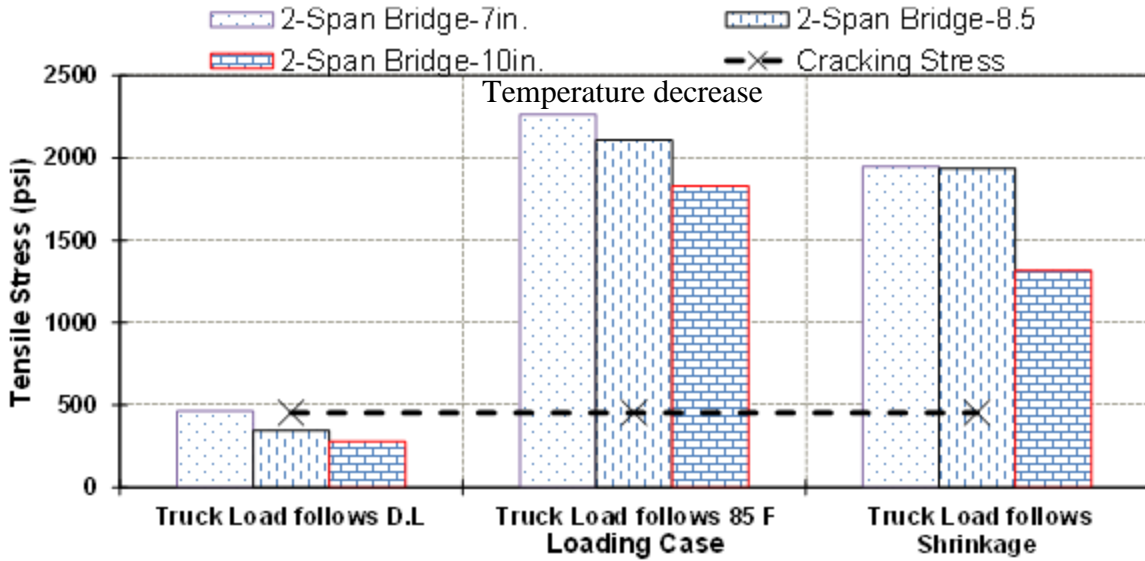


Figure 5-63: Longitudinal tensile stresses due to truck loads at 14 days (deck thickness)

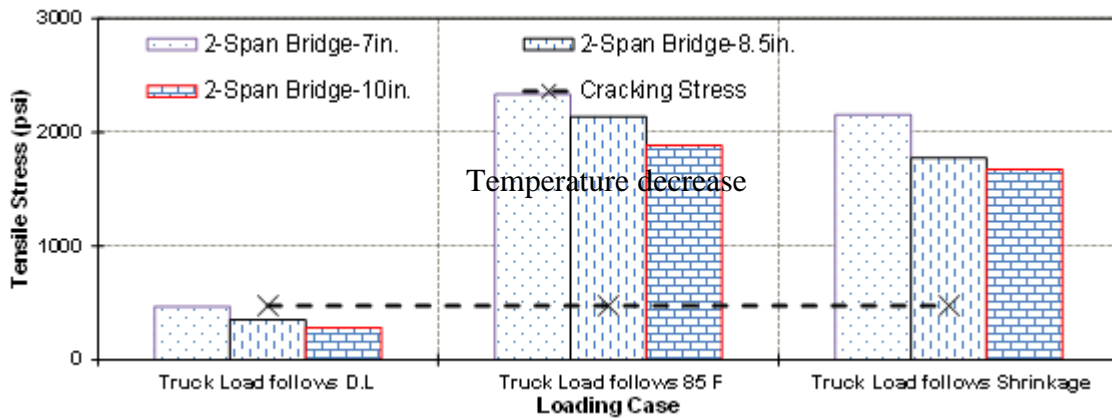


Figure 5-64: Longitudinal tensile stresses due to truck loads at 28 days (deck thickness)

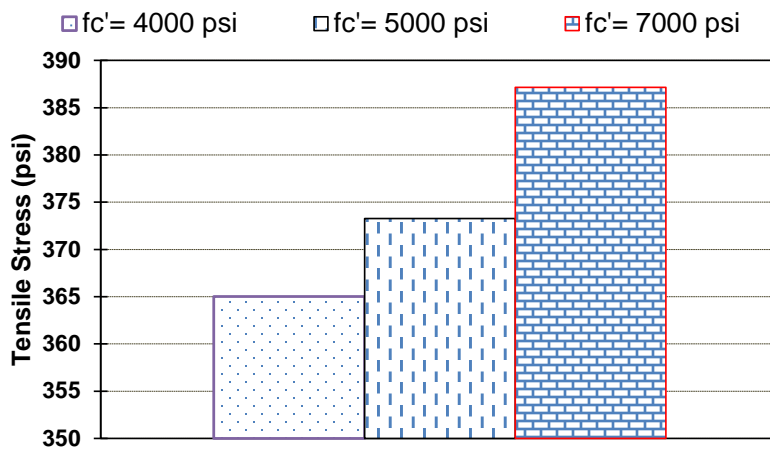


Figure 5-65: Longitudinal tensile stresses due to truck loads (concrete compressive strength)

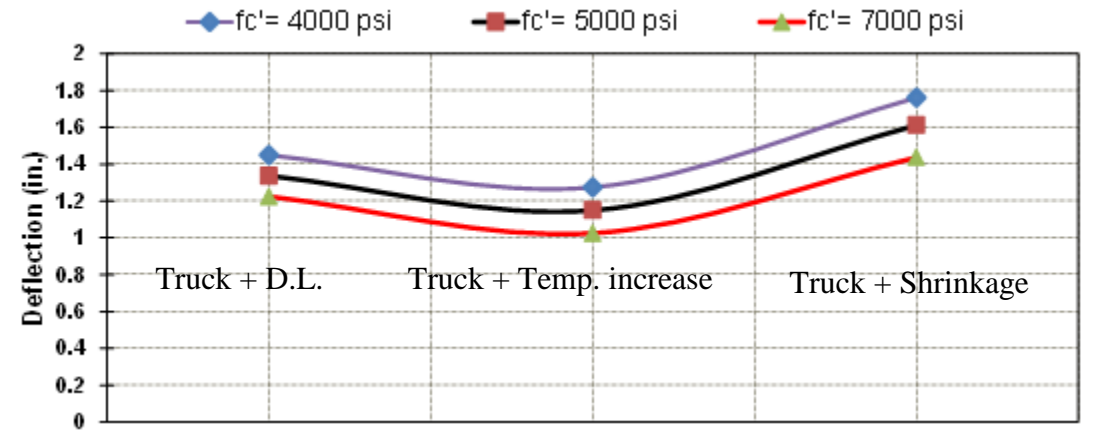


Figure 5-66: Bridge deflection (concrete compressive strength)

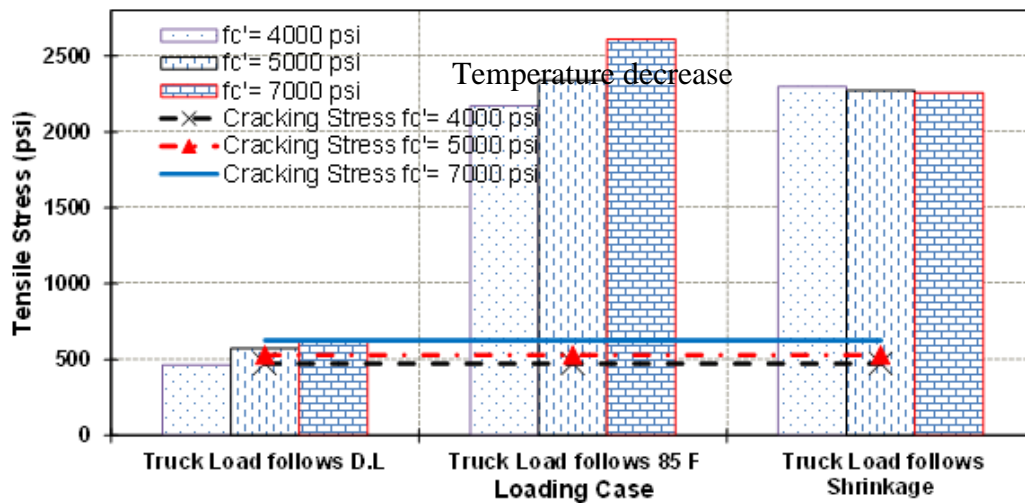


Figure 5-67: Longitudinal tensile stresses due to truck loads at 28 days (concrete compressive strength)

5.6. DESIGN IMPLICATIONS - EFFECT OF LOADING ON DEFLECTION & CRACK WIDTH

The bridge under study has the following properties:

- Bridge span length is 184 ft
- Three span bridge
- Girders spaced at 11'-3" o.c.

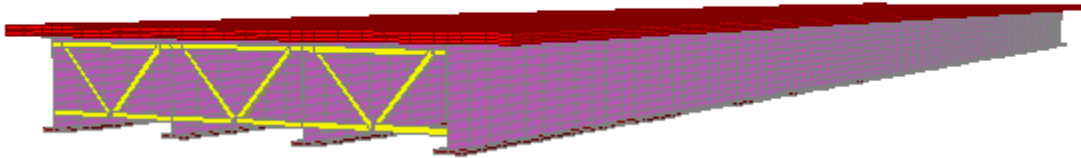


Figure 5-68: Bridge overview

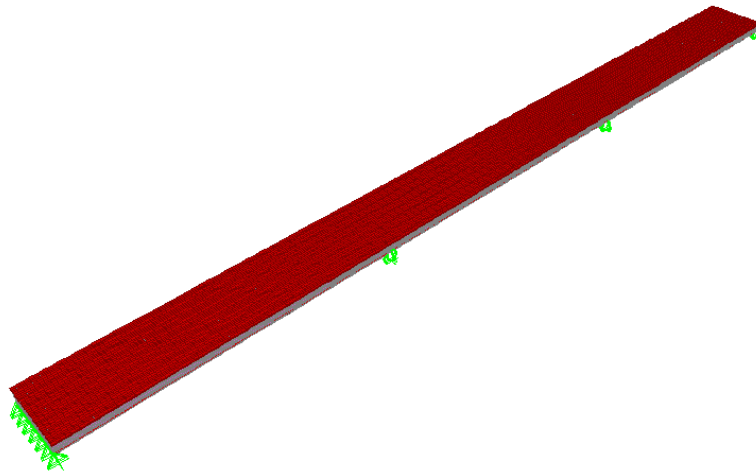
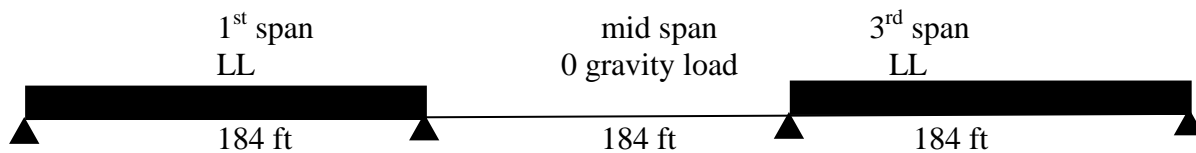


Figure 5-69: Three-span bridge

5.7. Loading Scenario

- The effect of dead load was not considered since unshored construction is a common practice.
- The 1st and 3rd spans were loaded with (LL) and mid span had no load



It is important to note that different types of loads were applied to the three-span bridge model. The applied loads included not only live load but also shrinkage, decrease of temperature, and increase of temperature. The temperature load was only applied to the bridge deck while the temperature of steel I-girders was assumed to remain unchanged. It was found that changing the temperature affects the tendency of the bridge deck to develop transverse cracking.

A summary of results is presented as shown in Tables 5-4 and 5-5.

Table 5-4: Loads and Loads Combinations Stresses, Moments, Deflections, and Crack Width

Loading Case	Moment (kip-ft)	Deflection (in.)	Crack width (in.)	Remarks
Shrinkage (SH)	1211	0.72↑	0.149	Cracked
Temp.(TE(+)) ¹	80	0.73↓	0	No cracks
Temp. (TE(-)) ²	963	0.60↑	0.118	Cracked
Truck (TR) ³	115	0.33↑	0	No cracks
SH + TR	1325	0.90↑	0.169	Cracked
(TE-Increase)+ TR	76	0.61↓	0	No cracks
(TE-Decrease)+ TR	1076	0.95↑	0.133	Cracked
SHR + TR + TE(+)	382	0.30↑	0.039	Cracked
SHR + TR + TE(-)	2287	1.68↑	0.299	Cracked

¹ Values presented are due to 85°F of an increase of temperature.

² Values presented are due to 85°F of a decrease of temperature.

³ 2.1 HS-20

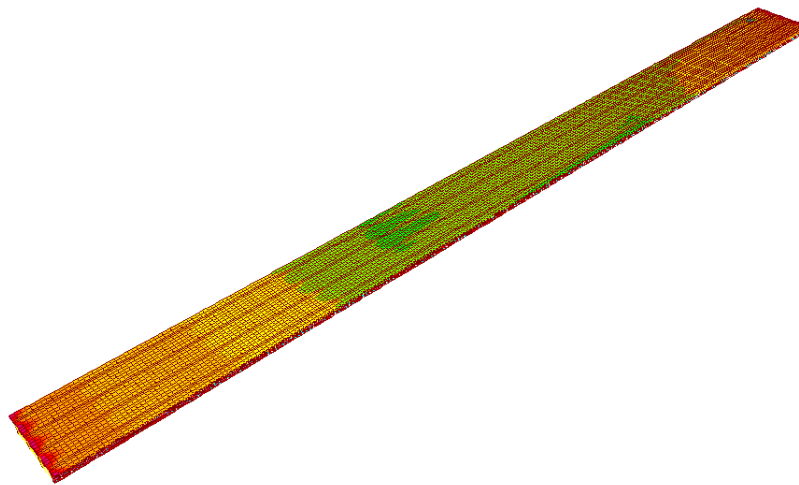


Figure 5-70: Stress contours due to shrinkage



Figure 5-71: Bridge deformed shape due to shrinkage

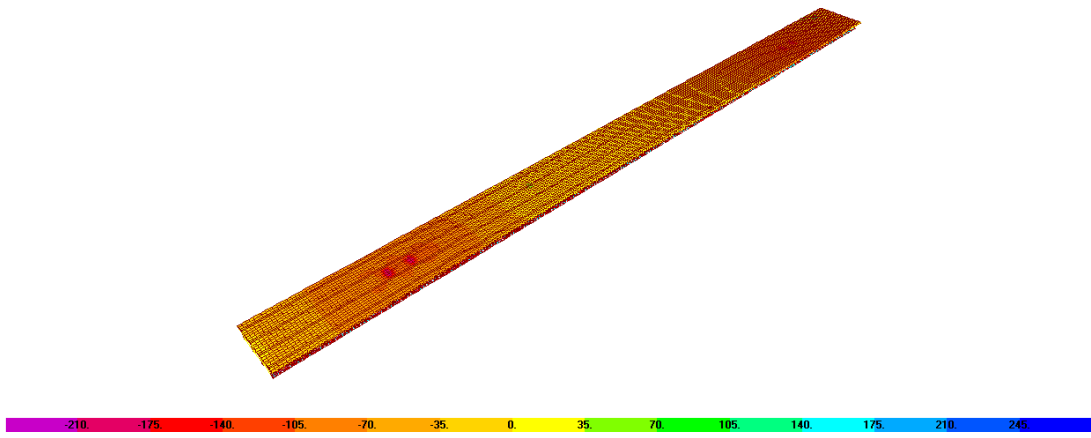


Figure 5-72: Stress contours due to Truck load



Figure 5-73: Bridge deformed shape due to Truck load

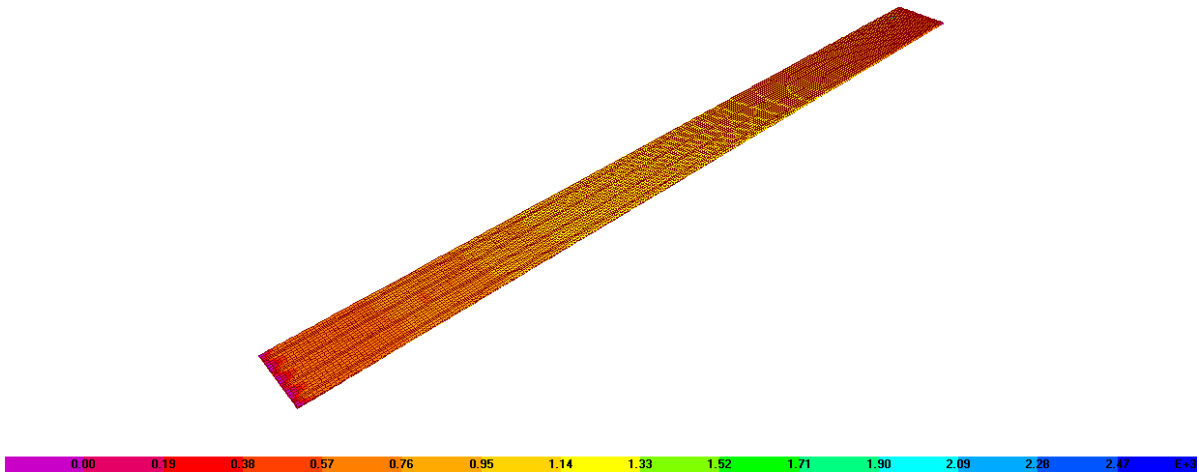


Figure 5-74: Stress contours due to Shrinkage and Truck – Top of Slab

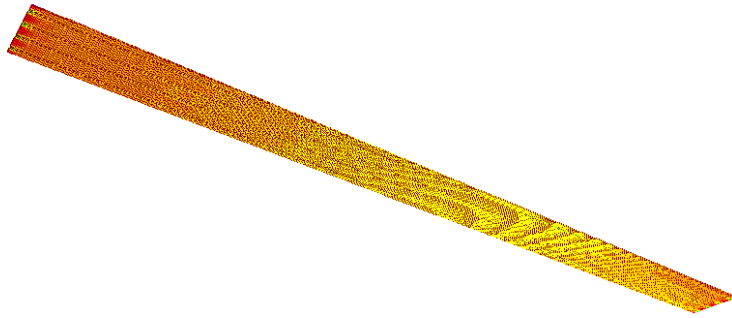


Figure 5-75: Stress contours due to shrinkage and Truck – bottom of slab

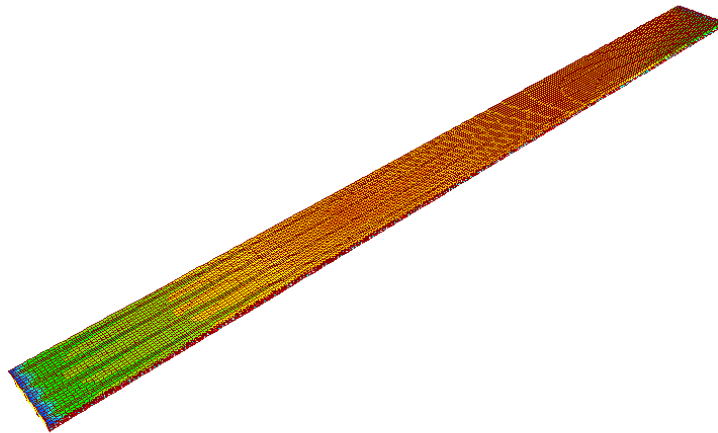


Figure 5-76: Stress contours due to 85°F increase of temperature



Figure 5-77: Bridge deformed shape due to 85°F increase of temperature

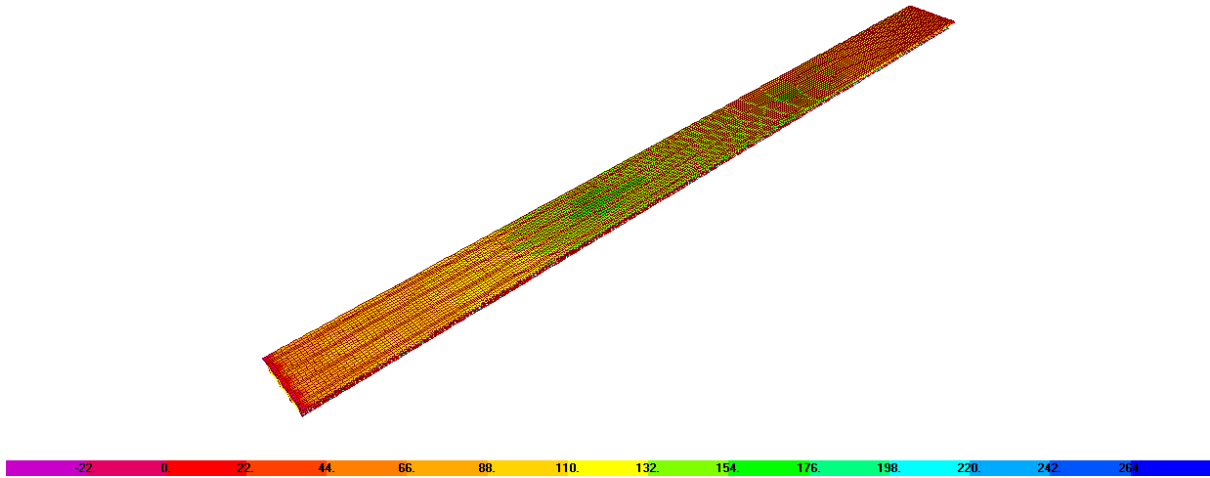


Figure 5-78: Stress contours due to 85°F decrease of temperature



Figure 5-79: Bridge deformed shape due to 85°F decrease of temperature

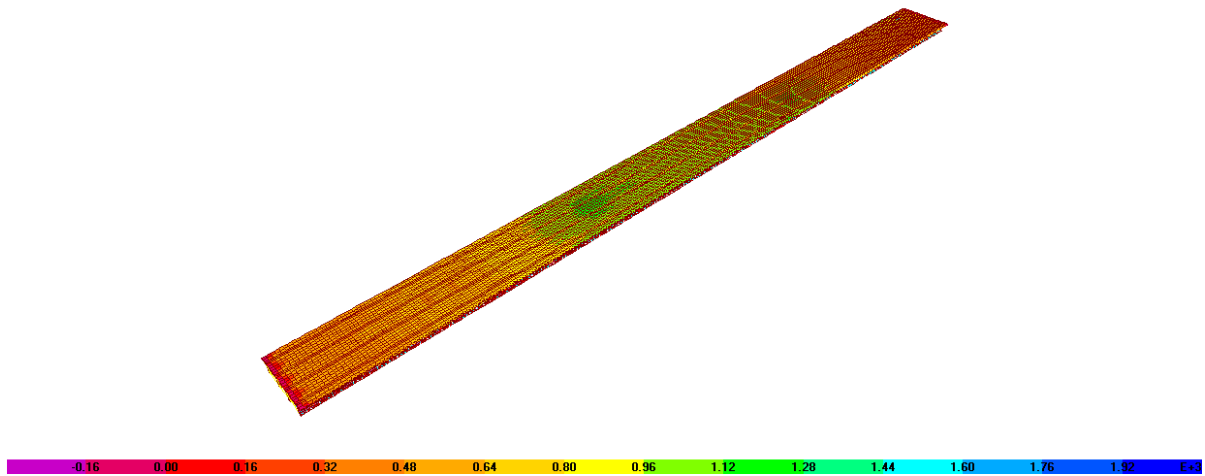


Figure 5-80: Stress contours due to 85°F decrease of temperature and Truck load

In order to study the effect of the increase of the live load applied to the bridge model on the widening of developed transverse cracks, the live load due to truck load was incrementally increased. The live load cases included application of 50%, 75%, 100%, and 125% of HS-20 truck load. The increase of the live load tends to further open the crack up and hence the crack width increased. It was important to specifically conduct this study on combined case of truck load with either shrinkage or decrease of temperature since shrinkage and decrease of temperature cases were proven to drive the development of transverse deck cracking. What was important is the clear trend of increased crack width with increased deflection due to incrementally increasing truck loading.

Table 5-5: Increase of Truck Load Effect with Shrinkage Load

Loading Case	Moment (kip-ft)	Deflection (in.)	Crack width (in.)
SH+0.5TR	1268	0.82↑	0.157
SH + 0.75TR	1296	0.86↑	0.161
SH + TR	1325	0.90↑	0.169
SH + 1.25TR	1353	0.93↑	0.173

Summary of results is shown in Table 5-6 for the cases of incremental increase of truck load and a decrease of temperature of 85°F.

Table 5-6: Increase of Truck Load Effect with Temperature Decrease Load

Loading Case	Moment (kip-ft)	Deflection (in.)	Crack width (in.)
TE¹+0.5TR	1020	0.87↑	0.126
TE + 0.75TR	1048	0.91↑	0.130
TE + TR	1076	0.95↑	0.134
TE + 1.25TR	1105	1.00↑	0.138

¹ Values presented are due to 85°F of a decrease of temperature

6. SPREADSHEET FOR EARLY AGE SHRINKAGE CRACK CALCULATIONS

6.1. INTRODUCTION

Understanding the concrete properties is important to accurately model the mechanisms contributing to the cracking of concrete decks. The user interface of the implemented computer Excel program will enable the user to input the properties of the concrete being monitored. The accompanied spreadsheet is designed to be a user-friendly calculation tool for concrete mixture proportioning, temperature prediction, thermal analysis, and tensile cracking prediction. It is designed specifically for concrete bridge decks but addresses a few different types of construction approaches including a deck with a stay-in-place galvanized metal pan, a deck with removable forms, or a deck on a precast panel. Though to obtain accurate temperatures, thermal stresses, and cracking risk calculations the user should have a good understanding of the fundamental principles and mechanics of hardening concrete. The aspects of hardening concrete addressed in the spreadsheet is subdivided into multiple sections; the first being concrete mixture proportioning, followed by temperature prediction, thermal stress analysis, and finally tensile cracking predictions.

6.2. NOTATIONS

k_c	is the concrete thermal conductivity
α	is the degree of hydration
k_{uc}	is the ultimate hardened concrete thermal conductivity.
c_{pconc}	is the specific heat of the concrete
ρ_{conc}	is the concrete density
W_c	is the weight of cement
W_a	is the weight of aggregate
W_w	is the weight of water
c_c	is the cement specific heat
c_a	is the aggregate specific heat
c_w	is the water specific heat
c_{ref}	is an average ultimate specific heat of the cement
α_u	is the ultimate degree of hydration
τ	is the hydration time parameter
β	is the hydration slope parameter
p_{C3S}	is the percent alite content in the Portland cement
p_{C3A}	is the percent aluminates in the Portland cement
p_{C2S}	is the percent belite in the Portland cement
p_{C4AF}	is the percent ferrite in the Portland cement
p_{SO3}	is the percent total sulfate in the Portland cement
p_{MgO}	is the percent MgO in the Portland cement
p_{freeCa}	is the percent CaO in the Portland cement

H_u is the ultimate heat of hydration
 H_{cem} is the heat of hydration of the Portland cement
 E_a is the activation energy of the concrete mixture
 t_e is the equivalent age of the concrete
 R is the universal gas constant
 T_r is the reference temperature
 T_{avg} is the average temperature during the time interval
 E_w is the water evaporation rate
 e_0 is the water surface saturated water vapor pressure
 e_a is the air water vapor pressure
 RH is the relative humidity (as a decimal)
 w is the wind speed
 E_c is the evaporation rate from concrete
 t is the time from mixing (hrs)
 a_{evap} is mixture dependent time constant
 ΔQ is the change in heat
 T_{sw} is the temperature of the surface water.
 T_a is the temperature of the air
 ϵ_a is the emissivity values for air
 ϵ_c is the emissivity values for concrete
 C_c is the percent of cloud cover
 G_{on} is the extraterrestrial radiation that would hit the surface
 ν is the Poisson's ratio
 E_c is the modulus of elasticity of the concrete
 α_{cteh} is the hardened concrete CTE
 α_{ca} is the coarse aggregate CTE
 V_{ca} is the coarse aggregate volume
 α_{fa} is the fine aggregate CTE
 V_{fa} is the fine aggregate volume
 α_p is the paste CTE
 V_p is the paste volume
 $f'_c(t)$ is the concrete compressive strength at any time t
 f'_c_{28} is the concrete compressive strength at 28 days
 $E_c(t)$ is the concrete modulus of elasticity at any time t
 E_{c28} is the concrete modulus of elasticity at 28 days
 s is a cement type coefficient
 ϵ_T is the thermal strain developed at time t
 $\epsilon_{sh}(t)$ is the mean shrinkage strain in the cross section
 $\epsilon_{sh\infty}$ is the time dependence of ultimate shrinkage
 kh is the humidity dependence
 $S(t)$ is the time dependence for shrinkage
 $\epsilon_{cr}(t)$ is the creep strain at any time t
 $J(t)$ is the creep compliance function
 $C_0(t)$ is the compliance function for basic creep at any time t

$C_d(t)$ is the compliance function for additional creep due to simultaneous drying
 K_r is the degree of restraint

6.3. SPREADSHEET ORGANIZATION

The spreadsheet is designed in such a way that the user can work their way through the multiple tabs from left to right where each tab is labeled by the process of computation. The tabs range in order from Deck and Concrete Inputs to Mix Design, Structural and Environmental Inputs, Cement Hydration, Temperature Analysis, Properties and Strengths, and Creep and Shrinkage Stresses. Each tab may contain various required user inputs, optional user inputs, default values, or calculated values. Each of the aforementioned cells are color coded with required inputs as bright yellow, optional inputs as pale yellow, default values as pinkish, and calculated values as grey. Examples of the two user input tabs are available, as shown in Figures 6-1 and 6-2.

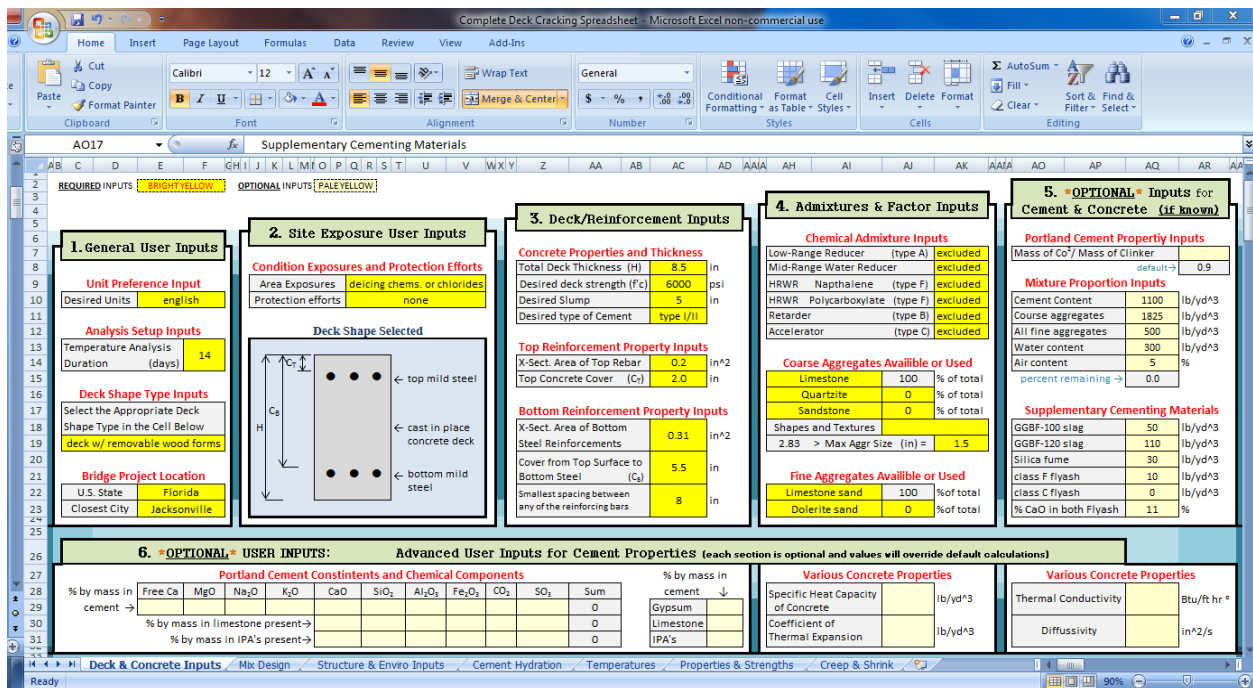


Figure 6-1: Visual example of deck and concrete user input tab

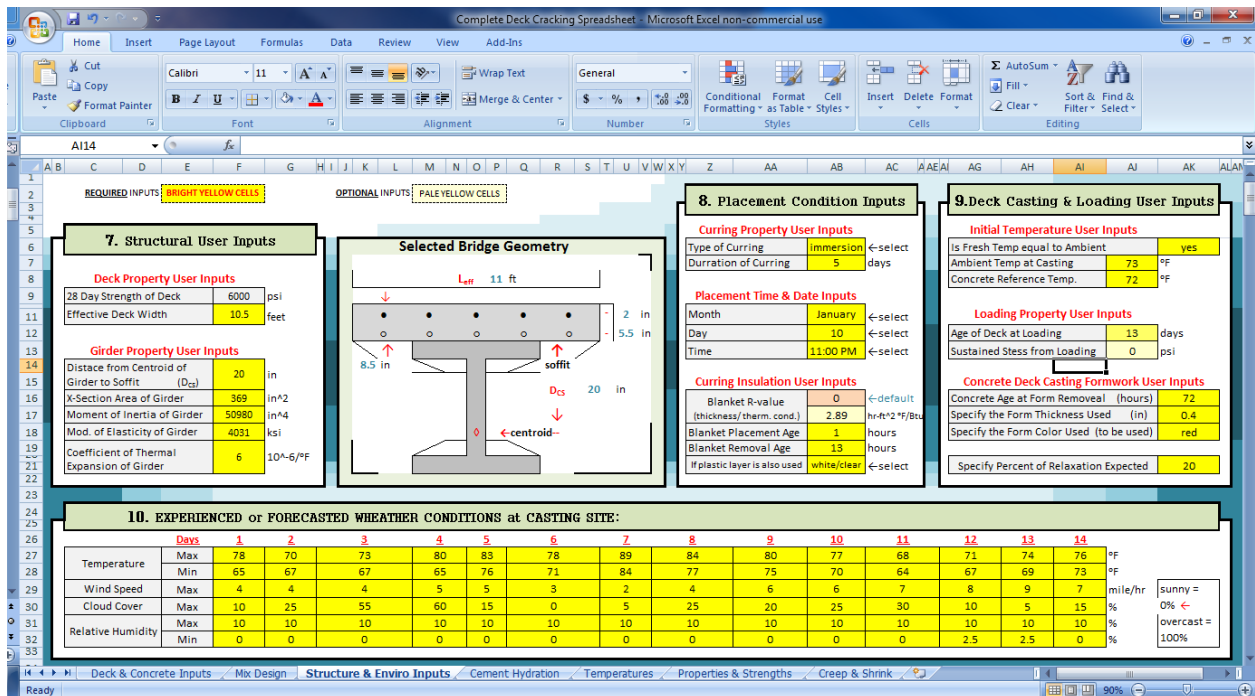


Figure 6-2: Visual example of structural and environmental user input tab

6.4. CONCRETE MIXTURE PROPORTIONING

The calculations for concrete mixture proportioning are only performed if the user does not specify a predetermined mixture. The primary source used for the mixture proportioning calculations in the accompanied spreadsheet is the ACI 211.1-91 document “Standard Practice for Selecting Proportions for Normal, Heavyweight, and Mass Concrete”. For a more detailed explanation of the proportioning method the user is recommended to read through the ACI 211 text.

When a user-specified mixture is not entered, the basic steps followed by the program are as follows:

1. Determine the amount of water needed to achieve a given slump for the maximum aggregate size selected by the user and to make the required adjustments to the water content based on the material properties, chemical admixtures, and entrained air properties.
2. Determine the water to cementitious ratio needed to achieve a desired strength with the percent of entrained air specified. Where the use of supplementary materials is assumed to not affect the water to cementitious ratio needed to achieve the desired strength.
3. Calculate the coarse aggregate fraction based on the maximum size of aggregate selected and the fine aggregate fineness modulus.

4. Calculate the required amount of fine aggregates to fill the remaining concrete volume which has already accounted for the cementitious materials, the water content, the coarse aggregate content and the percentage of air. The fine aggregate weight is then calculated from the volume using the specific gravity of the sands.

6.4.1. WATER ADJUSTMENTS

The water content is able to be adjusted for several factors both with and without a user defined concrete mixture proportion. User override values selected for water reducers should be based on prior experience or recommendations from the supplier/manufacturer. Air entrainment properties can be used to adjust the water content as they will also increase the concrete workability by both chemical and physical means. Similarly, supplementary material properties can be used to adjust the water content, for instance silica fume will greatly increase the water demand. Fly ash can, however, increase the workability, although the amount is very material dependent. Aggregates will also have a large effect on the concrete workability. Poorly shaped and graded aggregates will have a very high water demand. Round, smooth and well-graded aggregates will, however, decrease the concrete water demand. Experience with the local aggregates used is especially necessary when gauging the amount of water adjustment needed in the mixture proportioning. Likewise, material familiarity is necessary for the user to insure an adequate mixture is designed. The user should be familiar with concepts like using silica fume that are associated with using a high range water reducer that will aid in the dispersion due to the high water demand of the silica fume. Amounts and percentages for user override water adjustments are presented in Table 6-1 and shown in the display of the Excel tab labeled Figure 6-3.

Table 6-1: Range of User Override Water Adjustment Factors

Factor	Adjustment Ranges (negative is reduction)			
	Value	Unit	Value	Unit
Normal Range Water Reducer (ASTM type A)	0	%	-10	%
Mid-Range Water Reducer	-8	%	-15	%
High Range Water Reducer (ASTM type F)	-12	%	-30	%
Air Entrainment Effect	5	lbs/% air needed for desired		%
Aggregate Shape and Texture	-20	lbs	-45	lbs
Aggregate Gradation	10	%	-10	%
Supplementary Mineral Admixtures	15	%	-10	%
Other Un-specified Factors	10	%	-10	%

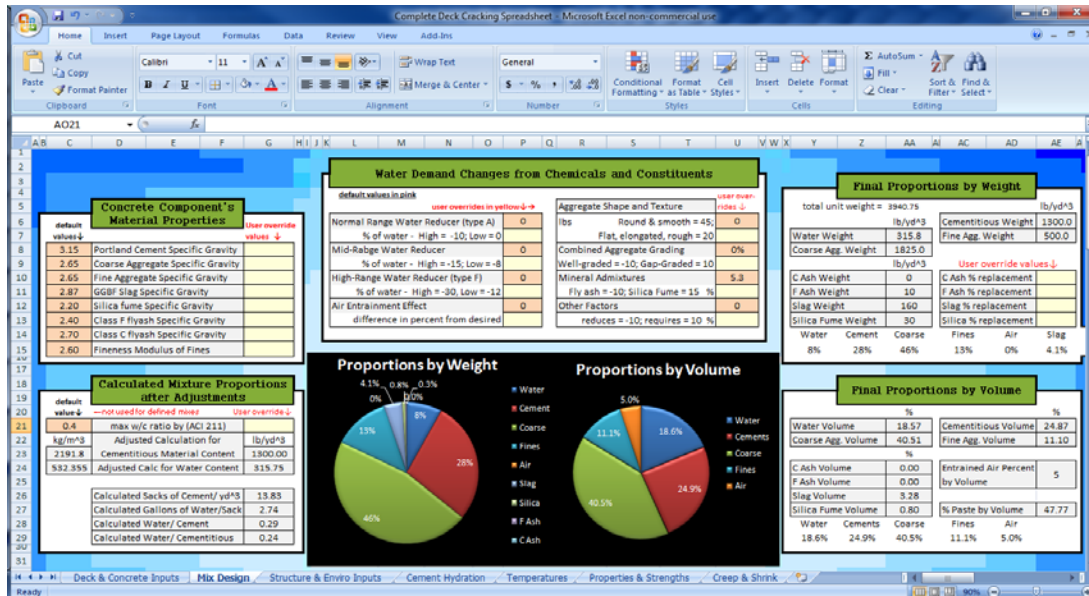


Figure 6-3: Concrete mixture portioning design tab of associated Excel spreadsheet

6.5. TEMPERATURE PREDICTION

Because of the constantly changing early age properties of concrete, the thermal properties of the concrete and its constituents are updated every time step. Some of the time dependent properties calculated include: thermal conductivity and the specific heat of the concrete.

6.5.1. CONCRETE THERMAL PROPERTIES

Thermal Conductivity: The thermal conductivity is known to be a function of “the moisture content, content and type of aggregate, porosity, density and temperature (Van Breugel, 1998).” The concrete thermal conductivity increases with increasing moisture content. Based on the recommendation of Schindler (2002), the spreadsheet assumes a linear decrease of the thermal conductivity with the degree of hydration from 1.33 times the ultimate thermal conductivity to the ultimate thermal conductivity as shown in Equation 6-1:

$$k_c(\alpha) = k_{uc} \cdot (1.33 - 0.33 \cdot \alpha) \quad (\text{Equation 6-1})$$

Where k_c is the concrete thermal conductivity (W/m/K), α is the degree of hydration, and k_{uc} is the ultimate hardened concrete thermal conductivity.

Specific Heat Capacity: The specific heat of concrete is also dependent on the mixture proportions, the degree of hydration, moisture levels, and the temperature (Schindler, 2002). A model proposed by Van Breugel accounts for changes in the specific heat based on degree of hydration, mixture proportions, and temperature as shown in Equation 6-2.

$$c_{pconc} = \frac{1}{\rho_{conc}} \cdot (W_c \cdot \alpha \cdot c_{ref} + W_c \cdot (1 - \alpha) \cdot c_c + W_a \cdot c_a + W_w \cdot c_w) \quad (\text{Equation 6-2})$$

Where c_{pconc} is the specific heat of the concrete (J/kg/K), ρ_{conc} is the concrete density (kg/m³), W_c is the weight of cement (kg/m³), W_a is the weight of aggregate (kg/m³), W_w is the weight of water (kg/m³), c_c is the cement specific heat (J/kg/K), c_a is the aggregate specific heat (J/kg/K), c_w is the water specific heat (J/kg/k), and c_{ref} is an average ultimate specific heat of the cement taken as 840 (J/kg/K).

6.5.2. CONCRETE HEAT OF HYDRATION

The concrete mix design is first modified using the Bogue calculations according to ASTM C 150. The concrete heat of hydration parameters H_u , τ , β , α_u , and E_a are then calculated based on the concrete mixture proportions and the constituent material properties. The τ , β , and α_u parameters are calculated from Equations 6-3, 6-4, and 6-5.

$$\alpha_u = \frac{1.031 \cdot w/cm}{0.194 + w/cm} + \exp \left\{ \begin{array}{l} -0.885 - 13.7 \cdot p_{C_4AF} \cdot p_{cem} \\ -283 \cdot p_{Na_2O_{eq}} \cdot p_{cem} \\ -9.9 \cdot p_{FA} \cdot p_{FA-CaO} \\ -339 \cdot WRRET - 95.4 \cdot PCHRWR \end{array} \right\} \quad (\text{Equation 6-3})$$

$$\tau = \exp \left\{ \begin{array}{l} 2.68 - 0.386 \cdot p_{C_3S} \cdot p_{cem} + 105 \cdot p_{Na_2O} \cdot p_{cem} + 1.75 \cdot p_{GGBF} \\ -5.33 \cdot p_{FA} \cdot p_{FA-CaO} - 12.6 \cdot ACCL + 97.3 \cdot WRRET \end{array} \right\} \quad (\text{Equation 6-4})$$

$$\beta = \exp \left\{ \begin{array}{l} -0.494 - 3.08 \cdot p_{C_3A} \cdot p_{cem} - 0.864 \cdot p_{GGBF} \\ +96.8 \cdot WRRET + 39.4 \cdot LRWR + 23.2 \cdot MRWR \\ +38.3 \cdot PCHRWR + 9.07 \cdot NHRWR \end{array} \right\} \quad (\text{Equation 6-5})$$

Similarly, the parameters of heat and activation energy are also calculated based on the concrete mixture proportions and the constituent material properties as described by Equations 6-6, 6-7, and 6-8.

$$H_u = \left\{ \begin{array}{l} H_{cem} \cdot p_{cem} + 461 \cdot p_{GGBF-100} + 550 \cdot p_{GGBF-120} \\ +1800 \cdot p_{FA-CaO} \cdot p_{FA} + 330 \cdot p_{S.F.} \end{array} \right\} \quad (\text{Equation 6-6})$$

$$H_{cem} = \left\{ \begin{array}{l} 500 \cdot p_{C_3S} + 260 \cdot p_{C_2S} + 866 \cdot p_{C_3A} + 420 \cdot p_{C_4AF} \\ +624 \cdot p_{SO_3} + 1186 \cdot p_{freeCa} + 850 \cdot p_{MgO} \end{array} \right\} \quad (\text{Equation 6-7})$$

$$E_a = \left\{ \begin{array}{l} 41230 + 8330 \cdot [(C_3A + C_4AF) \cdot p_{cem} \cdot Gypsum \cdot p_{cem}] \\ -3470 \cdot Na_2O_{eq} - 19.8 \cdot Blaine + 2.96 \cdot p_{FA} \cdot p_{CaO-FA} \\ +162 \cdot p_{GGBFS} - 516 \cdot p_{S.F.} - 30900 \cdot WRRET - 1450 \cdot ACCL \end{array} \right\} \quad (\text{Equation 6-8})$$

Where p_{C_3S} is the percent alite content in the Portland cement, p_{C_3A} is the percent aluminate in the Portland cement, p_{C_2S} is the percent belite in the Portland cement, p_{C_4AF} is the percent ferrite in the Portland cement, p_{SO_3} is the percent total sulfate in the Portland cement, p_{MgO} is the percent

MgO in the Portland cement and p_{freeCa} is the percent CaO in the Portland cement. If a user specifies to include any of the chemical admixtures but does not specify the dose the default amounts used are listed in Table 6-2.

Table 6-2: Default Chemical Admixture Dosages Assumed If Selected But Not Specified

Chemical Admixture	Default percents used if not specified	
LRWR	0.0029	% by mass of cementitious materials
MRWR	0.0032	% by mass of cementitious materials
WRRET	0.0035	% by mass of cementitious materials
NHRWR	0.0078	% by mass of cementitious materials
PCHRWR	0.0068	% by mass of cementitious materials
ACCL	0.013	% by mass of cementitious materials

The maturity method used to determine the rate of hydration of the cement is the equivalent age method described in ASTM C 1074 where the equivalent age of the concrete is calculated as described in Equation 7-9.

$$t_e = \sum e^{-\frac{E_a}{R} \left(\frac{1}{(T_a+273)} - \frac{1}{(T_r+273)} \right)} \Delta T \quad (\text{Equation 6-9})$$

The degree of hydration is next calculated by use of Equation 7-10 and ultimately the rate of heat generated is calculated using the parameter values from Equations 6-3 through 6-10 at each time step using Equation 6-11 (Schindler, 2004).

$$\alpha(t_e) = \alpha_u \cdot \exp\left(-\left[\frac{\tau}{t_e}\right]^\beta\right) \quad (\text{Equation 6-10})$$

$$Q(t) = H_u \cdot C_c \cdot \left(\frac{\tau}{t_e}\right)^\beta \cdot \left(\frac{\beta}{t_e}\right) \cdot \alpha_u \cdot \exp\left(-\left[\frac{\tau}{t_e}\right]^\beta\right) \cdot \exp\left(\frac{E_a}{R} \left(\frac{1}{273+T_r} - \frac{1}{273+T}\right)\right) \cdot \left(\frac{1}{3600}\right) \quad (\text{Equation 6-11})$$

Where t_e is the concrete equivalent age at the reference temperature as shown in Equation 6-9 (hrs), H_u is the total amount of heat generated at 100% hydration (J/kg), C_c is the total amount of cementitious materials (kg/m^3), τ is the hydration time parameter (hrs), β is the hydration slope parameter, α_u is the ultimate degree of hydration, E_a is the activation energy (J/mol), R is the universal gas constant (J/mol/K), T_r is the reference temperature ($^{\circ}\text{C}$), and T_a is the average temperature during the time interval. At this point the degree of hydration, concrete maturity, rate of heat generation, and the adiabatic temperature rise can be calculated. An example of the previously mentioned calculations is shown in Figure 6-4 which displays the graphs generated on the “Cement Hydration” tab of the Excel file.

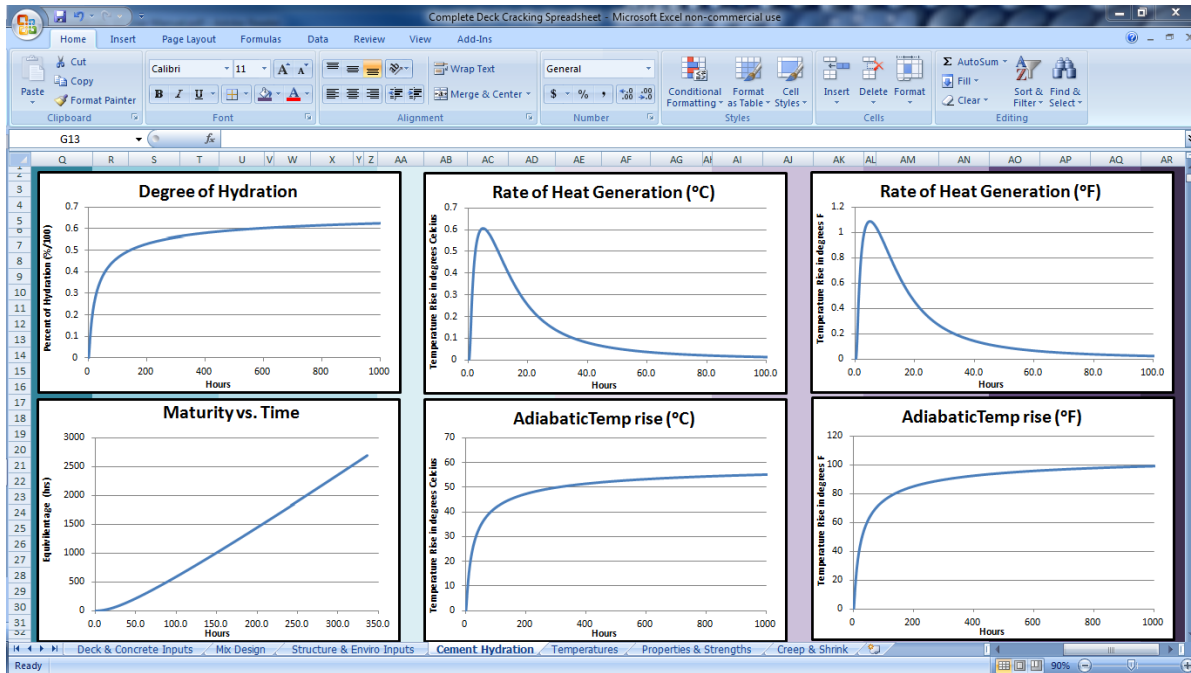


Figure 6-4: Example of “cement hydration” tab showing output graphs of hydration properties

6.6. BOUNDARY CONDITIONS

The boundary conditions considered for the temperature analysis include many heat sources and sinks. The primary conditions models include: evaporative cooling, free and forced convection, conduction, atmospheric radiation, solar radiation and irradiation. A depiction of the boundary conditions modeled is shown in Figure 6-5.

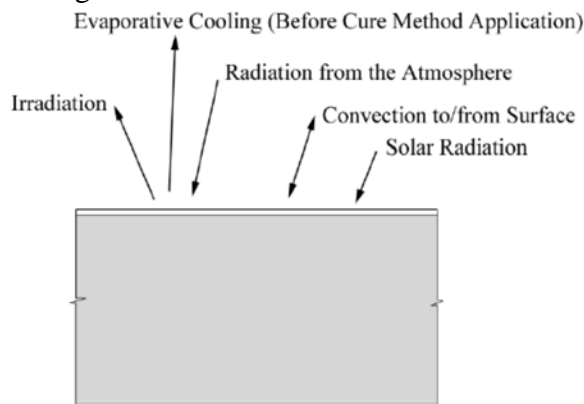


Figure 6-5: Boundary conditions used for temperature analysis model in Excel

Evaporative Cooling: The evaporative cooling model is from Schindler (2002). The model is reportedly based on the work of Menzel that applied water evaporation rate equations developed by Koehler to concrete. The evaporation rate follows Dalton’s law, which relates the water-vapor

pressure of the air, at the water surface, and the wind speed to the evaporation rate (Hover, 2006). Menzel's equation is shown as Equation 6-12 (Al-Fadhala and Hover, 2001).

$$E_w = 0.315(e_0 - RH \cdot e_a)(0.253 + 0.060w) \quad (\text{Equation 6-12})$$

Where E_w is the water evaporation rate ($\text{kg/m}^2/\text{hr}$), e_0 is the water surface saturated water vapor pressure (mmHg), e_a is the air water vapor pressure (mmHg), RH is the relative humidity (as a decimal), and w is the wind speed (m/s). The amount of evaporation from concrete may be related to the amount of evaporation from a water surface by Equation 6-13 (Schindler 2002):

$$E_c = E_w \cdot \exp \left[- \left(\frac{t}{a_{\text{evap}}} \right)^{1.5} \right] \quad (\text{Equation 6-13})$$

Where E_c is the evaporation rate from concrete ($\text{kg/m}^2/\text{hr}$), t is the time from mixing (hrs), and a_{evap} is mixture dependent time constant (hrs). The default value for a_{evap} is equal to 3.75 hr and the evaporative cooling model is applied until either a cure method is applied or 24 hours after placing. The final change in heat due to evaporative cooling is calculated using Equation 6-14.

$$\Delta Q = -E_c \cdot h_{\text{lat}} \quad (\text{Equation 6-14})$$

Where ΔQ is the heat lost due to evaporative cooling, E_c is the evaporation rate from the concrete as calculated in Equation 6-13, and h_{lat} is calculated by using Equation 6-15 where T_{sw} is the temperature of the surface water.

$$h_{\text{lat}} = 2500000 + 1859 \cdot T_{\text{sw}} \quad (\text{Equation 6-15})$$

Convection: Both the free and forced convection heat exchanges are modeled using Equations 6-16 and 6-17. Equation 6-16 is defining the change in heat due to the convection process and Equation 6-17 is defining the convection coefficient.

$$\Delta Q = h(T_s - T_a) \quad (\text{Equation 6-16})$$

$$h = C \cdot 0.2782 \cdot \left(\left[\frac{1}{T_{\text{avg}} + 17.8} \right]^{0.181} \right) \cdot (|T_s - T_a|^{0.266}) \cdot \left(\sqrt{1 + (2.8566 \cdot w)} \right) \quad (\text{Equation 6-17})$$

Where ΔQ is the change in heat, h is the convection coefficient, T_s is the temperature of the concrete surface, T_a is the temperature of the air, and T_{avg} is the average of the two temperatures.

Conduction: Conduction is the heat lost or gained from the contact of the concrete with any other material or substance. Conduction can be considered to act between the concrete and the air, between the concrete and the form work, or between the concrete and stagnate surface water; and is calculated using Equation 6-18.

$$\Delta Q = -k \cdot A \cdot \frac{\Delta T}{\Delta y} \cdot \Delta t \quad (\text{Equation 6-18})$$

Where ΔQ is the change in heat, k is the thermal conductivity of the concrete, A is the area of contact, ΔT is the difference in temperature of the two materials, Δy is the thickness of the volume considered, and Δt is the duration of the time interval.

Radiation: The radiation that affects the curing concrete deck occurs as solar radiation, atmospheric radiation, and irradiation. The atmospheric radiation and irradiation are easiest to calculate and the respectful equations are listed below in Equations 6-19 and 6-20.

$$\Delta Q = \sigma \cdot \epsilon_a \cdot T_a^4 \quad \text{(Equation 6-19)}$$

$$\Delta Q = \epsilon_c \cdot \sigma \cdot T_c^4 \quad \text{(Equation 6-20)}$$

Where ΔQ is the change in heat due to the radiation, σ is the Boltzmann constant (W/m^2K^4), ϵ_a and ϵ_c are the emissivity values for either the air or the concrete, and T_a and T_c are the temperatures of either the air or the concrete. Solar radiations are much more complicated of calculations requiring calculated values for extraterrestrial radiation, solar declination angles, solar hour angles, and angles of incidence. These values are calculated based on the latitude and longitude of the nearest location selected by the user and follow the procedures outlined in “Solar Engineering of Thermal Processes: Third Edition” by J.A. Duffie and W.A. Beckman. However the final equation used to calculate the solar radiation on the deck surface at each time step is defined in Equation 6-21.

$$\Delta Q = (0.91 - 0.7 \cdot Cc) \cdot G_{on} \cdot Ab_c \quad \text{(Equation 6-21)}$$

Where ΔQ is the change in heat due to solar radiation, Cc is the percent of cloud cover, G_{on} is the extraterrestrial radiation that would hit the surface, and Ab_c is the absorptiveness of the concrete. Using the values calculated for Equations 6-14, 6-16, 6-18, 6-19, 6-20, and 6-21 the final temperature of the concrete accounting for the energy lost or gained is ultimately compiled to generate a graph of temperature vs. time. An example of the generated graphs is available in Figure 6-6 which displays a screen shot of the temperature analysis tab of the associated excel spreadsheet.

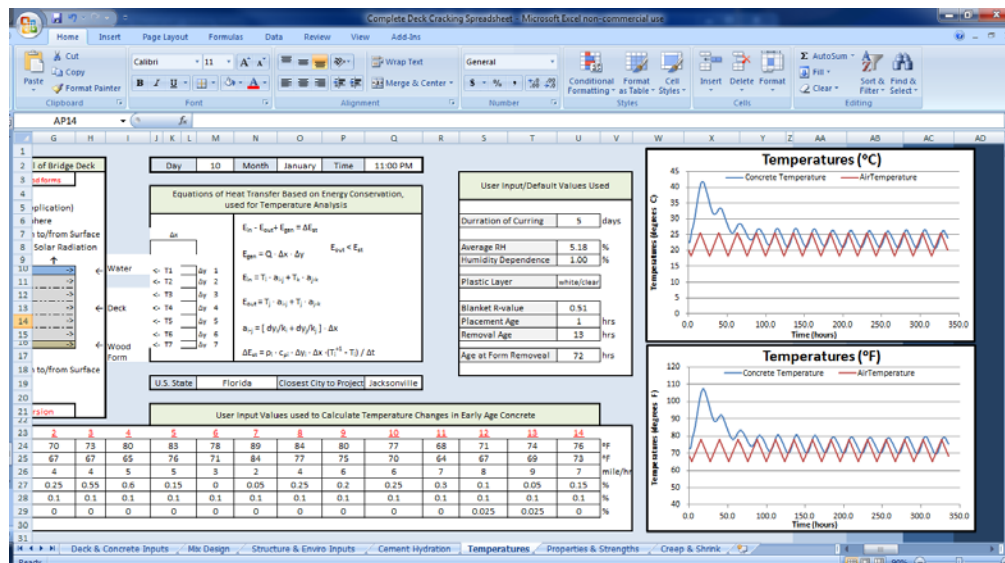


Figure 6-6: Depiction of temperature analysis tab, displaying output graphs of temperatures

6.7. THERMAL STRESS ANALYSIS

Thermal stress modeling in concrete members is non-linear because of changing early age material properties such as Poisson's ratio, the coefficient of thermal expansion (CTE), the modulus of elasticity, and the concrete strength. The non-linearity is also attributed to differential temperature development and creep. The thermal stress analysis includes the evaluation of thermal expansion stresses, shrinkage stresses, the degrees of restraint, and the creep stresses developed over time. The B3 Model associated with Zdenek P. Bazant and Sandeep Baweja was the primary source for the creep and shrinkage calculations where thermal, shrinkage, and creep strains are calculated and converted to stresses. The stresses are calculated from the strain values using Equation 6-22.

$$\sigma = \frac{E_c \varepsilon}{(1+\nu) \cdot (1-2\nu)} \quad (\text{Equation 6-22})$$

Where σ is the developed stress, ε is the previously calculated strain, ν is the Poisson's ratio, and E_c is the modulus of elasticity of the concrete.

6.7.1. CONCRETE MECHANICAL PROPERTIES

Concrete mechanical property development at early-ages is dependent on the concrete degree of hydration and temperature development. The mechanical property development is calculated using the equivalent age maturity (ASTM C 1074, 2004) as previously discussed.

Poisson's ratio: A multitude of different equations have been developed to relate the maturity to the development of Poisson's ratio. The accompanied spreadsheet uses a proposed model from De Schutter and Taerwe, 1996; where Poisson's ratio is based on the degree of hydration as described in Equation 6-23.

$$\nu(\alpha) = 0.18 \cdot \sin\left(\frac{\pi \cdot \alpha}{2}\right) + 0.5e^{-10\alpha} \quad (\text{Equation 6-23})$$

Where $\nu(\alpha)$ is Poisson's ratio at that degree of hydration and α is the degree of hydration as calculated from the heat of hydration analysis. An example of the graphical display of the Poisson's ratio from the accompanied spreadsheet is displayed in Figure 6-7 (full hydration is not achieved in this example).

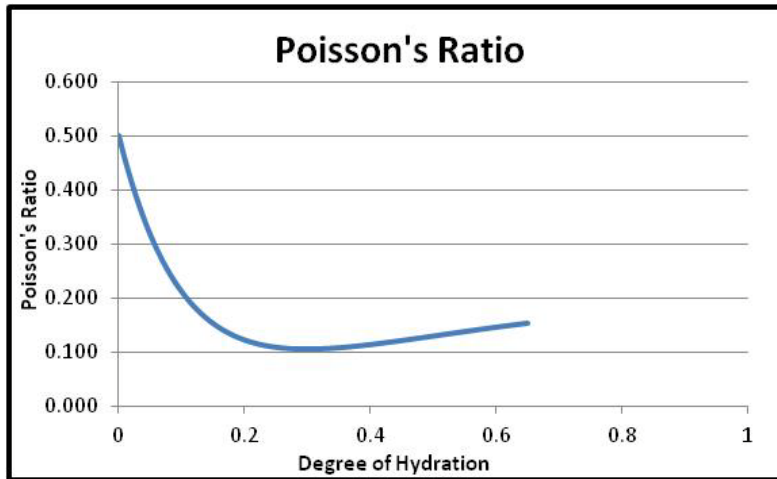


Figure 6-7: Graphical depiction of example poisson's ratio development from spreadsheet

Coefficient of thermal expansion: The accompanied spreadsheet uses a constant CTE, because of the lack of a data to model how the mixture proportions relate to CTE development. The constant coefficient of thermal expansion used is calculated from the mixture proportions and the aggregate type using the method proposed by Emanuel and Hulsey (1977) shown in Equation 6-24.

$$\alpha_{cteh} = \frac{\alpha_{ca} \cdot V_{ca} + \alpha_{fa} \cdot V_{fa} + \alpha_p \cdot V_p}{V_{ca} + V_{fa} + V_p} \quad (\text{Equation 6-24})$$

Where α_{cteh} is the hardened concrete CTE, α_{ca} is the coarse aggregate CTE ($\mu\epsilon/^\circ\text{C}$), V_{ca} is the coarse aggregate volume (kg/m^3), α_{fa} is the fine aggregate CTE ($\mu\epsilon/^\circ\text{C}$), V_{fa} is the fine aggregate volume (kg/m^3), α_p is the paste CTE ($\mu\epsilon/^\circ\text{C}$), and V_p is the paste volume (kg/m^3). Unless optional user inputs or user overrides are modified, the default values of CTE for various constituents presented in Table 6-3 are used for evaluation of the concrete's CTE in Equation 6-24.

Table 6-3: Default CTE Values of Concrete Constituents Used If No Modifications are Selected by User

Possible Concrete Constituents	Default CTE Values Used
Hardened Cement Paste	10.8 $\mu \text{E} / ^\circ\text{C}$
Limestone Aggregates	3.5 $\mu \text{E} / ^\circ\text{C}$
Siliceous River Gravel and Sands	11 $\mu \text{E} / ^\circ\text{C}$
Granite Aggregates	7.5 $\mu \text{E} / ^\circ\text{C}$
Dolomitic Limestone Aggregates	7 $\mu \text{E} / ^\circ\text{C}$

Compressive Strength: The compressive strength of the concrete can be calculated in a number of ways. The accompanied spreadsheet calculated the compressive strength of the concrete using two different methods and averages the results. The first method is described by Equation 6-25.

$$f'c(t) = f'c_{28} \cdot \exp\left(-\left[\frac{\tau_s}{t}\right]^\beta\right) \quad (\text{Equation 6-25})$$

Where $f'c(t)$ is the concrete compressive strength at any time t , $f'c_{28}$ is the concrete compressive strength at 28 days, τ_s is a fit parameter taken as 0.721, and β is another fit parameter taken as 27.8. In the other method, Equation 6-26 is solved for $f'c(t)$ using the value from Equation 6-27 as $E_c(t)$ and is averaged with the value attained from Equation 6-25.

Modulus of Elasticity: The elastic modulus provides the correlation between restrained strains and stresses and it is known to be dependent on the mixture proportions, unit weight, maturity, aggregate modulus, strength, and moisture condition. The elastic modulus is also known to develop faster than the tensile and compressive strengths. In the accompanied spreadsheet two methods of calculating the modulus are performed and then averaged. The two methods are described by Equations 6-26 and 6-27 where Equation 6-26 is from the ACI 318 document and Equation 6-27 is from the CEB-FIP document.

$$E_c(t) = 57000\sqrt{f'c(t)} \quad (\text{Equation 6-26})$$

$$E_c(t) = E_{c28}e^{[s/2(1-\sqrt{28/t})]} \quad (\text{Equation 6-27})$$

Where $E_c(t)$ is the concrete modulus of elasticity at any time t , E_{c28} is the concrete modulus of elasticity at 28 days, and s is a cement type coefficient which is 0.2 for high early strength cements, 0.25 for normal hardening cements, and 0.38 for slow hardening cements.

6.7.2. THERMAL EXPANSION

Thermal dilation stresses developed in the concrete are the easiest stresses to calculate using the B3 model. The thermal dilation strain is defined as listed in Equation 6-28.

$$\varepsilon_T(t) = \alpha \cdot \Delta T(t) \quad (\text{Equation 6-28})$$

Where ε_T is the thermal strain developed at time t , α is the concrete CTE as calculated in Equation 6-24, and $\Delta T(t)$ is the difference in temperature from the reference temperature at time t . The relating thermal stresses are then calculated using Equation 6-22.

6.7.3. SHRINKAGE

Concrete early-age free shrinkage strains are dependent on the concrete degree of hydration and temperature development. The free shrinkage strain is composed of the concrete thermal strains, the autogenous strains, the drying shrinkage strains, and the plastic shrinkage strains. In the B3 Model the shrinkage is first estimated from the concrete strength and composition.

$$\varepsilon_{sh}(t) = -\varepsilon_{sh\infty} \cdot k_h \cdot S(t) \quad (\text{Equation 6-29})$$

Where $\varepsilon_{sh}(t)$ is the mean shrinkage strain in the cross section, $\varepsilon_{sh\infty}$ is the time dependence of ultimate shrinkage, k_h is the humidity dependence, and $S(t)$ is the time dependence for shrinkage. These variables can easily be calculated using the B3 model.

6.7.4. CREEP

The creep calculated for the associated spreadsheet is primarily due to the applied stresses from early age thermal stresses and shrinkage stresses prior to loading. The final equation for the calculation of the early age creep strains are as defined in Equation 6-30.

$$\varepsilon_{cr}(t) = J(t) \cdot \sigma(t) \quad (\text{Equation 6-30})$$

Where $\varepsilon_{cr}(t)$ is the creep strain at any time t , $J(t)$ is the creep compliance function as described in Equation 6-31, and $\sigma(t)$ is the stress felt by the concrete at any time t .

$$J(t) = q_1 + C_0(t) + C_d(t) \quad (\text{Equation 6-31})$$

Where $J(t)$ is as previously defined, q_1 is the instantaneous strain due to a unit stress, $C_0(t)$ is the compliance function for basic creep at any time t , and $C_d(t)$ is the compliance function for additional creep due to simultaneous drying. The aforementioned compliance functions can also be easily calculated following the B3 model for creep and shrinkage. An example of the developed stresses calculated by the spreadsheet is available in Figure 6-8.

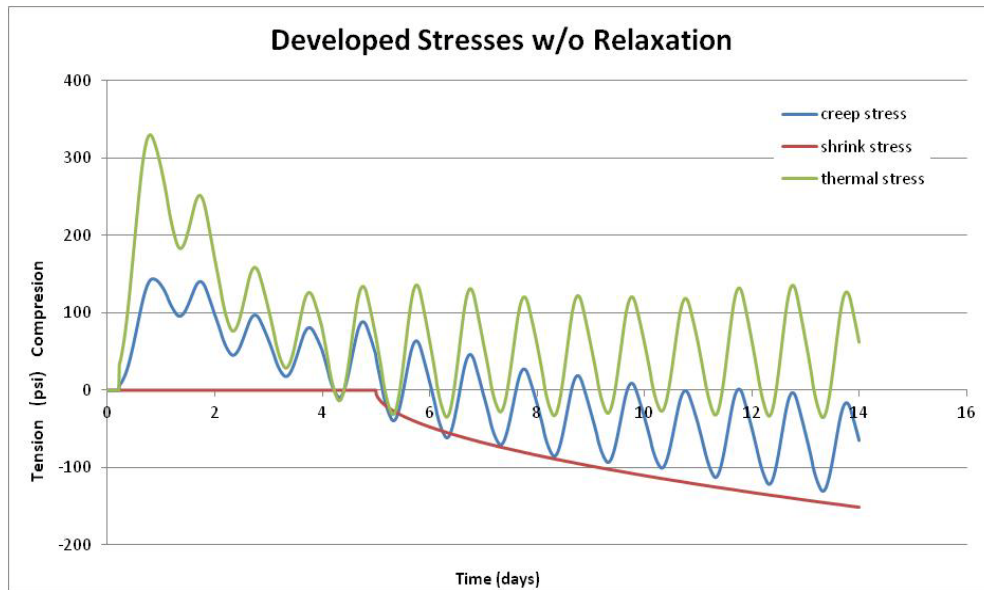


Figure 6-8: Example of stresses w/o relaxation calculated by spreadsheet

6.8. TENSILE CRACKING PREDICTION

6.8.1. DEGREES OF RESTRAINT

For the degree of restraint the restraining materials modulus is defined as E_f and the modulus of the freshly casted concrete is E_c . The ratio of the two moduli defines the degree of restraint as described in Equation 6-32.

$$K_r = \left\{ \begin{array}{ll} 0.2 & \text{when } \frac{E_f}{E_c} \leq .1 \\ .33 & \text{when } .1 < \frac{E_f}{E_c} \leq .2 \\ .56 & \text{when } .2 < \frac{E_f}{E_c} \leq .5 \\ .71 & \text{when } .5 < \frac{E_f}{E_c} \leq 1 \\ .83 & \text{when } 1 < \frac{E_f}{E_c} \end{array} \right\} \quad (\text{Equation 6-32})$$

6.8.2. TOTAL DEVELOPED STRESSES

Then using the stresses calculated from the strains in Equations 6-28, 6-29, and 6-30 the total stress in the newly casted deck can be calculated from Equation 6-33.

$$\sigma_{total} = K_r \cdot (\sigma_J + \sigma_T + \sigma_{cr}) \quad (\text{Equation 6-33})$$

6.8.3. TIME OF FIRST DEVELOPED CRACK

Finally, the tensile strength can be calculated by Equation 6-34; where $f'c$ is as calculated in Equation 6-25 and w is the calculated unit weight of the concrete determined from the mix design.

$$f_t = \frac{\sqrt{f'c \cdot w}}{3} \quad \text{(Equation 6-34)}$$

The moment of initial cracking of the deck can be approximated by comparing the developed tensile strength of the concrete to the stresses developed in the concrete. An example of this comparison can made in the spreadsheet can be seen in Figure 6-9.

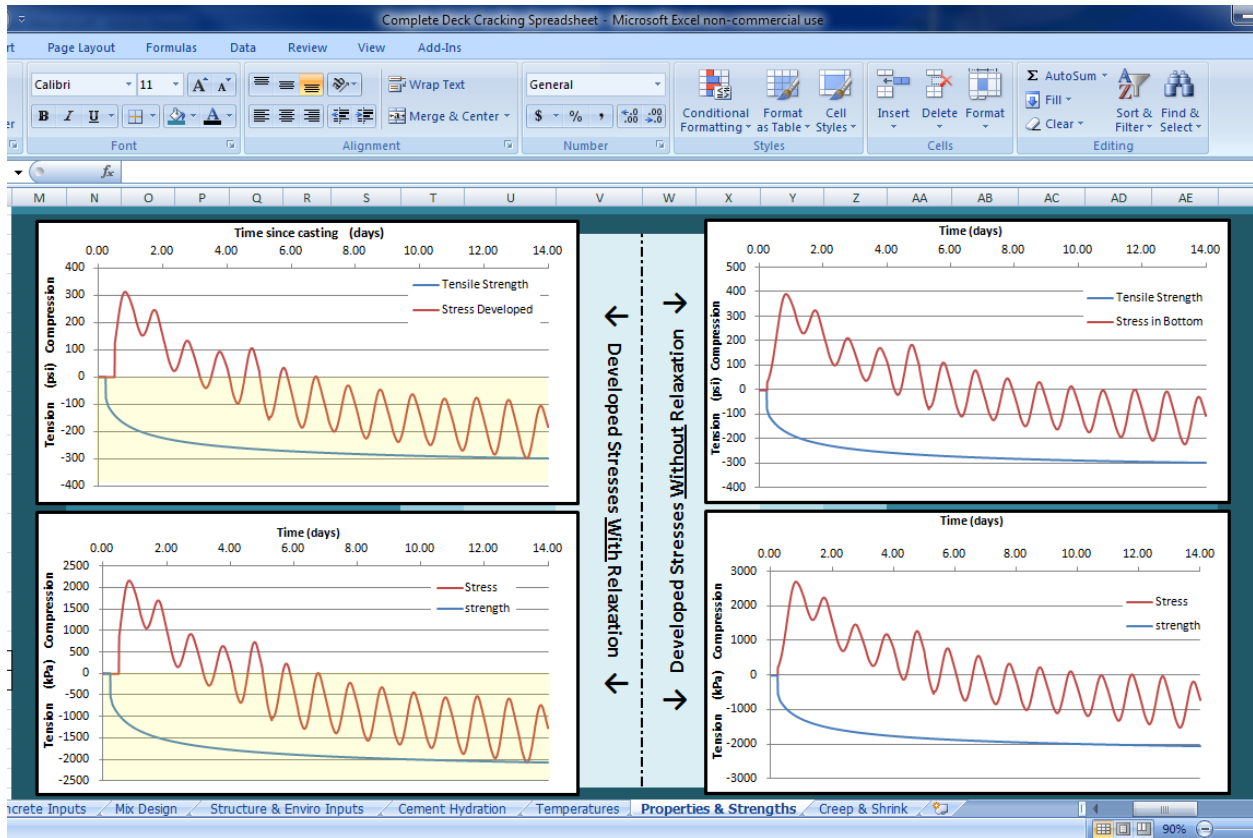


Figure 6-9: Screen cap of properties and strength tab displaying stresses and tensile strengths

Similar to the reference documents, when relaxation effects are taken into consideration a point of zero stress can be identified and the moment in time of cracking is shown by the first intersection of the two graphed properties (developed strength and developed stresses). An example of the theory is depicted in Figure 6-10 which was taken from Schindler, 2002. The

associated spreadsheet developed a graph which equates to the concept in Figure 6-10 and it is shown in Figure 6-11 where the moment in time of first cracking can be easily identified.

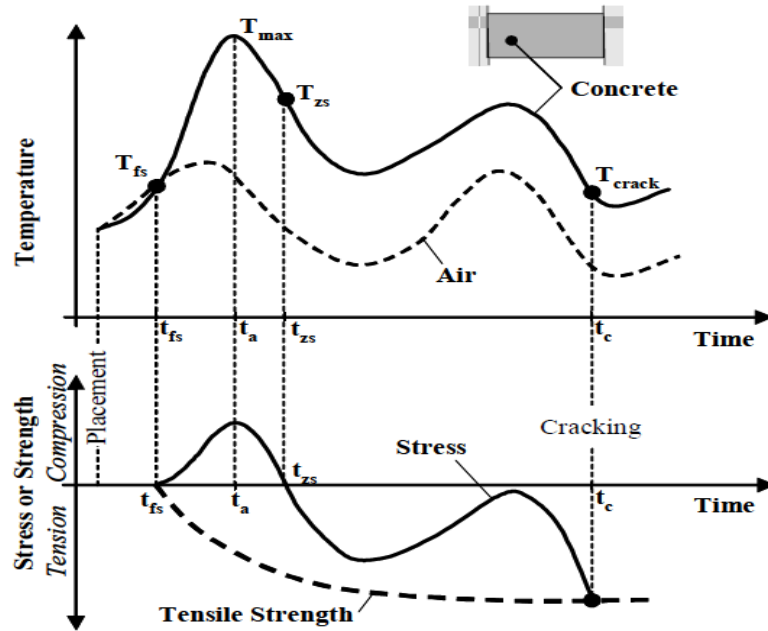


Figure 6-10: Documented behavior of hardening concrete and crack identification (Schindler et al. 2002)

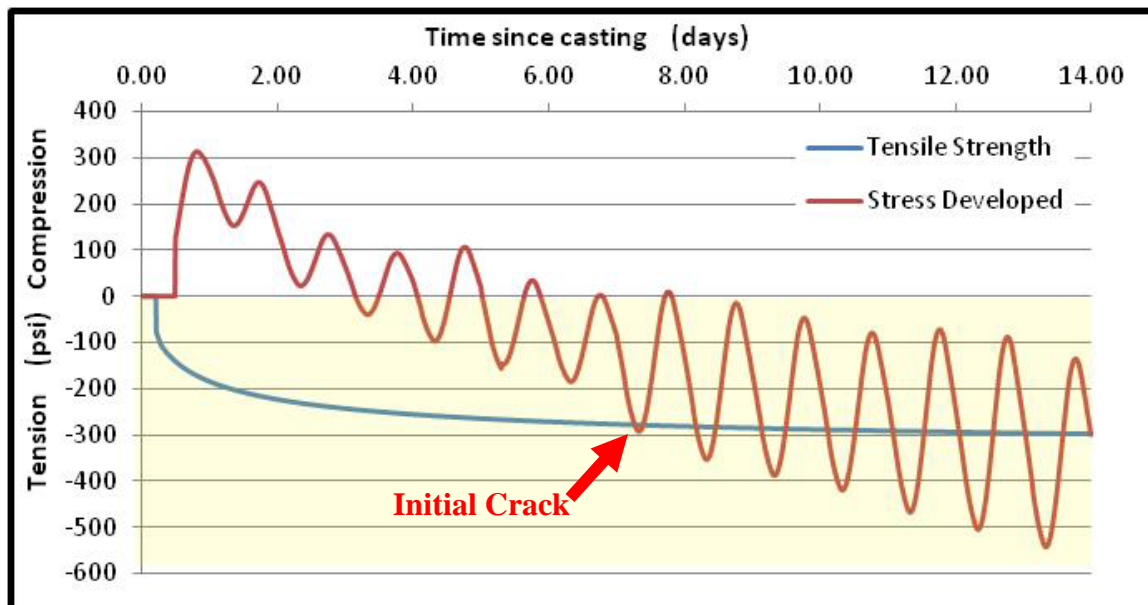


Figure 6-11: Spreadsheet calculated behavior of hardening concrete sample and crack identification

7. CONCLUSIONS

The conclusions drawn from this study are:

1. All of the tested sealers performed well with respect to the penetration depth. In addition to exhibiting good penetration, the sealers bonded well to the crack walls in most of the cases.
2. The flexural capacity of the cracked slabs was restored after sealing. The sealed slabs performed close to the control slabs.
3. Sealer debonding was minimal when reloading the repaired slabs, which indicated a good bond performance of the sealers.
4. The test results of all the sealers indicated discrepancies from the claimed values in the data sheets in all performed tests including tensile strength and elongation. The material samples were prepared by the product suppliers and tested twice at the FDOT material labs.
5. Performance of sealers complied with many of the requirements of the FDOT specifications. Special attention could be paid to modify the FDOT requirements to reflect a minimum elongation value.
6. From the analysis of the experimental and field test results, the authors recommend a minimum elongation for the sealers to be 10%.
7. Based on the test results of different sealers, the authors recommend that the minimum tensile strength of the sealant material should be higher than the tensile capacity of concrete and should be at least 1000 psi. This is recommended to restore the flexural strength of concrete and to prevent sealer failure under future loads.
8. The Finite Element (FE) analysis of bridges indicated that in most cases, no cracking occurred under truck loads only. However, the combined effect of truck load with shrinkage or truck load with thermal effect causes transverse deck cracking.
9. From the results of the Finite Element (FE) analysis of bridges, it was indicated that some of the primary causes of deck cracking are shrinkage alone, thermal alone, the combined effect of truck load and shrinkage effect, and the combined effect of truck load and thermal effect.
10. Based on the Finite Element (FE) analysis of bridges, shrinkage solely or in combination with truck loading may cause transverse cracking in bridge decks.
11. The FE model of tested slabs simulated well the tensile stresses that developed in the deck.
12. The FE analysis of bridge model indicated an increase of deflection and crack widths due to the increase of live load applied to bridges. The transverse cracks were already developed due to shrinkage or thermal effects and then widened under truck load.
13. Deck cracks initiated due to shrinkage and/or temperature effects typically become working cracks, as external loads are ultimately applied to the deck. The cracks can widen due to these applied loads.
14. There was a clear correlation between increasing crack width with increasing deflection due to incrementally increasing truck loading, based on FE model and analytical study.

15. Based on the analytical study, the authors recommend limiting the vertical deflection of bridge superstructure system. Limiting superstructure flexibility controls the vertical deflection.
16. From the analysis of the analytical study, increasing deck thickness reduces deck stresses.
17. From analyzing the results of the developed Excel spreadsheet, continuation of wet curing for 14 days rather than 7 days helped mitigating early age deck cracking.

8. REFERENCES

1. American Association of State Highway and Transportation Officials, *AASHTO LRFD Bridge Design Specification*, 2nd Edition. Washington D.C., 1998.
2. American Association of State Highway and Transportation Officials (AASHTO), 2007, *LRFD Bridge Design Specifications*, 4th Edition, Washington D.C.
3. ACI committee 209. Prediction of Creep, Shrinkage, and Temperature Effects. Detroit, 1978.
4. ACI Committee 207. Shrinkage and Creep effects in Concrete. Detroit, 1986.
5. ACI Committee 224, 2001, *Control of Cracking in Concrete Structures*, (ACI 224R-01), American Concrete Institute, Farmington Hills, MI.
6. ACI committee 308, *Standard Practice for Curing Concrete*. Detroit, 1986.
7. American Concrete Institute, ACI Manual of Concrete Practice- Part 1: *Materials and general Properties of Concrete*, Detroit, 1986.
8. Altoubat, S.A., and Lange, D.A., 2000, "Creep, Shrinkage and Cracking of Restrained Concrete at Early Age", University of Illinois at Urbana-Champaign, Urbana, IL.
9. Altoubat, S. and D.A. Lange, "Creep, Shrinkage, and Cracking of Early Age Concrete Discussion," *ACI Materials Journal*, Vol. 99, No. 3, pp. 326-7, 2002.
10. K. Babaei and R.L. Purvis, "Premature Cracking of Concrete Bridge Decks: Cause and Methods of prevention" Proceedings, 4th International Bridge Engineering Conference, 1996.
11. Babaei, K., and Purvis, R., *Prevention of Cracks in Concrete Bridge Decks: Report on Laboratory Investigation of Concrete Shrinkage*, Report for Research Project 89-01. Pennsylvania Department of Transportation, Oct. 1994.
12. Babaei, K., and Hawkins, N.M., Evaluation of Bridge Deck Protective Strategies. NCHRP Report 297, TRB, National Research Council, Washington, D.C., September 1987.
13. BASF (2010). *Degadeck Crack Sealer Plus Product Data*, Shakopee, MN. <http://www.basf.com>.
14. BASF (2010). *Degadur 332 Product Data*, Shakopee, MN. <http://www.basf.com>.
15. R.L. Blaine, H.T. Arni, D.H. Evans, M.R. Defore, J.R. Clifton, and R.G. Methey. "Interrelation between Cement and Concrete Properties", Building Research Division of National Bureau of Standards, 1953.
16. Cady, P. D., Carrier, R. E., Bakr, T. A., and Theisen, J. C., 1971, Final Report, *Durability of Bridge Deck Concrete*, Pennsylvania Department of Transportation, Harrisburg, PA.
17. Cao, L.C. and Shing, P.B., (1999), "Simplified analysis method for slab-on-girder highway bridge decks," *J. Struct. Eng.*, 125(1), 49-59.
18. ChemMasters, (2010). *Duraguard HM Sealer Product Data*, Madison, OH. <http://www.chemmasters.net>
19. ChemMasters, (2010). *Duraguard 401 Product Data*, Madison, OH. <http://www.chemmasters.net>.
20. T.T.H. Cheng and D.W. Johnston, *Incidence Assessment of Transverse Cracking in Concrete Bridge Decks: Construction and Material Considerations*, Report FHWA/NC/85-002, Vol. 1, North Carolina State University, Raleigh, 1985, 232 pp.

21. F.H. Dakhil, P.D. Cady and R.E. Carrier, "Cracking of Fresh Concrete as Related to Reinforcement", *ACI Struct. Journal*, 72(8), pp. 421-428, 1975.
22. Delatte, N., Miller, D., and Mrkajic, A., 2007, "*Portland cement pervious concrete pavement: Field performance investigation on parking lot and roadway pavements*, Final Report, Ready Mix Concrete Research and Education Foundation, Silver Springs, Md.
23. J. Ducret and J. Lebet. "Measurements on a Composite Bridge: Effect of Concrete Hydration", *Proceedings of an Engineering Foundation Conference*, American Society of Civil Engineers, New York, 1996.
24. Eppers, L., French, C., and Hajjar, J. F., "Transverse Cracking in Bridge Decks: Parametric Study", Mn/DOT Final Report, 1998.
25. La Fraugh, R. W., and Perenchio, W. F., (1989), *Phase I Report of Bridge Deck Cracking Study West Seattle Bridge*, Rep. No. 890716, Wiss, Janney, Elstner Associates, Northbrook, Ill.
26. C. French, L. Eppers, Q. Le, and J.F. Hajjar, "Transverse cracking in concrete bridge decks" *Transportation Research Record*. n 1688 Nov 1999. p 21-29.
27. R.J. Frosch, R.D. Radabaugh, and D.T. Blackman, "Investigation of Transverse Deck Cracking", *ASCE Structures Congress*, Denver, April 2002.
28. Frosch, R., Blackman, D., and Radabaugh, R. (2003). *Investigation of Bridge Deck Cracking in Various Bridge Superstructure Systems*, Report Number FHWA/IN/JTRP-2002/25, Indiana Department of Transportation, Division of Research, West Lafayette, IN.
29. Frosch, R.J., (2002), "Modeling and Control of Side Face Beam Cracking," *ACI Structural Journal*, Vol. 99, No. 3, May-June 2002, pp. 376-385.
30. Hadidi, R. and Saadeghvaziri, M.A., "Transverse Cracking of Concrete Bridge Decks: State of the Art", *Journal of Bridge Engineering: American Society of Civil Engineer*, 2005.
31. Iowa Department of Transportation. *A study of Transverse Cracks in the Keokuk Bridge Deck*, Final Report, Iowa Department of Transportation, July 1986.
32. M.A. Issa, "Investigation of cracking in concrete bridge decks at early ages", *Journal of Bridge Engineering*, V 4 n 2 1999, p 116-124.
33. T. Kochanski, J. Parry, D. Pruess, L. Schuchardt, and J. Ziehr, J., *Prematur, Cracking of Bridge Decks Stud*, Wisconsin Dept. of Transportation, Madison, Wisconsin, 1990.
34. P.D. Krauss and E.A. Rogalla, *Transverse Cracking in Newly Constructed Bridge Decks*, NCHRP Report 380, Transportation Research Board, Washington, DC, 1996.
35. Lasa, I.R., Powers, R.G., and Kessler, R.J., (1980), *Evaluation of Rohm and Haas, High Molecular Weight Methacrylate Monomer as a Crack Sealer on the Seven Mile Bridge in Florida One Year after Application*, State of Florida Department of Transportation, December, Tallahassee, Florida.
36. Le, Q. T. C., French, C., and Hajjar, J. F., "Transverse Cracking in Bridge Decks: Parametric Study," Mn/DOT Final Report, 1998.
37. C. Meyers., 1982, *Survey of Cracking on Underside of Classes B-1 and B-2 Concrete Bridge Decks in District 4. Investigation 82-2*, Division of Material and Research, Missouri Highway and Transportation Department, Jefferson City, Mo.

38. Ministry of Transportation and Communications, 1983, *Ontario highway bridge design code*. Ministry of Transportation and Communications, Downsview, Ontario. Canada. 357 pp.
39. Minnetyan, L., and Assamany, A., (2004). "Serviceability of high performance concrete." Presented at the Central New York ASCE, ASME, IEEE, NSPE Engineering Expo, Syracuse, NY, November 15, 2004.
40. M. Paillere, M. Buil and J.J. Serrano, "Effect of Fiber Addition on the Autogenous Shrinkage of Silica Fume Concrete", *ACI Material Journal*, V.86, No.2, Mar.-Apr., pp. 139-144, 1989.
41. PCA (1970), *Durability of Concrete Bridge Decks*, Final Report, 35 pp.
42. Perfetti, G. R., Johnston, D. W., and Bingham, W. L., 1985, *Incidence Assessment of Transverse Cracking in Concrete Bridge Decks: Structural Considerations*, Report No. FHWA/NC/88002, Vol. 2, North Carolina State University, Raleigh, Dept. of Civil Engineering, 201 pp.
43. Portland Cement Association, 1969, Final Report, *Design of Continuous Highway Bridges with Precast Prestressed Concrete Girders*, Portland Cement Association.
44. Portland Cement Association, Final Report, *Durability of Bridge Decks - A cooperative Study*, Skokie, Illinois, 1970.
45. Purvis, R.; Babei, K.; Udani, N.; Qanbari, A.; and Williams, W., 1995, "Premature Cracking of Concrete Bridge Decks: Causes and Methods of Prevention," Proceedings of the 4th International Bridge Engineering Conference, Washington, D.C.
46. G.E. Ramey, A.R. Wolff, R.L. Wright. "Structural design actions to mitigate bridge deck cracking", *Practice Periodical on Structural Design & Construction*, v 2 n 3, p118-124, 1997.
47. Saadeghvaziri, M.; Hadidi, R., 2002, *Cause and Control of Transverse Cracking in Concrete Bridge Decks*, Final Report FHWA-NJ-2002-019, New Jersey Department of Transportation, Trenton, NJ.
48. Schmitt, T. R., and Darwin, D., 1999, "Effect of Material Properties on Cracking in Bridge Decks", *Journal of Bridge Engineering*, ASCE, February, Vol. 4, No. 1, pp. 8-13.
49. Stewart, C.F., and Gunderson, B.J. *Factors Affecting the Durability of Concrete Bridge Decks*. Interim Report No.2, Research and Development Section of Bridge Department, State of California, November 1969.
50. Tadros, M. K., Al-Omaishi, N., Seguirant, S. J., and Gallt, J. G., (2003), "Prestress Losses in Pretensioned High Strength Concrete Girder Bridges", Washington, D.C.: Transportation Research Board.
51. Transpo Industries, (2010), "Sealate T-70/30 MX Product Data", New Rochelle, NY. <http://www.transpo.com>.
52. Unitex, (2010), *Pro-Poxy 40LV LM Product Data*, Kansas City, MO. <http://www.unitex-chemicals.com>.
53. Wallace T. McKeel, Jr., 1985, *Evaluation of deck durability on continuous beam highway bridges*, Virginia Center for Transportation Innovation and Research, VHTRC 85-R32.
54. Wiegink, K., Marikunte, S., and Shah, S. P., (1996), "Shrinkage cracking of high-strength concrete." *ACI Materials Journal*, 93(5), 409-415.

55. Xi, Y., Shing, B., Abu-Hejleh, N., Asiz, A., Suwito, A., Xie, Z., and Ababneh, A., 2003, *Assessment of the Cracking Problem in Newly Constructed Bridge Decks in Colorado*, Final Report CDOT-DTD-R-2003-3, Colorado Department of Transportation, CO.
56. Yazdani, N., Green, P. and Haroon, S., “Wind Missile Impact Capacity of Essential Facilities”, *Journal of Emergency Management*, Vol. 5, No. 2, pp. 27-40, March/April 2007.
57. S. Zhou, D.C. Rizos, and M.F. Petrou, (2004), “Effects of superstructure flexibility on strength of reinforced concrete bridge decks,” Elsevier Ltd, *Computers and Structures* 82 (2004).

9. APPENDIX A: SEALERS MATERIAL APPLICATION

Figure 9-1 shows sealer material application in the field.



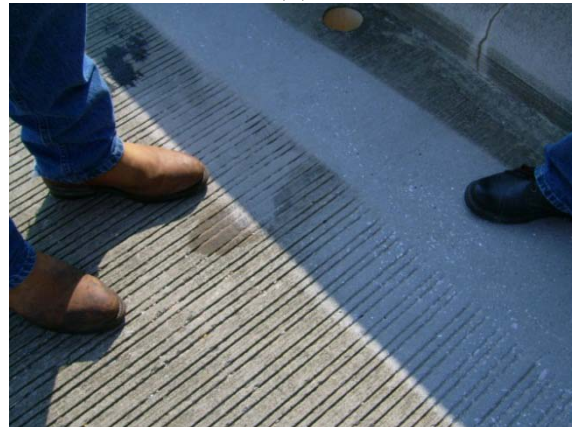
(a)



(b)



(c)



(d)



(e)



(f)



(g)



(h)



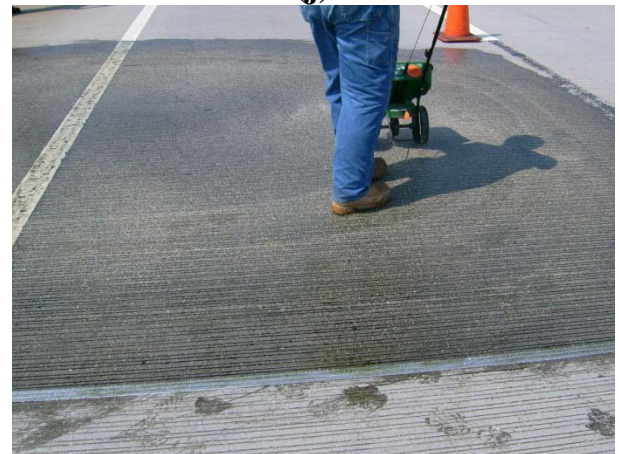
(i)



(j)



(k)



(l)

Figure 9-1: Sealer application

10. APPENDIX B: INSPECTED BRIDGES

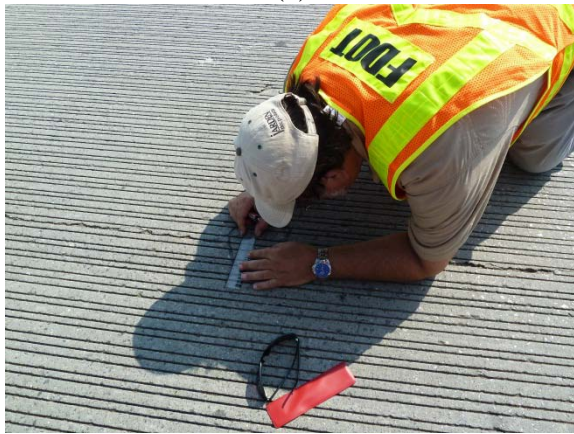
Figures 10-1 to 10-6 present the inspected bridges and field investigation.



(a)



(b)



(c)



(d)



(e)



(f)

Figure 10-1: Site inspection - Blackwater River Bridge (Pensacola)



(a)



(b)



(c)



(d)



(e)



(f)



(g)



(h)

Figure 10-2: Sampling



(a)



(b)



(c)



(d)



(e)



(f)

Figure 10-3: Site inspection - Fort Lauderdale



(a)



(b)



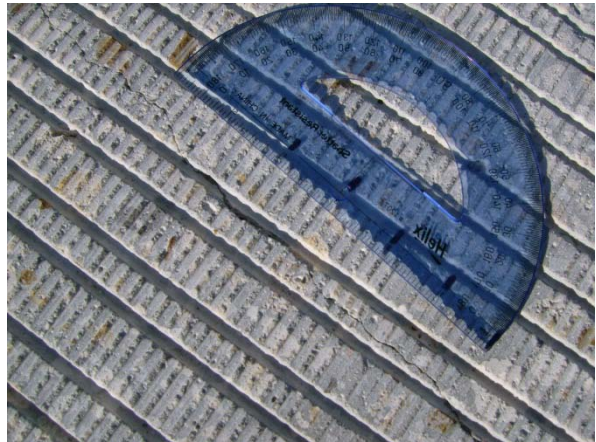
(c)



(d)



(e)



(f)

Figure 10-4: Site inspection - U.S. 1 Bridge (Jacksonville)



(a)



(b)



(c)



(d)

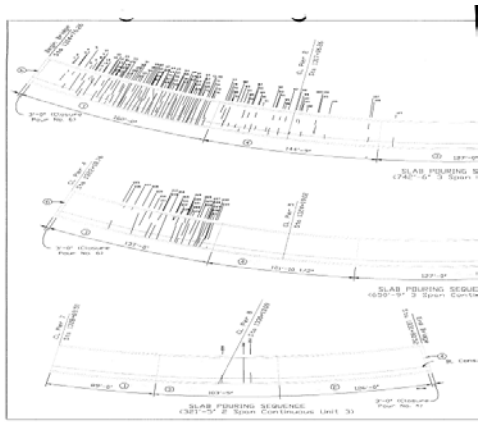


(e)

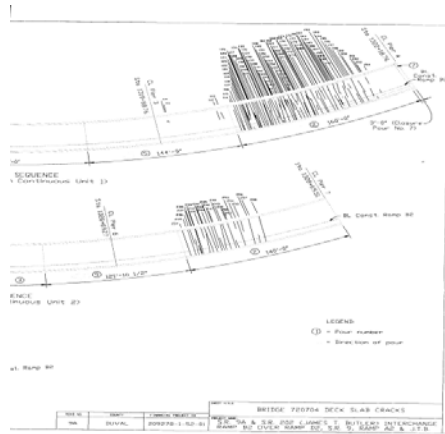


(f)

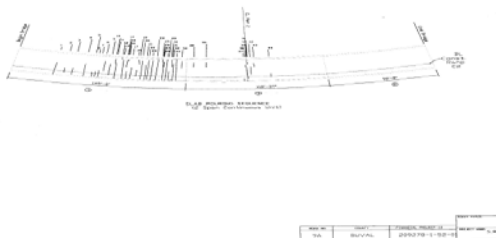
Figure 10-5: Concrete placement - U.S. 1 Bridge (Jacksonville)



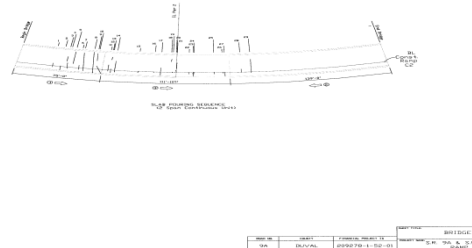
(a)



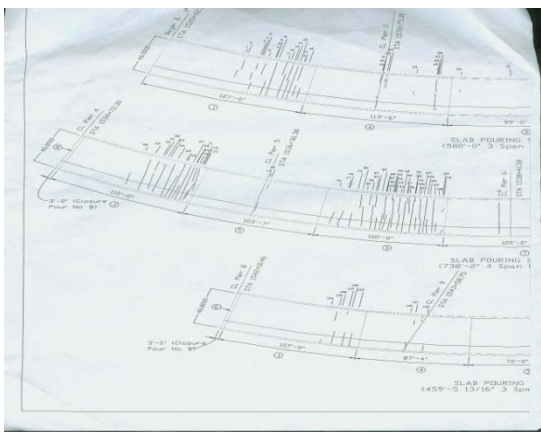
(b)



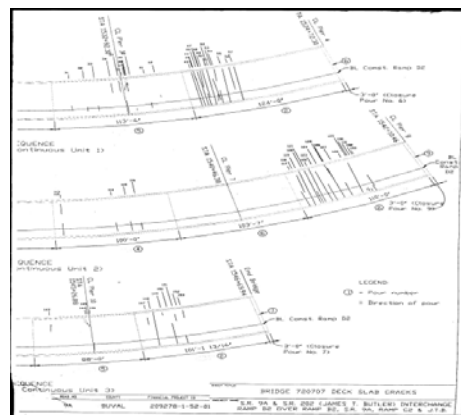
(c)



(d)



(e)

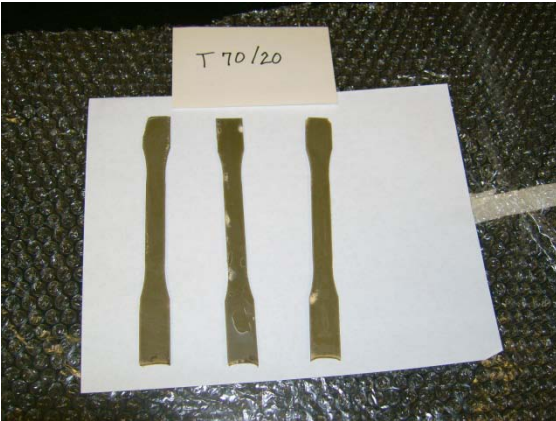


(f)

Figure 10-6: Crack locations - JTB Bridge (Jacksonville)

11. APPENDIX C: SEALER TESTING

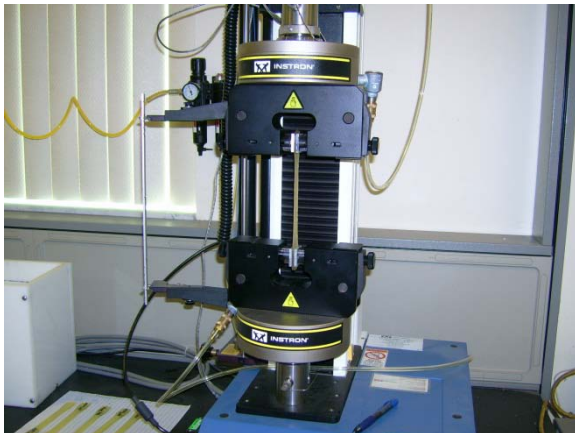
The following Figures (Figures 11-1 to 11-3) show the lab tests including sealer and core testing.



(a)



(b)



(c)



(d)



(e)



(f)

Figure 11-1: Sealer tensile testing



(a)



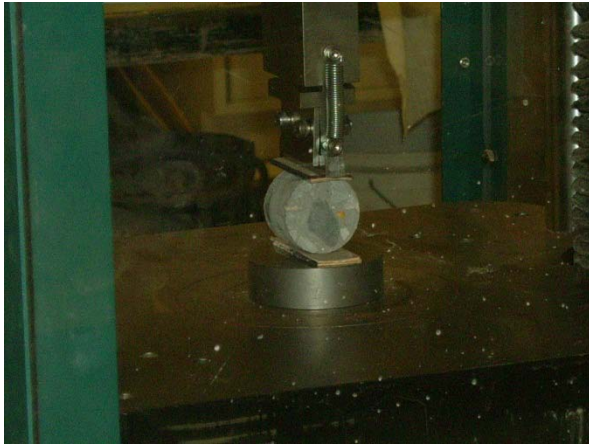
(b)



(c)



(d)



(e)



(f)

Figure 11-2: Site core testing - site core testing



(a)



(b)



(c)



(d)



(e)



(f)



(g)



(h)

Figure 11-3: UNF – Lab testing and core testing

12. APPENDIX D: SHRINKAGE STRAIN CALCULATIONS

12.1. Calculations of Strain due to Shrinkage

The equation developed by Saadeghvaziri and Hadidi (2002) and presented before was used to determine the strain due to shrinkage (ξ_{sh}) at different ages of concrete. A summary of equations is shown in the following Figures (Figure 12-1 to Figure 12-7).

Drying shrinkage of concrete is defined as a decrease in volume under constant temperature due to loss of moisture after concrete has hardened	
Tadros and Al-Omaishi (2003)	It should be noted that the value 0.48×10^{-3} simply represents an estimate for the ultimate shrinkage strain in the concrete.
$\epsilon_{sh} = -k_{sh}k_{vs}k_{h}k_{f}k_{td}(0.48 \times 10^{-3})$	(5.1)
Saadeghvaziri and Hadidi 2002	
$\epsilon_{sh} = -(1.2)k_{vs}k_{h}k_{f}k_{td}(0.78 \times 10^{-3})$	(5.2)
$k_{vs} = 1.45 - 0.13(V/S) \geq 1.0$	(5.3) The coefficient k_{vs} is a factor for considering the effect of the volume-to-surface ratio of the concrete. where V is the volume of concrete and S is the surface area of concrete.
$k_h = 2.00 - 0.014H$	(5.4) The coefficient k_h is a humidity factor that accounts for the fact that shrinkage tends to be greater in dry climates than humid climates. where H is the relative humidity (%) of the environment
$k_f = \frac{3}{14f'_c}$	(5.5) The coefficient k_f is a factor to take into consideration the effect of concrete strength where f'_c is the specified compressive strength of concrete at the time of initial loading (ksi). However, because the age of the concrete at the time of loading is unknown, Tadros and Hadidi (2003) suggests the use of 0.80f' when examining this factor
$k_{td} = \frac{t}{91-47t+7t^2}$	(5.6) The coefficient k_{td} is a time development factor where t is the maturity of the concrete (in days). Maturity is defined as the age of concrete between the end of curing and the time being considered. However, for bridge decks where the curing time may be unknown (or varying), the time immediately following placement is used as an initial time



Figure 5.25 Topographic Map of United States Humidity (Tadros and Al-Omaishi 2003).

Figure 12-1: Bridge model single-span-N-4000-8.5-4, two-span-N-4000-8.5-4, three-span-N-4000-8.5-4

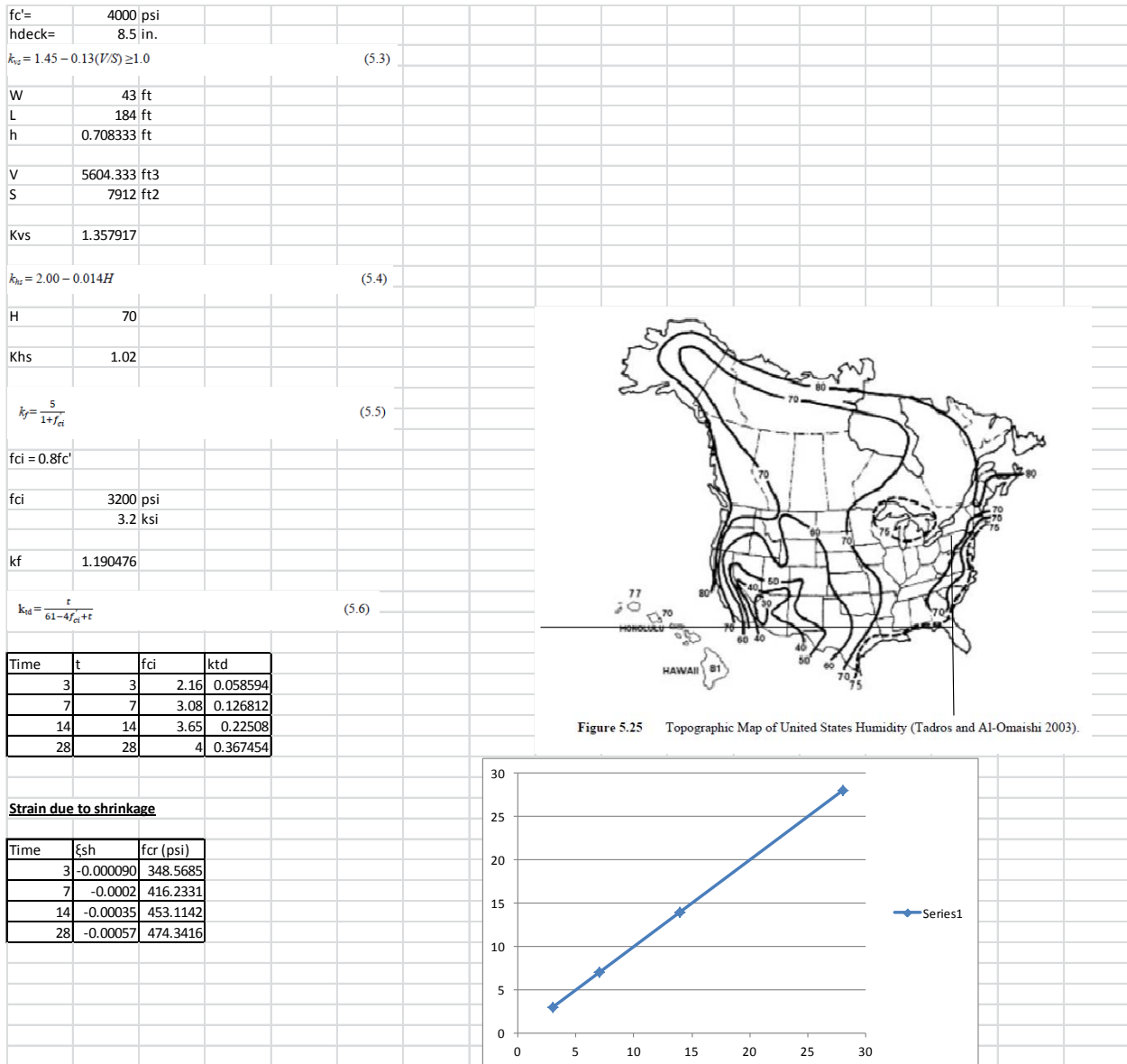


Figure 12-2: Bridge model two-span-half-4000-8.5-4

fc'	4000 psi			
hdeck	8.5 in.			
$k_{tz} = 1.45 - 0.13(V/S) \geq 1.0$			(5.3)	
W	43 ft			
L	92 ft			
h	0.708333 ft			
V	2802.167 ft3			
S	3956 ft2			
Kvs	1.357917			
$k_{tz} = 2.00 - 0.014H$			(5.4)	
H	70			
Khs	1.02			
$k_{tz} = \frac{5}{1+f_c}$			(5.5)	
fci = 0.8fc'				
fci	3200 psi 3.2 ksi			
kf	1.190476			
$k_{td} = \frac{r}{61-4f_{ci}+r}$			(5.6)	
Time	t	fci	ktd	
	3	2.16	0.058594	
	7	3.08	0.126812	
	14	3.65	0.22508	
	28	4	0.367454	
Strain due to shrinkage				
Time	ξ_{sh}	fcr (psi)		
	3	-9E-05	348.5685	
	7	-0.0002	416.2331	
	14	-0.00035	453.1142	
	28	-0.00057	474.3416	



Figure 5.25 Topographic Map of United States Humidity (Tadros and Al-Omaishi 2003).

Figure 12-3: Bridge model two-span-N-4000-7-4

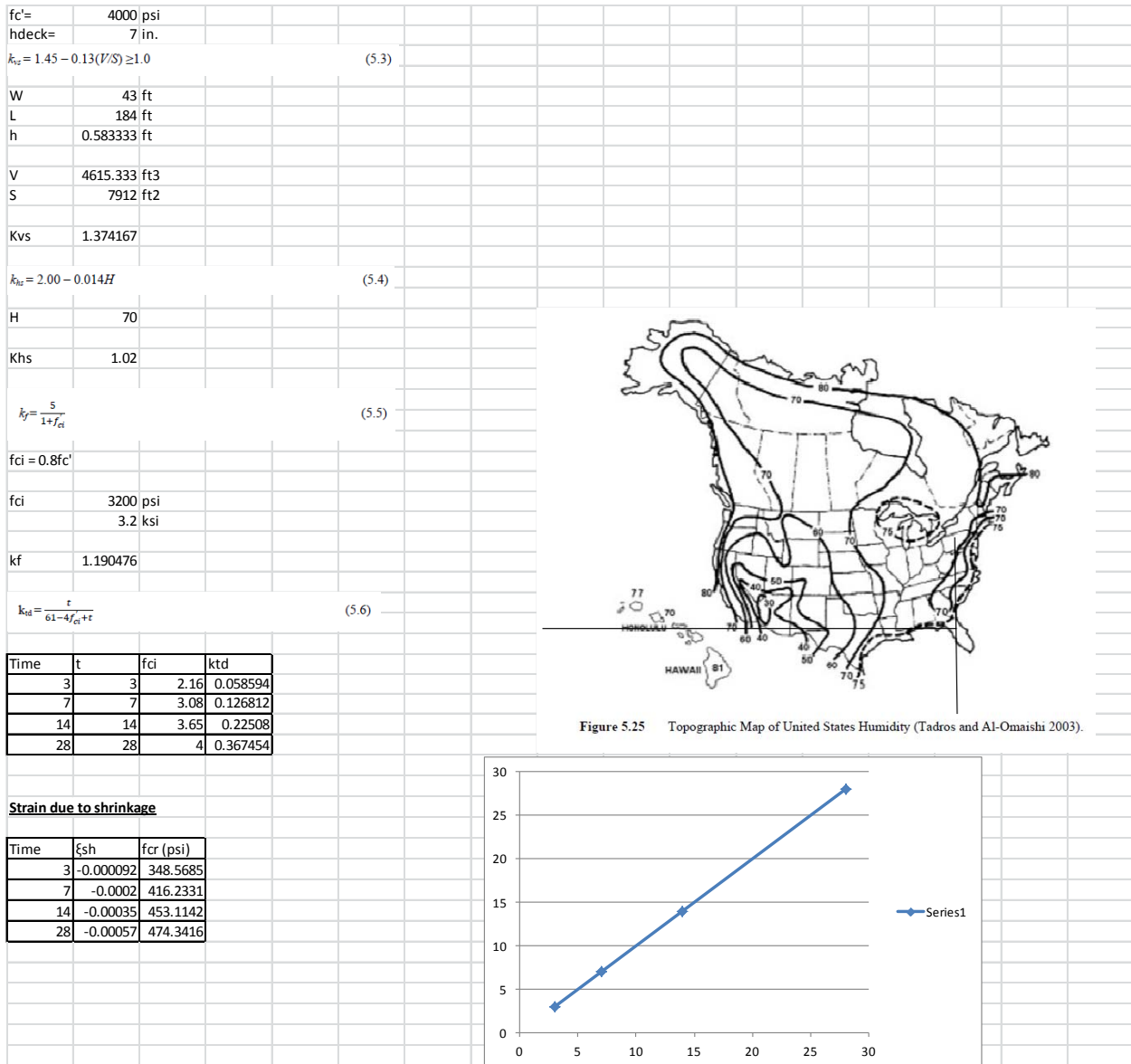


Figure 12-4: Bridge model two-span-N-4000-10-4

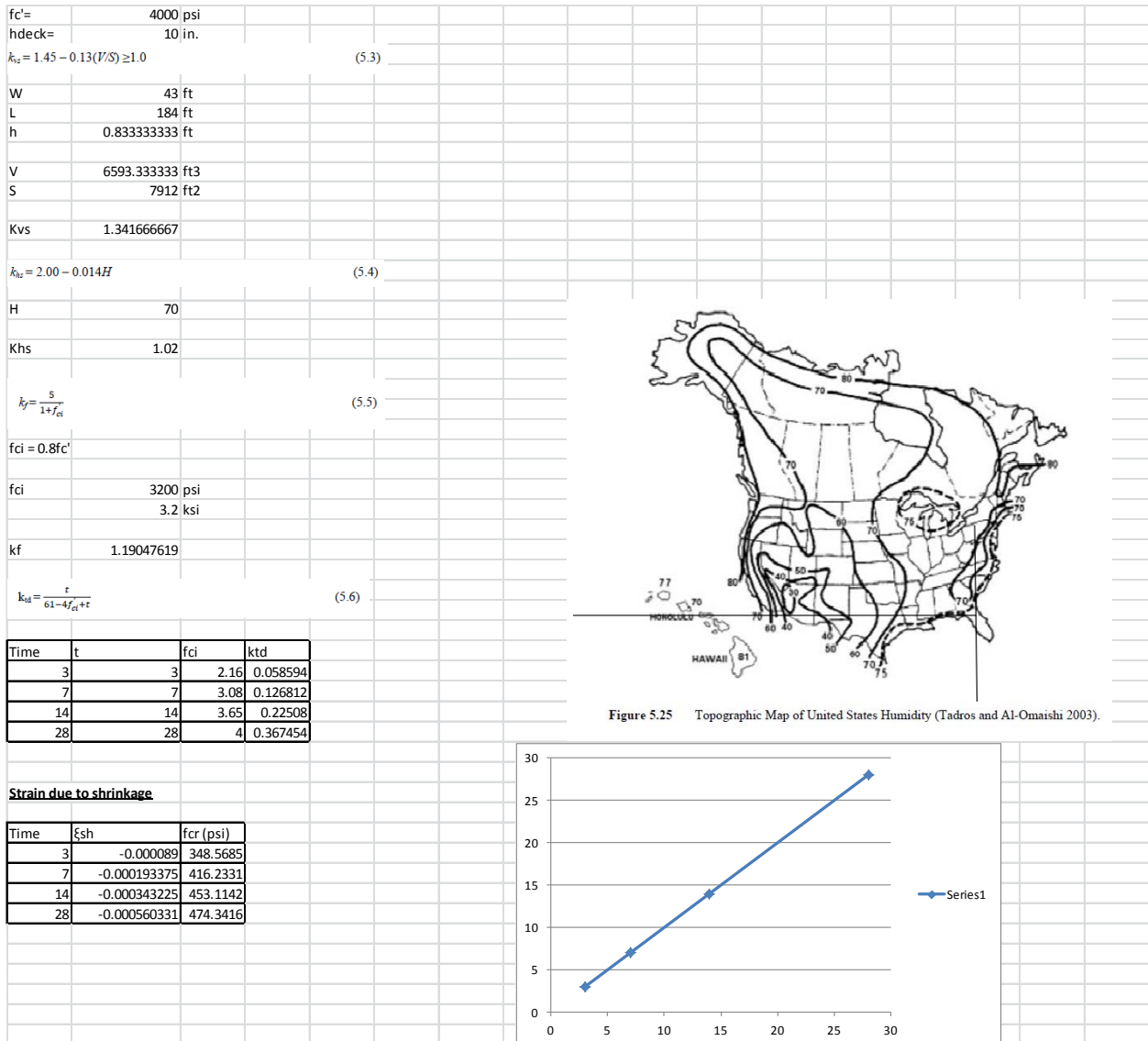


Figure 12-5: Bridge model two-span-N-5000-8.5-4

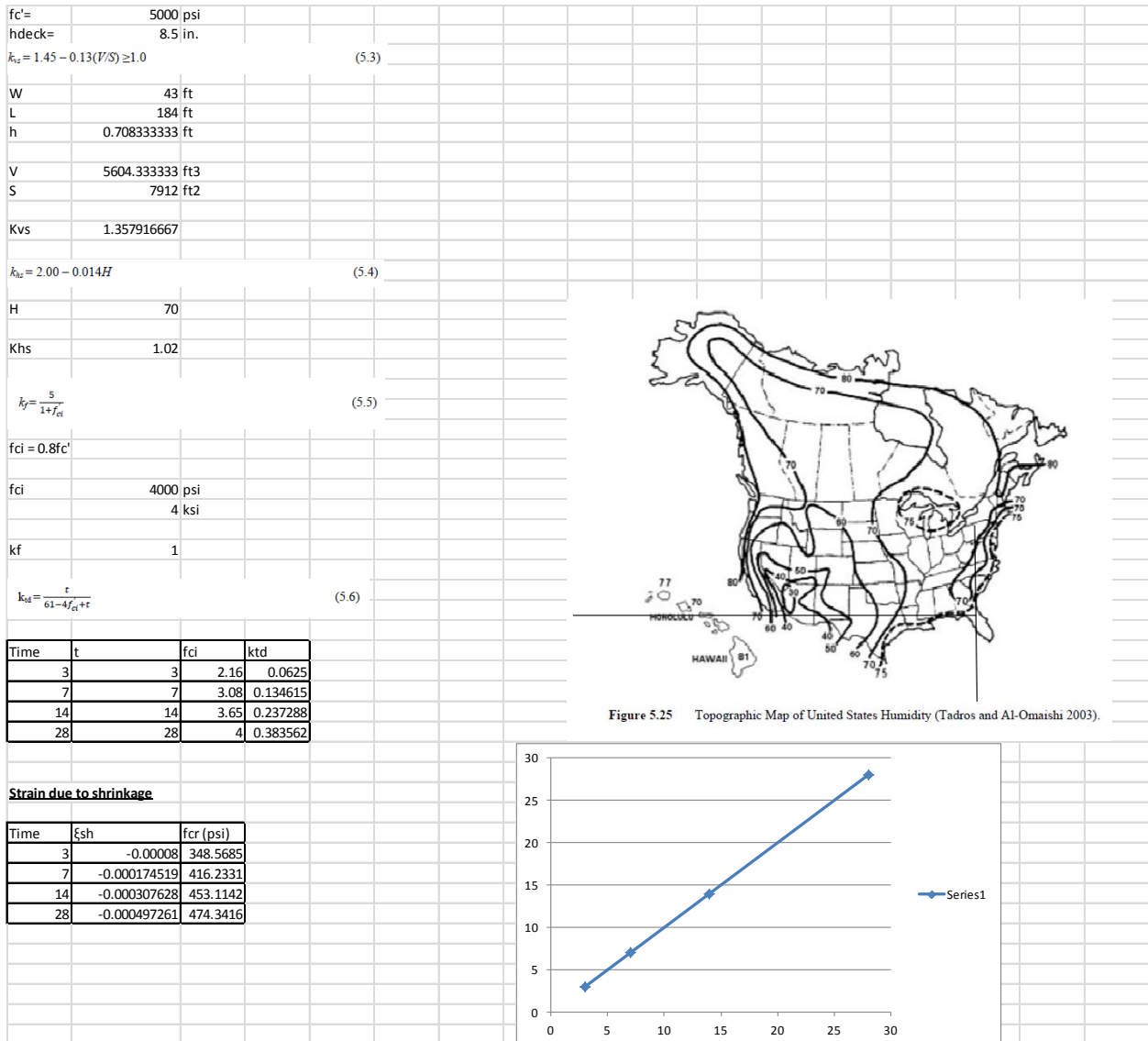


Figure 12-6: Bridge model two-span-N-7000-8.5-4

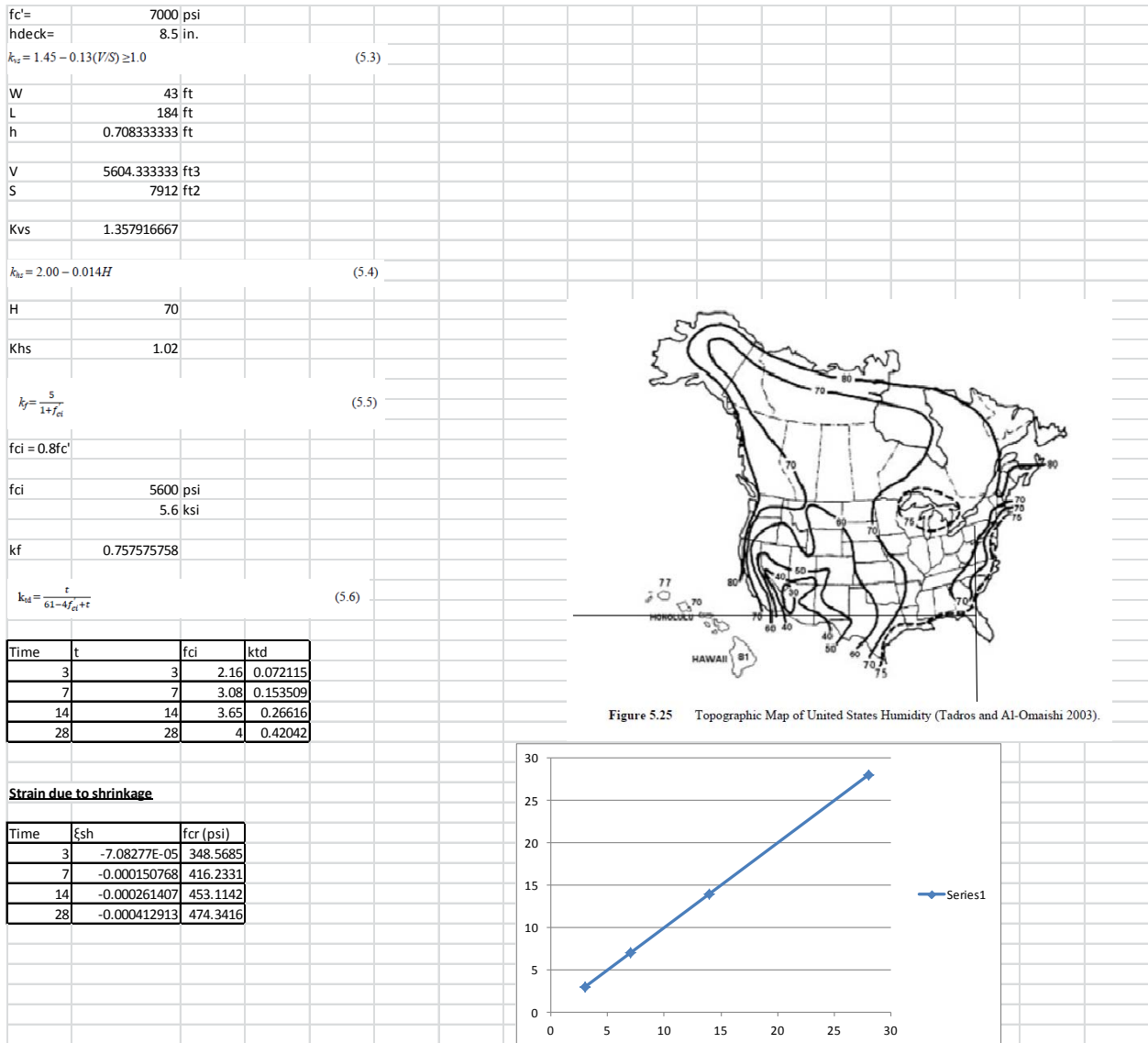



Figure 12-7: Another bridge model

13. APPENDIX E: CREEP STRAINS CALCULATIONS

13.1. Calculations of Creep Coefficient

The creep coefficient is calculated using PCA (1969) equations for all of the bridge models. The creep coefficient is multiplied by strain developed dead load then applied to bridge decks.

A summary of the equations is presented below in Figure 13-1.

PCA "Design of Continuous Highway Bridges with Precast Prestressed Concrete Girders" August 1969	
The creep coefficient is the ratio between creep strain and the strain due to permanent stress.	
$\Psi_{(\infty,1)} = 3.5k_c k_f (1.58 - H/120) t_i^{-0.118} [(t-t_i)^{0.6} / (10.0 + (t-t_i)^{0.6})]$	
$k_c = \left[\frac{\left(\frac{t}{26e^{0.36(V/S)_b} + t} \right)}{\left(\frac{t}{45+t} \right)} \right] \left[\frac{1.80 + 1.77e^{-0.54(V/S)_b}}{2.587} \right] \quad (SC5.4.2.3.2-1)$	<p>the volume to surface area factor, k_c t = maturity of concrete = infinite days</p> <p>e = natural log base (approx. 2.71828)</p> <p>$(V/S)_b$ = volume to surface ratio</p>
$k_f = 1/[0.67 + (f'_c/9)]$	<p>the concrete strength factor, k_f f'_c is the specified compressive strength of concrete</p>
	<p>H = the relative humidity (%) of the environment t_i = age of concrete when load is initially applied t = age of concrete at time of interest</p>
<p>Figure 5.25 Topographic Map of United States Humidity (Tadros and Al-Omaishi 2003).</p>	

(a)

$k_c = \left[\frac{t}{2C_p^{0.34}(V/S)_h + t} \right] \left[\frac{1.80 + 1.77e^{-0.34(V/S)_h}}{2.537} \right]$	(SC5.4.2.3.2-1)	
W	43 ft	
L	92 ft	
h	0.708333 ft	
V	2802.167 ft3	
S	3956 ft2	
V/S	8.5 in.	
t	infinite days	
k _c	0.702733	
$k_f = 1/[0.67 + (f'_c/9)]$		
f' _c	4 ksi	
k _f	0.897308	
H	70	
t _i	1 day	
t	450 days	maximum time used
ψ(450,1)	1.75096	
ψ(∞,1)	2.199632	
Two Span Bridge (Fixed-Fixed)		
E	57000vfc'	3604.997 ksi
σ	0.404 ksi	stress due to dead load from analyses
ξ	σ/E	strain due to dead load from analyses
	0.000112	
ξ _{cr}	ψξ	0.000247



Figure 5.25 Topographic Map of United States Humidity (Tadros and Al-Omaishi 2003).

(b)

$k_c = \frac{\left(\frac{t}{2c e^{0.36(t/2c)} + t} \right)}{\left(\frac{t}{45+t} \right)} \left[\frac{1.80 + 1.77 e^{-0.54(t/2c)}}{2.587} \right] \quad (\text{SC5.4.2.3.2-1})$		
W	43 ft	
L	184 ft	
h	0.833333 ft	
V	6593.333 ft ³	
S	7912 ft ²	
V/S	10 in.	
t	infinite days	
k _c	0.698877	
$k_f = 1/[0.67 + (f'_c/9)]$		
f _c '	4 ksi	
k _f	0.897308	
H	70	
t _i	1 day	
t	450 days	maximum time used
ψ(450,1)	1.741352	
ψ(∞,1)	2.187561	
Two Span Bridge		
E	57000/f _c '	3604.997 ksi
σ	0.08 ksi	stress due to dead load from analyses
ξ	σ/E	strain due to dead load from analyses
	2.22E-05	
ξ _{cr}	ψξ	4.85E-05



Figure 5.25 Topographic Map of United States Humidity (Tadros and Al-Omaishi 2003).

(C)

$k_c = \left[\frac{t}{2.0e^{0.36(100\%)} + t} \right] \left[\frac{1.80 + 1.77e^{-0.54(100\%)}}{2.587} \right]$	(SC5.4.2.3.2-1)	
W	43 ft	
L	184 ft	
h	0.708333 ft	
V	5604.333 ft ³	
S	7912 ft ²	
V/S	8.5 in.	
t	infinite days	
k _c	0.702733	
$k_f = 1/[0.67 + (f'_c/9)]$		
f _c '	5 ksi	
k _f	0.815956	
H	70	
t _i	1 day	
t	450 days	maximum time used
ψ(450,1)	1.592215	
ψ(∞,1)	2.000209	
Two Span Bridge		
E	57000vf'	4030.509 ksi
σ	0.169 ksi	stress due to dead load from analyses
ξ	σ/E	strain due to dead load from analyses
	4.19E-05	
ξ _{cr}	ψξ	8.39E-05



Figure 5.25 Topographic Map of United States Humidity (Tadros and Al-Omaishi 2003).

(d)

$k_c = \frac{\left(\frac{t}{2c e^{0.36(t/c)}} + t \right)}{\left(\frac{t}{45+t} \right)} \left[\frac{1.80 + 1.77 e^{-0.54(t/E)}}{2.587} \right] \quad (\text{SC5.4.2.3.2-1})$		
W	43 ft	
L	184 ft	
h	0.708333 ft	
V	5604.333 ft ³	
S	7912 ft ²	
V/S	8.5 in.	
t	infinite days	
k _c	0.702733	
$k_f = 1/[0.67 + (f'_c/9)]$		
f _c '	7 ksi	
k _f	0.690714	
H	70	
t _i	1 day	
t	450 days	maximum time used
ψ(450,1)	1.347823	
ψ(∞,1)	1.693193	
Two Span Bridge		
E	57000f _c '	4768.962 ksi
σ	0.182 ksi	stress due to dead load from analyses
ξ	σ/E	strain due to dead load from analyses
		3.82E-05
ξ _{cr}	ψξ	6.46E-05



Figure 5.25 Topographic Map of United States Humidity (Tadros and Al-Omaishi 2003).

(e)

Figure 13-1: PCA equations for creep